REGIONAL GEOCHEMICAL DISPERSION OF ELEMENTS IN THE REGOLITH OF THE GIRILAMBONE REGION, CENTRAL WEST NSW

By

KAMAL KHIDER

A thesis submitted to the Australian National University in fulfilment of the requirements for the degree of Doctor of Philosophy

2007

ABSTRACT

Geochemical exploration has provided a major contribution to the discovery of mineral deposits in the Cobar-Girilambone region. The areas of bedrock exposure have generally been well explored and further discoveries will significantly depend on a better understanding of element dispersion, movement and accumulation within the extensive areas of *in situ* and transported regolith cover.

This study evaluates the background levels of target and pathfinder elements in various sampling media including groundwater, the top metre, transported and *in situ* regolith; and the influences of secondary enrichment (calcrete, iron and manganese) on the element association in the regolith of the Girilambone region. It also demonstrated that the bedrock geology could be identified by geochemical signatures preserved in *in situe* regolith. This improved knowledge of the regolith geochemistry and parent bedrock will assist mineral exploration in the region.

Thresholds and anomalies for key target and pathfinder elements (As, Au, Co, Cr, Cu, Mo, Ni, Pb, Sb, V, W, Zn) are estimated using Boxplot and MAD methods. The highest threshold, which possibly indicates a local background, is indicated by the Boxplot method, whereas the MAD method indicates a lower regional background for elements. The thresholds of Au, Cu, Pb and Zn are higher in the *in situ* regolith facies. Arsenic, Cr and V show higher backgrounds when associated with enrichments of hematite and goethite in the Fe-enriched regolith zone. Four major element associations are recognized by cluster analysis. These include elements associated with Ca and Mg (carbonate group), with MnO (manganese oxide), with Fe_2O_3 (iron oxide) and with Ni and Cr (mafic group). Principal component analysis indicates similar groups representing calcretization (Ca+Mg), adsorption (Fe-Mn oxides) and bedrock influences.

A groundwater aquifer is present within the *in situ* regolith in phyllitic siltstone-sandstone layers. Water levels mirror topography, indicating an unconfined aquifer system, and groundwater is flowing to the northeast in the Hermidale area and in part of the Byrock area. The groundwater in the region is mainly of chloride type, rich in

Na, Cl and SO_4 compared to less common calcium-bicarbonate and bicarbonate-chloride types. The correlation between Br/Cl and Na/Cl shows three processes affect the groundwater composition: evaporation, water-rock interaction and water mixing. Calculation of groundwater ages based on $^{36}Cl/Cl$ indicates that the groundwater in the Byrock area (418000-516000 years) is older than that in the Hermidale area (241000-492000 years). Calculated saturation indices of $ZnSiO_3$, malachite and tenorite appear to show a vector towards sites of known mineralisation. The correlation between the groundwater and regolith composition suggests at least two sites (drill holes CBAC217 and CBAC219) of potential mineralisation in the Byrock area.

Slightly weathered and deeply weathered saprolith can be discriminated using the Chemical Index of Alteration (CIA) and major element trends (Al_2O_3- (Na2O+CaO)-K_2O). These trends also indicate the chemical history of regolith profiles in the Girilambone region. Four zones of weathering are recognised based on the CIA value ranging from zone I (CIA>85), zone II (75>CIA≥ 85), zone III (55>CIA≤75) and zone IV (CIA≤55).

Immobile element ratios Zr/Sc versus Th/Sc indicate the level of sediment recycling. A significant increase of Zr/Sc (>10) with insignificant or no increase in Th/Sc (≈1.0), suggests significant recycling of much of the material through weathering processes. Al_2O_3/SiO_2 and TiO_2/Zr ratios are used in association with the $15Al_2O_3$-$300TiO_2$-Zr diagram to discriminate between sandstone, shale and mafic to felsic igneous composition. Ti/Th and Ce/La ratios are used to discriminate between saprolith materials that are derived from the Cobar Supergroup and Girilambone Group. Cobar Supergroup data are clustered in limited ranges of Ti/Th ($0.039 \geq Ti/Th \geq 0.03$) and Ce/La ($2.2 \geq Ce/La \geq 1.9$) ratios, whereas those related to the Girilambone group are characterised by a relatively small range of Ti/Th ($0.03 \geq Ti/Th \geq 0.005$) and Ce/La ($2.3 \geq Ce/La \geq 1.8$).

Calcrete, Fe-Mn oxides or oxyhydroxides appear to be the major regolith components that host Au and base metals (Cu, Zn, Pb) in transported and *in situ* regolith in the Girilambone region. The association of Au with calcrete in the region appears to reflect a chemical environment within both transported and *in situ* regolith that is

conducive to precipitation of both carbonate and mobilised gold, rather than a direct control on gold fixation by calcrete. Sampling the upper part of the calcrete zone within shallow transported and *in situ* regolith during air-core drilling, as part of the strategy for gold exploration in this region, is recommended.

A Mn-enriched zone is variably distributed in the regolith of the Girilambone region and is concentrated in the *in situ* regolith. The highest MnO contents are in the southwest of the Hermidale area and generally decrease toward the east. A stratified concentration of Mn above the present water table along the groundwater flow path indicates previous water levels where the manganese oxides were precipitated due to redox changes.

Enrichments of Au (> 0.009 ppm) and As (>40 ppm) match Fe_2O_3 increases related to the abundance of ferruginous clasts in the Fe-enriched zone, and these indicate a mechanical dispersion of remnant primary Au in ferruginous regolith.

An association of elevated Fe, Zn, Cu and Pb is correlated with the presence of weathered mafic rocks in the region. Over most of the area there is no systematic correlation of elevated Au, As, Zn, Cu and Pb with Fe_2O_3 in either the transported or *in situ* regolith ($r^2 \leq 0.006$, 0.003, 0.04, ≤ 0.16 respectively). These elements are normally considered to be strongly adsorbed or incorporated into goethite and hematite, particularly around mineralisation, but in this case the relationship is not strongly expressed, probably because of the low levels of the trace elements in much of the area and the different adsorption patterns of goethite and hematite.

Certificate of authorship

All results, interpretations and arguments presented in this thesis are my own, except where acknowledged.

Kamal Khider

ACKNOWLEDGMENTS

This work was supported by the Australian Government's Cooperative Research Centre Program, within CRC LEME through a CRCLEME postgraduate award and access to CRCLEME project funding.

Special thanks to my supervisors Ken McQueen and Bear McPhail who were always there for me, advising and discussing outcomes, returning chapter drafts with insightful comments " How, Why...and Refs. !!" with an optimistic "onward". They are the best supervisors that the "luckiest' PhD student could ever have.

I could not mention supervisors without thanking Keith Scott (CSIRO, North Ryde) for his periodic discussions and constructive suggestions and Professor Graham Taylor (University of Canberra) for his judgment and discussion in the early stages of the study.

The drilling for this study was carried out by the NSW Department of Primary Industries, as part of a collaborative project with CRC LEME. Most of the regolith samples were collected by CRC LEME and NSW DPI staff as part of the Girilambone project.

Rainwater data for the study area were provided by Patrice de Caritat (Geoscience Australia) whose support is gratefully acknowledged. Five groundwater samples (Hermidale area) were collected by K. McQueen.

Thanks to Professor Keith Fifield (Department of Nuclear Physics, ANU) for his assistance in analysing chlorine- 36 samples.

Thanks to the following people from the Department of Earth and Marine Sciences, ANU; Judith Shelley for reading the initial drafts and for her invaluable linguistic corrections, Maite Le Gleuher for her assistance in analysing the manganese oxides and for her stimulating discussions, and Ulrike Troitzsch for her help in XRD analysis.

I thank Rushdy Othman (University of NSW) and my co-workers from CRC LEME, Roslyn Chan, Ian Roach and Tan Kok Piang for their various assistance and discussions.

Thanks to John Spring and Aleksandra Plazinska (Bureau of Rural Sciences) for providing valuable field and laboratory assistance.

Finally, thanks to my family particularly to my supportive wife Haifa, who I can't thank enough for her kindness, patience and help over the years, especially during the protracted writing up of the thesis.

Table of Contents

Abstract i

Certificate of authorship iv

Acknowledgements v

1.Chapter one: Introduction 1

1.1Preamble 1

1.2Aims and approaches of the study 3

1.3 Thesis outline 4

2.Chapter two: Regional and site characteristics 6

2.1 Location of study area 6

2.2 Climate, vegetation and landuse 7

2.3 Regolith landforms 8

2.4 Previous work on the geochemistry and regolith in the Girilambone region 10

3. Chapter three: Regional geology and mineralisation 14

3.1 Regional setting of southeastern Australia 14

3.2 Regional tectonic history 17

3.3 Local stratigraphy and intrusions 21

3.3.1 Introduction 21

3.3.2 Girilambone Group 21

3.3.3 Ultramafic and related rocks 23

3.3.4 Silurian volcano- sedimentary sequence 24

3.3.5 Cobar Supergroup and related intrusives 24

3.4 Economic geology and known styles of mineralisation 25

3.4.1 Deposits related to the Girilambone Group 25

3.4.1.1 Girilambone 26

3.4.1.2 Tritton 26

3.4.2 Deposits related to the Cobar Supergroup 27

3.4.2.1 Canbelego -Mount Boppy 27

3.4.2.2 Cobar –type deposits 28

3.5 Mineral deposits in the study area 28

3.5.1 Deposits associated with the Girilambone Group 28
3.5.1.1 Budgery mine 30
3.5.1.2 Bylong 30
3.5.1.3 Calcite crystal rise, North Pole prospect and Chert Ridge prospect 30
3.5.1.4 Mount Dijou – Bald Hills 32
3.5.2 Deposits related to Silurian granitoids 32
3.5.2.1 Beanbah prospect 32
3.5.3 Deposits in unnamed Silurian volcano-sedimentary sequences 32
3.5.4 Deposits in the Cobar Supergroup 34
3.5.4.1 Glengarry gossan and related deposits 35

4.Chapter four: Sampling methodology 36

5.Chapter five: Data analysis techniques 39
5.1 Introduction 39
5.2 Exploratory Data Analysis 40
5.3 Recognition of outliers by boxplot 41
5.4 Transformations 43
5.5 Transformation to avoid closure 43
5.6 Quality control of data 44
5.7 Detection limit 49
5.8 Cluster Analysis 50
5.8.1 Amalgamation or linkage rules 51
5.8.2 Distance measures 52
5.9 Principal Component Analysis 53
5.10 Summary and conclusions 53

6. Chapter six: Geochemical background, anomalies and element associations 55
6.1 Definitions and methodology 55
6.1.1 Introduction 55
6.1.2 Definitions (background, threshold, and anomaly) 55

6.1.3 Techniques used to determine the background and anomaly 56
6.1.4 Evaluation of the statistical techniques 56
6.2 Regolith units and geochemical backgrounds, thresholds and anomalies 58
6.2.1 Introduction 58
6.2.2 Background and threshold values 60
6.2.2.1 Element thresholds for the top meter 60
6.2.2.2 Element thresholds for the transported regolith 61
6.2.2.3 Element thresholds for the *in situ* regolith 62
6.3 Geochemical anomalies 63
6.3.1 Anomalies in the top metre 63
6.3.1.1 Anomalies in the clay-silt- gravel facies 63
6.3.1.2 Anomalies in the regolith carbonate facies 64
6.3.2 Anomalies in transported regolith 64
6.3.2.1 Anomalies in the clay-silt-gravel facies 64
6.3.2.2 Anomalies in the regolith carbonate facies 71
6.3.2.3 Anomalies in the iron- rich facies 71
6.3.3 Anomalies in the *in situ* regolith 71
6.3.3.1 Clay-silt-gravel facies 71
6.3.3.2 Anomalies in the regolith carbonate facies 76
6.3.3.3 Anomalies of the iron-rich regolith facies 76
6.3.3.4 Anomalies in the manganese-rich facies 76
6.4 Element associations 80
6.5 Summary and conclusions 87

7. Chapter seven: Groundwater chemistry and hydrogeology 89
7.1 Introduction 89
7.2 Site descriptions 89
7.3 Hydrogeology 93
7.4 Electrical conductivity, pH/Eh and temperature 94
7.5 Alkalinity 97
7.6 Major ions geochemistry 99
7.7 Groundwater type and origin of dissolved ions 100
7.8 Chloride-36 105

7.9 Identification of aquifer minerals 107
7.9.1 Weathering of silicate minerals 109
7.9.2 Saturation indices 111
7.10 Implications for exploration 112
7.11 Summary and conclusions 117

8. Chapter eight: Weathering processes and provenance 118
8.1 Introduction 118
8.2 Geochemical approaches to evaluate sedimentary processes 119
8.2.1 Testing element immobility 120
8.2.2 Weathering and Chemical Index of Alteration (CIA) 121
8.2.3 Metasomatism 127
8.2.4 Sedimentary recycling 128
8.2.5 Sedimentary sorting 128
8.3 Bedrock, weathering profiles and sediment compositions 132
8.3.1 Weathering zones 132
8.3.2 Bedrock identification 134
8.4 Summary and conclusions 138

9. Chapter nine: Element dispersion in calcrete- manganese - iron-dominant regolith 140
9.1 Introduction 140
9.2 Element associations and dispersion in regolith carbonate zones 141
9.2.1 Introduction 141
9.2.2 Nature and regional distribution of regolith carbonate 141
9.2.3 Calcrete composition 145
9.2.4. Gold concentration in calcrete 154
9.2.4.1 Association of Au with calcrete in the *in situ* regolith 156
9.2.4.2 Association of Au with calcrete in the transported regolith 158
9.2.5 Minor and trace element characteristics of regolith carbonate zones 160
9.2.5.1 Silver, arsenic, bismuth, antimony and tungsten 160
9.2.5.2 Barium and strontium 162

9.2.5.3 Other trace elements 165
9.2.6 Origin of carbonate 165
9.2.7 Summary and conclusions 166
9.3 Element associations and dispersion in Mn-rich regolith 166
9.3.1 Introduction 166
9.3.2 Occurrence of Mn-rich horizons 167
9.3.3 Manganese oxide/oxyhydroxide minerals 167
9.3.4 Accumulation of manganese oxides and oxyhydroxides 176
9.3.5 Major and trace elements characteristics of manganese oxides/oxyhydroxides 177
9.3.5.1 Gold concentration in Mn-rich regolith 178
9.3.5.2 Minor and trace element characteristics 185
9.3.6 Groundwater and Mn-rich regolith 188
9.3.7 Summary and conclusions 193
9.4 Element association and dispersion in Fe-enriched regolith 193
9.4.1 Introduction 193
9.4.2 Iron oxide/oxyhydroxide minerals 194
9.4.3 Trace element characteristics of Fe-enriched regolith 198
9.4.3.1 Gold in Fe-enriched regolith 198
9.4.3.2 Zinc, copper and lead associated with Fe oxides/ oxyhydroxides 201
9.4.4 Summary and conclusions 207
10. Chapter ten: Conclusions and recommendations 208
10.1 Anomaly, background and element associations 209
10.2 Groundwater chemistry and hydrogeology 209
10.3 Sedimentary weathering processes and source composition 210
10.4 Element dispersion in calcrete- manganese- iron –dominant regolith 211
10.5 Recommendations for further work 212

References 215

Appendices 245

LIST OF FIGURES

Figure 2.1 Location map of study area in western NSW. 6

Figure 2.2 Monthly rainfalls in the Cobar area. 7

Figure 2.3 Basic regolith landforms on the Girilambone region. 9

Figure 3.1 Main structural entities in the basement of eastern Australia. 15

Figure 3.2 Provinces of the Lachlan Fold Belt. 16

Figure 3.3 Elements of the early Palaeozoic geology of the Lachlan Fold Belt. 17

Figure 3.4 Cambrian to Middle Devonian development of the Lachlan Fold Belt. 19

Figure 3.5 Interpretive geological map of study area. 22

Figure 3.6 Location map showing drill hole and mineralisation sites in the Sussex area. 29

Figure 3.7 location map showing drill holes and mineralisation sites in the Hermidale area. 31

Figure 3.8 Location map showing drill holes and mineralisation sites in the Byrock area. 33

Figure 5.1 An example of boxplot application. 42

Figure 5.2 Plots showing results of replicate analysis. 48

Figure 5.3 Correlation between duplicate and original element. 49

Figure 6.1. Summary profiles of thickness of transported and *in situ* regolith in the Byrock (A), Sussex (B) and Hermidale (C) areas. 59

Figure 6.2. Distribution pattern of Au anomalies. 64

Figure 6.3. Distribution pattern of Co anomalies. 65

Figure 6.4. Distribution pattern of Cr anomalies. 65

Figure 6.5. Distribution pattern of Cu anomalies. 66

Figure 6.6. Distribution pattern of Mo anomalies. 66

Figure 6.7. Distribution pattern of Ni anomalies. 67

Figure 6.8. Distribution pattern of Pb anomalies. 67

Figure 6.9. Distribution pattern of Sb anomalies. 68

Figure 6.10. Distribution pattern of V anomalies. 68

Figure 6.11. Distribution pattern of W anomalies. 69

Figure 6.12. Distribution pattern of Zn anomalies. 69

Figure 6.13. Anomalies in Cr and Mo for the regolith carbonate facies in the top metre samples from drill holes CBAC191 and CBAC 92. 70

Figure 6.14. Anomalies in the regolith carbonate facies of the transported regolith. 74
Figure 6.15. Anomalies in the Fe-rich facies of the transported regolith. 75

Figure 6.16. Anomalies in the *in situ* clay-silt- gravel facies. 77
Figure 6.17. Anomalies in the regolith carbonate facies of the *in situ* regolith 78
Figure 6.18. Anomalies in the Fe-rich facies of the *in situ* regolith. 79
Figure 6.19. Anomalies in the *in situ* Mn- rich facies. 81
Figure 6.20. Elements cluster dendrograms of the clay-silt-gravel facies of the top metre regolith unit. 82
Figure 6.21. Elements cluster dendrograms of the *in situ* regolith unit 82
Figure 7.1. Geologic map of the Girilambone region showing some known mineralisation sites, drill hole locations 90
Figure 7.2 Digital elevation model of the Byrock area. 91
Figure 7.3 Digital elevation model of the Hermidale area. 92
Figure 7.4 Magnetics imagery of the Byrock area. 92
Figure 7.5 Magnetics imagery of the Hermidale area. 93
Figure 7.6 Lithologic cross-section along the groundwater flow between and CBAC217 and CBAC227. 94
Figure 7.7 Lithologic cross-section showing the water in the northern part of the Hermidale area. 95
Figure 7.8 Lithologic cross-section showing the water table in the southern part of Hermidale area. 95
Figure 7.9 General hydraulic contours (m) in the Byrock area. 96
Figure 7.10 General hydraulic contours (m) in the Hermidale area. 96
Figure 7.11 Eh-pH diagram. 98
Figure 7.12. Piper plots illustrating different types of groundwater. 101
Figure 7.13 Scatterplots of alkalinity vs (Na + K + Ca+Mg). 102
Figure 7.14 Scatterplots of $(Ca^{2+}+Mg^{2+})$ vs $(K^{+}+N^{+})$. 102
Figure 7.15 Scatterplot of Na^{+} vs Cl^{-}. 104
Figure 7.16 Scatterplot of Na/Br vs Cl/Br. 104
Figure 7.17 Scatterplot of Cl^{-} vs $SO4^{2-}$. 105
Figure 7.18 Scatterplot of Ca^{2+} vs $SO4^{2-}$. 105
Figure 7.19 ^{36}Cl /Cl versus chloride for the Byrock groundwater samples. 108

Figure 7.20 ^{36}Cl /Cl versus chloride for the Hermidale groundwater samples. 109
Figure 7.21 Hermidale and Byrock groundwater plotted on apportion of the log (a K^+/H^+) versus log a Mg^{++}/H^+*2 diagram. 110
Figure 7.22 Calculated saturation indices of $ZnSiO_3$ (A), malachite (B), and tenorite (C) in Hermidale groundwaters. 112
Figure 7.23 The Hermidale and Byrock groundwater compositions, mineral stability fields. 114
Figure 7.24 The distribution pattern of Cu and Zn in the groundwater. 115
Figure 7.25 Distribution profiles of Cu and Zn in the regolith of the Byrock drill holes CBAC217, CBAC219 and CBAC248. 115
Figure 7.26 Distribution patterns of EC, SO_4^{2-}, Cl^-, Cu and Zn in groundwater. 116
Figure 8.1 Scattergrams showing correlations between likely immobile elements. 122
Figure 8.2 Scattergrams showing immobility test correlations. 123
Figure 8.3. Scattergram showing correlation between Al_2O_3 and high CaO of base of the hole saprolith samples. 124
Figure 8.4. Ternary plots of molecular proportions of Al_2O_3- (Na_2O+CaO*) -K_2O with the Chemical Index of Alteration (CIA). 126
Figure 8.5 Plot of Th/Sc verse Zr/Sc for saprolith sample. 129
Figure 8.6 Al_2O_3/SiO_2 -100TiO_2/Zr diagram for saprolith samples. 130
Figure 8.7 Ternary plot of 15Al_2O_3-300TiO_2-Zr. 131
Figure 8.8 An idealized weathering profile developed on granitic bedrock. 133
Figure 8.9 A-CN-K diagram shows the weathering zones. 134
Figure 8.10 Scattergram of 30TiO_2/Al_2O_3 and Ce. 136
Figure 8.11 Scattergram of 30TiO_2/Al_2O_3 and La. 137
Figure 8.12 Ti/Th - Ce/La diagram of saprolith materials. 137
Figure 8.13 CIA – $(Ce/La)_N$ diagram of saprolith materials. 138
Figure 9.1 Classification of calcrete by hydrological setting. 143
Figure 9.2 Distribution of calcrete and associated soils in Australia. 144
Figure 9.3 Examples of calcrete from the Girilambone region. 146
Figure 9.4 Drill hole plots showing distribution of calcrete-bearing zones in the transported regolith of the Byrock area. 147
Figure 9.5 Drill hole plots showing distribution of calcrete-bearing zones in the transported regolith of the Hermidale area. 148

Figure 9.6 Drill hole plots showing distribution of calcrete-bearing zones in the transported regolith of the Sussex area. 149
Figure 9.7 Drill hole plots showing distribution of calcrete-bearing zones in the *in situ* regolith of the Byrock area. 150
Figure 9.8 Drill hole plots showing distribution of calcrete-bearing zones in the *in situ* regolith of the Hermidale area. 151
Figure 9.9 Drill hole plots showing distribution of calcrete-bearing zones in the *in situ* regolith of the Sussex area. 152
Figure 9.10 Triangular (MgO-CaO-Al_2O_3) compositional diagram of the transported and in-situ regolith. 153
Figure 9.11 Bivariate MgO-CaO diagram of the transported calcrete–bearing Regolith. 153
Figure 9.12 Bivariate MgO-CaO diagram of the *in situ* calcrete-bearing. 154
Figure 9.13 Scattergrams of major components in the regolith carbonate zones. 155
Figure 9.14 Distributions of Au, Bi, CaO, MgO and total Fe_2O_3 (wt %) within *in situ* regolith in drill hole CBAC2. 156
Figure 9.15 Distributions of Au, W, CaO, MgO and Fe_2O_3 (total) in drill hole CBAC188. 157
Figure 9.16 Distributions of Au, CaO, MgO and Fe_2O_3 (total) within *in situ* regolith in drill hole CBAC41. 158
Figure 9.17 Distributions of Au (ppm), CaO, MgO and total Fe_2O_3 (wt %) within *in situ* regolith in drill hole CBAC204. 158
Figure 9.18 Distribution of Au (ppm), CaO, MgO and total Fe_2O_3 (wt %) within transported regolith in drill holes CBAC78 and CBAC159. 159
Figure 9.19 Scattergrams showing correlation of detectable Ag with major elements. 160
Figure 9.20 Distribution profile showing the relationships between Fe_2O_3, MnO, MgO, CaO (wt %), Ag, As, Au and Mo (ppm) in drill hole CBAC188. 161
Figure 9.21 Arsenic distribution profiles and the relationships between As (ppm) and MgO, CaO, Fe_2O_3, MnO (wt %), in drill holes CBAC13, CBAC159 and CBAC184 . 163
Figure 9.22 Scattergrams showing correlations between Sr and Ba and other elements in the regolith carbonates. 164

Figure 9.23 Showing distributions of Sr ppm, Ba ppm, S wt %, CaO wt % and MgO wt % in drill hole CBAC213. 165
Figure 9.24 Drill hole plots showing distribution of Mn-enriched zones in the *in situ* regolith. 168
Figure 9.25 SEM photomicrograph showing large flakes of mica (muscovite) and microcrystalline Mn oxides (cryptomelane). 170
Figure 9.26 EDXA spectra showing the chemical compositions. 171
Figure 9.27 SEM photomicrograph showing a quartz crystal and microcrystalline Mn oxides. 172
Figure 9.28 EDXA spectrum showing the chemical compositions. 172
Figure 9.29 SEM photomicrograph showing microcrystalline Mn oxides clustered between clay crystals. 173
Figure 9.30 EDXA spectrum showing the chemical compositions. 173
Figure 9.31 SEM photomicrograph showing well-developed Mn(lithiophorite) crystals forming sheaves in voids, mica crystals. 174
Figure 9.32 EDXA spectrum showing the chemical compositions. 175
Figure 8.33 EDXA spectrum showing the chemical compositions of microcrystalline Mn oxides (pyrolusite). 175
Figure 9.34 Mineral sequences in the weathering of Mn-bearing silicates. 176
Figure 9.35 Distribution profile of Mn (wt %) and Mn-minerals in drill holes CBAC176, CBAC177 and CBAC180. 178
Figure 9.36 Scattergrams of major elements in the Mn-dominant regolith. 179
Figure 9.37 Scattergrams of trace elements in the Mn-enriched regolith. 180
Figure 9.38 Distribution profiles in the Mn-dominant horizon of CBAC119. 182
Figure 9.39 Distribution profiles in the Mn-dominant horizon of CBAC191. 182
Figure 9.40 Distribution profiles in the Mn-dominant horizon of CBAC195. 183
Figure 9.41 Distribution profiles in the Mn-dominant horizon of CBAC198. 183
Figure 9.42 Distribution profiles in the Mn-dominant horizon of CBAC201. 184
Figure 9.43 Distribution profiles in the Mn-dominant horizon of CBAC211. 185
Figure 9.44 Scattergrams showing the correlation between Mn and Ba, Co, Cr, Pb, Ni and Zn. 187
Figure 9.45 Distribution patterns in the Mn-dominant regolith of CBAC122, CBAC177, CBAC198, and CBAC211. 188

Figure 9.46 A cross section showing the Mn-rich zone and watertable along the flow path of the groundwater. 190
Figure 9.47 Distribution patterns in the Mn-rich regolith of CBAC173. 191
Figure 9.48 Distribution patterns in the Mn-rich regolith of CBAC181. 191
Figure 9.49 Distribution patterns in the Mn-rich regolith of CBAC185. 192
Figure 9.50 Distribution patterns in the Mn-rich regolith of CBAC182. 192
Figure 9.51 Plan showing the location of drill holes with observed Fe-enriched zones in the regolith from the Sussex area. 195
Figure 9.52 Plan showing the location of drill holes with observed Fe-enriched zones in the regolith from the Hermidale area. 196
Figure 9.53 Plan showing the location of drill holes with observed Fe-enriched zones in the regolith from the Byrock area. 197
Figure 9.54 Scattergrams of trace elements in the Fe-enriched regolith. 199
Figure 9.55 Distribution profiles in the Fe- dominant horizons of CBAC103. 200
Figure 9.56 Distribution profiles in the Fe- dominant horizons of CBAC204. 200
Figure 9.57 Distribution profiles in the Fe- dominant horizons of CBAC27. 202
Figure 9.58 Distribution profiles in the Fe- dominant horizons of CBAC246. 202
Figure 9.59 Distribution profiles in the Fe- dominant horizons of CBAC243. 203
Figure 9.60 Distribution profiles in the Fe- dominant horizons of CBAC200. 204
Figure 9.61 Distribution profiles in the Fe- dominant horizons of CBAC205. 205
Figure 9.62 Distribution profiles in the Fe- dominant horizons of CBAC218. 206
Figure 9.63 Distribution profiles in the Fe- dominant horizons of CBAC224. 206

LIST OF TABLES

Table 5.1. Standard deviation (s), mean ($\bar{y}$), coefficient of variation (CV) and precision (P) of five replicate samples from CBAC150, Hermidale area. 47

Table 5.2 Types of distance measures. 52

Table 6.1. Threshold values of elements estimated by Median+2MAD and Boxplot methods for clay-silt-gravel, regolith carbonate, Fe-rich and Mn-rich facies of the top metre, transported and *in situ* regolith units in the Girilambone region. 62

Table 6.2 Anomalies of As, Au, Co, Cr, Cu, Ni, Pb, V, and Zn from the transported clay-silt-gravel facies of the Sussex and Hermidale areas. 72

Table 6.3 Anomalies of Co, Cr, Mo, Ni, Pb and V from the transported clay-silt-gravel facies of the Byrock area. 73

Table 6.4 The rotated factor matrices with loading of elements on each component of the principle component analysis. 84

Table 6.5 The rotated factor matrices with loading of elements on each component of the principle component analysis. 85

Table 6.6 Elemental groups as are suggested by cluster analysis (CA) and principal component analyses (PCA) from the top metre, transported and *in situ* regolith facies. 86

Table 7.1 Sample depth, Electrical conductivity (EC), pH, Eh, temperature and alkalinity of the groundwater samples from the Byrock and Hermidale areas. 98

Table 7.2 ^{36}Cl determinations for the Byrock and Hermidale groundwaters. 108

Table 9.1 Morphological classification of calcrete. 142

Table 9.2 Chemical compositions of the common Mn oxide minerals 170

1. CHAPTER ONE: INTRODUCTION

1.1 PREAMBLE

During the last decade there has been an increasing interest in the regolith and the tectonic, climatic and surface processes that control it. Large areas of the Earth are characterised by thick regolith cover. These areas are mainly located within the tropical to sub-tropical zone (between latitudes 40° north and south). Most of Australia's surface is distinguished by low relief and this, together with its location in mid to low latitude (11°-43°), has affected the types of landform and the manner of landscape development. As the search for buried ore deposits continues throughout Australia (e.g., Butt, 1998; Morris *et al.*, 2003; Cameron *et al.*, 2004; Tonuie *et al.*, 2003) and the world (e.g., Kauranne *et al.*, 1992; Roy *et al.*, 2004), the use of regolith geochemistry will continue to play an important role in mineral exploration. The use of geochemistry in mineral exploration has progressed from evaluating local targets using weathered bedrock recovered by auger or aircore drilling to reconnaissance mode exploration, where targets are defined over prospective stratigraphic and structural features (Cohen *et al.*, 1996). In Australia, exploration is focussed on regolith geochemistry as a tool, particularly in areas of deep *in situ* and transported regolith cover (e.g., Butt *et al.*, 2005). Proper application of regolith multi element geochemistry as well as specific sampling media in regolith-dominated terrains has led to the discovery of buried ore deposits (Butt and Zeegers, 1989). The geochemical behaviour, dispersion and accumulation of elements in the regolith results from interaction between parent rock that may host mineralisation, weathering processes and groundwater that disperse and /or accumulate target and pathfinder elements (e.g., Taylor and Eggleton, 2001).

The hydrogeochemistry of groundwater has been used in Australia as a tool to understand the origins of dryland salinity (e.g. Cartwright *et al.*, 2004) and to assist mineral exploration under cover. For example a regional study of groundwater chemistry has been conducted within the Carpentaria and Eromanga Basins, NW Queensland, where the underlying basement rocks belong to the Georgetown and Mt Isa inliers (Giblin 1996b; 2001). A detailed hydrogeochemical study was also performed at the undisturbed Halfmile Lake and Restigouche Zn-Pb deposits in New Brunswick (Leybourne *et al.*, 2002). Both these studies showed a significant

relationship between groundwater chemistry and mineralisation. Whitford *et al.* (1998) detected mineralisation by groundwater geochemistry at the Abra deposit in Western Australia, from both major and trace elements, and isotope signatures of S, Pb and Sr. However, the variability of factors that control behaviour and dispersion of elements through water-rock interactions can limit groundwater as a sampling medium Carr *et al.* (1999). The interpretation of uranium ore-mineral equilibrium calculations in groundwater was used to assist uranium exploration in South Australia (Pirlo and Giblin, 2004). Caritat *et al.* (2003; 2005) used the relative concentration of S, Sr and Pb isotopes as a hydrogeochemical tool to target and suggest new prospective mineralisation sites under cover from the Curnamona province in the Broken Hill area.

This study examines the nature of regolith-related chemical dispersion in part of the Girilambone landscape dominated by erosion and well developed *in situ* regolith. The area is located in western New South Wales and covers a strip from north of Nymagee to south of Bourke on the Hermidale, Coolabah, Sussex, and Byrock 1: 100 000 map sheets. The scarcity of bedrock outcrops, a thick regolith with deep weathering and extensive transported cover that masking the geology (Chan *et al.*, 2001; 2002; 2004) and the desire by explorationists to be able to conduct geochemical surveys using surficial regolith samples necessitate a need for better understanding of the regolith geochemistry of this poorly known and explored region. Exploration in this region has been hindered by a number of factors. These include multiple deformations and metamorphism of bedrocks and the style and geometry of ore deposits (McQueen, 2004a). The regolith is very old and complete and for geochemical exploration it is essential to understand the controls on element dispersion in the regolith, regional associations, backgrounds and anomalies of elements and the influence of weathering processes, bedrock geology and groundwater on element associations.

Between 2001 and 2004 a major drilling program was conducted in this region by the Cooperative Research Centre for Landscape Environments and Mineral Exploration (CRC LEME) and the New South Wales Department of Mineral Resources (now Department of Primary Industry (DPI)). This drilling program provided a significant amount of data including chemical analysis, which facilitated this study.

1.2 AIMS AND APPROACHES OF THE STUDY

This study investigates using regolith materials (top metre, transported and *in situ*) in the Girilambone region, in addition to groundwater, as sampling media, to understand element dispersion patterns and the formation of secondary geochemical haloes. The outcomes may provide confidence in vectoring towards possible mineralisation in this region. The research also aims to estimate background levels of target and pathfinder elements in the regolith. The aims of the study can be summarised as follows:

- to develop improved geochemical exploration strategies through a better understanding of multi-element geochemical associations, anomalies and backgrounds;
- to identify processes of weathering, transportation and dispersion of elements in the unmineralised and weakly mineralised regolith of the Hermidale- Sussex- Byrock region;
- to understand the behaviour of potential target and pathfinder elements during weathering processes, and particularly the controls on Au, Cu, Zn and Pb dispersion and concentration in carbonate, iron and manganese-enriched regolith and variably weathered background settings;
- to use groundwater chemistry to identify weathering water-rock interaction processes, and target concealed mineralisation;
- to identify the parent materials of the regolith in the region; and
- to appraise the composite geochemical sampling media available in the region and to make suggestions to assist mineral exploration in the region and elsewhere.

The approach taken has been to:

- examine the distribution pattern, local and regional background levels, and thresholds for a range of target and pathfinder elements;
- identify geochemical associations and special lateral and vertical distribution patterns of certain elements by using cluster analysis;
- examine and identify secondary minerals by visual and petrographic examination, testing with hydrochloric acid, X-Ray Diffraction (XRD), Scanning Electron Microscope (SEM) and Energy Dispersive X-ray Analysis (EDXA);
- analyse groundwater at selected sites by Inductively Coupled Plasma –Optical Emission Spectrometry (ICP OES) and radioisotope chlorine-36 measurements; and

- recognise the geochemical signatures of bedrock samples from the base of drill holes by using immobile major and trace element ratios measured by X- Ray Fluorescence (XRF) spectroscopy analysis.

1.3 THESIS OUTLINE

The thesis is organised as follows:

- The current chapter is an introduction to the study outlining the aims and approaches;

- Chapter Two introduces the regional and site characteristics of the study area including climate, vegetation, landuse, regolith landforms and previous work on the geochemistry and regolith in the Girilambone region.

- Chapter Three summarises the geology and metallogeny of the region, and describes previous geochemical investigations in the region;

- Chapter Four describes sampling methodology.

- Chapter Five describes the methods of data manipulation, quality control, basic and multivariate statical techniques that were employed in the study.

- Chapter Six includes a detailed geochemical investigation, using cluster and principal component analyses, to determine the characteristic geochemical associations of the studied regolith units (top metre, transported, *in situ*) and to identify background, and anomalous levels for elements in the region;

- Chapter Seven describes the types of groundwater samples, and the processes that control the nature of the groundwaters, (e.g., evaporation and mixing), investigates the rock-water interactions, and estimates the relative ages using ^{36}Cl measurements;

- Chapter Eight presents a method for identifying the geochemical signatures of underlying bedrock in partially weathered bottom of hole samples.

- Chapter Nine includes a description of the weathering profiles, element associations in the secondary calcrete-, iron- and manganese- enriched regolith zones; and

- Chapter Ten presents the conclusions and recommendations of the study.

2. CHAPTER TWO: REGIONAL AND SITE CHARACTERISTICS

2.1 LOCATION OF STUDY AREA

The Girilambone region is located in western New South Wales, approximately 700 km north west of Sydney. The area covers a strip from north of Nymagee to south of Bourke; including the Hermidale, Coolabah, Sussex, and Byrock1: 100 000 map sheets, within the latitudes 30° 30` to 32° 00` south and longitude 146° 00` to 147° 00` east (Figure 2.1).

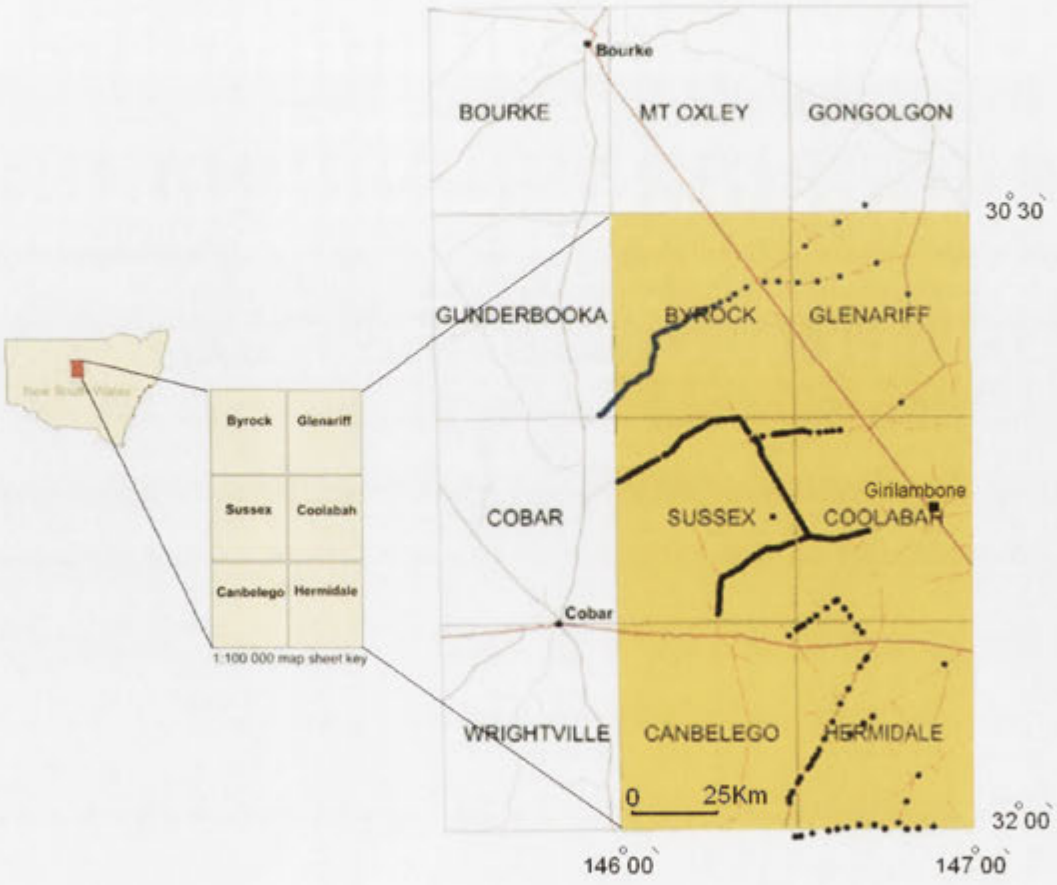

Figure 2.1 Location map of study area in western NSW. Large map shows 1:100,000 sheet areas and sampled drill hole sites along road traverses.

2.2 CLIMATE, VEGETATION AND LANDUSE

The study area has a sub-arid climate. Average monthly maximum temperatures range from 13 °C to 20 °C in winter to between 28 °C to 39 °C in summer. Average monthly minimum temperatures range from 2 °C to 8 °C in winter to 14 °C to 24 °C in summer. The humidity is low. During the summer the average relative humidity is about 30 % in the afternoon and about 50 % at 9 am. In winter it is about 45 % at 3 pm, whilst it is about 75 % at 9 am. On average, rainfall tends to be uniformly distributed throughout the year, with a median annual rainfall for Cobar of 390 mm (Australian Bureau of Meteorology). Figure 2.2 shows the monthly rainfall in the Cobar area.

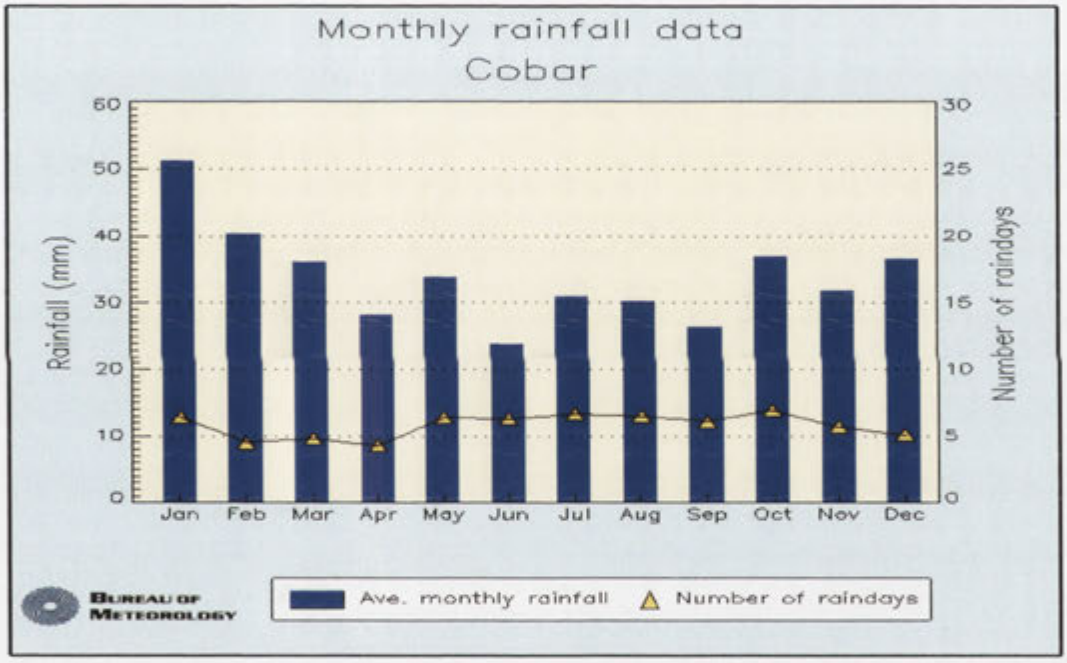

Figure 2.2 Monthly rainfalls in the Cobar area. (from Australian Bureau of Meteorology).

Livestock grazing is the main agricultural enterprise (Tate, 2003). Wheat is the predominant crop further to the south of Cobar, but cropping is limited in the Girilambone-Cobar region due to the low nutrient content of the soils and poor annual rainfall (Cunningham *et al.*, 1981). Mining is also a major industry within the region where Au, Cu, Zn and Pb are mined (e.g., Stegman and Stegman, 1996).

The Girilambone region is host to many species of grasses, shrubs and trees, which can be used as surrogates for identification of different regolith and landforms. Belah and River Oak are noticed in large well-developed stands in or close to the drainage channels, whereas White Cypress Pine are commonly found growing in coarse textured red and brown earth (Munro, 2003), occasionally associated with streams, and shallow soils well up the slopes of hills. Small communities of Black Cypress Pine are present on hills and stony ridges, commonly associated with Kurrajong, Mugga Ironbark and Green Mallee communities (Cunningham *et al.*, 1981). Extensive areas of Mulga have developed to form an almost impassable scrub.

2.3 REGOLITH LANDFORMS

The Girilambone region lies within the Cobar Pediplain. This Pediplain is largely underlain by outcrop and subcrop of the Cambro-Ordovician Girilambone Group, the Early to Middle Devonian Cobar Supergroup and the Middle to Late Devonian Mulga Down Group (Glen, 1994). The pediplain is characterised by gently undulating hills averaging 250 metres above sea level, with a few isolated peaks and ranges rising to 100 metres above this level (Leah, 1996). The Pediplain is bounded by sedimentary sequences associated with the Neogene Murray Basin and the Quaternary Darling, Bogan and Lachlan River system (Gilligan and Byrnes, 1995).

Most of the study area is covered by colluvial and alluvial sediments with small areas of weathered bedrock rises (9-30 m relief). In the Hermidale (particularly in the southwestern part) and Sussex areas there are some low hills (30-90 m relief), and in the Byrock area more extensive highly weathered bedrock rises. A few small volcanic plateaux of slightly weathered leucitite basalt occur in the Sussex and Byrock areas (Chan *et al.*, 2001; 2004; Glanville *et al.*, 2003). Colluvial sheetwash sediments on rises dominate in the Sussex area, whereas colluvial sheetwash sediments on erosional plains and depositional plains dominate in the Hermidale area (Chan *et al.*, 2001; 2002; 2004). Regolith landform units were used in the compilation of the Girilambone 1:100,000 regolith-landform map (Figure 2.3). *In situ* saprolite and saprock and transported components are distinguished according to the degree of weathering of weatherable

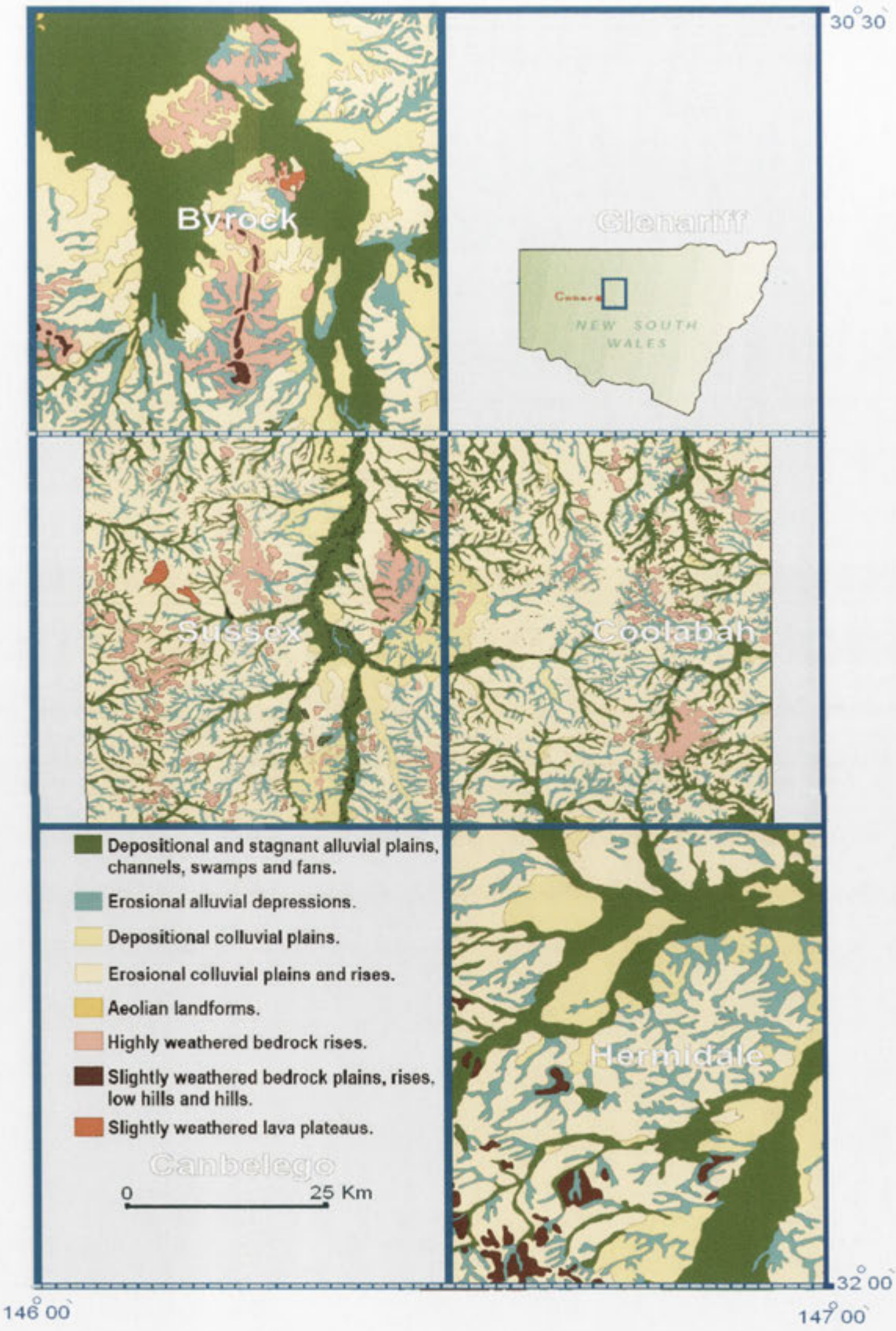

Figure 2.3 Basic regolith landforms on the Girilambone region. Named sheets are 1:100,000 sheets (source CRC LEME and NSW DPI Girilambone-Cobar project).

minerals as well as clay mineral assemblages. Generally the transported regolith consists of clay and minor quartz silt-sand-gravel sediments, whereas the *in situ* regolith consists of a variety of sandstone/siltstone to metasandstone/siltstone, claystone to shale/phyllite (micaceous in places), and silty claystone/ phyllite (Chan *et al.*, 2001; 2002; 2004).

2.4 PREVIOUS WORK ON THE GEOCHEMISTRY AND REGOLITH IN THE GIRILAMBONE REGION

In the Girilambone region, the Cobar area has been a major focus for geological investigation and modern mineral exploration, particularly for gold, since the mid-1980s (Stegman and Stegman, 1996). Earlier, Andrews (1915) and Rayner (1961) studied the stratigraphy, structure and tectonic history of the Cobar region and described the Cobar copper and gold deposits with detailed investigation of the geology, ore deposits and operating mines. Other previous geological investigations in the Byrock area (e.g., Hall, Ralph &Associates, 1969; Eastmet Minerals N.L., 1970) concluded that the dominant outcrops in the area belong to the Girilambone Group (Ordovician) and also noted that no economic mineralisation had been reported, except an abandoned copper prospect to the north and a gold lode to the west. The regional geology and mineralisation of the Cobar region and study area are discussed in Chapter 3.

Geochemical dispersion and associated depletion haloes in fresh rocks and regolith surrounding orebodies have been investigated in numerous studies at selected mineralised sites including at the Elura and CSA mines in the Cobar area. These studies employed different analytical techniques and sample media (Cohen *et al.*, 1996). However, the present review only covers previous work concerned with using chemical analysis of regolith and/or groundwater (as sampling medium) to target mineralisation sites in the region.

The principles and mechanisms of geochemical dispersion, weathering, landscape development, formation of regolith and anomalies have been discussed in different geochemical exploration models (e.g. Butt, 1987; Butt and Zeegers, 1989; Taylor and Butt 1998; Butt *et al.*, 2000). Leah (1996) classified the weathering profiles in the Cobar district into relict lateritic profiles preserved within deeply weathered Palaeozoic

bedrock terranes with partial oxidation ranging in depth between 80 and 100 metres with ferruginous lag morphologies resting on the weathered bedrock and reworked ferruginous regolith materials within overlying alluvium. Rutherford (2000) considered oxidation (redox processes), which mainly affects the sulfide component and metal species, and hydration of the silicate minerals as the main geochemical processes that control the chemistry of the weathering profile in the Cobar area. Although these processes are important in the formation of the weathered profile and movement of metals, they are controlled by the paleoclimatic and recent climatic regimes (e.g., Campbell and Claridge, 1992).

Secondary dispersion of elements in the Cobar region has been interpreted as a result of paleodrainage channel activity (Taylor *et al.*, 1984), mechanical dispersion of ferricrete from an earlier lateritic weathering profile (Dunlop *et al.*, 1983) and weathering of the sulfides. Studies have shown that Cu and Zn are preferentially concentrated in goethite and that Pb is commonly concentrated in hematite (Scott, 2002). Different techniques and sampling media were employed to understand factors controlling element dispersion in the Cobar region (e.g., Alipour *et al.*, 1995; 1996; 1997; Cohen, *et al.*, 1998; Pwa *et al.*, 1999; Cairns *et al.*, 2001; Khider, 2004; McQueen *et al.*, 2004; Whitbread and Moore, 2004; Khider and McQueen, 2006; McQueen, 2006).

Geochemical dispersion and resulting anomalies in residual and transported regolith along the drainage system near the CSA mine displayed three element associations: Cu - Zn - Mn ± Au ± Pb; the As-Sb ± Au; and the As- Sb-Pb ± Au (Shen *et al.*, 1998). These associations were recorded from deep saprolite, residual regolith and interbedded gravels and silts of paleo-channel deposits respectively. Gold has irregular anomalies correlated with near-surface carbonate accumulation (Hill *et al.* 1998; McQueen *et al.* 1999) and economic Au hosted in the oxidised zones (e.g., McKinnons regolith) without significant base metals (Piang, 1996).

Pwa *et al.* (1999; 2002) showed that in the Cobar region Cu, Zn, Pb, Ni, As, Mo, Ag, Sb, Ba, Bi and W are enriched around mineralisation, and K, Al, Ca, Ti, Ga, Rb, Sr, Zr, Y, V, Na are generally depleted because of feldspar and mica weathering in regolith at selected mineralised sites. Scott *et al.* (1991) related the secondary dispersion of Cu, Zn, and some Au to the fluctuation of water table in the area. However, lack of

chemical analysis of the groundwater made it difficult to understand rock-water interactions along the water table in this region.

Investigation of the behaviour of pathfinder elements in the intensely weathered Cobar terrain by McQueen and Munro (2003) revealed that at the new Cobar Au- Cu deposit there is a progressive change in mineral hosts. Goethite, hematite and cryptomelane and alunite-jarosite minerals were identified as important hosts for Zn- Cu- As, Cu- Pb- Sb and Co-Cu- Ni element groups respectively. Secondary Fe and Mn oxides and oxyhydroxides are major host phases for base metal cations within *in situ* regolith near the Peak in the Cobar area (Cairns *et al.*, 2001). These oxides were developed in a dominantly erosional setting. No clear association was found between gold and any particular secondary mineral. Pathfinder element associations in the Nyngan-Bourke-Nymagee area include an "evaporitic" association of Ca-Mg ± Au, a redox association of Mn-Co-Zn ± Ni – Cu ± Au related to redox boundary accumulations of Mn oxides/oxyhdroxides, a goethite association of Fe-Cu-Zn and a hematite association of Fe-As-Pb ± Sb ± Bi (McQueen, 2004b). These groups of elements were proposed as background associations but the study did not specify or link any of these associations to transported or residual regolith units. Distribution of these elements through the weathering profile around the New Cobar deposits was interpreted as due to the interplay between chemical (hydromorphic) and mechanical dispersions (McQueen *et al.*, 2004). Elements such as Pb, As, Bi, Sb and W showed limited chemical dispersion deeper in the profile but were mechanically dispersed in hematitic lag at the surface.

The association of Au with calcrete in the Girilambone region was studied by Khider and McQueen (2006) and McQueen (2006) These studies have revealed that the presence of carbonate is an indicator of a geochemical environment conducive to precipitation of chemically mobilised gold rather than a direct control on gold fixation by calcrete. The total carbonate content is probably not a significant control on the Au concentration.

The hydrogeology of the Nymagee area was summarised by Menzies (1969) as being controlled by three main rock type settings:

- Thin Quaternary deposits that are unlikely to contain usable water;

- Devonian rocks classified into the Amphitheatre and Mulga Downs Stages. The Amphitheatre Stage is characterised by relatively porous and highly impervious rocks. Many of the latter are quartzites, which are full of joints and cracks that make them capable of holding underground water. The Mulga Downs Stage consists mainly of coarse sandy rocks, which are commonly silicified. Some of these rocks are porous sandstone and many of the quartzite beds are heavily jointed and carry useful supplies of water; and
- Pre-Devonian rocks, which generally contain water with high quantities of salts.

The groundwater chemistry and hydrogeology of the Girilambone region were investigated by Khider (2004) and Khider and McPhail (2005). These studies showed that the aquifer is an unconfined system within the *in situ* regolith areas and consists of phyllitic siltstone - sandstone layers. The groundwater generally flows to the northeast in the Hermidale area and in part of the Byrock area. The groundwater in the region is mainly of chloride type, rich in Na, Cl and SO_4 .The other calcium-bicarbonate and bicarbonate – chloride types are not predominant and the main processes that affected the groundwater composition are evaporation, water –rock and mixing.

3. CHAPTER THREE: REGIONAL GEOLOGY AND MINERALISATION

3.1 REGIONAL SETTING OF SOUTHEASTERN AUSTRALIA

The geological structure of the eastern third of Australia, which includes New South Wales, is summarised by Scheibner (1999) as being composed of three main entities (Figure 3.1):

1. the Palaeo-Proterozoic to Mesozoic Australian Craton to the west of the Tasman Line, which is mostly concealed by platform basins. In places these basins have been deformed into within-plate fold belts (e.g., Adelaide Fold Belt);
2. the Neoproterozoic to Mesozoic Tasman Fold Belt System or Orogenic Zone, which represents an orogenic or active plate margin east of the Tasman Line; and
3. the Late Carboniferous to Cainozoic platform cover of sedimentary and intraplate igneous, dominantly volcanic, rocks.

Most of New South Wales lies in the Tasman Fold Belt System, which consists of five fold belts. The important ones are the Kanmantoo, Lachlan and New England Fold Belts, the last two being separated by the Sydney-Bowen Basin. Small parts of the Thomson and Adelaide Fold Belts occur in the north and the west respectively (Figure 3.1; Scheibner, 1999).

The Girilambone region, the focus of this study, is located in the NW Lachlan Fold Belt (LFB). The LFB has Cambrian to Carboniferous rock assemblages developed over 700 km across strike and subdivided into western, central and eastern subprovinces (Figure 3.2; Gray, 1997; Gray and Foster, 1997; 1998; Foster *et al.*, 1999; Fergusson, 2003; Neef, 2004). The western and central subprovinces include structural evidence of east-directed and west-directed thrusting, respectively (Gray *et al.*, 2002).

Glen (1992,1995) subdivided the LFB based on the distribution of constrained and unconstrained sediment packages (lithotectonic associations) into the Western, Southwestern, Central, and Eastern belts. Early Ordovician turbidites occur across the Lachlan Fold Belt, but in the Late Ordovician, turbidites were restricted to the central part of the Southwestern belt and the western part of the Western belt (Glen,

1992;Vandenberg and Stewart, 1992; Glen, 1995). The study area lies in Glen's 1995's Central belt (Figure 3.3).

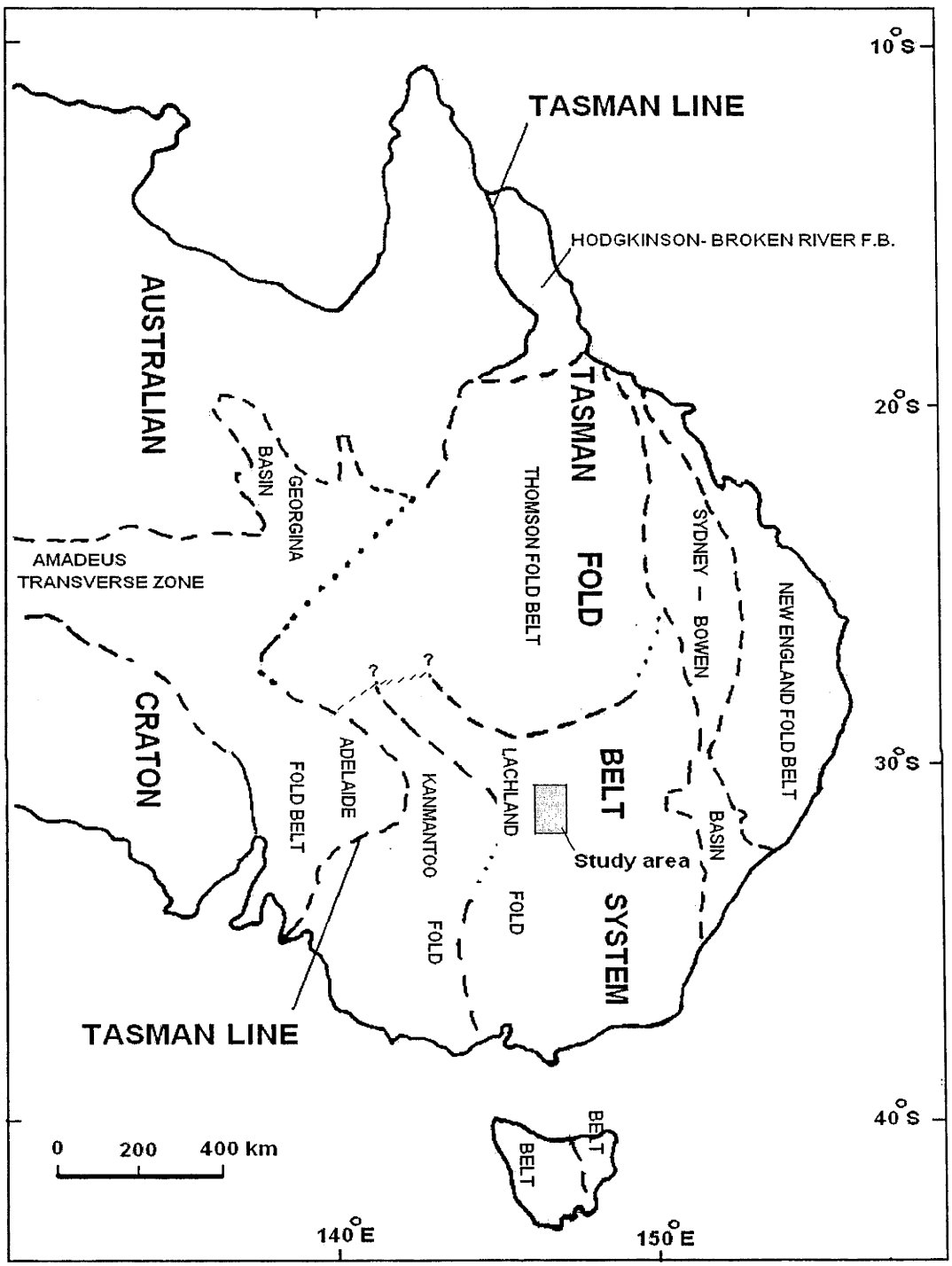

Figure 3.1 Main structural entities in the basement of eastern Australia (from Scheibner, 1999).

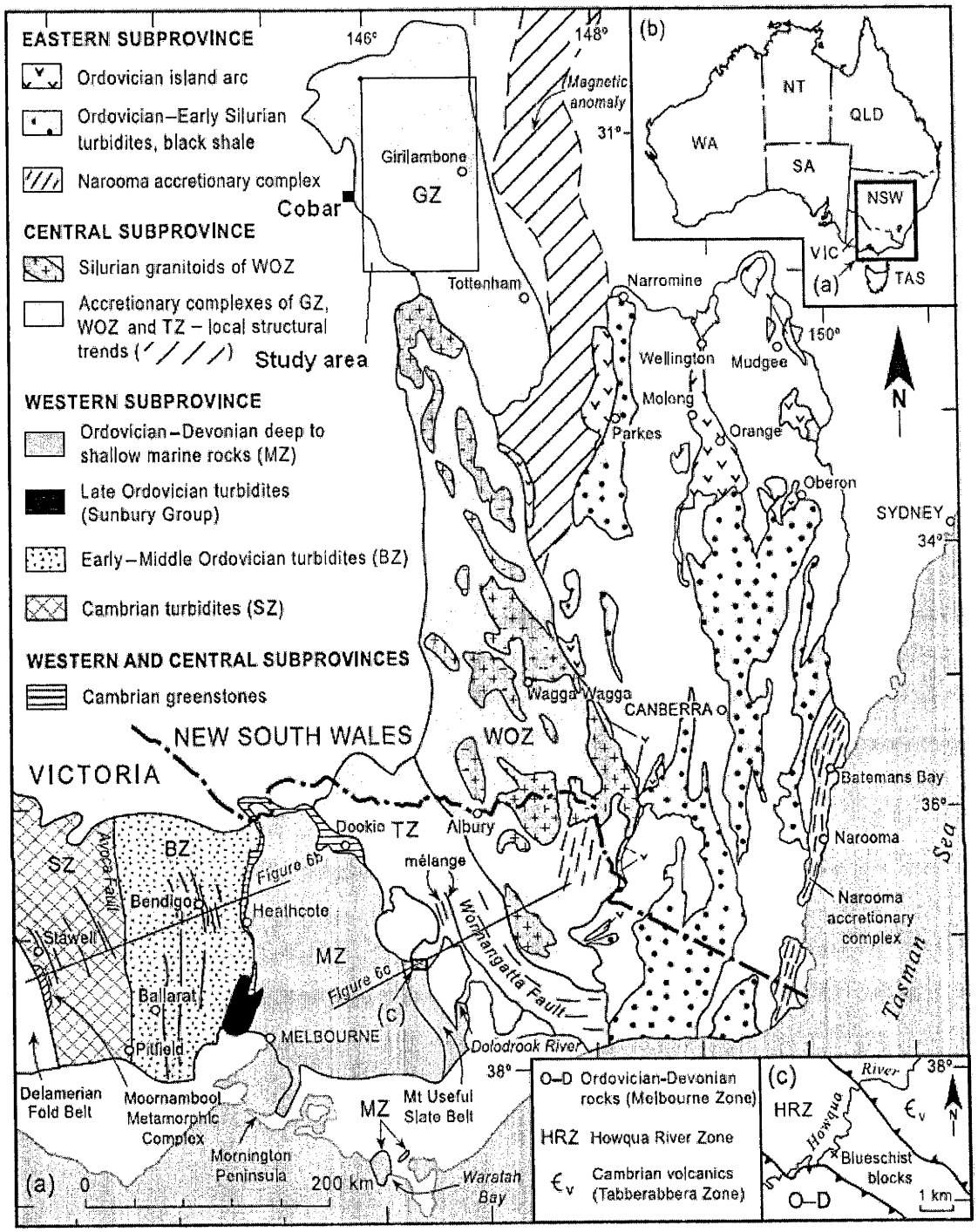

Figure 3.2 Provinces of the Lachlan Fold Belt (from Fergusson, 2003).

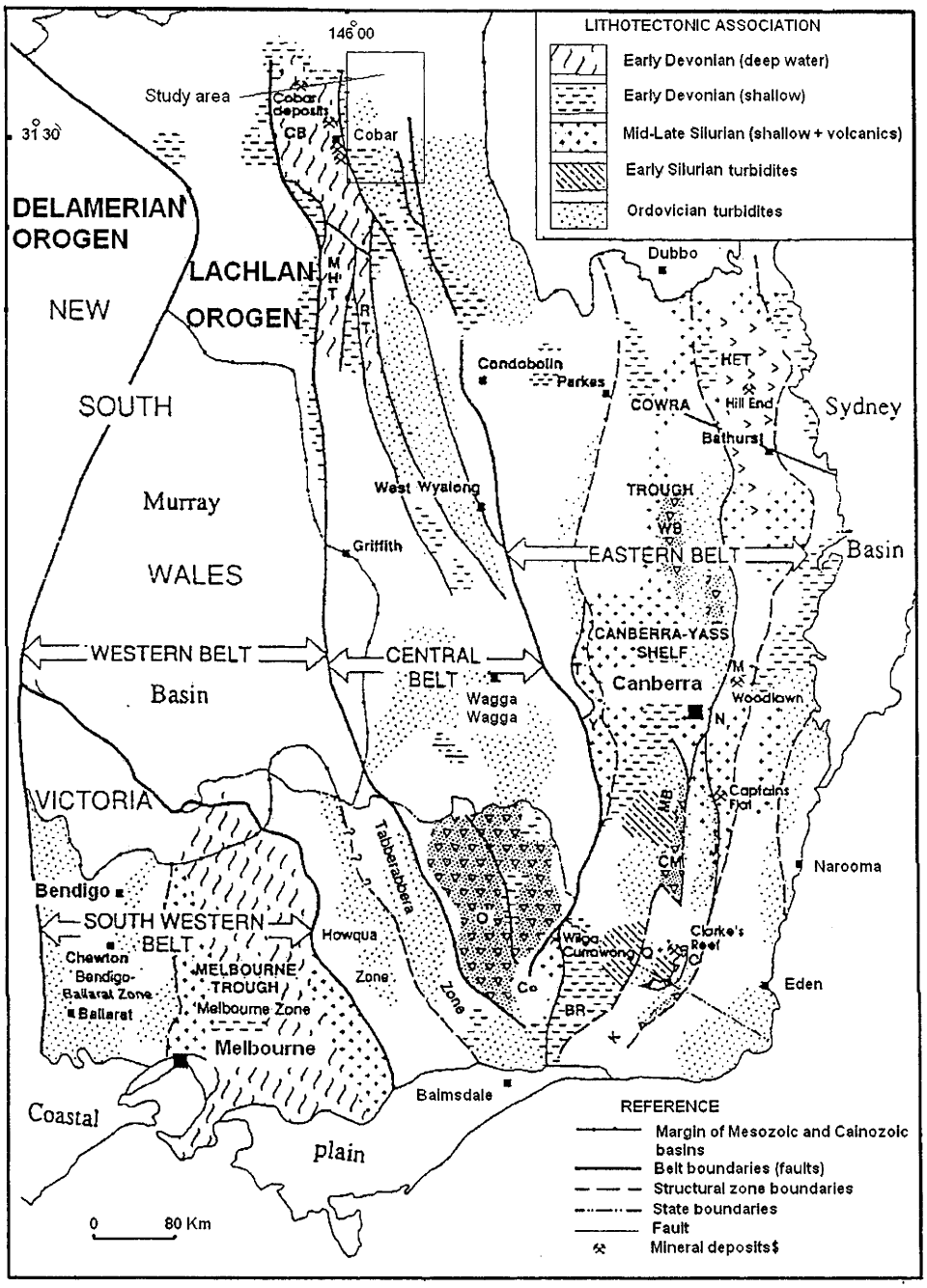

Figure 3.3 Elements of the early Palaeozoic geology of the Lachlan Fold Belt (from Glen, 1995).

3.2 REGIONAL TECTONIC HISTORY

The tectonism that has affected the Girilambone (Bourke-Cobar-Nymagee) region can be considered in five stages:

1. Pre-Devonian tectonism;
2. Regional crustal extension in the Late Silurian to Early Devonian;

3. Late Early Devonian transgressional tectonism;
4. Carboniferous tectonism; and
5. Neotectonism.

1. Pre-Devonian tectonism

The Lachlan Fold Belt in pre-Ordovician time was characterised by an oceanic setting without any deformation in the belt itself, slowly filling in with thick deep-marine turbidite sequences (Fergusson and Coney, 1992). The study area was in the ocean on the continental side of the Molong Volcanic Arc (Byrnes, 1993) and the oldest rocks in the Girilambone region were probably deposited from this time. To the west of this arc, sedimentation of turbiditic basinal sediments (Wagga Marginal Basin) began in the earliest Ordovician (Kilpatrick and Fleming, 1980). To the east was a fore-arc basin (Monaro Slope and Basin; Figure 3.4A).

During the Late Ordovician to Early Silurian the Benambran Orogeny caused strong deformation in the western and central parts of the Lachlan Fold Belt. The Molong Volcanic Arc and its microcontinental basement collided with the fill of its back-arc basin (Wagga Marginal Basin), causing strong deformation and large-scale imbrication of the basinal sequences (Pogson, 1982).

The geochemical and isotopic signatures of rocks from this province indicate their genesis in a subduction- related island-arc setting (Carr *et al.*, 2003). The line of collision is known as the Gilmore Suture (Figure 3.4 C). This structure is oriented approximately north-south and its northern continuation is less well-defined (Scheibner, 1983,1999). It appears to connect with the faults in the Mineral Hill region (Pogson, 1991) and further north it terminates against the east-north-easterly trending Nandewar Lineament (Byrnes, 1993). The deformation, thrust pile-up and consequent tectonic thickening of the Wagga Marginal Basin fill in the high heat flow regime of the back-arc basin (Pogson, 1982) resulted in high-temperature, low-pressure style metamorphism leading to formation of anatectic granites. Some of these granites were emplaced syntectonically, but most are post-tectonic. This orogenic activity formed the Wagga-Omeo Metamorphic Belt (Figure 3.4B; Byrnes, 1993).

2. Regional crustal extension in the Late Silurian to Early Devonian

During the Silurian the Lachlan Fold Belt entered a tensional phase. Early Silurian extension formed new troughs in the eastern half of the Lachlan Fold Belt, followed by localised Late Silurian-Early Devonian deformation during the Bowning-Bindi

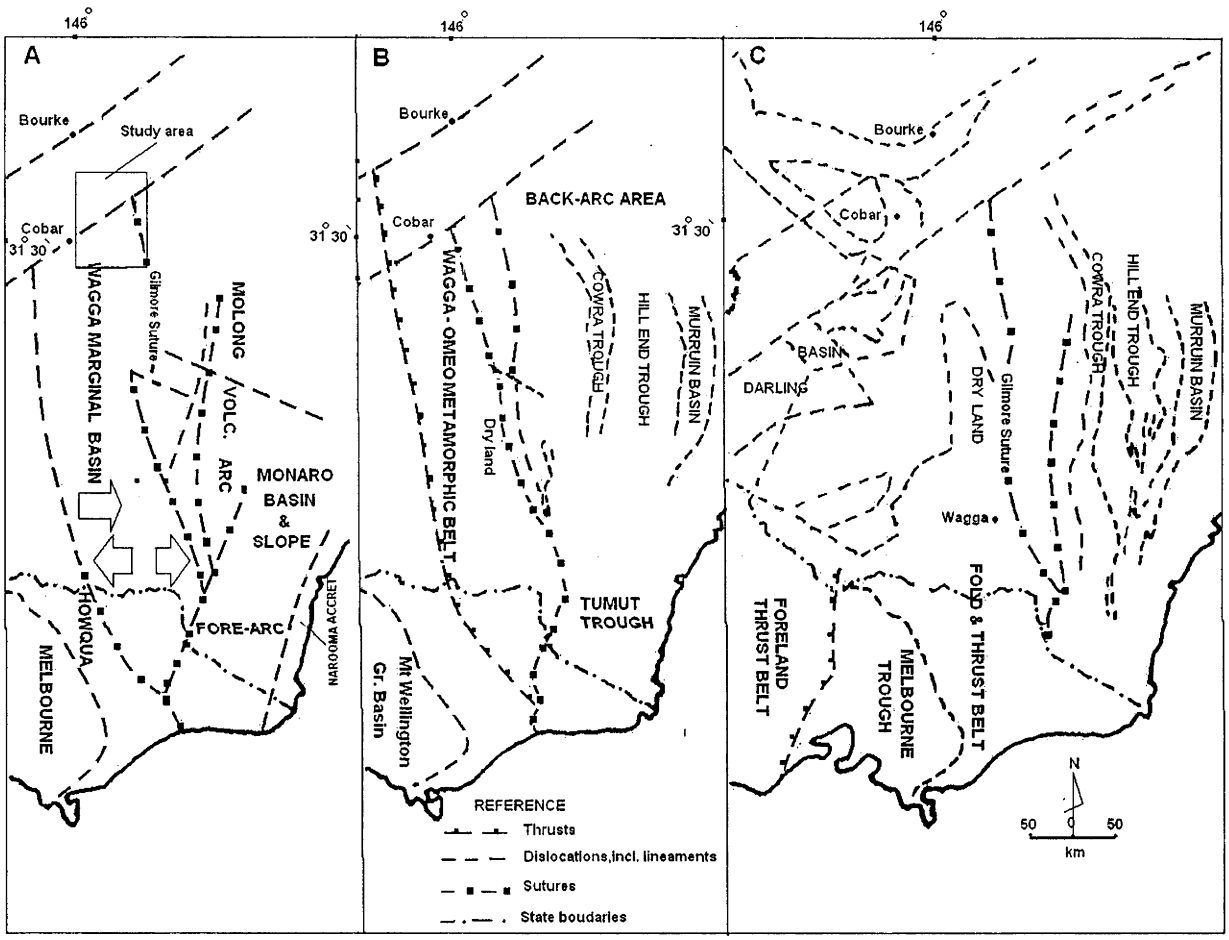

Figure 3.4 Cambrian to Middle Devonian development of the Lachlan Fold Belt (after Byrnes, 1993).

Orogeny (Scheibner, 1999). However, west of the Gilmore Suture, extension facilitated the emplacement, into the upper crust, of anatectic granitoid melts generated during the Benambran tectonism (425-450 Ma). Further, brittle crust extensional tectonism west of the Gilmore Suture in the earliest Devonian resulted in subsidence and the formation of the composite Darling Basin in which the Cobar Supergroup was deposited (Figure 3.4C; Byrnes, 1993).

3. Late Early Devonian transgressional tectonism

The Middle Devonian Tabberabberan Orogeny terminated the pre-cratonic development of the Lachlan Fold Belt. Radiometric dating (Glen *et al.*, 1992) suggests that deformation and metamorphism of the easternmost Darling Basin fill occurred at the close of the Early Devonian (395-400 Ma), as an early expression of the Tabberabberan Orogeny, which affected the Lachlan region in a number of ways (Powell, 1984). Former zones of extension probably suffered severe deformation from this orogeny. It is also possible that former extensional faults became reverse faults and developed into thrusts of thick-skin and thin-skin tectonic styles (Glen, 1988). This deformation was followed by molassic overlap sedimentation, which in the Cobar-Bourke area is represented by the Mulga Downs Group sedimentation in the Barka Basin.

4. Carboniferous tectonism

Kanimblan tectonism in the Carboniferous (335-360 Ma) resulted in relatively mild deformation of the Mulga Downs Group sediments in the Barka Basin and further deformation of the underlying Cobar Supergroup. Deformation of these cover sequences was probably controlled by reactivation of the normal and cross faults (Neef and Bottrill, 2001), which were active during Early Devonian sedimentation. The faults are probably reactivated basement faults (Glen, 1985, 1988). The Kanimblan Orogeny resulted in the formation of large warps and open folds, such as the Gunderbooka Syncline, without developing an axial plane cleavage.

The Kanimblan Orogeny further metamorphosed Lachlan Fold Belt rocks. Post-kinematic granites intruded into the eastern part of the Lachlan Fold Belt. The existence of some granitic intrusions of this age is considered possible in the Bourke-Cobar region, but these intrusions are probably of small volumetric importance by comparison with Siluro-Devonian plutons. Carboniferous low- temperature metamorphic effects further east are best recognised from folded and thrust relicts of the Mulga Downs Group in the Bourke area (Glen *et al.*, 1996). A possible Carboniferous age cannot be excluded for some of the least deformed felsic and andesite intrusives in the Bourke and Cobar sheet areas.

5. Neotectonism

The Kanimblan Orogeny converted the LFB into a neocraton, and subsequent Late Carboniferous-Holocene sedimentation has been of platformal character (Scheibner and Basden, 1996) with some reactivation of the Palaeozoic structural framework during Cainozoic time (Duk-Rodkin *et al.*, 2003).

3.3 LOCAL STRATIGRAPHY AND INTRUSIONS

3.3.1 INTRODUCTION

The main Palaeozoic litho-tectonic units recognised in the study area are: The Older Basement (Cambrian-Late Silurian); Cobar Supergroup (Late Silurian- late Early Devonian); and the Mulga Downs Group (Early to Late Devonian).

The recognised rocks of the Older Basement in the study area are:

1. turbidites, chert and minor basic volcanics of the Girilambone Group;
2. intruded ultramafic and related rocks in the eastern part; and
3. a Silurian volcano- sedimentary sequence.

3.3.2 GIRILAMBONE GROUP

The Girilambone Group, as mapped on the Bourke, Cobar and Nymagee 1: 250,000 sheets (Byrnes, 1993; Suppel and Gilligan, 1993) crops out poorly to the east of Cobar between Nymagee and Bourke (Figure 3.5). The Girilambone Group consists of rhythmically bedded, poorly sorted, fine and coarse-grained quartzose sandstone with subordinate quartzo-feldspathic sandstone, siltstone and chert, together with minor intercalated basic volcanics and minor conglomerate, marl and serpentinite. This group has undergone low- to medium- grade regional metamorphism, ranging from low greenschist to low amphibolite facies (Gilligan and Byrnes, 1995).

The upper part of the Girilambone Group is characterised by a turbidite sequence comprising medium to thickly bedded quartz-rich sandstone interbedded with siltstone, slate, and minor chert beds occurring either as thin layers interbedded with slates or as

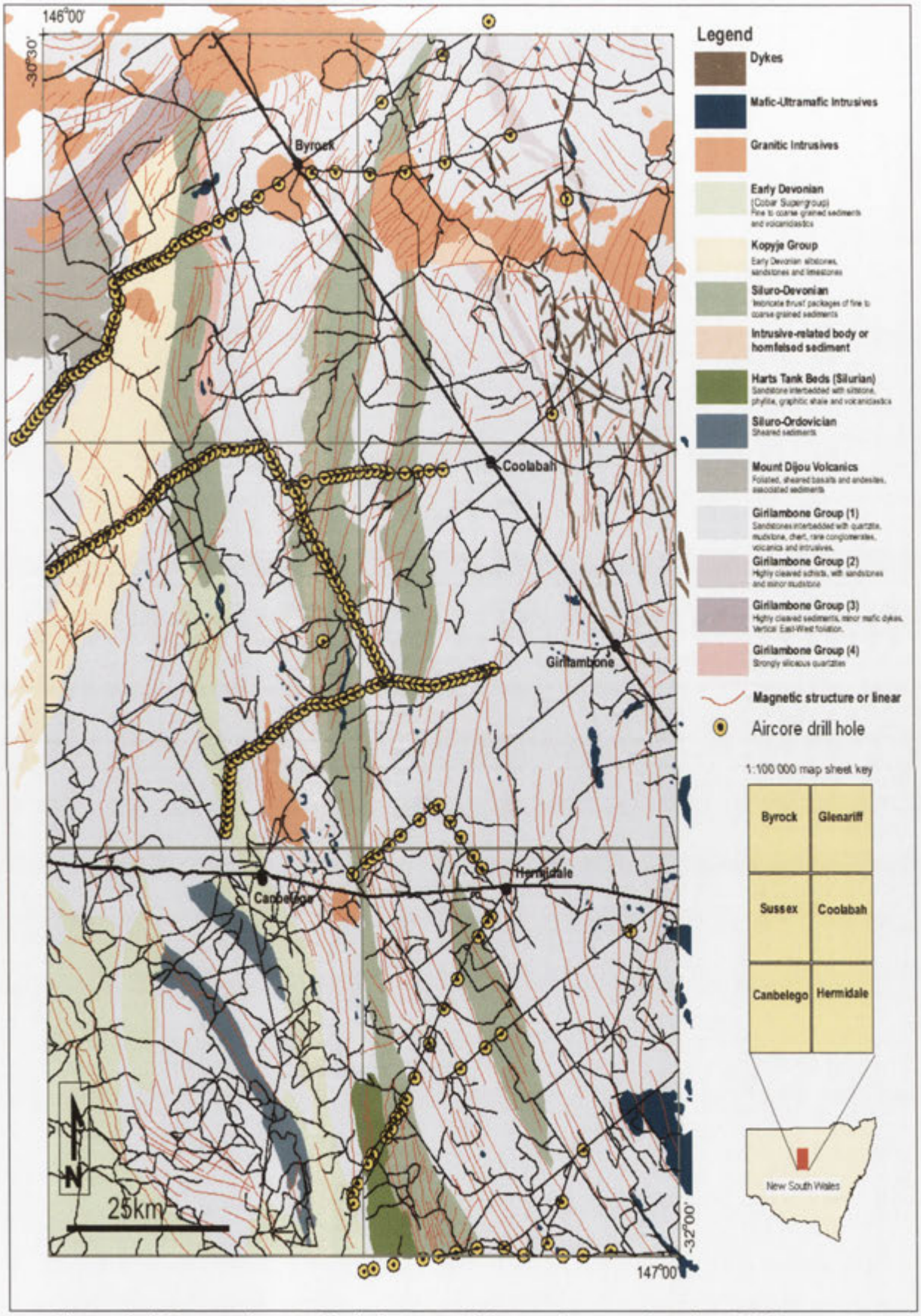

Figure 3.5 Interpretive geological map of the study area showing drilling traverses (after Fleming *et al.*, 2002).

mappable chert zones such as the Alandoon Chert and Whinfell Chert (Pogson, 1991). The turbidites range from clay-rich shales to quartz-rich greywacke. Unmetamorphosed turbidites consist dominantly of clay minerals and quartz. Other minerals, notably feldspar, are present in small amounts (Chappell, 1998). Chemical analysis of turbidites of the Lachlan Fold Belt has shown that these are distinctively low in the elements of typical feldspar (i.e., Na, Ca and Sr; Wyborn and Chappell, 1986). The lower turbidite sequence consists of well-bedded, thin to thick beds of meta-sandstone interbedded with phyllite and schist. Metamorphosed limestone and calc-silicate rocks were reported from Cobar (Rayner, 1969; Brunker, 1970; Feltone 1981) and Bourke (Byrnes, 1993) 1:250,000 sheets. The relationship of these lithological units to the Girilambone Group is uncertain. It is thought that rather than being part of the Girilambone Group, they represent another lithostratigraphic unit (of Silurian or Ordovician age and possible volcanic `arc' affinity), which may have been imbricated with the turbidites (Gilligan and Byrnes, 1995).

The Girilambone Group in the Hermidale, Coolabah and Sussex regions of the Cobar 1:250,000 sheet and the Bobadah-Nymagee 1:250,000 sheets is generally recognised as undifferentiated thick and thin bedded, graded, parallel–laminated and ripple cross-laminated, poorly sorted fine to coarse-grained, micaceous quartz sandstones interbedded with quartzite, minor quartz feldspathic sandstone and thinly bedded chert, quartz-sericite schist, quartz- muscovite- chlorite-biotite-albite-andalusite schist and rare metabasic volcanics (Suppel and Gilligan, 1993). In the Byrock-Glenariff area of the Bourke 1:250,000 sheet, the Girilambone Group is more recognisable as a group of quartzose and quartz lithic sandstone, pelite and chert, minor intercalations of polymictic conglomerate, carbonate-rich rocks, calc silicate homfels and marble, and some magnetite-rich schist (Byrnes, 1993). A minor occurrence of Alandoon Chert has also been recorded from the Hermidale area (Chan *et al.*, 2002).

3.3.3 ULTRAMAFIC AND RELATED ROCKS

Two main types of ultramafic rocks occur in the study area. The Honeybugle Complex consists of hornblende pyroxenite, hornblendite, serpentinite, gabbro, syenodiorite, quartz norite, monzogabbro and monzonite (Byrnes, 1993). This complex trends north-westerly (Gilligan and Byrnes, 1995), and has been recorded from the southeastern

corner of the Hermidale sheet (Chan *et al.*, 2002). Serpentinised ultramafic rocks are recorded at Miandetta on the east edge of the Hermidale sheet (Chan *et al.*, 2002). These rocks are interpreted as the northern extension of the Alaskan type intrusive belt developed to the south (Elliott and Martin, 1991).

3.3.4 SILURIAN VOLCANO- SEDIMENTARY SEQUENCE

A Silurian volcano- sedimentary sequence consisting of felsic volcanics intercalated with a sedimentary sequence forms a poorly known belt of rocks in the vicinity of Harts Tank north of Nymagee (Gilligan and Byrnes, 1995). In the study area the Silurian Harts Tank Beds were recorded at Rainbow Ridge. These beds comprise a complex sequence of fine- grained sandstone, siltstone, phyllite, black graphitic shale, chert, rhyodacitic volcaniclastics and minor related andesitic lavas and tuffs (Pan Australian Mining Ltd, 1986; Chan *et al.*, 2002). The widespread geochemical anomalies associated with this sequence suggest a Silurian igneous association (Gilligan and Byrnes, 1995).

3.3.5 COBAR SUPERGROUP AND RELATED INTRUSIVES

The Cobar Supergroup comprises a sedimentary and volcanic sequence deposited in the Cobar region during the Early Devonian. Sedimentation varied from shallow water shelf deposition of the Kopyje, Mouramba, Winduck and Walter Range shelves to deeper water turbidite deposition represented by the Cobar Basin, Mount Hope, Rast and Melrose Troughs (Glen, 1985). The only group that has been definitely recorded from the study area is the Kopyje Group (Chan *et al.*, 2002).

The Cobar Supergroup overlies older basement rocks with regional unconformity /nonconformity or with a faulted relationship. Minor terrestrial sedimentation is preserved at the base of the sequence in the marginal area of the Cobar Supergroup. Volcanism was mainly submarine but with some subaerial accumulations on shelf areas (Suppel and Gilligan, 1993). The Supergroup was deposited in a fault- controlled basin, and troughs developed as a result of rifting at the beginning of the Early Devonian

(Glen, 1985, 1990). The known margins of the basin and troughs were north-northwesterly to northerly trending basement fractures (Suppel and Gilligan, 1993).

The major volcanic centres related to the Babinda and Majuba Volcanics contain thick accumulations of felsic pyroclastics, consisting largely of ashflow and airfall tuffs with rhyolite and dacite flows and minor tuffaceous siltstone. In the study area the Babinda Volcanics, which form a series of hills, and the Florida Volcanics were recorded from the southwest corner of the Hermidale sheet and east of Canbelego respectively (Chan *et al.*, 2002).

3.4 ECONOMIC GEOLOGY AND STYLES OF MINERALISATION

The central western region of New South Wales is one of the richest mineral provinces in the Lachlan Fold Belt. Mining commenced in the Cobar area when copper was discovered in 1870 in a waterhole at the site of the Great Cobar Copper Mine. Later, the Cobar Mining Field became one of Australia's main sources of copper. Gold mining in the area started soon afterwards at the Great Cobar, the New Occidental, New Cobar, Chesney, Mt Boppy, Mt Drysdale and Peak mines (Stegman and Stegman, 1996). The major deposits occur near Cobar, around Girilambone, Nymagee and Canbelego. Metallogenic maps with the mineral deposit sites have been compiled by Byrnes (1993), Suppel and Gilligan (1993) and Gilligan and Byrnes (1995). The major mineralisation styles of the region were summarised by Chan *et al.* (2001, 2002).

The mineral deposits in the Cobar-Girilambone region can be grouped according to lithostratigraphic host units, unless they are related to granitoids, as follows:

1. Deposits related to the Girilambone Group.
2. Deposits related to the Cobar Supergroup.

3.4.1 DEPOSITS RELATED TO THE GIRILAMBONE GROUP

The Girilambone Group contains strongly deformed sequences with probable juxtapositioning of different crustal blocks and sequences (Glen and Fleming, 2000). Some of the rocks assigned to the Girilambone Group exhibit evidence of multiple deformation. Minor puckering is common and in places chevron kinking is well

developed (Byrnes, 1993). The age of the Girilambone metasedimentary and metavolcanic rocks is thought to be Cambro- Ordovician, but some probable Late Silurian- Early Devonian sedimentary units have probably been infaulted (Chan *et al.*, 2001). The main mineral deposits in the Girilambone terrain are predominantly of copper and gold.

3.4.1.1. GIRILAMBONE

The Girilambone copper deposit is the most significant (124,000 t Cu) deposit of this type. It occurs 5 km west of Girilambone (Figure 3.6) and is hosted by chlorite-sericite schists and the banded quartzite member of the Caro Schist Formation, the basal formation of the Girilambone Group (Shields, 1996). Copper mineralisation at this site occurs mainly as strongly folded layers and bands or lenses of sulfide in quartzite, and as disseminated sulfides within chloritic schists. The occurrence of quartzite as the dominant host rock and the layered style of sulfide mineralisation suggested to early workers that the deposit represents a deformed, stratiform volcanogenic massive sulfide deposit of possibly "Besshi" type. The dominant quartzite host rocks were possibly exhalative chemical sediments (Shields, 1996; Chan *et al.*, 2001). The main primary sulfides are pyrite and chalcopyrite with secondary chalcocite developed in partly oxidised ores. Malachite, azurite, cuprite and native copper occur in the main oxidised zone, while rare phosphate minerals are reported from the upper section of the oxide zone (Shields, 1996). Secondary processes, including economically significant oxidation, supergene enrichment and leaching extend to 65, 45, and 30 metres below the surface respectively (Gilligan and Byrnes, 1995). Alternative ore genesis models suggest that the Girilambone deposit is a structurally controlled, epigenetic vein and lode system (Chan *et al.*, 2001).

3.4.1.2 TRITTON

The Tritton deposit is located 65 km NW of Nyngan and 20 km SW of the Girilambone mine (Figure 3.6). It is a structurally controlled, sediment-hosted, copper deposit discovered in 1995 (Tritton Resources Ltd, 2003). The deposit is hosted by a part of the Girilambone Group, which consists of pelitic schists, mafic schists, greywackes and quartzites. It does not crop out. The total resource is about 11 million tonnes of 2.8 wt % copper at a 1wt % cut-off (Nord Pacific Ltd, 1998). The deposit comprises two

distinct *en-echelon* lenses of massive, mainly copper sulfide mineralisation, which plunge to the SE. Copper is primarily present as chalcopyrite. Gold occurs various with hematite-impregnated schist, gossans, parent sulphides, copper ore and possibly quartz veins (Fogarty 1996; Register of Australian Mining, 2003/2004).

Mineralisation occurs in three zones, upper, central and lower, which are continuous for up to 450 m in strike length, up to 35 m wide and open at depth below 1000 m (Fogarty, 1998). Mineralisation in the upper zone is hosted by a quartzite unit and occurs approximately 180 m below the present land surface (Fogarty, 2001). Primary mineralisation consists of massive pyrite and chalcopyrite, occurring as pipe-like massive sulfide zones. The lower zone consists of massive and banded pyrite-chalcopyrite lenses in chloritic and semi-pelitic schist immediately overlying carbonated mafic schist. Chlorite, epidote and carbonate alteration assemblages are also common throughout the Tritton deposit, with siderite alteration in the hanging wall closely associated with sulfide mineralisation (Berthelsen, 1998). Unlike the nearby Girilambone deposits, little secondary mineralisation is developed within the weathered profile of the Tritton copper deposits (Ackerman and Chivas, 2004).

3.4.2 DEPOSITS RELATED TO THE COBAR SUPERGROUP

3.4.2.1 CANBELEGO -MOUNT BOPPY

Gold mineralisation occurs near Canbelego (Figure 3.6) as free gold or associated with chalcopyrite or iron-rich sphalerite. The host rocks are laminated quartz-mica schists, phyllite, siliceous breccia, lithic sandstone, calcareous siltstone, and polymictic conglomerate of the Early Devonian (Kopyje Group). The style of mineralisation is quartz-vein stockworks in brecciated host rocks. Gilligan (1982) considered the deposits to be of volcanic exhalative origin associated with local volcanism. The primary ore minerals are sphalerite, galena and pyrite, whereas the main secondary minerals are limonite and hematite.

The major Mt Boppy deposit (14.2 t of produced gold) is hosted by a conglomeratic unit of the Baledmud Formation, near its unconformable boundary with the underlying Girilambone group. The oxidation in the deposits extends to 91 metres and other

secondary processes (supergene enrichment and leaching) are reported to be economically significant (Gilligan and Byrnes, 1995).

3.4.2.2 COBAR –TYPE DEPOSITS

Polymetallic sulfide mineralisation near Cobar occurs in high-strain areas along the eastern side and northern edge of the Cobar Basin (Glen, 1995). The deposits vary in metal type and abundance. Some are dominantly copper deposits, some have silver-lead-zinc lenses in addition to copper, some are gold rich and one (the Elura deposit, north-west of Cobar) is lead-zinc-silver-rich with only minor copper. All these deposits are hosted by folded and cleaved Early Devonian thin-bedded turbidites and lie oblique to the bedding (Glen, 1987).

The CSA deposit, north of Cobar comprises systems of lenses that encompass veins, disseminations and semi-massive to massive Cu-Pb-Zn ores (Giles and Marshall, 2004). Deposits occur as multiple vein and massive sulphide pods and lenses that are typically confined to steeply plunging pipe-like concentrations within the steeply dipping host structures. Consequently, most ore bodies have a small ellipsoidal surface expression and a large down-plunge extension (Stegman and Pocock, 1996). Oxidation extends down to 100 metres below the surface with variable supergene enrichment at the present water table. The structural setting and fluid inclusion data suggest that high temperature hydrothermal ore-bearing fluids migrated along major faults during inversion of the Cobar Basin (Glen, 1987; Sun and Seccombe, 2000; Giles and Marshall, 2004).

3.5 MINERAL DEPOSITS IN THE STUDY AREA

3.5.1 DEPOSITS ASSOCIATED WITH THE GIRILAMBONE GROUP

Many minor mineral deposits and occurrences were described in the study area by Byrnes (1993), Suppel and Gilligan (1993) and Gilligan and Byrnes (1995). The following deposits are geographically closest to study sites within the Hermidale, Sussex, Coolabah and Byrock 1:100,000 sheet areas.

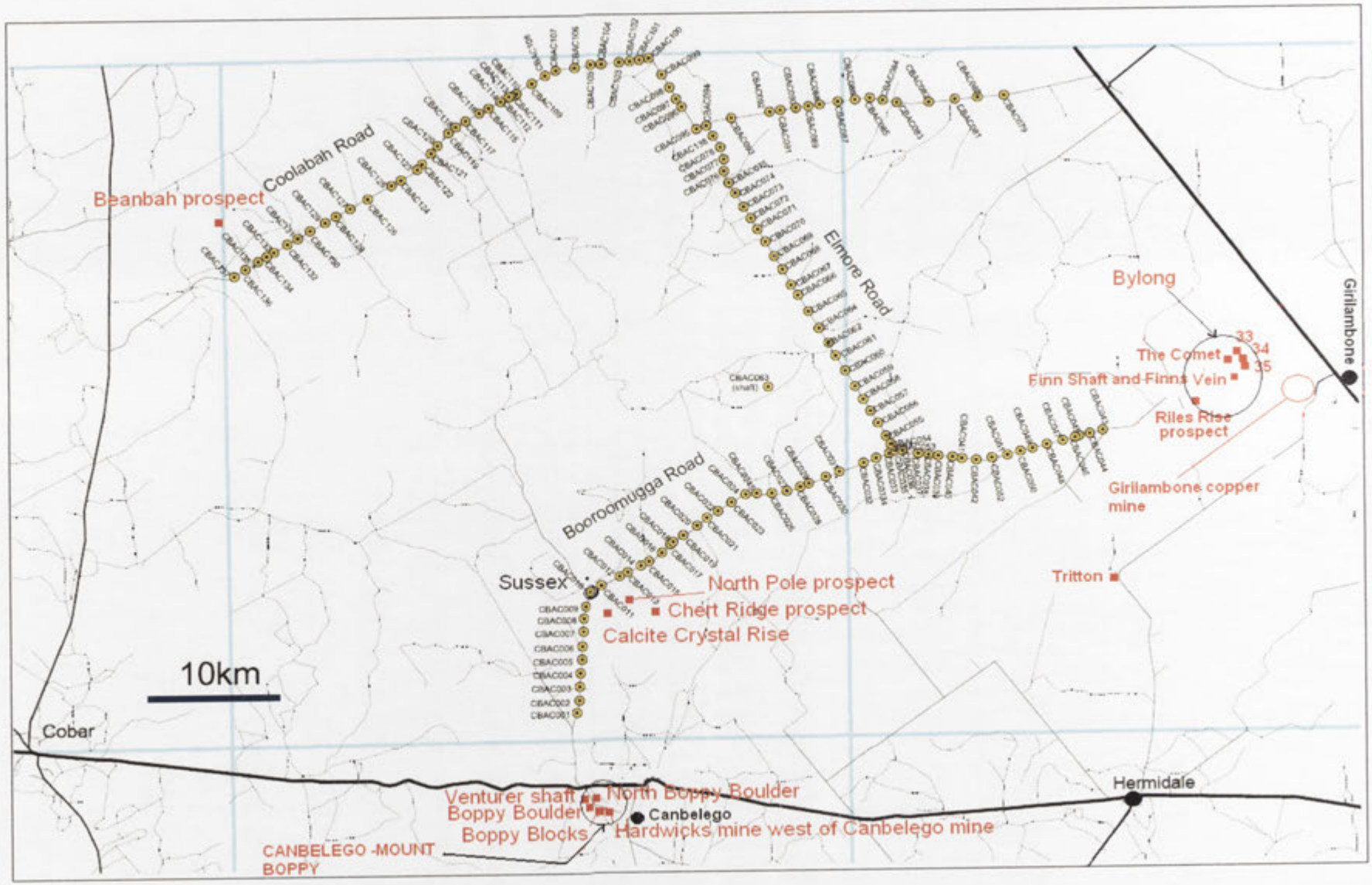

Figure 3.6 Location map showing drill hole and mineralisation sites in the Sussex area.

3.5.1.1 BUDGERY MINE

The Budgery deposit is located about 10 km to the northwest of Hermidale. It consists of a pipe-like copper sulfide orebody that plunges south- southeast at 45°. It contains a 20 m vertical interval above the water table in which rich ores, both supergene sulphides and oxide masses, were found (Gilligan and Byrnes, 1995). The deposit is associated with mafic rocks of the Girilambone Group. Drill hole CBAC151 is located 1.5 km northwest of the Budgery Mine (Figure 3.7).

3.5.1.2 BYLONG

Byrnes (1993) identified the Riles Rise prospect (Fe), the Comet (Au) and the Finn Shaft and Finns Vein (Au) gold and ironstone deposits and three other unnamed deposits numbered 33, 34 and 35 on the Cobar metallogenic map in the Bylong area about 30-50 km W-NW of Girilambone. These small gold workings are mostly on iron-stained quartz veins developed along fractures and schistosity. The veins vary from 2-5 cm to 15-25 cm wide (Gilligan and Byrnes, 1995). These deposits are hosted by schist of the Girilambone Group. The closest drill hole to this area is CBAC 43, located about 25 km to the southwest (Figure 3.6).

3.5.1.3 CALCITE CRYSTAL RISE, NORTH POLE PROSPECT AND CHERT RIDGE PROSPECT

These prospects are located south of Booroomugga Road (close to drill holes CBAC8-12) about 5 km southeast Sussex (Figure 3.6), and are considered to comprise a stratigraphic trend, containing possible syngenetic mineralisation (Gilligan and Byrnes, 1995).

Calcite Crystal Rise (Pb) consists of two parallel gossanous quartz veins, which are present in weakly-mineralised metasediment of the Girilambone Group. The best auger hole values in this prospect showed 1700 ppm Pb, 390 ppm Zn and 350 ppm Cu (Gilligan and Byrnes, 1995).

The North Pole prospect (Pb, Au) occupies a fault or shear zone with fractured chert, quartz veining and iron staining. There is some minor gossanous development. Low anomalous silver is widespread and occurs in both chert and ironstone. Maximum base metal values recorded from the gossanous ironstone are 4000 ppm Cu, 6000 ppm Pb and 2900 ppm Zn (Gilligan and Byrnes, 1995).

At the Chert Ridge prospect (Pb, Zn, Cu) geochemical prospecting has showed anomalous lead values along a chert-rich ridge. Values are up to 1.8 wt% Pb, 665 ppm Cu and 1250 ppm Zn. On the chert ridge weak traces of mineralisation probably continue north through the North Pole line of pits.

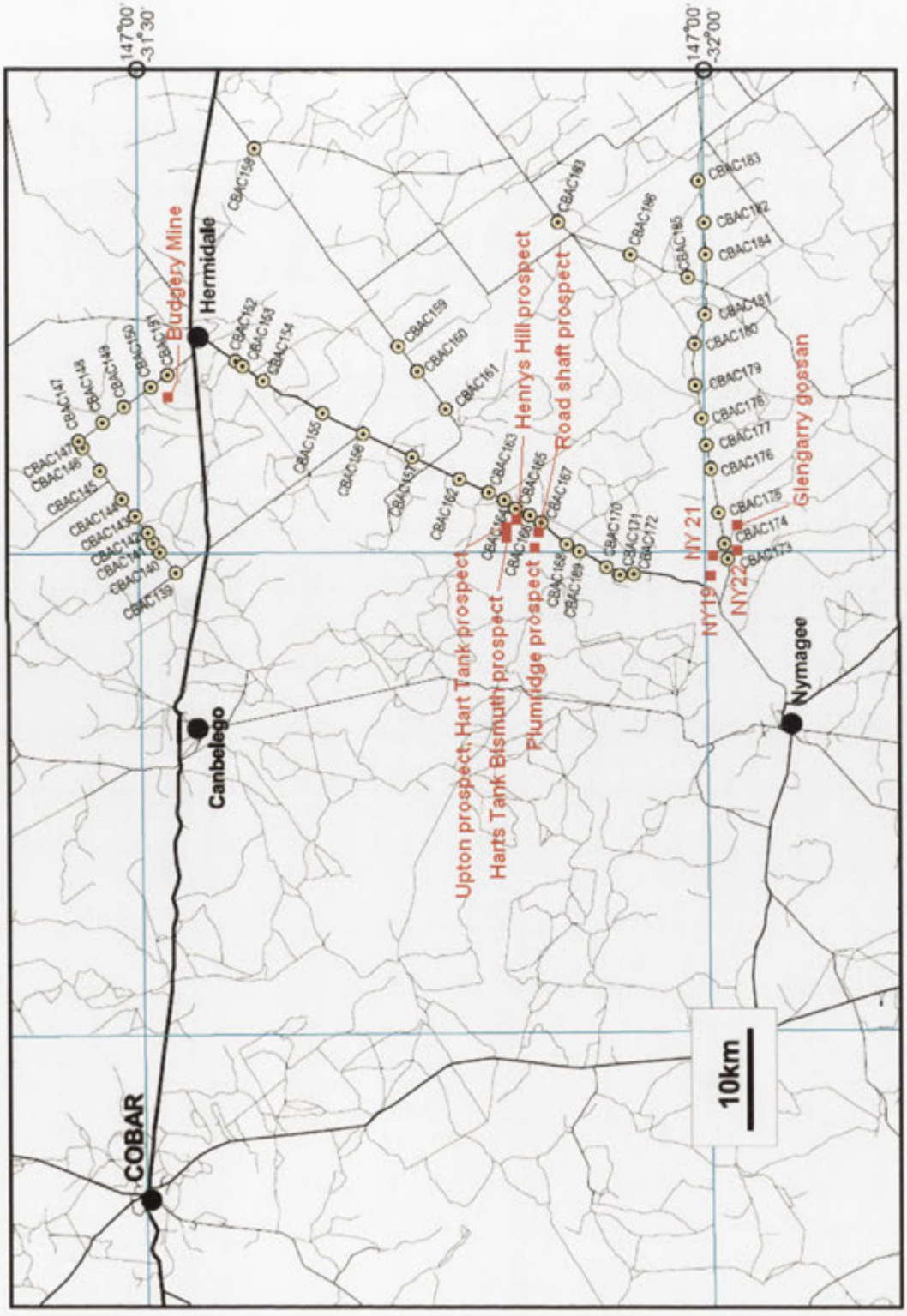

Figure3.7 Location map showing drill hole locations and mineralisation sites in the Hermidale area.

3.5.1.4 MOUNT DIJOU – BALD HILLS

Deposits in the Mt Dijou-Bald Hills area are associated with deformed mafic volcanic rocks (including pillow lavas) and enclosing metasediments. Mineralisation appears to be structurally controlled, occurring in fault breccias, quartz veins and lodes with associated silicification and minor sulfides (Byrnes, 1993). Early descriptions of the deposits (gold and silver) refer to mineralisation occurring in horizons or jasper-ironstone lodes, probably reflecting near surface oxidised portions of the mineralisation. Mafic units (dykes or interbedded volcanics) were recorded in nearby aircore holes (McQueen, 2004a). Drill holes CBAC 199-202 are located close to the Mount Dijou-Bald Hill area (Figure 3.8).

3.5.2 DEPOSITS RELATED TO SILURIAN GRANITOIDS

3.5.2.1 BEANBAH PROSPECT

The Beanbah prospect is an old working located northeast of Coronga Downs and related to Silurian granitoids in the Beanbah area. It is hosted by silicified metasediments of the Girilambone Group, which have been intruded by porphyritic rocks and the Beanbah Granite. Quartz veining and silicification are common, with anomalous values of Mo, Sn, W and locally Cu, Pb and As (De Ross, 1978). Maximum rock chip values from the prospect are 0.35 wt% Cu, 1.28 wt% Pb, 10.2wt% As, 410 ppm Zn, 95 ppm Ag, 70 ppm Sn and 2500 ppm Mo (Gilligan and Byrnes, 1995). In the present study CBAC 137 is the closest drill hole to this deposit (Figure 3.7).

3.5.3 DEPOSITS IN UNNAMED SILURIAN VOLCANO - SEDIMENTARY SEQUENCES

The following mineralisation sites are located to the northwest of Rainbow Ridge and close to the studied drill holes CBAC 165, CBAC 166 and CBAC 167 in the Harts Tank area:

Harts Tank Bismuth prospect Bi (Cu, W);

Upton prospect, Hart Tank prospect Zn, Pb, (Cu, W);

Bills Retirement, Au;

Henrys Hill prospect Cu (Zn);

Henrys prospect Au;

Plumridge prospect Au (Bi); and

Road shaft prospect Pb (Zn, Cu).

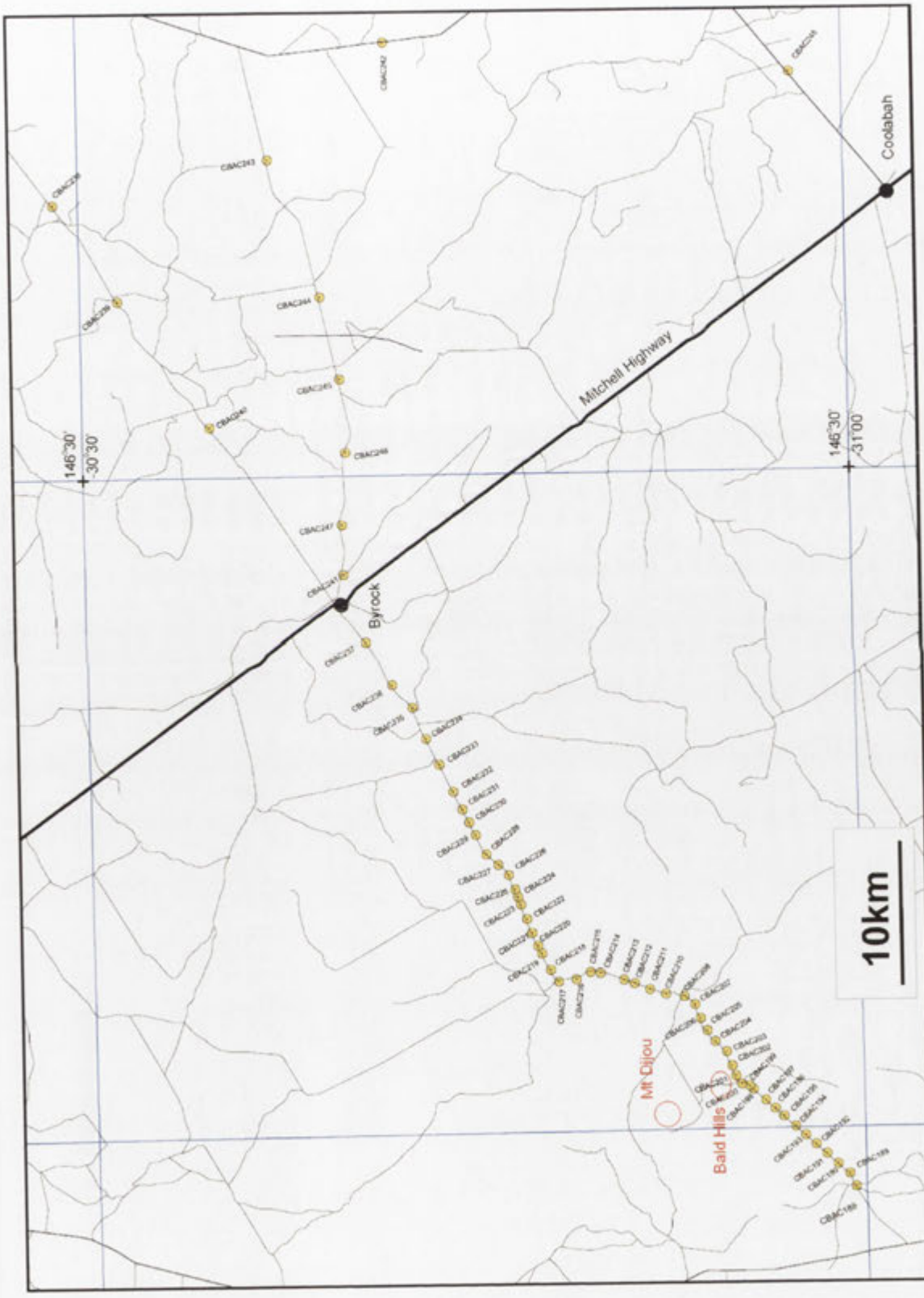

Figure 3.8 Location map showing drill holes and mineralisation sites in the Byrock area

Gilligan and Byrnes (1995) recorded these deposits within unnamed Silurian volcano — sedimentary sequences. The Harts Tank area was originally prospected for gold and Pan Australian Mining Ltd explored the area for base metals and gold in the late 1980's (Pan Australian Mining Ltd, 1986). The geochemical anomalies are mainly associated with ferruginous siliceous outcrops. The gold values are mostly below 1g/t. Bismuth was reported from a small fault zone passing through the Harts Tank Bismuth prospect and north of the Upton prospect (Gilligan and Byrnes, 1995).

Mineralisation at Plumridge is hosted by intermediate volcanics and greenschist of Canbro-Ordovician age. The host rocks in the Road shaft prospect are greenschist felsic volcanics, interbedded with Canbro-Ordovician sedimentary rocks. Rock samples contain up to 325 ppm Cu and 2660 ppm Zn. Some ultra-silicified pyritic dolomite contains up to 0.32 ppm Au, 6550 ppm Pb and 830 ppm As. Hydrothermal alteration is predominant both at this prospect and Henrys Hill prospect (Gilligan and Byrnes, 1995).

3.5.4 DEPOSITS IN THE COBAR SUPERGROUP

A major concentration of gold and base metals occurs in and around Canbelego (Figure 3.6). The Mount Boppy mine was one of the major producers in the state early last century. In addition, there are numerous smaller deposits that were prospected or mined around this area. The following deposits are the closest to the study area:

Venturer shaft	Au;
Boppy Boulder	Au (Ag, Pb);
North Boppy Boulder	Fe (Mn, Au);
Boppy Blocks	Fe, Mn (Au, Pb, Zn); and
Hardwicks mine west of Canbelego mine	Au, Mn (Ag, Zn, Co).

The deposit occurrences in the Canbelego area are related to the basal part of the Baledmund Formation or to the fault zone at or near the Girilambone Group basement-Baledmund Formation cover contact. The Venturer shaft and Boppy Boulder deposits occur as veins hosted by Early Devonian interbedded sedimentary rocks, greenschist, and phyllite. Metaquartzite, greenschist and conglomerate host the North Boppy Boulder and Boppy Blocks deposits. The Hardwicks deposits mainly occupy a fault or

shear zone and are hosted by conglomerate (Gilligan and Byrnes, 1995). In this study CBAC 1 is the closest borehole to this site (Figure 3.6).

3.5.4.1 GLENGARRY GOSSAN AND RELATED DEPOSITS

The Glengarry Gossan and related deposits (coded as NY19, NY21, and NY22 in Nymagee Mineral data sheet; Suppel and Gilligan, 1993) are located in the northwestern corner of the Bobadah and northeastern corner of the Nymagee (100 000) sheets. The gold and /or silver deposits in this area are concentrated along veins in felsic volcanic rocks, except NY 19, which occurs in siltstone of the Baledmund Formation of the Kopyje Group. The following mineral deposits were described by Suppel and Gilligan (1993) from this area:

NY19	Pb, Au (Cu, Ag);
NY 21	Au;
NY22	Au; and
Glengarry gossan	Pb, Cu, Zn (Ag).

The primary and secondary minerals of these deposits are pyrite and iron or manganese oxides, respectively. In this study drill holes CBAC 173, CBAC174 and CBAC 175 are close to these deposits (Figure 3.7).

4. CHAPTER FOUR: SAMPLING METHODOLOGY

A total of 247 drill holes (138 for Sussex-Coolabah, 49 for Hermidale, and 60 for the Byrock sheets areas) were drilled in the study area using a small 6-wheel aircore rig supplied by Geological Ore Search, Cobar. The drilling was conducted along roadside traverses with holes generally spaced at 2-4 km. In some cases the spacing ranged from 1-8 km. Depth of drilling ranged from 6-82 m. Standard drill log sheets combining requirements for both CRC LEME and NSW DPI were used. Chip tray samples were collected for every metre for the first ten metres then 2 metres thereafter. Approximately 4 kg samples were taken for geochemical analysis every 1 m for the first 10 metres and then composite samples were collected every 1-3 metres until the end of hole. The water table level was noted in the field at the time of drilling (Chan *et al.*, 2001; 2002, Fleming and Hicks, 2002). Samples were taken with a PVC sample spear from bagged bulk samples collected by cyclone on the drill rig. Samples were collected by the CRC LEME and NSW DPI sampling team.

Byrock and Hermidale samples were analysed for 28 elements (Ag, Al, As, Ba, Be, Bi, Ca, Cd, Co, Cr, Cu, Fe, K, Mg, Mn, Mo, Na, Ni, P, Pb, S, Sb, Sr, Ti, V, W, Zn and Zr) using Inductively Coupled Plasma Atomic Emission Spectrometry (ICP AES), following a multi acid digest (HF- HNO_3- HCO_4 digestion, HCl leach) using method ME- ICP61 of ALS – Chemex Laboratories in Orange. Sussex samples were processed by ANALABS of Cobar using ICP AES (method I104) and ICP MS (method M104) after multi acid digestion (Appendix 1). Although the analytical method used is not a total analysis technique for some elements (Eaton at al., 1995), it gives a good first pass indication of element abundances, particularly for most (but not all) elements of direct interest as commodities or pathfinders (Chan *et al.*, 2002). Each sample was also analysed for Au by graphite furnace AAS analysis (method: AU-GF42 of ALS – Chemex or F614 of ANALABS) following aqua *regia* digest and solvent extraction (Appendix 1).

Four-kilogram samples were collected from the bottom 1 m interval of the 230 air core holes. The depth of sampling varied from 3 m to 82 m, depending on the thickness of the weathering profile and the depth of drill refusal. Samples were pulverised in a

tungsten carbide mill and analysed for major elements by X-ray fluorescence spectrometry (XRF) and trace elements by inductively coupled plasma mass spectrometry (ICP MS) at Geoscience Australia (Appendix 2).

Groundwater samples (1000 ml) were collected by stainless steel bailer (1 m length by 5 cm diameter, and 50 cm by 5 cm) from 14 drill holes (9 from the Byrock area, which are CBAC217, CBAC218, CBAC219, CBAC227, CBAC231, CBAC235, CBAC242, CBAC243 and CBAC248 and five drill holes CBAC150, CBAC154, CBAC158, CBAC160 and CBAC173 from the Hermidale area). The water depth, electrical conductivity (EC), pH, Eh and water temperature (T) were measured on site using portable Orion^{TM} electrodes and meters. All samples were collected after the third bailing attempt to ensure that water representative of the groundwater in the hole was being considered. Water samples were filtered with 0.45μm filters and separated into 500 ml for cation analyses (acidified with 2 ml concentrated HNO_3) and 500 ml for anion analyses (unacidified). Sample handling was carried out with talcum-free non-sterile latex gloves. All sampling bottles were new and rinsed three times with the water to be sampled prior to collection of the actual sample. Chemicals were added using glass or disposable polyethylene pipettes. The alkalinity of the unacidified samples was measured by titration in the laboratory and cation and anion concentrations were measured by conventional methods using ICP OES at the Bureau of Rural Science (BRS), for major (Na, K, Ca, Mg, Si, Cl, SO_4) and trace elements (Al, Ba, Cu, Fe, Mn, Sr, Zn; Appendix 3). Seven water samples from drill holes CBAC150, CBAC158, CBAC160, CBAC173, CBAC 217, CBAC227 and CBAC231 were analysed for ^{36}Cl at the Department of Nuclear Physics of the Australian National University.

Manganese-rich grains and Mn-coated dark coloured grains (>1 mm diameter) from five Mn-dominant intervals in the drill holes CBAC 176 (37-39 m), CBAC177 (8-9 m, 13-15 m), and CBAC180 (6-7 m, 7-8 m) were examined using JEOL 6400 scanning electron microscope (SEM) and energy dispersive X-ray (EDX) analysis system operating at 15 KeV in Australian National University.

The mineralogy of 34 samples were examined by X-Ray Diffraction (XRD) to identify carbonate, manganese oxides and iron oxides minerals and the semi-quantitative determination of the mineral abundance was achieved using *SiroQuant* software at the

Department of Earth and Marine Sciences of the Australian National University (Appendix 4).

Standard, blanks, replicates and duplicates were used to ensure the accuracy and precision as described in Chapter 5 (Appendix 5).

5. CHAPTER FIVE: DATA ANALYSIS TECHNIQUES

5.1 INTRODUCTION

Data analysis involves condensing large volumes of information into a form that is more concise, but no less accurate, from which conclusions and /or decisions can be made more easily and efficiently. Over the last century a large body of literature on the statistical treatment of geochemical data has been published and computer packages have been developed, with some designed for the peculiarities of geochemical models and processes (e.g., Rollinson, 1993; Davis, 2002).

The patterns of geochemical data are generally complex because they are controlled by different geological processes that influence the material from which the geochemical samples are collected. Since Krumbein and Graybill (1965), statisticians have tried to develop improved methods to analyse geological variables. The particular nature of these variables, including the ubiquitous relationship between the location where a measurement is made and the value of this measurement, has required the development of appropriate statistical methods (Davis, 2002). Some non-statistical methods e.g., exploratory data analysis, element ratio, bivariate and triangle plots have also been used to analyse geochemical variables (Rollinson, 1993).

In this study, different media, such as regolith (transported and residual) and groundwater are sampled and the samples are analysed for their chemical and mineralogical contents (e.g., by ICP AES & MS, XRF and XRD). The geochemical data are derived from particular locations in space and time and are characterised by sample weight, sampling densities, sample distributions and the analytical techniques applied.

This chapter includes techniques that are used to analyse the collected geochemical data to:

- identify the distribution pattern and outliers ;
- avoid closure and investigate data transformation and quality control; and
- identify element associations using multivariate statistical methods (cluster analysis (CA) and principal component analysis (PCA).

Data in this study, as generally in geochemical analysis (Helsel and Hirsch, 1992), are characterised by:

- a lower boundary of zero, no negative values are possible;
- presence of 'outliers', i.e. observations considerably higher or lower than many of the data;
- positive skewness and non-normal distribution; and
- censored data, reported only as below or above some threshold (e.g., detection limit).

5.2 EXPLORATORY DATA ANALYSIS

Exploratory Data Analysis (EDA) is the manipulation, summarisation and display of data using simple arithmetic techniques to make them more comprehensible with the intention of uncovering underlying structure in the data and detecting important departures from this structure (Tukey, 1977; Kelly *et al.*, 1992; Dale, 1995). EDA is an approach philosophy for data analysis that employs a variety of techniques (mostly graphical) to maximise insight into a data set, uncover underlying structure, extract important variables, detect outliers and anomalies, test underlying assumptions, develop conservative models, and determine optimal factor settings (e.g., Abonyi *et al.*, 2004).

EDA is similar to classic statistical data analysis in that both start with a general scientific problem and yield scientific conclusions. The difference is the sequence and focus of the intermediate steps. For classic statistical analysis, the sequence is Problem => Data => Model => Analysis => Conclusions, whereas for EDA, the sequence is Problem => Data => Analysis => Model => Conclusions (Dale, 1995; NIST/SEMATCH, 2005). Accordingly for classical analysis, the data collection is followed by the imposition of a model (e.g. normality, linearity, etc.) and the analysis, estimation, and testing that follows are focused on the parameters of that model. For EDA, the data collection is not followed by assuming a model but by analysis with a goal of inferring what model would be appropriate (NIST/SEMATCH, 2005).
Most geochemical studies (Reimann and Filzmoser, 2000; Grunfeld, 2005) consider using EDA as a first step in understanding the distribution of the measured variables and a combination of different graphics of histogram, boxplot and a one dimensional scattergram will give an excellent one-dimensional insight into the data.

In this study, data were analyzed using a mixture of both EDA and classic statistical approaches (as well as other approaches e.g. multivariate analysis). Many graphical techniques of EDA such as boxplots, scatter plots and ratio plots are proposed and used to analyse the raw data to detect the outlier values (thresholds and anomalies), and to discover the relationship between different major and trace elements in the regolith. Classic statistics, such as mean, median and standard deviation are used in indicating the quality (accuracy and precision) of the data and in estimating the background and anomaly thresholds for the elements.

5.3 RECOGNITION OF OUTLIERS BY BOXPLOT

A boxplot consists of a rectangular box from first quartile ($q0.25$) to third quartile ($q0.75$), with tick marks at the median ($q0.5$). The distance between the top and bottom of the box is the interquartile range (IQR). The line in the middle of the box is the sample median. If the median is not centred in the box, it is an indication of skewness. The "whiskers" are lines extending above and below the box. They show the extent of the rest of the sample set (unless there are outliers). The suspected outliers and extreme outliers are values that are more than 1.5 and 3.0 times the interquartile range away from the top or bottom of the box respectively (Tukey, 1977). The plotted outlier points may be the result of a data entry error, a poor measurement or an anomaly in the measured data. The effectiveness of boxplots has been demonstrated in summarizing the results of a field survey (Reese, 2005) and in processing the geochemical data of the Cobar region (Cohen *et al.*, 1996).

A single boxplot or multiple boxplots can be drawn together to compare multiple data sets or to compare groups in a single data set. An example of a comparative application of boxplot is given in Figure 5.1. Small boxes represent consistent values of elements, whereas large boxes display a wide range of variation in element concentration. Outliers are extreme high or low measurements (outliers on the high side are more common) that are sometimes referred to as "spurious" data because they are highly divergent from the main population of data. Outliers may arise from matrix interferences or errors in transcription, sampling technique, datacoding, analytical methods and / or instrument calibration. Alternatively, what may appear to be outliers

may simply represent inherent variability in the regional background geochemistry. This will be particularly true for background areas in which the geochemistry is heterogeneous (e.g., SWEDIF and EFAWEST, 1998).

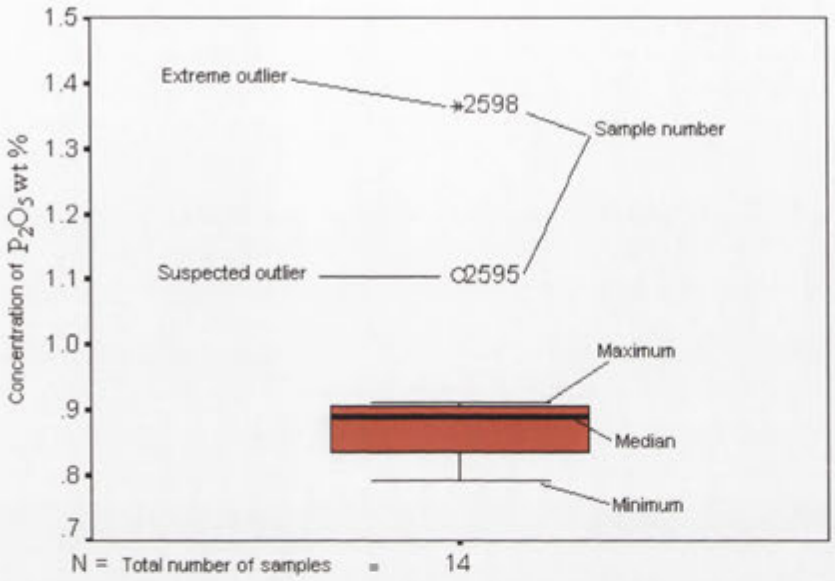

Figure 5.1 An example of a boxplot for samples of transported regolith in the Byrock area.

Outliers are a controversial issue in geochemical analysis; some geochemists (e.g., Goncalves *et al.*, 1998; Borrego and Gutierrez, 2000; Lalor and Zhang, 2002) have considered them as analytical errors so they are often dealt with by removing them prior to multivariate analyses of data or prior to some of the hypothesis test procedures. Others (e.g., Helsel and Hirsch, 1992) have considered the outlier as the most important records in the data set, and argue they should be carefully investigated based on available geological information. In this study the term "outlier" is applied to both genuine anomalous observations that might relate to potential mineralization, and to spurious data points resulting from sampling, analytical and other sources of error. Accordingly, during background data interpretation, statistical outliers are provisionally accepted as geochemical variations and their credibility is deferred until follow-up investigation. The quartile (boxplot) and classic statistical techniques are used to identify the geochemical (thresholds and anomalies in the regolith of the Girilambone region (Chapter 6) in which the outliers represent potential geochemical anomalies. Outliers were removed from the multivariate analysis (CA and PCA) data as discussed below.

5.4 TRANSFORMATIONS

Transformation is typically employed in geochemistry to de-skew data for use in modelling methods that assume normality of distribution. Employment of transformation is not merely an arbitrary choice, because serious problems can occur when procedures assuming symmetry, linearity or homoscedasticity (constant variance) are used on data, which do not possess these required characteristics (Helsel and Hirsch, 1992; Kotlyar *et al.*, 1998).

To normalise geochemical data, the most commonly used transformation is logarithmic, because the lognormal distribution has long been recognised as a useful model in the evaluation of geological variables whose value distribution is often extremely skewed (Rendu, 1988; Limpert *et al.*, 2001; Ohta *et al.*, 2004; 2005). However, a number of studies (e.g., Reimann and Filzmoser, 2000; Grunfeld, 2005) have shown that this has not been a general rule of thumb when regional datasets are considered. Some geochemical data rarely follow normal or even lognormal distributions (Reimann and Filzmoser, 2000) and a practical problem remains that the lognormal model is often only an approximation of the true distribution of geological data (Rendu, 1988).

The Girilambone geochemical data are not normally or log normally distributed. The normal probability and detrended normal plots of the studied geochemical data (element concentration) showed that the outliers make the distribution pattern of the studied elements not normal (Appendix 8). Therefore, to avoid the "abnormal" influences of these outliers on element association, and because some multivariate analysis (i.e., PCA) are sensitive to outlier values (Davis, 2002) these outliers were removed before multivariate statistical analysis. The data are also log-centred ratio transformed to avoid the closure effect (as discussed below).

5.5 TRANSFORMATION TO AVOID CLOSURE

Geochemical data are typically reported as proportions (weight %, parts per million, etc.). For a given observation, compositional proportions (i.e.; weight%) always sum to a constant (100%). Closed data, by definition, are points of the simplex, which are a

part of n-dimensional real space. The elements of points on the simplex are vectors of real numbers that satisfy the constant sum constraint. Statistical measures, such as measures of correlation and covariance can be misleading and can result in an incorrect assessment of correlation or other measures of association (Davis, 2002). Aitchison (1986) advocated the use of centred log-ratio transformations to overcome the effect of closure. The centred log-ratio transformation of an observation consists of taking the logarithm of each variable after the variables have been divided by the geometric mean calculated across all variables.

The log-centred ratio is useful because it maintains the concept of distance (i.e.; Euclidean) between two compositions in the cluster analysis (Aitchison et al., 2000). Also, closure can be avoided by utilising mass balance approaches based on fixing volume, mass or concentration changes between samples of parent and daughter lithologies. However, this is a restrictive approach and is impractical in the weathering (regolith) environments where the equivalent fresh parent rock may be difficult to obtain.

Another practical technique to remove closure effects is using element ratios (i.e., Mg/Ca, Al/Si, K/Al). This can be explained mathematically as follow:

$$Y_1 / Y_2 = (X_1 / X_D)/(X_2/X_D) \quad \text{.....(1)}$$

$$Y_1/Y_2=X_1/X_2 \quad \text{.....(2)}$$

Where Y_1 and Y_2 are the concentrations (weight % or mole %) of elements 1 and 2 in the closed data, X_1 and X_2 are the pre closed amount of the elements 1 and 2 respectively, and X_D is the total sum of all element (1+ 2+3,....D)

In this study the effect of closure was largely avoided by using the log centred ratio. This transformation is applied on the data of multivariate cluster analysis and principal component analysis (Chapter 6), whereas ratios are predominantly used to identify the parent materials (Chapter 8).

5.6 QUALITY CONTROL OF DATA

Exploration investment commonly hinges on the results and interpretation of geochemical data. A measure of confidence of the data must be ensured, and this can be

obtained only from a reliable quality assurance/quality control (QA/QC) program, which depends upon the quality of field sampling and laboratory analytical procedures. An appropriate QA/QC program should minimize inconsistencies and uncertainties within the data. Failure to monitor analytical quality may lead to incorrect estimation of thresholds and result in geochemical anomalies that are laboratory error and sampling artefacts. The objectives of a QA/QC program are to:

- document the procedures and methods of sample collection, preparation and analysis;
- provide assurance as to reliability of analyses using replicate samples, cross-laboratory checks;
- provide assurance as to the precision and accuracy from duplicate samples.
- provide assurance as to the accuracy from using recognized reference standards.
- provide reliable information regarding the interpretation of data with respect to the behaviour of a mineral and its mineral component(s) during weathering.

Analytical quality control is essential in the initial stage of data analysis (Levinson, 1974). The principal indicators of data quality are their bias, precision and accuracy. Bias is a consistent deviation of measured values from the true value, caused by systematic errors in procedure that can be attributed to either the technique or the laboratory's use of the technique. Precision is the nearness with which measurements of a given sample agree with each other. In other words it is a measure of the degree of agreement among replicate analysis of a sample, usually expressed as the standard deviation. Accuracy is a combination of bias and precision of an analytical procedure, which reflects the closeness of a measured value to a true value (Clesceri *et al.*, 1989). Precision and accuracy are complex issues and are not the same for all elements and all concentration levels (Nash *et al.*, 2001).

Guides to analytical quality control (Plant *et al.*, 1975; Fletcher, 1981) explain the statistical basis of control and/or the precautions that must be observed. A comprehensive account of the theory of error in geochemical data is given by Miesch (1967). However, it does not give a detailed description of practical methods for estimating the various forms of analytical error.

James (1970), Thompson and Howarth (1978) and Thompson (1983; 1992) described the statistical basis of analytical quality control, an approach to the estimation of analytical precision and the factors that need to be controlled in any analytical procedure. These factors were classified to within-batch variations, between-batch variations and overall accuracy. The within-batch variations are either random, uncontrolled variation that arises at every stage of analytical procedure, which can be quantified simply as within-batch precision, or are systematic changes within the batch. They may become apparent as a change in accuracy, in the form of drift, a periodic variation, or discontinuity. The between-batch variations represent changes in accuracy between the batches or an additional source of variance, the between- batch precision. The overall accuracy is the ability to have correct results of whole multi-batch analysis. The purpose of a geochemical survey is to give a description of the geochemical variation in sampling media within a region. Numerically this can be expressed in terms of the natural " geochemical variance" of the area. Geochemical information content is diminished by the two processes of measurement: the act of taking a sample adds a random error with " sampling variance" and the act of chemical analysis adds another random error with " analytical variance" (Ramsey *et al.* 1992).

In this study, standards (9 tests by MB-6 standard and 9 tests STSD-2 standard of ALS Chemex) and blanks were used to ensure the accuracy (Appendix 5). The analysis of these standards showed that some elements (Be, P and Cd) significantly recorded higher than the standard upper limits, whereas potassium, Fe and Ti values are lower than the standard lower limit (Appendix 5). This possibly indicates analytical errors and /or changes in the composition of the chemical standard.

Five replicates were used to investigate sub-sampling precision and analytical accuracy and 65 duplicate (49 from Sussex-Coolabah, 6 from Hermidale and 10 from Byrock; Appendix 5) samples have been used to estimate the precision of analysis in the three batches of data. Replicates were used to calculate the standard error (standard deviation (s) of the mean ($\bar{y}$) and the probability or the confidence level of the data. Estimations of uncertainty of the data are based on definition of the precision in geochemistry (Thompson, 1983; Plouffe and Bond, 2003) as $P = (2s/\bar{y}) * 100\%$, where the coefficient of variation (CV), and the relative standard deviation are $(s/\bar{y}) *100\%$ and s/

ȳ, respectively, and graphically by simply plotting the concentration of different batches against each other (Table 5.1; Figure 5.2). Potassium, Bi, Sb and Au concentrations show high variation and low precision, which are the result of the analytical procedure (e.g., K & Sb, Chan *et al., 2002*) and/or variation in detecting low concentrated trace elements (e.g., Au). Elements with low variation (<7%) such as Al, Ba, Be, Co, Cr, Cu, Fe, Mg, Mn, Na, Ni, P, Pb, Sr, V, Zn and Zr (Table 5.1), indicate high (≥ 93%) analytical precision. A significant similarity in sub- sample replicate compositions indicates that these sub-samples are high-quality representatives of the bulk composite sample.

Graphical correlation between the duplicates and original samples generally shows significant correlation between the analysed elements (Figure 5.3), which indicates a high analytical precision.

Table 5.1. Standard deviation (s), mean (ȳ), coefficient of variation (CV) and precision (P) of five replicate samples from CBAC150, Hermidale area. Silver, Mo, Cd, W, and S are excluded from the data because they are below the detection limits. Bold numbers (in Bi, Ca and Sb) represent half of detection limit.

Sample	Au ppm	Al %	As ppm	Ba ppm	Be ppm	Bi ppm	Ca %	Co ppm	Cr ppm	Cu ppm	Fe %	K %
R1	0.004	11.16	12	824	4.3	4	0.01	2	96	33	5.37	2.21
R2	0.004	11.46	11	833	4.7	1	0.01	2	104	36	5.49	1.11
R3	0.002	11.61	17	849	4.7	7	0.01	2	110	35	5.48	2.57
R4	0.002	10.13	13	760	4.7	6	**0.005**	2	114	35	5.23	1.98
R5	0.002	9.78	14	716	4.8	6	**0.005**	2	115	35	5.21	1.9
S	0.16	0.03	0.07	0.03	0.02	0.35	0.16	0.00	0.03	0.01	0.01	0.14
ȳ	0.42	1.03	1.12	2.90	0.67	0.60	1.88	0.30	2.03	1.54	0.73	0.28
CV	39.12	3.24	6.42	1.08	2.81	57.88	8.77	0.00	1.60	0.90	1.48	50.21
P	78.25	6.48	12.83	2.16	5.62	115.76	17.54	0.00	3.20	1.80	2.96	100.41
Sample	**Mg %**	**Mn ppm**	**Na %**	**Ni ppm**	**P ppm**	**Pb ppm**	**Sb ppm**	**Sr ppm**	**Ti %**	**V ppm**	**Zn ppm**	**Zr ppm**
R1	0.52	67	0.09	24	574	32	6	41	0.13	124	84	93
R2	0.52	70	0.09	26	692	33	**2.5**	42	0.37	131	86	105
R3	0.53	70	0.09	26	667	32	**2.5**	44	0.34	130	86	106
R4	0.47	68	0.09	25	647	28	9	35	0.27	132	85	102
R5	0.45	65	0.09	25	645	26	**2.5**	34	0.31	131	84	103
S	0.03	0.01	0.00	0.01	0.03	0.04	0.26	0.05	0.18	0.01	0.01	0.02
ȳ	3.70	1.83	2.95	1.40	2.81	1.48	0.59	1.59	3.43	2.11	1.93	2.01
CV	0.86	0.74	0.00	1.03	1.08	3.03	45.10	3.14	5.32	0.52	0.26	1.13
P	1.71	1.49	0.00	2.07	2.17	6.07	90.19	6.29	10.64	1.03	0.53	2.26

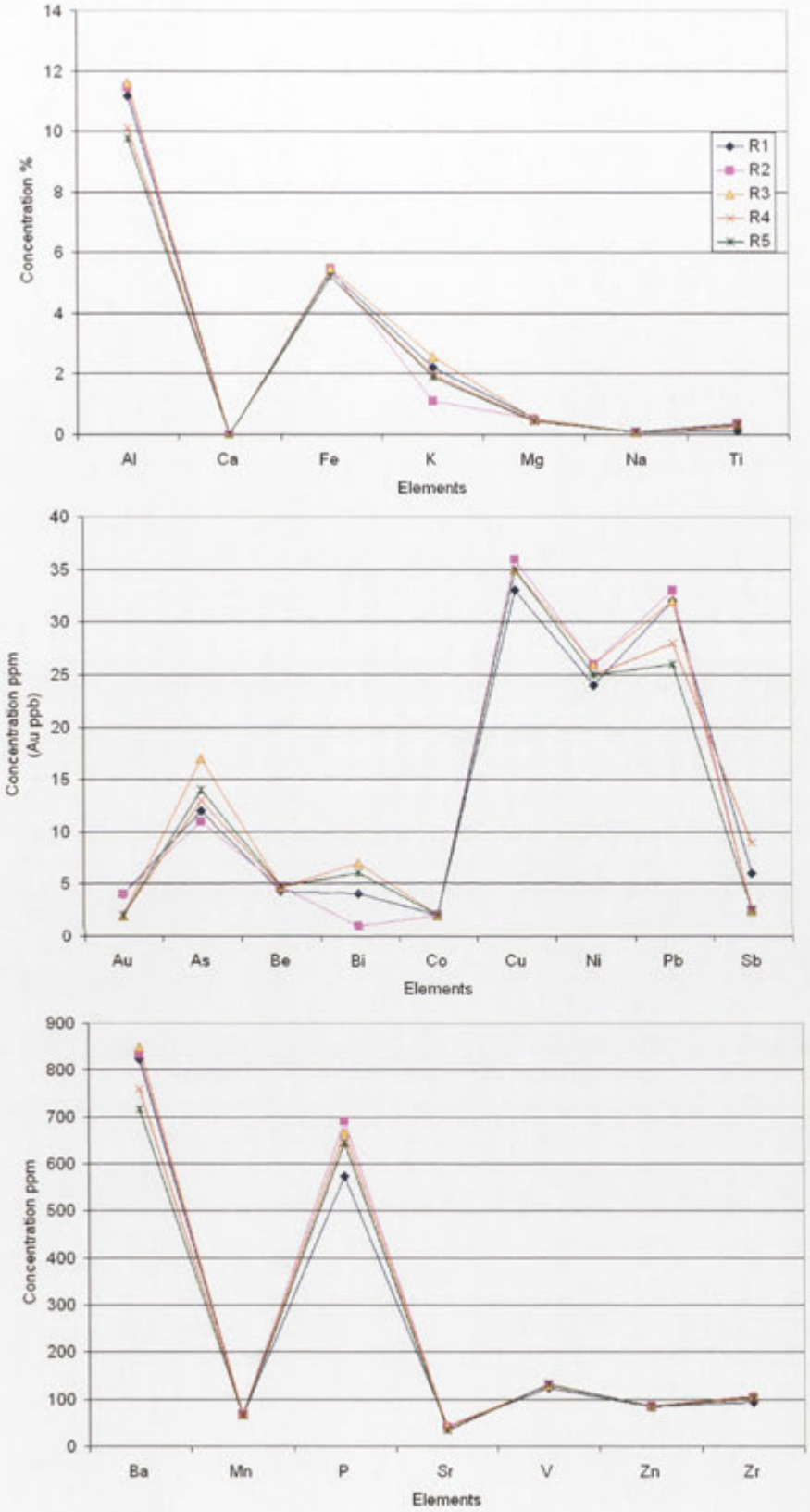

Figure 5.2 Plots showing results of replicate analysis of major, minor and trace elements for 5 replicates (sub-samples) from CBAC150 32-33m in the Hermidale area.

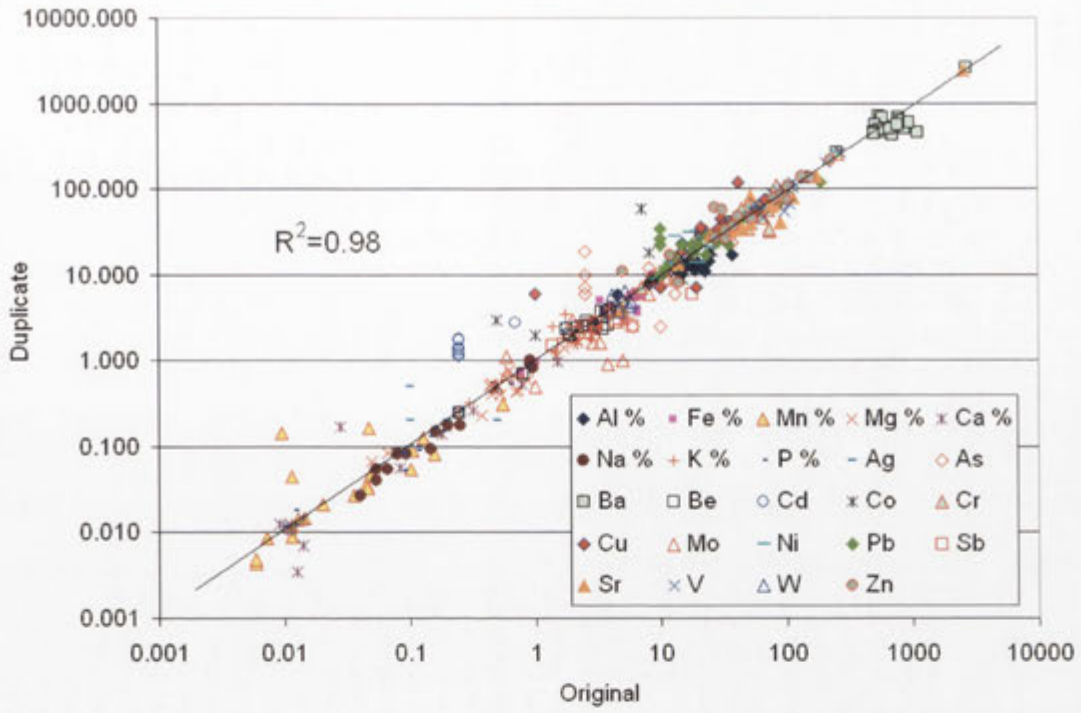

Figure 5.3 Correlation between duplicate and original element concentrations in the regolith of the Girilambone region shows a high correlation coefficient, $r^2 = 0.98$. Data are in ppm unless are nominated.

5.7 DETECTION LIMIT

The limit of detection is the lowest concentration, which can be measured by a specific analytical method and is a function of the level of background noise relative to an element signal (Norrish and Chappell, 1967). This value varies greatly from one method to another and from one matrix (host rock material) to another (Levinson, 1974). The data less than the detection limit are known as left censored data (Last, 1988). Investigators apply various strategies to estimate values below the detection limit (DL), including replacement of measurements below a DL with a single value, for example DL, DL/2 or Dl/$\sqrt{2}$ (Helsel, 1990; Hornung and Reed, 1990). If the distribution of measured data is log- normal, then the expected values of the missing measurement are conditional on being less than the DL (Gleit, 1985).

In general, censoring means that observations at one or both extremes are not available (Gleit, 1985). If censored data make up more than about 30%, the application of parametric statistics may lead to unreliable results (Lubin *et al.*, 2004). For less than 30%, a common and acceptable practice is for them to be converted to the value of half

of the detection limit (e.g. Ellis and Gilbert, 1980; Grunsky and Smee, 1999). This method is widely used, but has no theoretical basis (Helsel, 1990). DL/2 was used as an average value between the DL value and zero (Gleit, 1985). In this study, elements with > 30% censored values are excluded from statistical analysis, whereas those with <30% are replaced by half of the detection limit.

5.8 CLUSTER ANALYSIS

The cluster analysis method divides a large number of objects into a smaller number of homogeneous groups on the basis of correlation structure (Hartigan, 1975). As an explorative technique, cluster analysis provides a description of a reduction in the dimension of the data. It classifies a set of observations into two or more mutually exclusive unknown groups based on combinations of many variables. This analysis has been used to group geological records (Hesp and Rigby, 1975; Guerzoni *et al.*, 1996; Goncalves, 1998; Maerz and Zhou, 1999; Bucker *et al.*, 2000; Edwards *et al.*, 2000; Jerram and Cheadle, 2000; Zhou and Maerz, 2001), identify regional seismic events (Young *et al.*, 2001), group geochemical data (Roy, 1981; Goncalves and Ewert, 1998;Whiticar and Harris, 2000; Hwang *et al.*, 2001; Lee *et al.*, 2001; Zhang and Lalor, 2003; Reinders *et al.*, 2003), and recognise the relationship of constituents and geochemical associations (Baudo *et al.*, 2000; Peruzzo and Busa, 2000; Popov, 2002) and of background and contamination levels (Salman and Rukah, 1999; Hwang *et al.*, 2001).

The purpose of cluster analysis is to assemble observations into relatively homogenous groups or "clusters", the members of which are at once alike and unlike members of other groups. Clustering procedures can be classified into partitioning methods, arbitrary origin methods, mutual similarity procedures and hierarchical clustering (Davis, 2002). The hierarchical clustering techniques are most widely applied in the earth sciences, probably because their development has been closely linked with numerical categorisation of geological data.

Methods of hierarchical cluster analysis follow a prescribed set of steps as follows (e.g., Davis, 2002):

- collecting a data matrix whose columns stand for the objects (samples) to be cluster-analysed and whose rows are the attributes that describe the objects (variables);
- optionally standardising the data matrix; and
- using the standardised data matrix to compute the values of resemblance coefficients and measure the similarities among all pairs of variables and objects, which results in a diagram called a tree, or dendrogram, that shows the hierarchy of similarities among all pairs of variables and objects.

5.8.1 AMALGAMATION OR LINKAGE RULES

At each step of the hierarchical process, the value of an objective function or clustering criterion must be computed to determine which two groups are to be joined. The objective function is usually based on a measure of proximity between groups. In other words it is necessary to identify a linkage or amalgamation rule to determine when two clusters are sufficiently similar to be linked together. The common linkage methods (e.g., Sokal and Sneath, 1963; Johnson and Wichern, 1982; Davis, 2002) can be summarised as follows:

- single linkage (nearest neighbor);
- complete linkage (furthest neighbor);
- unweighted pair-group method using arithmetic averages (UPGMA);
- weighted pair-group method using arithmetic averages (WPGMA);
- unweighted pair-group method using the centroid average (UPGMC);
- weighted pair-group method using the centroid average (WPGMC); and
- Ward's method.

In this study, Ward's method (Ward, 1963) is used to identify the linkage between clusters. This method consists of using the analysis of variance approach to evaluate the distance between clusters by minimizing the sum of squares of any two hypothetical clusters that can be formed at each step. The advantages of this technique are i) any coherent group will not split among different categories, ii) the methodology readily allows consideration of all variables and iii) the boundaries between clusters fall, by definition, in regions of multivariate space where there are few points. If this

subdivision results from geological processes, the boundaries would be natural (Guerzoni *et al.*, 1996).

5.8.2 DISTANCE MEASURES

The joining or tree clustering method uses the dissimilarities (similarities) or distances between objects when forming the clusters. Similarities are a set of rules that serve as criteria for grouping or separating items. These distances (similarities) can be based on a single dimension or multiple dimensions, with each dimension representing a rule or condition for grouping objects. Different types of distance measures are summarised in Table 5.2 (StatSoft, 2004).

Table 5.2 Types of distance measures. p and r values are defined by user. Xi and Yi the coordinates of the objects X and Y.

Distance	**Expressions**
Euclidean	$\sqrt{\sum (x_i - y_i)^2}$
Squared Euclidean	$\sum (x_i - y_i)^2$
Manhattan	$\sum \lvert x_i - y_i \rvert$
Chebychev	$\text{Max} \lvert x_i - y_i \rvert$
Power	$\sqrt[r]{\sum (x_i - y_i)^p}$

In this study the Euclidean distance, the most straightforward way of computing distances between objects in a multi-dimensional space, was used to calculate the distances between clusters. This is probably the most commonly used measure of similarity between objects in a standardised m-space (Davis, 2002). The distance coefficient is the geometric distance in the multidimensional space and it is computed as:

$$d_{(x,y)} = \{\sum_i (x_i - y_i)^2\}^{1/2}$$

Where x_i denotes the variable measured on object x and y_i is the variable measured on object y and the $d_{(x,y)}$ is the distance between object x and object y.

The advantage of this method is that the distance between any two objects is not affected by the addition of new objects to the analysis, which may be outliers.

However, the distances can be greatly affected by differences in scale among the dimensions from which the distances are computed. Therefore the data must be standardised by subtracting the column means and dividing by the column standard deviation prior to computing distance measurements (Davis, 2002). This ensures that each variable is weighted equally. Otherwise, the distance will be influenced most strongly by the variable that has the greatest magnitude.

5.9 PRINCIPAL COMPONENT ANALYSIS

Principal component analysis (PCA) is a data reduction technique designed to reduce a large number of variables to a small set of underlying components that summarise the essential information contained in the variables. A number of steps comprise the PCA procedure. These are computation of the correlation matrix (to determine the appropriateness of the factor (component) analytical model, component extraction (to determine the number of components that are necessary to represent the data and rotation (to make the component structure more interpretable; Coakes and Steed, 2001).

PCA uses measures of association such as covariances or correlations to produce the principal component (Cohen, 2001). However, selecting the association is important in PCA because elemental association that is defined by covariance is possibly affected by the scale of measurement values (ppm vs weight % data). This means elements with large scale and large numerical values will dominate the variance-covariance matrix from which PCA results are generated. The correlation matrix is not affected by scale and is actually the standardised equivalent of the covariance matrix therefore all elements are equally represented in the correlation matrix. In this study the correlation matrix is used for all PCA association. The statistical background and the procedure of PCA are summarised in Coakes and Steed (2001) and Davis (2002).

5.10 SUMMARY AND CONCLUSIONS

The most useful steps in data inspection and analysis are found to be:

- Displaying data using exploratory data analysis methods (Histogram, Boxplot) and separating extreme or outlying values of elements as a subset of the data.

- Examining the normality of the data by plotting the data against the normal score using the quartile-quartile diagram. This showed that the Girilambone regolith geochemical data are neither normal nor lognormal. Therefore, to closely normalise these data, the outliers and data with >30% of their values below detection limit are excluded in CA and PCA.
- Determining the accuracy and precision of the data by graphical plotting and computing the coefficient of variation (CV) and the relative standard deviation. The graphical method of determining precision is more reliable particularly for small number of replicates.
- Applying multivariate cluster and principal component analyses to group the geochemical variables.

6. CHAPTER SIX: GEOCHEMICAL BACKGROUND, ANOMALIES AND ELEMENT ASSOCIATIONS

6.1 DEFINITIONS AND METHODOLOGY

6.1.1 INTRODUCTION

One of the major objectives of this regional geochemical study is to establish the normal or background variations of elements used in geochemical exploration in this area of ancient and complex regolith cover. This chapter describes the concept and definition of the term "background" and the approach used to estimate the geochemical backgrounds and anomalies of elements in the top metre, transported and *in situ* units of regolith in the Girilambone region. The chapter also defines element associations based on statistical calculation of the distance similarity coefficient between these elements using cluster analysis. These element associations are further investigated by principal component analysis.

6.1.2 DEFINITIONS (BACKGROUND, THRESHOLD, AND ANOMALY)

The geochemical background is the normal range of concentration for an element or elements in an area excluding mineralised samples (Levinson, 1974). By definition, a geochemical anomaly is a deviation from the norm and is a departure from the geochemical patterns that are normal for a given area or geochemical landscape. To differentiate between background and anomaly, the term threshold is introduced. The threshold is the upper limit of normal background values (Levinson, 1974). Threshold values, like background values, vary for each element in each rock type, and in each area. Values higher than the threshold are considered anomalous and worthy of cautious inspection. The problem with defining the background is identifying what is the normal range or abundance. In other words what is the geochemical meaning of the words "normal range" and how can it be recognised?

Several rules of thumb have been proposed to identify the background and anomalous values. Hawkes and Webb (1962) suggested the best approximation for a single population of values (one element from one type of rock) is to take the median value as

background, the mean plus twice the standard deviation as threshold and to consider only the highest 2.5 percent as anomalous (or above the threshold). Boyle (1971) suggested samples that contain an amount of element twice the background, or more, are generally considered anomalous.

6.1.3 TECHNIQUES USED TO DETERMINE THE BACKGROUND AND ANOMALY

Hawkes and Webb (1962) and Levinson (1974) suggest the following techniques for estimating the background and anomaly values:

- In an area of known mineral occurrences, carrying out an orientation survey around and away from the mineral occurrence(s) and plotting the data of element concentration as a map, histograms and/or cumulative frequency plots, and selecting a value that differentiates mineral occurrence-related data from the remainder;
- In the common, often unavoidable absence of orientation information (in non/or weakly mineralised sites with a thick weathering profile) and/or reliable data from the literature, it is necessary to examine the data themselves for unusual behaviour (Chen *et al.*, 1998) and this leads to the concept of the statistical anomaly. Various ways of identifying such anomalies are described below.

6.1.4 EVALUATION OF THE STATISTICAL TECHNIQUES

The widely used statistical techniques to estimate threshold values are briefly summarised below.

1. METHOD OF MEAN PLUS TWO STANDARD DEVIATION (M+2S)

This method of selecting threshold values is still used, but is probably not appropriate in many situations. It involves calculating the arithmetic mean (M) and standard deviation (S) of the data set and applying the classification "anomalous" to values exceeding M+2S. The use of the mean plus two standard deviations is not based on some fundamental relationship to mineralisation (Chen *et al.*, 1998). It is merely equivalent, in a normal, unskewed distribution to the 97.5 percentile. Although it is difficult to transform the geochemical data to a typical normal distribution, the use of

this parameter as a threshold is equivalent to selecting the uppermost 2.5 percent of any sample population. This method of deriving the 97.5 percentile was developed before computers were widely available and summary statistics for large populations of analytical values took a long time to process.

2. MEDIAN + 2 MEDIAN ABSOLUTE DEVIATION (MAD) METHOD

Starting geochemical data analysis with statistical tests based on assumptions of normality, independence and identical distribution may not be warranted, therefore using the median + 2 Median Absolute Deviation (MAD) is an alternate more robust analogy to M + 2S. In the median + 2MAD method the arithmetic mean is replaced by the median and the standard deviation by the median absolute deviation (MAD), defined as the median of the absolute deviations from the median of all data (Tukey, 1977). This method is strongly dependent on the lowest threshold value (median value) (Levinson, 1974) without statistical assumptions. Also when a summary value is desired that is not strongly influenced by a few extreme observations (outliers), the median is preferable to the mean (Helsel and Hirsch, 1992). The mean value in (mean+2S) is possibly pulled towards the outliers (becoming higher), whereas the median is resistant to the effect of a change in value in the presence of outlying observations. This method is useful when the data contains less than 10% outliers (Reimann *et al.*, 2005).

3. BOXPLOT METHOD

The boxplot method was explained in detail in Chapter 4. In this approach the calculation of the threshold value is based on the quartile and interquartile range of the data as 1.5 times the interquartile range (IQR=Q3-Q1) away from the top (upper hinge) or bottom (lower hinge) of the box respectively. This boxplot method is the most powerful as long as the outliers comprise less than 15% of the data set (Reimann *et al.*, 2005).

In this study the boxplot and median +2 MAD techniques are applied to calculate the geochemical threshold of the different regolith (top metre, transported and *in situ*) units because the preliminary inspection of the studied data showed that the outlier values are less than 15%. The identified thresholds were plotted along the studied traverses to

show how the value of the threshold varies for a single element in different regolith units of the study areas.

6.2 REGOLITH UNITS AND GEOCHEMICAL BACKGROUNDS, THRESHOLDS AND ANOMALIES

6.2.1 INTRODUCTION

In the study area the regolith can be conveniently divided in to three basic types:

- the top metre (largely comprising soil in most of the area);
- transported ; and
- *in situ* (residual).

The top metre samples from drilling have been used to understand the geochemical signature of element associations and the nature and the pattern of element dispersion in the surface and near-surface environments. Generally the material of the top metre has a homogenous appearance. It consists of silty red-brown clay with pebbles, patches of organic substances and regolith carbonate, that if present occurs in the second half metre. The known soil horizons are uncertain and difficult to establish. The soil types in the Girilambone area have been classified as solonised brown, solodic, red brown earths and red calcareous and non-calcareous earths (e.g., Cohen *et al.*, 1998). Soils have been widely used as sampling media for geochemical exploration in the Cobar area (Cohen *et al.*, 1998; Cairns *et al.*, 2001; Scott, 2002).

Transported regolith can be recognised from visual observation and Portable Infrared Mineral Analysis (PIMA) spectra variations. Identification of clay minerals and the kaolinite crystallinity index were used to define the unconformity between transported regolith that contains kaolinite ± illite ± smectite and *in situ* regolith, which is characterised by highly crystalline kaolinite associated with muscovite/ phengite ± illite ± smectite (Chan *et al.*, 2002; 2004). The depth of transported regolith varies in the study area. It extends to at least 66 m depth in the Byrock region, 35 m in the Sussex region and 42 m in the Hermidale region (Figures 6.1 A-C).

Cyclic leaching of trace elements during weathering, aeolian contamination of fine fractions and the thick transported regolith profile all have the potential to dilute

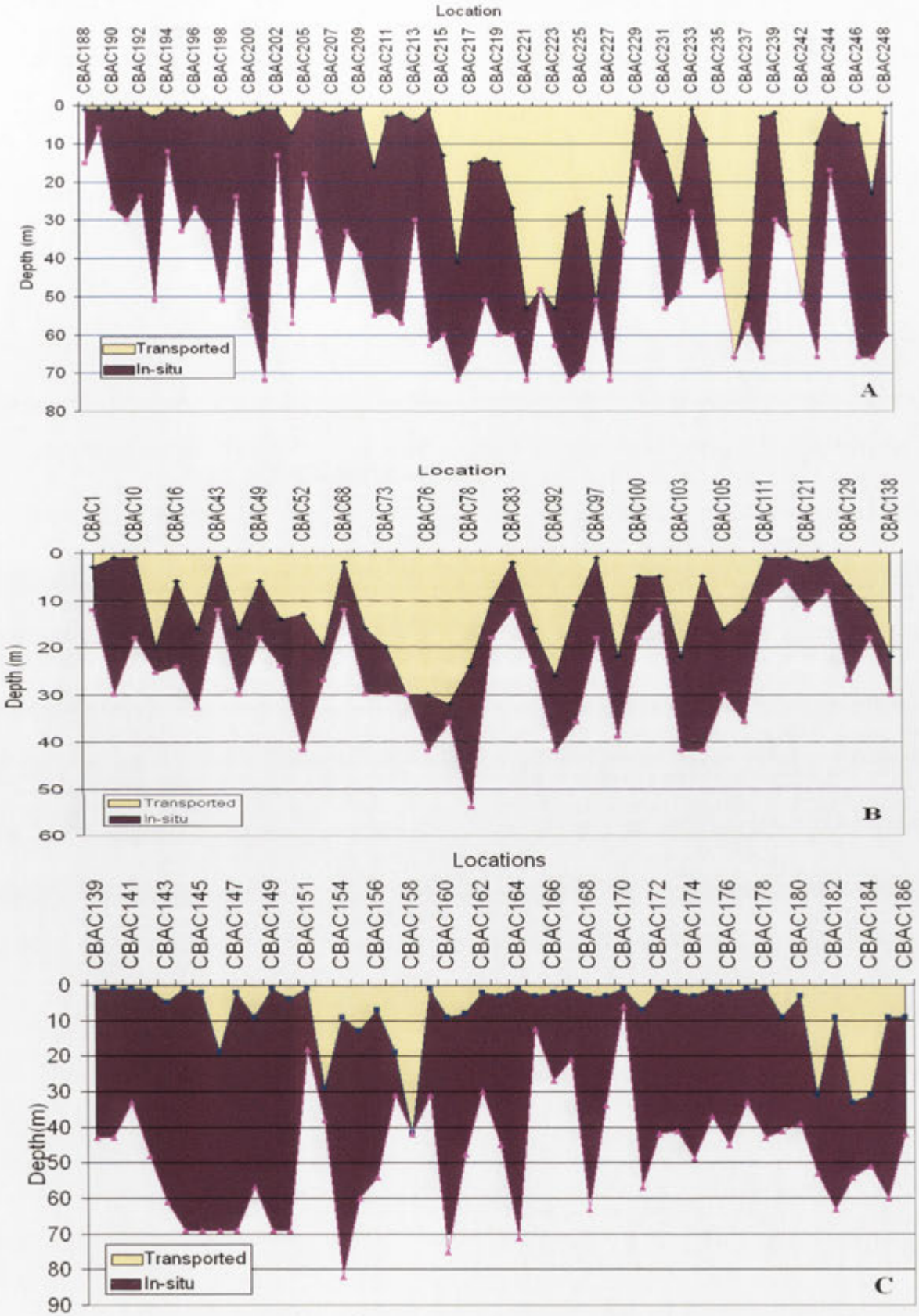

Figure 6.1 Summary profiles of thickness of transported and *in situ* regolith in the Byrock (A), Sussex (B) and Hermidale (C) areas. Drill holes locations in the Sussex, Hermidale and Byrock areas are shown in Figures (3.6-8).

geochemical anomalies. To detect these weaker anomalies it is important to understand the behaviour of pathfinder elements during chemical weathering and soil formation. Grouping these elements according to their occurrences and geochemical behaviours (e.g., mobility of elements) can enhance detection of weaker anomalies and improve interpretation.

The regolith (top metre, transported and *in situ*) samples were also classified into different regolith facies based on their main secondary enrichments produced during weathering. These include a clay-silt-gravel facies (without any enrichment of CaO, MgO, Fe_2O_3 or MnO), regolith carbonate facies (CaO and MgO are $\geq$ 1% wt %), iron-dominant facies (Fe_2O_3 total $\geq$8.5 wt %) and relatively manganese-dominant facies (MnO $\geq$0.1 wt %). The concentration levels are arbitrarily chosen based on comparing the chemical analysis with petrographic description of the samples (Appendix 7).

6.2.2 BACKGROUND AND THRESHOLD VALUES

Most of the area covered in this study is only weakly mineralised or totally unmineralised. It thus provides an opportunity to establish typical background values for elements of interest and threshold values for anomalies generated by regolith-forming processes. Composite samples of the top metre, transported and *in situ* regolith are used to recognise regional backgrounds, anomalies and local geochemical associations of elements. Elements that have more than 30% of their values below the detection limits (BDL) were excluded or treated separately.

The threshold values of the Au, As, Co, Cr, Cu, Mo, Ni, Pb, Sb, and Zn are summarised in Table 6.1. These elements were selected because of their exploration importance as "pathfinders" for ore deposits (e.g. Levinson, 1974). Generally the estimated threshold values derived from the MAD method are less than those for the boxplot method (Table 6.1), which probably represent the minimum threshold values.

6.2.2.1 ELEMENT THRESHOLDS FOR THE TOP METRE

Background concentrations of elements in the surface and near-surface pedogenic environments are primarily influenced by soil forming factors (Davies and Wixson, 1987). The apparent geochemical patterns and elemental composition of different soils

have been attributed to the effects of climate on soil formation (Chen *et al.*, 1999) and degree of weathering (Holmgren *et al.*, 1993). Parent materials and secondary enrichment of carbonate (calcrete), iron oxides and manganese oxides during duricrust formation are also major factors influencing elemental association and background levels (Pierce *et al.*, 1982; Ames and Prych, 1995; Taylor and Eggleton, 2001). Other factors, such as agricultural and industrial activities also influence elemental concentrations in the near-surface regolith.

Two facies were recognised in the top meter of regolith. These are a clay-silt-gravel facies and regolith carbonate facies. The threshold values for As (20 ppm and 27 ppm, MAD method and boxplot method respectively), Cu (30 ppm and 38 ppm), Ni (36 ppm and 41ppm), Pb (40 ppm and 82.5 ppm), and Zn (91 ppm and 99 ppm) are significantly higher in the carbonate facies compared to the clay gravel facies (Table 6.1). This possibly indicates that the regolith carbonate facies has higher potential to accumulate these elements. However, these differences in the background levels must be treated cautiously because they are possibly influenced by a small number of the regolith carbonate samples. Gold has approximately equal threshold values in the clay-gravel facies (0.004-0.006 ppm) and in the carbonate-rich facies (0.004 ppm). Threshold concentrations of Cr are higher in the clay-gravel facies (90 ppm and 116 ppm, Table 6.1).

6.2.2.2 ELEMENT THRESHOLDS FOR THE TRANSPORTED REGOLITH

Three regolith facies are recognised in the transported regolith. These are clay-silt-gravel, regolith carbonate and iron-rich facies. Comparative statistical data of element thresholds for these facies (Table 6.1) show that Au threshold values are approximately equal 0.004 ppm in all three, increasing to 0.006 ppm in the regolith carbonate facies. Also Ni, Mo, Sb and Zn threshold ranges are higher in regolith carbonate, which indicates that regolith carbonate is an appropriate facies to accommodate these elements.

Generally the iron-rich facies is characterised by higher thresholds for As, Cr, Pb, V and W. This reflects the occurrence of iron oxide minerals (e.g., goethite, hematite) that are characterised by high element absorption (scavenging) capacity. No significant differences are observed in Co threshold values.

Table 6.1 Threshold values of elements estimated by Median+2MAD and Boxplot methods for clay-silt-gravel, regolith carbonate, Fe-rich and Mn-rich facies of the top metre, transported and *in situ* regolith units.

REGO.UNIT / FACIES	Statistical estimation	Au ppm	As ppm	Co ppm	Cr ppm	Cu ppm	Mo ppm	Ni ppm	Pb ppm	Sb ppm	V ppm	W ppm	Zn ppm
TOP METRE													
Clay-Silt-Gravel	Number of samples	97	83	145	188	188	149	188	137	117	188	106	188
	Median+2MAD	0.004	17.0	13.0	90.0	30.0	2.3	32.0	34.0	1.9	112.0	4.4	59.5
	3rdQ+1.5IQR	0.006	21.3	14.5	116.0	38.5	6.5	40.5	45.0	3.6	139.6	6.9	77.4
Regolith carbonate	Number of samples	9	9		9	9	9	9	9		9		9
	Median+2MAD	0.004	20.0		80.0	30.0	1.7	36.0	40.0		116.0		91.0
	3rdQ+1.5IQR	0.004	27.5		85.0	39.5	3.5	41.0	82.5		147.0		99.0
TRANSPORTED													
Clay-Silt-Gravel	Number of samples	272	284	484	589	589	589	589	418	296	589	274	589
	Median+2MAD	0.004	17.0	10.0	77.0	23.0	1.4	30.0	30.0	2.0	106.0	4.6	45.0
	3rdQ+1.5IQR	0.004	20.5	16.5	107.5	33.5	6.5	42.0	39.0	2.8	138.0	6.9	66.5
Regolith carbonate	Number of samples	42	77	82	92	92	70	92	63	50	92	38	92
	Median+2MAD	0.004	17.0	13.0	73.0	23.0	3.9	33.0	28.0	2.1	107.0	3.9	53.0
	3rdQ+1.5IQR	0.006	25.0	16.0	96.5	30.5	8.2	44.5	51.5	10.8	144.0	5.5	67.3
Fe-rich	Number of samples	60	140	95	140	140	140	127	123	111	140	106	140
	Median+2MAD	0.001	27.0	11.0	156.0	24.0	2.6	26.0	39.0	5.6	216.0	5.9	44.0
	3rdQ+1.5IQR	0.004	40.0	15.0	217.0	33.0	6.2	35.0	62.8	9.6	303.5	9.2	63.5
IN SITU													
Clay-Silt-Gravel	Number of samples	545	735	570	1292	1292	1046	1292	1031	705	1292	661	1292
	Median+2MAD	0.004	20.0	10.0	94.0	37.0	2.2	34.0	44.0	2.9	127.0	6.2	81.0
	3rdQ+1.5IQR	0.011	27.5	19.5	135.0	50.5	6.5	48.0	69.5	5.4	170.5	9.9	120.0
Regolith carbonate	Number of samples	128	185	121	310	310	263	310	203	211	310	189	310
	Median+2MAD	0.004	19.0	11.0	89.0	34.0	1.8	27.0	49.0	2.9	133.0	5.1	72.0
	3rdQ+1.5IQR	0.009	28.5	14.5	115.4	48.0	4.3	38.0	84.5	4.8	170.1	6.5	114.5
Fe-rich	Number of samples	41	86	38	91	91	87	91	71	53	91	52	91
	Median+2MAD	0.004	26.0	12.0	132.0	47.0	2.0	31.0	54.0	4.1	208.0	6.4	107.0
	3rdQ+1.5IQR	0.009	37.0	18.6	183.8	65.0	4.0	41.0	86.8	5.4	304.6	9.9	161.4
Mn-rich	Number of samples	69	67	81	81	81		81	81		81		81
	Median+2MAD	0.011	21.0	87.0	92.0	62.0		80.0	51.0		20.0		172.0
	3rdQ+1.5IQR	0.02	27.0	160.0	123.5	87.0		118.0	66.5		117.0		255.5

6.2.2.3 ELEMENT THRESHOLDS FOR THE *IN SITU* REGOLITH

In situ regolith consists of clay-silt, regolith carbonate, iron and manganese- rich facies. The *in situ* regolith is characterised by high abundances of Au, Co, Cu, Ni, Pb, V, W and Zn compared to the top metre and transported regolith. This is probably related to reduced dispersion and dilution in the *in situ* regolith.

The higher threshold for Au (0.11-0.02 ppm), in addition to Co, Ni, Cu and Zn, in the Mn-rich facies could be related to either high concentrations of these elements within Mn-rich parent rocks or their scavenging by Mn oxide during the weathering process. The highest threshold values for Cr, As and V were recorded in the Fe- rich facies. The abundance of Cr, V and Fe probably reflects their concentration in iron oxide minerals.

6.3 GEOCHEMICAL ANOMALIES

Discriminating between ore-related and regional background anomalies is difficult and often requires intensive, expensive and unrewarding fieldwork. However, a sufficient amount of geological and geochemical information obtained through a major drilling program will assist in following the anomalies in the third dimension (downhole) and evaluating sampling media and the exploration approach. The threshold values obtained from the MAD and boxpot methods were used to assess possible anomalous values of elements. Some observed values of the top metre samples are significantly greater than the boxplot threshold values and therefore are considered as anomalies. These samples are separated into sub-data sets for additional investigation down the regolith profile.

6.3.1 ANOMALIES IN THE TOP METRE

6.3.1.1 ANOMALIES IN THE CLAY-SILT-GRAVEL FACIES

The anomalous concentration range of elements in the top metre, clay-silt-gravel facies samples are as follows: Au 0.007-0.027 ppm, Co 15-22 ppm, Cr 126-130 ppm, Cu 40-232 ppm, Mo 7-12 ppm, Ni 42-73 ppm, Pb 48-160 ppm, Sb 3.9-11 ppm, V 143-151 ppm, W 7.1-10.4 ppm and Zn 71-128 ppm (Appendix 7). No anomalous values have found for As. Elevated values (> boxplot threshold) of Au were detected from drill holes CBAC6, 32, 112 and 239, Co from CBAC3, 10, 45, 177, 201 and 204, Cr from CBAC 23, and 231, Mo from CBAC 15, 189, 193, 199, 200, 204, 209, 211, 223, 229, 231 and 232, Ni from CBAC 22-25, 166, 189 and 242, Pb from CBAC 6, 43, 60, 82, 85, 86, 88, 105, 115 and 188, Sb from CBAC 82, 139, 140, 149, 151, 152, 157, 159, 161, 162, 164, 172, and 177, V from CBAC 5 and 82, W from CBAC79, 85, 104, 106, 107 and 116 and Zn from CBAC1, 8, 10, 39, 68, 96, 104, 105, and 117. (Figures 6.2-12, Appendix 7).

Gold anomalies are not associated with any other element except Cu (53 ppm) and Pb (74 ppm) in drill hole CBAC6. Copper anomalies are accompanied by elevated Zn values in drill holes CBAC1, 96, and 117. High Cu concentrations are associated with elevated Mo in drill hole CBAC15 and elevated Sb in drill hole CBAC139. Elevated Zn values were observed in drill holes CBAC104-106. A significant enrichment of Ni is recorded from drill holes CBAC22-25 (Figure 6.7, Appendix 7).

6.3.1.2 ANOMALIES IN THE REGOLITH CARBONATE FACIES

The regolith carbonate facies in the top metre displays anomalies in two drill holes, CBAC 191 and 192. Anomalies for Cr (95 ppm) and Mo (13 ppm) occur in CBAC192. Elevated Mo (4 ppm) was detected in CBAC191 (Figure 6.13, Appendix 7).

6.3.2 ANOMALIES IN TRANSPORTED REGOLITH

6.3.2.1 ANOMALIES IN THE CLAY-SILT-GRAVEL FACIES

The clay-silt-gravel facies of the transported regolith shows Au anomalies (0.005-0.098 ppm) concentrated in the central and southern part of the region (Sussex-Hermidale areas). These anomalies do not have associated As anomalies except in drill hole CBAC64, where the elevated Au (0.005 ppm) is associated with elevated As (24 ppm) and Co (25 ppm). Gold anomalies are associated with elevated Cr (115ppm) in drill

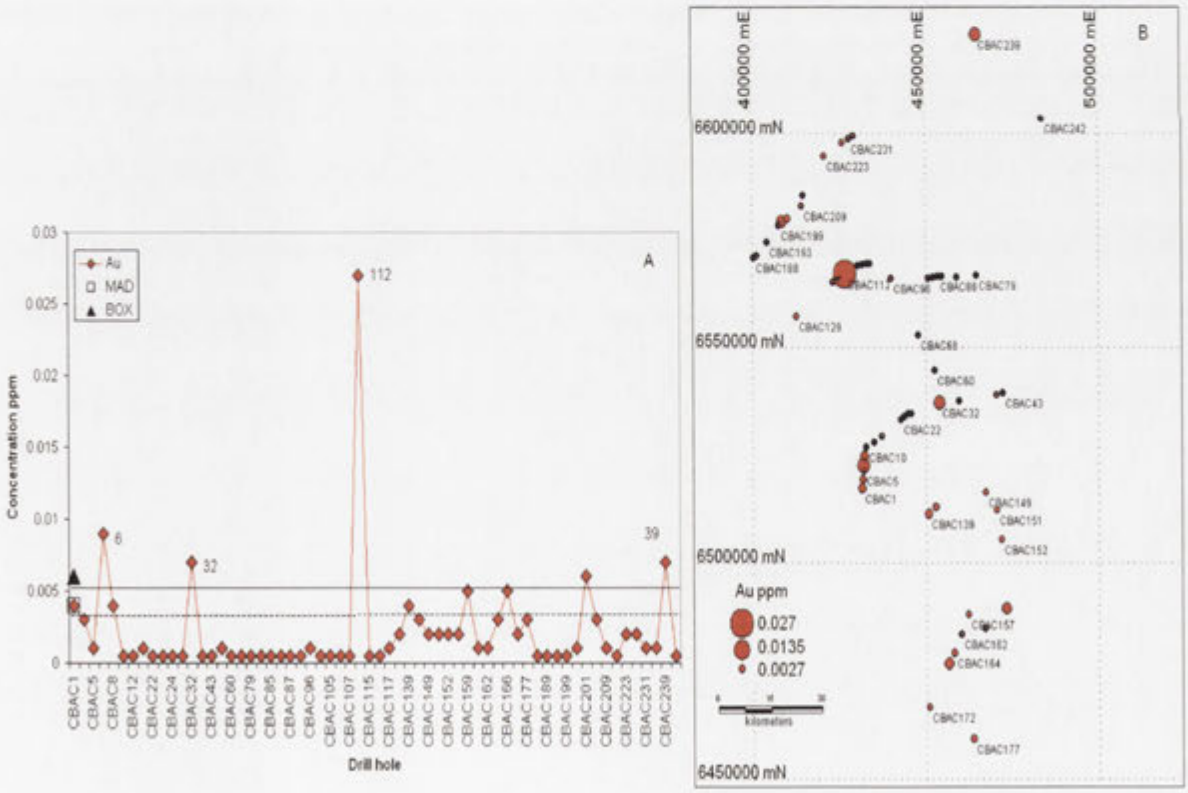

Figure 6.2 Distribution pattern of Au anomalies with MAD and boxplot (BOX) threshold values (A) and a thematic map of anomalous Au in the top metre clay-silt-gravel facies (B).

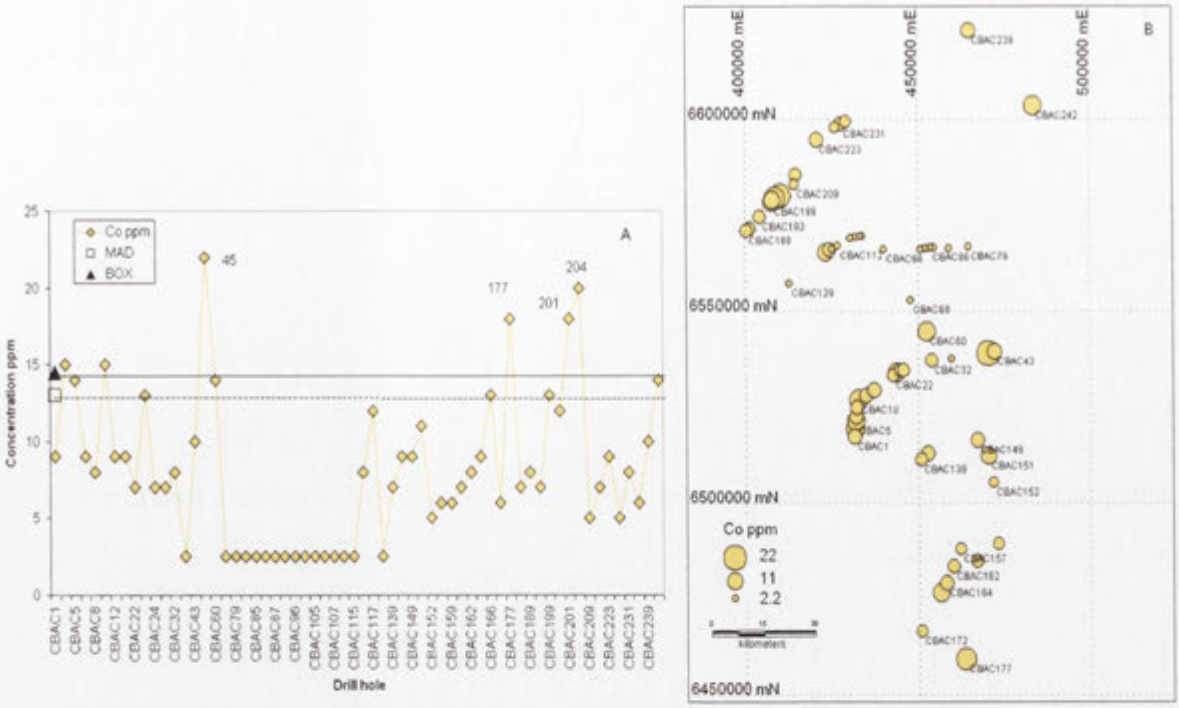

Figure 6.3 Distribution pattern of Co anomalies with MAD and boxplot (BOX) threshold values (A) and a thematic map of anomalous Co in the top metre clay-silt-gravel facies (B).

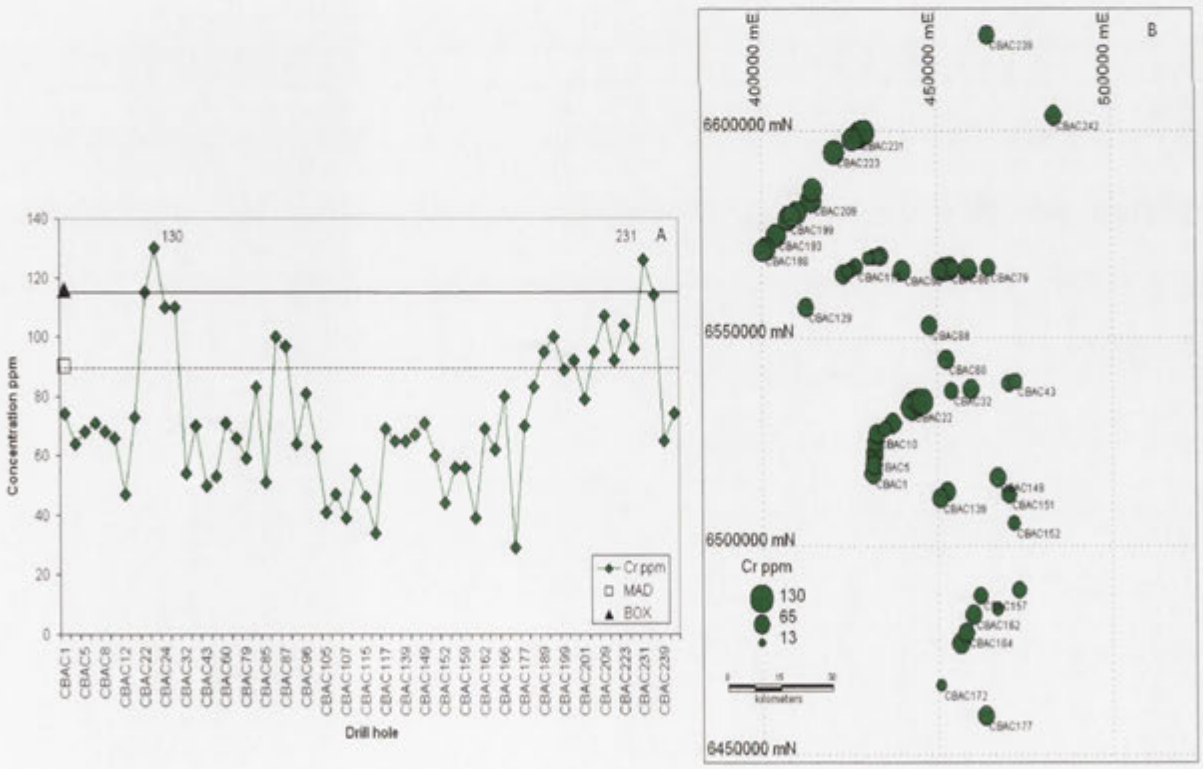

Figure 6.4 Distribution pattern of Cr anomalies with MAD and boxplot (BOX) threshold values (A) and a thematic map of anomalous Cr in the top metre clay-silt-gravel facies (B).

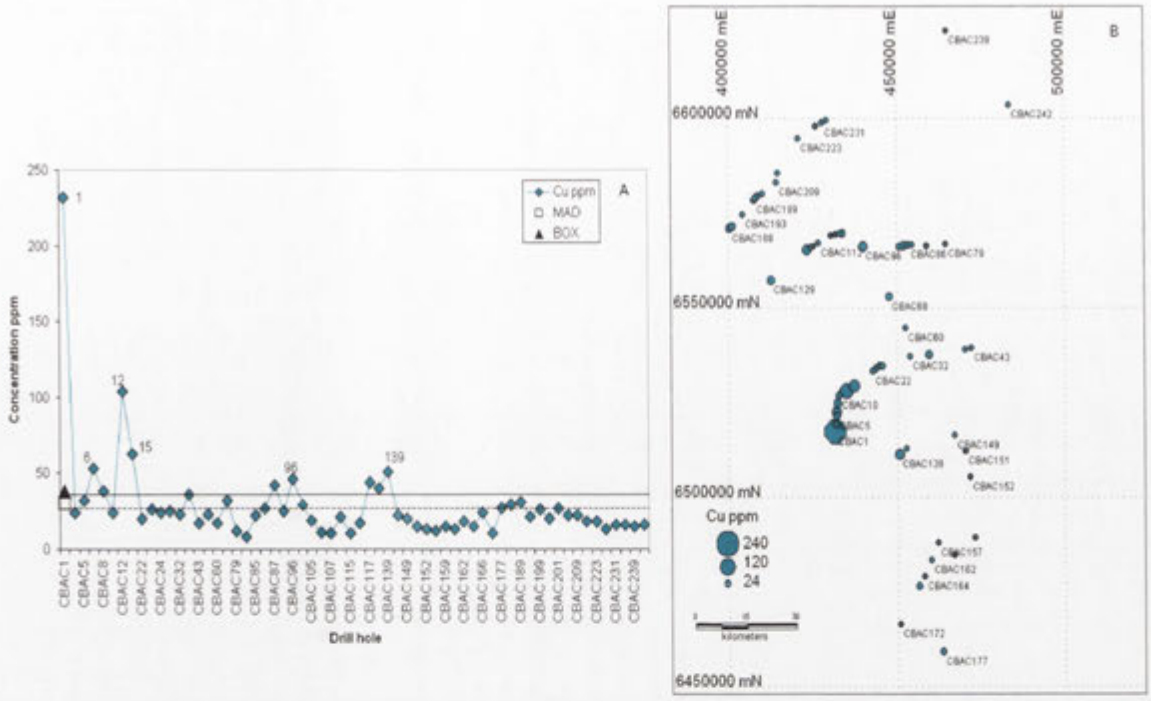

Figure 6.5 Distribution pattern of Cu anomalies with MAD and boxplot (BOX) threshold values (A) and a thematic map of anomalous Cu in the top metre clay-silt-gravel facies (B).

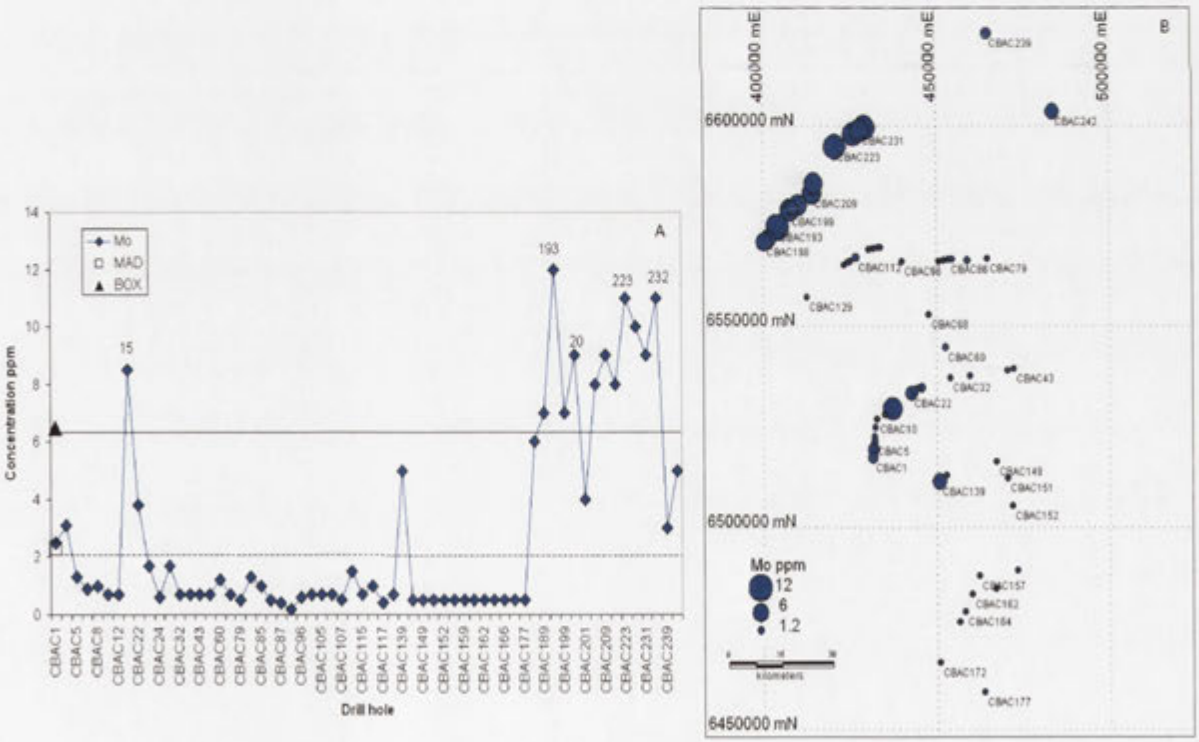

Figure 6.6 Distribution pattern of Mo anomalies with MAD and boxplot (BOX) threshold values (A) and a thematic map of anomalous Mo in the top metre clay-silt-gravel facies (B).

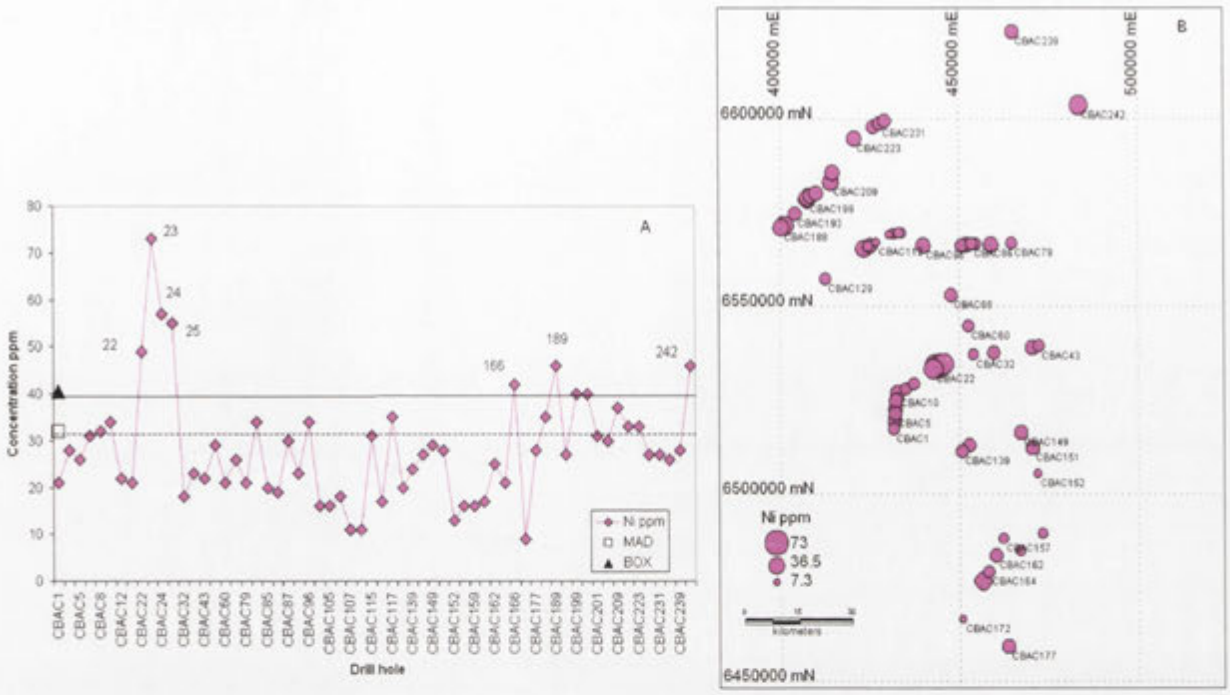

Figure 6.7 Distribution pattern of Ni anomalies with MAD and boxplot (BOX) threshold values (A) and a thematic map of anomalous Ni in the top metre clay-silt-gravel facies (B).

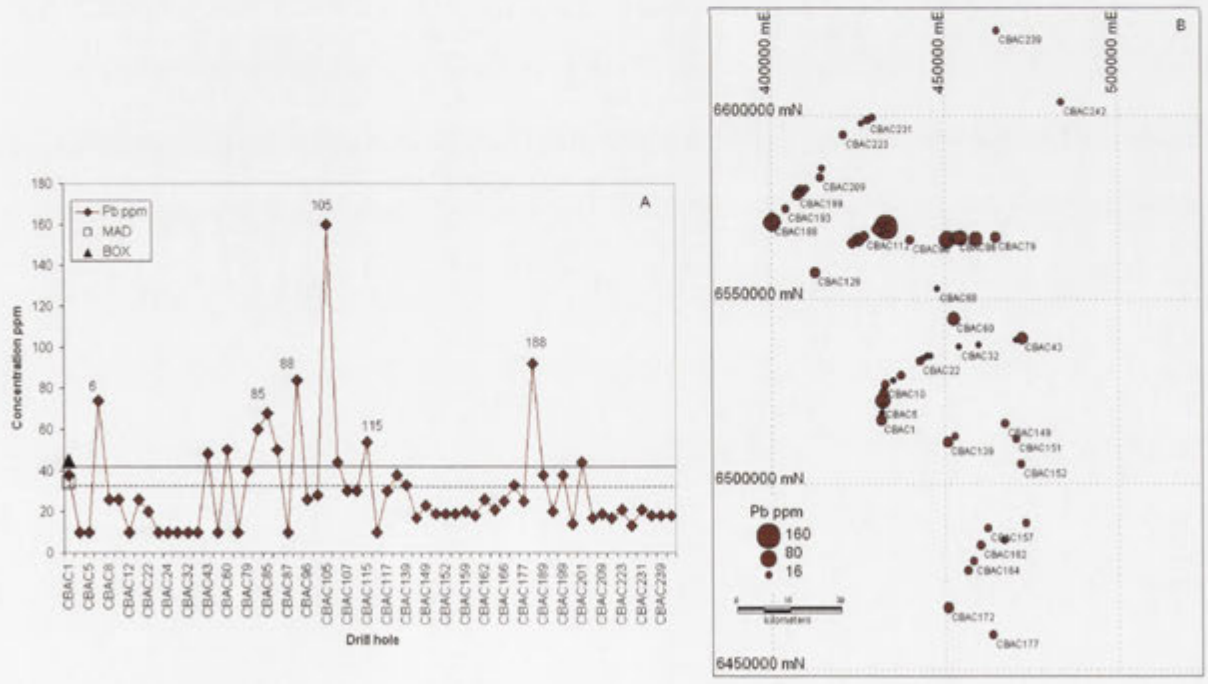

Figure 6.8 Distribution pattern of Pb anomalies with MAD and boxplot (BOX) threshold values (A) and a thematic map of anomalous Pb in the top metre clay-silt-gravel facies (B).

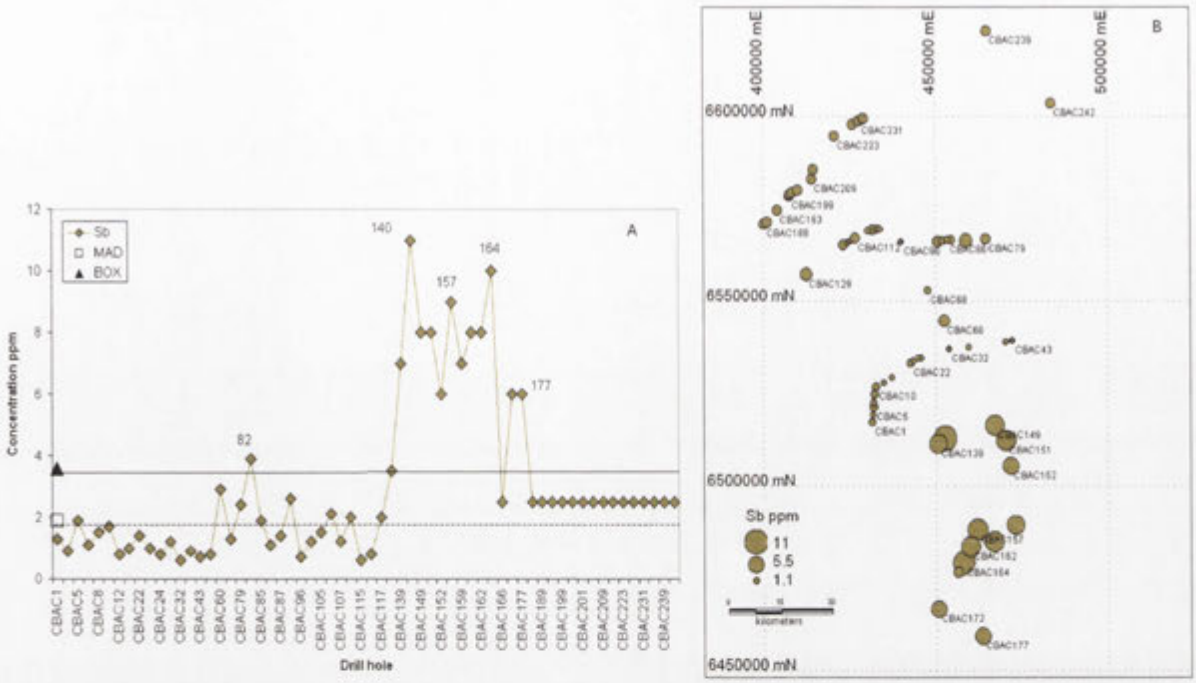

Figure 6.9 Distribution pattern of Sb anomalies with MAD and boxplot (BOX) threshold values (A) and a thematic map of anomalous Sb in the top metre clay-silt-gravel facies (B).

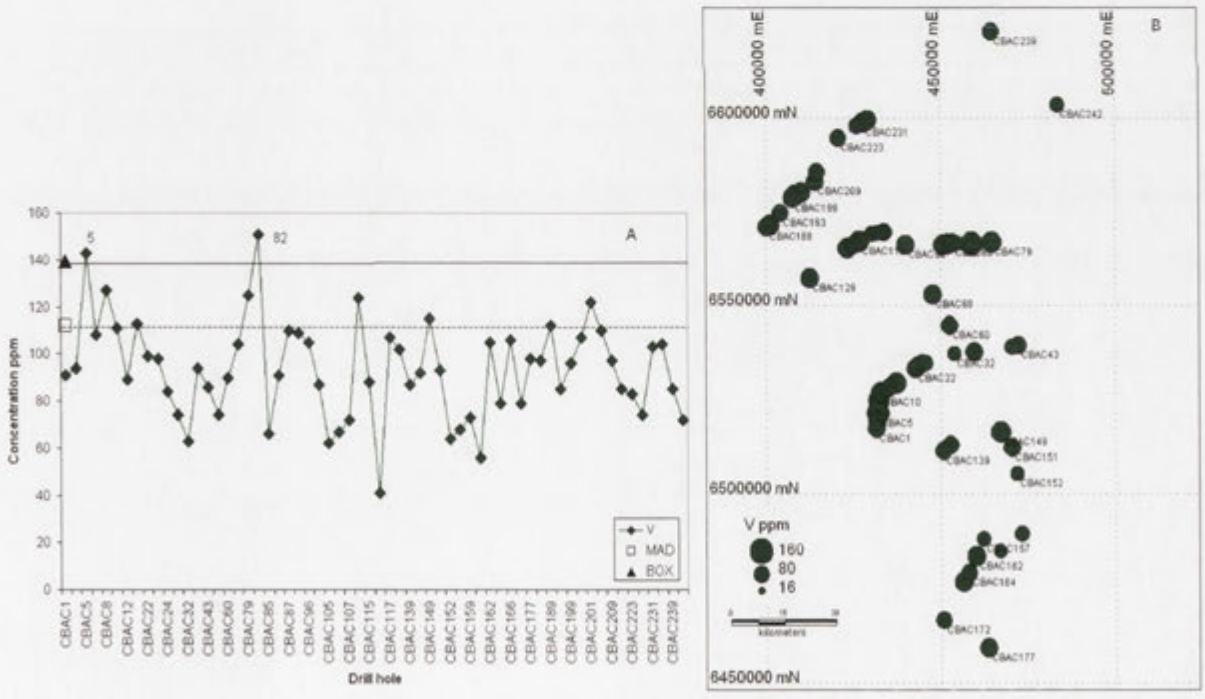

Figure 6.10 Distribution pattern of V anomalies with MAD and boxplot (BOX) threshold values (A) and a thematic map of anomalous V in the top metre clay-silt-gravel facies (B).

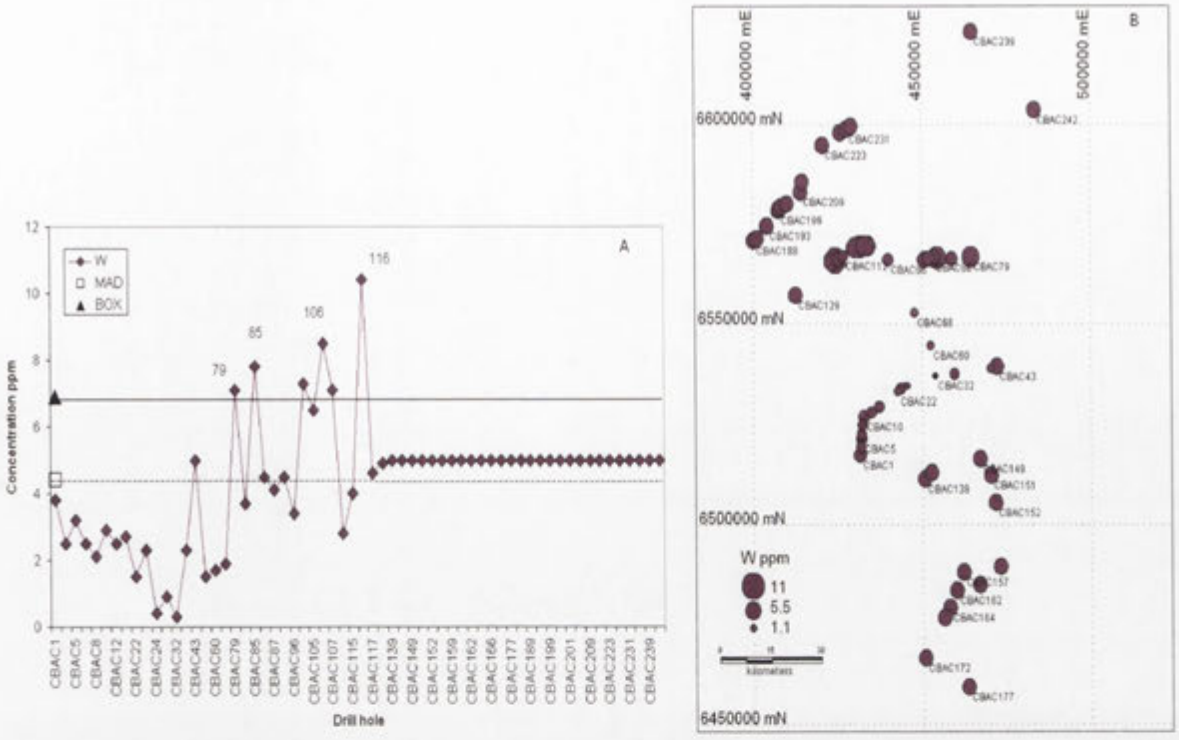

Figure 6.11 Distribution pattern of W anomalies with MAD and boxplot (BOX) threshold values (A) and a thematic map of anomalous W in the top metre clay-silt-gravel facies (B).

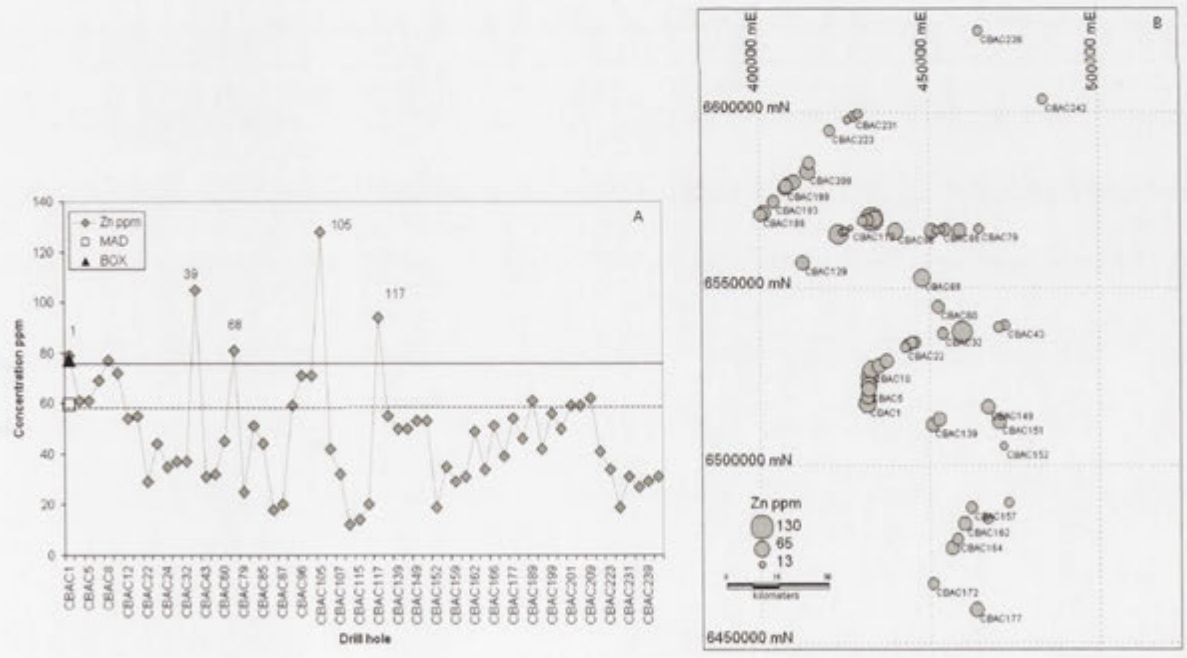

Figure 6.12 Distribution pattern of Zn anomalies with MAD and boxplot (BOX) threshold values (A) and a thematic map of anomalous Zn in the top metre clay-silt-gravel facies (B).

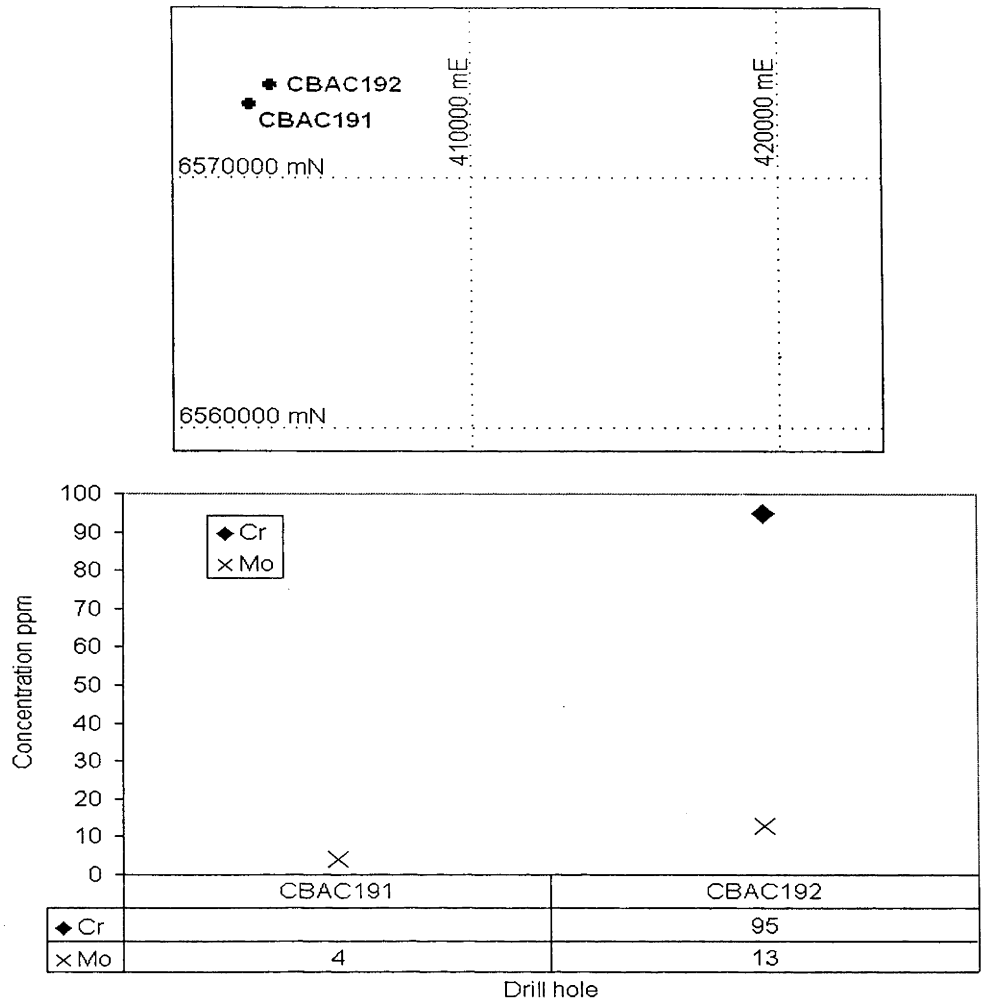

Figure 6.13 Anomalies in Cr and Mo for the regolith carbonate facies in the top metre samples from drill holes CBAC191 and CBAC 92.

hole CBAC29 and with elevated Cu (38 ppm) in drill hole CBAC157. Copper anomalies were also detected from the Sussex and Hermidale areas and range from 31 ppm to 257 ppm. Elevated Cu values are occur in drill holes CBAC1 (257 ppm) and CBAC153 (162 ppm).

Anomalous Cu values are associated with elevated Zn in drill holes CBAC 68, 101, 117, 121 and 124, and with elevated Pb in drill holes CBAC93 and CBAC227. In addition, anomalous Pb is associated with Cr and Ni anomalies in drill holes CBAC224, 225 and 237. Elevated Cr and Ni probably reflect the presence of weathered mafic rocks and elevated Pb could reflect the greater abundance of iron oxides (i.e., hematite) at these sites. Anomalous concentrations of Pb are widely spread over the study area

with notable concentration in the north. The highest anomalous value for Pb (406 ppm) is in drill hole CBAC241 (Tables 6.2,3).

6.3.2.2 ANOMALIES IN THE REGOLITH CARBONATE FACIES

The regolith carbonate facies of the transported regolith is characterised by a number of Au anomalies (Figure 6.14). This gold is not associated with any gold pathfinder elements. Copper anomalies were recorded from drill holes CBAC 20 (52 ppm) and CBAC184 (34 ppm associated with As). Drill hole CBAC162 shows elevated Zn (84 ppm) with elevated Sb (11 ppm). Lead anomalies occur in drill holes CBAC228, CBAC218 and CBAC242 (52 ppm, 57 ppm and 87 ppm respectively) and are not associated within other element anomalies. A single chromium anomaly (106 ppm) was recorded in drill hole CBAC231 (Figure 6.14, Appendix 7).

6.3.2.3 ANOMALIES IN THE IRON- RICH FACIES

The iron-rich facies of the transported regolith is characterised by a number of Au anomalous values ranges from 0.007 ppm to 0.026 ppm. Elevated Au (>0.01 ppm) values were recorded from CBAC103 and CBAC143. These anomalies are not associated with anomalous values of other elements. Elevated values of As, Cr, Pb, Sb and V were observed in CBAC80. Associated Cu and Zn anomalies were observed in CBAC81 (with Au and Ni) and CBAC223 (with Ni). An additional Zn anomaly is also detected from CBAC207 (Figure 6.15 Appendix 7).

6.3.3 ANOMALIES IN THE *IN SITU* REGOLITH

6.3.3.1 CLAY-SILT-GRAVEL FACIES

The clay-silt-gravel facies of the *in situ* regolith contains elevated Au concentrations in drill holes CBAC 63, 157, 188-191 and 217-220. Anomalous Au values are also occur in drill holes CBAC122, 123, 142, 161, 185 (with Co, Sb, W), 195, 199, 211, 238 (with Zn) and 243 (with W). Anomalous Cu is widespread in the area, without any significant correlation with any other element except Zn in drill hole CBAC167. Elevated values of Cu are present in drill holes CBAC1, 7, 37, 50, 80, 115, 116, 119 (with Co, Ni, Zn), 121, 122, 125, 139,143, 155, 168, 171, 177, 195, 205 and 243 (with V). Additional Zn

Table 6.2 Anomalies of As, Au, Co, Cr, Cu, Ni, Pb, V, and Zn from the transported clay–silt-gravel facies of the Sussex and Hermidale areas.

Source	Hole_No.	from (m)	to (m)	As ppm	Au ppm	Co ppm	Cr ppm	Cu ppm	Ni ppm	Pb ppm	Sb ppm	V ppm	W ppm	Zn ppm
Sussex	CBAC1	2	3					257			3.20			
Sussex	CBAC7	1	2					35						
Sussex	CBAC14	3	4	34							3.20	248		
Sussex	CBAC15	3	3.5										7.0	
Sussex	CBAC18	3	4			17.0								
Sussex	CBAC18	8	9				110				3.00	183		
Sussex	CBAC20	1	2					38						
Sussex	CBAC22	1	2						50					
Sussex	CBAC22	4	5						44					
Sussex	CBAC22	5	6						51					
Sussex	CBAC22	9	10				115							
Sussex	CBAC22	10	11						44					
Sussex	CBAC22	11	12						43					
Sussex	CBAC22	20	24	21										
Sussex	CBAC23	1	2						55					
Sussex	CBAC23	5	6						46					
Sussex	CBAC23	6	7						42					
Sussex	CBAC23	7	8				110		46					
Sussex	CBAC29	16	20		0.018		115					158		
Sussex	CBAC30	8	9										10.5	
Sussex	CBAC46	3	4										7.9	
Sussex	CBAC52	5	6		0.024									
Sussex	CBAC52	9	10		0.012									
Sussex	CBAC53	10	11		0.005									
Sussex	CBAC63	1	2		0.098									
Sussex	CBAC64	1	2	24	0.005	25.0								
Sussex	CBAC65	2	3		0.005									
Sussex	CBAC67	2	3										8.0	
Sussex	CBAC68	1	2					35						81.0
Sussex	CBAC72	1	2					32						
Sussex	CBAC73	1	2									166		
Sussex	CBAC73	2	3											67.0
Sussex	CBAC74	1	2							42				
Sussex	CBAC74	18	24		0.007									
Sussex	CBAC74	24	30		0.005									
Sussex	CBAC76	5	6		0.011									
Sussex	CBAC77	1	2									202		
Sussex	CBAC78	4	5					31						
Sussex	CBAC78	5	6			20.0								
Sussex	CBAC78	8	9					36						
Sussex	CBAC78	12	18					32						
Sussex	CBAC80	1	2											86.0
Sussex	CBAC83	1	2					34						
Sussex	CBAC84	1	2								2.90			
Sussex	CBAC92	1	2					39						
Sussex	CBAC93	1	2					44		92				
Sussex	CBAC93	5	6					34						
Sussex	CBAC94	3	4		0.005									
Sussex	CBAC99	1	2							40				
Sussex	CBAC100	1	2		0.005									121.0
Sussex	CBAC101	1	2					41				148	7.1	97.0
Sussex	CBAC102	1	2									142		
Sussex	CBAC103	1	2										7.3	
Sussex	CBAC104	1	2											77.0
Sussex	CBAC104	9	10								3.00		8.3	
Sussex	CBAC105	1	2							40				
Sussex	CBAC105	11	12											
Sussex	CBAC106	1	2							50			13.7	
Sussex	CBAC116	1	2										12.6	
Sussex	CBAC117	1	2					54						86.0
Sussex	CBAC121	1	2					49					10.0	79.0
Sussex	CBAC124	1	2					39					8.5	80.0
Sussex	CBAC126	1	2							60				
Sussex	CBAC128	4	5					40						
Sussex	CBAC137	4	5										7.4	
Sussex	CBAC138	7	8										11.4	
Sussex	CBAC138	9	10										9.9	
Sussex	CBAC138	10	11		0.026									
Hermidale	CBAC146	3	4								6.00			
Hermidale	CBAC146	6	7								7.00			
Hermidale	CBAC148	3	4								11.00			
Hermidale	CBAC148	5	6								13.00			
Hermidale	CBAC150	1	2								8.00			
Hermidale	CBAC150	3	4								10.00			
Hermidale	CBAC153	1	2		0.005									
Hermidale	CBAC153	2	3		0.006						6.00			
Hermidale	CBAC153	3	4					162						
Hermidale	CBAC153	6	7								7.00			
Hermidale	CBAC154	7	8								7.00			
Hermidale	CBAC154	8	9		0.005									
Hermidale	CBAC155	1	2											67.0
Hermidale	CBAC155	9	11		0.023									
Hermidale	CBAC155	11	13		0.005									
Hermidale	CBAC155	13	15		0.006									
Hermidale	CBAC157	2	3								6.00			
Hermidale	CBAC157	3	4											
Hermidale	CBAC157	5	6		0.005			38			6.00			
Hermidale	CBAC157	7	8		0.007									
Hermidale	CBAC158	17	21											81.0
Hermidale	CBAC159	0	1		0.005						7.00			
Hermidale	CBAC169	1	2								5.00			
Hermidale	CBAC169	2	3								7.00			
Hermidale	CBAC182	1	2			17.0								
Hermidale	CBAC183	8	9		0.008									
Hermidale	CBAC183	29	33								7.00			
Hermidale	CBAC185	5	6								8.00			
Hermidale	CBAC185	6	7								10.00			
Hermidale	CBAC185	7	8								7.00			
Hermidale	CBAC186	2	3								6.00			
Hermidale	CBAC186	7	8								5.00			
Hermidale	CBAC187	3	4								6.00			
Hermidale	CBAC187	6	7								7.00			

Table 6.3 Anomalies of Co, Cr, Mo, Ni, Pb and V from the transported clay-silt-gravel facies of the Byrock area.

Source	Hole_No.	from (m)	to (m)	Co ppm	Cr ppm	Cu ppm	Mo ppm	Ni ppm	Pb ppm	V ppm	W ppm
Byrock	CBAC199	2	3		189						
Byrock	CBAC218	6	7						40		
Byrock	CBAC219	5	6				10.0				
Byrock	CBAC220	3	4				8.0				
Byrock	CBAC221	5	6	18.0							
Byrock	CBAC221	7	8				10.0				
Byrock	CBAC221	12	13				10.0				
Byrock	CBAC222	2	3				8.0				
Byrock	CBAC222	3	4		108		14.0				
Byrock	CBAC222	4	5				10.0				
Byrock	CBAC223	4	5				17.0	44			
Byrock	CBAC223	6	7				9.0		45		
Byrock	CBAC223	7	8				7.0				
Byrock	CBAC223	8	9				14.0				
Byrock	CBAC223	9	10				12.0		41		
Byrock	CBAC223	15	16				10.0	50			
Byrock	CBAC223	19	20				8.0				
Byrock	CBAC224	2	3				7.0				
Byrock	CBAC224	3	4		110		17.0	52	42		
Byrock	CBAC224	4	5		110		11.0		66		
Byrock	CBAC224	5	6						41		
Byrock	CBAC224	9	10						61		
Byrock	CBAC224	12	13				12.0				
Byrock	CBAC225	4	5				9.0				
Byrock	CBAC225	5	6		115		12.0	83	43		
Byrock	CBAC225	15	16				10.0		51		
Byrock	CBAC225	18	19						50		
Byrock	CBAC225	21	22				8.0				
Byrock	CBAC225	24	25				11.0		45		
Byrock	CBAC226	15	16				10.0				
Byrock	CBAC226	21	22				8.0				
Byrock	CBAC226	24	25								
Byrock	CBAC226	30	31		73		11.0		55		
Byrock	CBAC226	33	34		115		9.0		55		
Byrock	CBAC227	15	16			32	11.0		53		
Byrock	CBAC228	17	18							205	
Byrock	CBAC232	2	3	17.0			7.0				
Byrock	CBAC232	3	4				7.0				
Byrock	CBAC232	4	5				8.0				
Byrock	CBAC232	5	6	23.0				47			
Byrock	CBAC232	6	7				13.0		131		
Byrock	CBAC232	7	8				11.0		53		
Byrock	CBAC234	4	5								11.0
Byrock	CBAC234	5	6						46		
Byrock	CBAC234	6	7						51		13.0
Byrock	CBAC234	8	9								12.0
Byrock	CBAC237	2	3				8.0				
Byrock	CBAC237	15	16				7.0				
Byrock	CBAC237	18	19				7.0				
Byrock	CBAC237	27					7.0				
Byrock	CBAC237	30	31				8.0		52		
Byrock	CBAC237	33	34		253		24.0	48	177		
Byrock	CBAC237	36	37				9.0		44		
Byrock	CBAC237	39	40				16.0		49		
Byrock	CBAC237	42	43				13.0		115		
Byrock	CBAC238	1	2				7.0				
Byrock	CBAC241	1	2	19.0				43			
Byrock	CBAC241	2	3				9.0				
Byrock	CBAC241	3	4				12.0				
Byrock	CBAC241	8	9				9.0				
Byrock	CBAC241	25	31						211		
Byrock	CBAC241	26	27						48		
Byrock	CBAC241	27	28						406		
Byrock	CBAC241	28	29						203		
Byrock	CBAC241	29	30						130		10.0
Byrock	CBAC241	30	31						70		10.0
Byrock	CBAC241	31	34						53		
Byrock	CBAC242	8	9				14.0				
Byrock	CBAC242	9	10		130		27.0	57			
Byrock	CBAC242	12	13				13.0				
Byrock	CBAC242	14	15								
Byrock	CBAC242	17	18				14.0				
Byrock	CBAC243	1	2								
Byrock	CBAC243	2	3				9.0				
Byrock	CBAC243	7	8				10.0		40		
Byrock	CBAC243	9	10				8.0				
Byrock	CBAC245	4	5				7.0				
Byrock	CBAC247	1	2	21.0				51			
Byrock	CBAC247	2	3				12.0				
Byrock	CBAC247	3	4				9.0				
Byrock	CBAC247	8	9				7.0			140	
Byrock	CBAC247	14	15				7.0				10.0
Byrock	CBAC247	15	21								

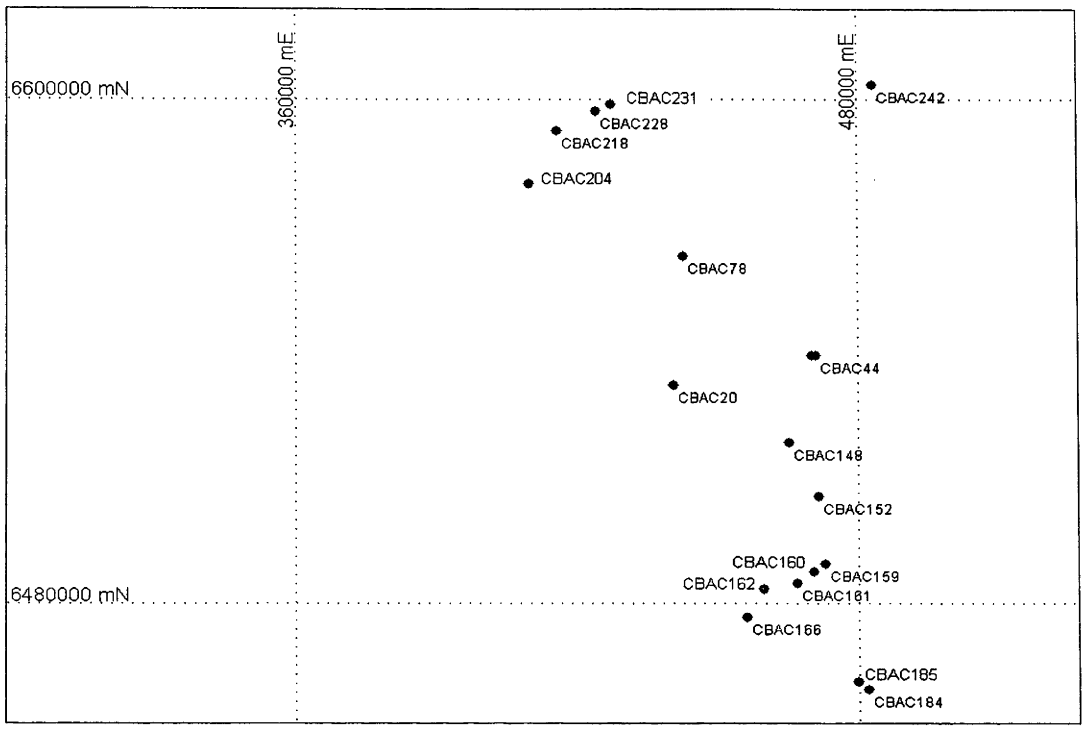

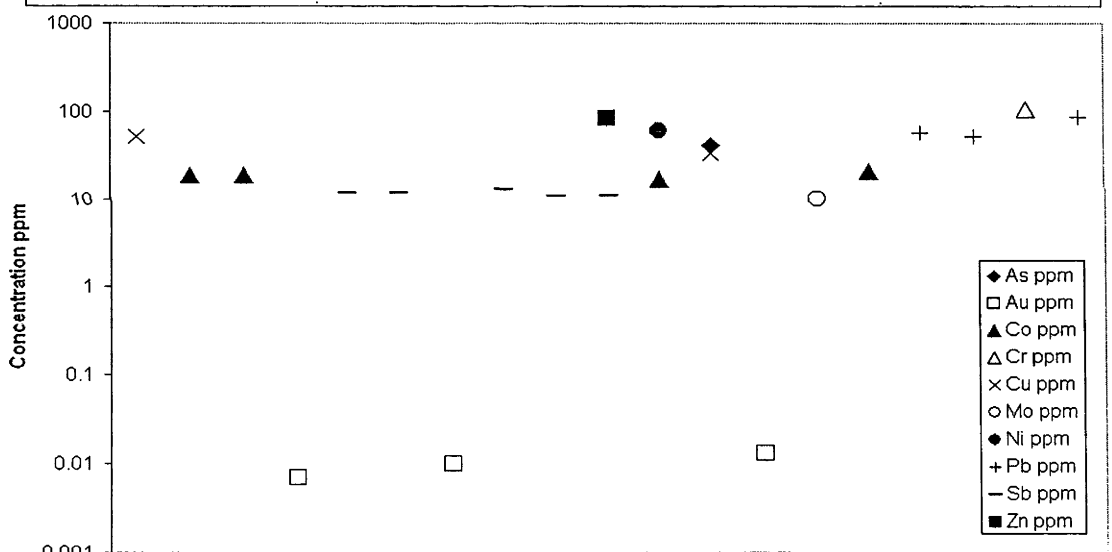

	CBAC20	CBAC44	CBAC45	CBAC78	CBAC148	CBAC152	CBAC159	CBAC160	CBAC161	CBAC162	CBAC166	CBAC184	CBAC185	CBAC204	CBAC204	CBAC218	CBAC228	CBAC231	CBAC242
From m	2	2	1	6	2	6	1	4	1	1	1	3	8	1	2	7	9	5	3
To m	3	3	2	7	3	7	2	5	2	2	2	4	9	2	3	8	10	6	4

Figure 6.14 Anomalies of As, Au, Co, Cr, Cu, Mo, Ni, Pb, Sb, V and Zn in the regolith carbonate facies of the transported regolith.

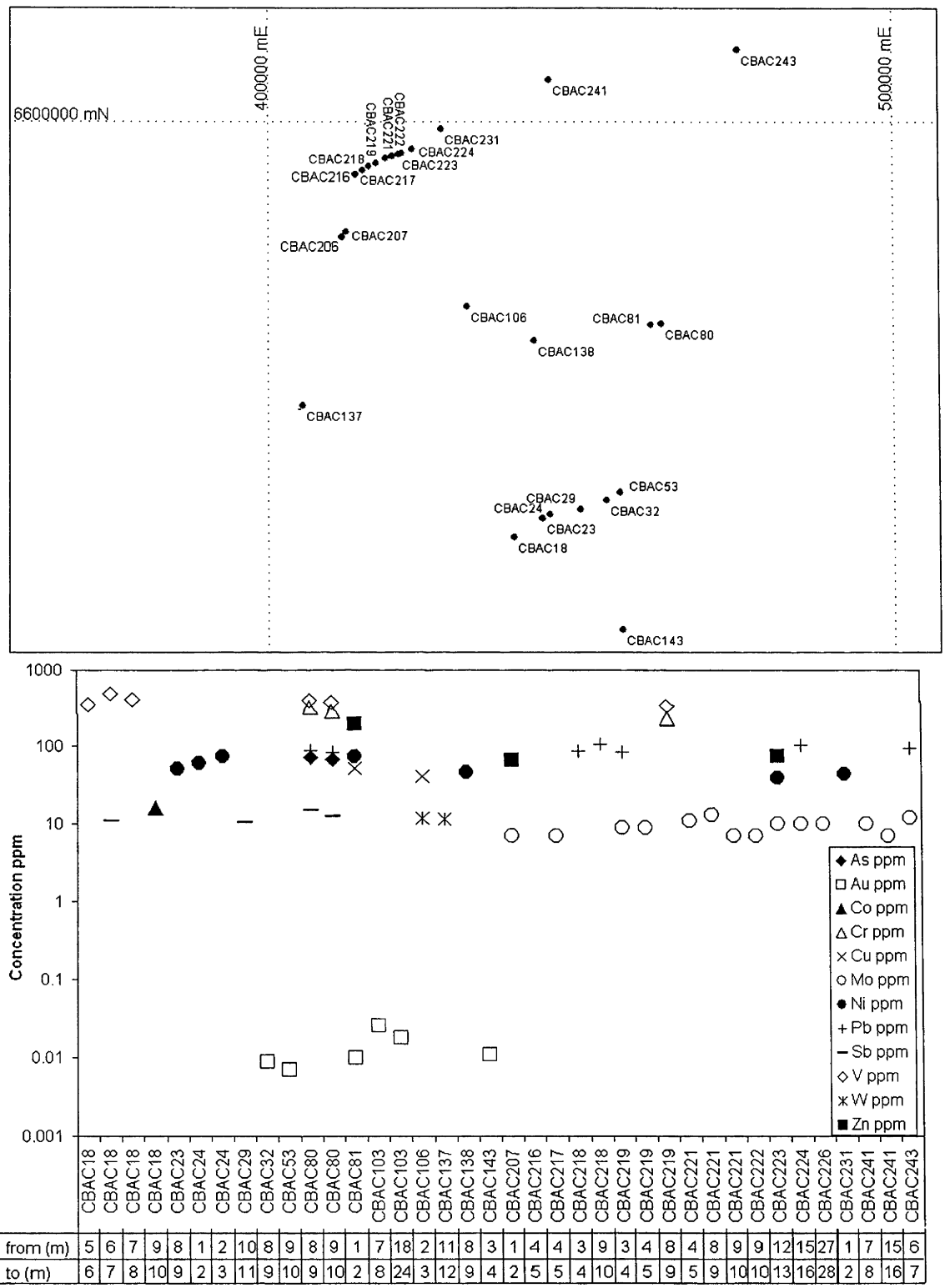

Figure 6.15 Anomalies of As, Au, Cr, Cu, Mo, Ni, Pb, Sb, V, W, and Zn in the Fe-rich facies of the transported regolith.

anomalies also occur in drill holes CBAC104, 109, 120,142,144, 146, 175, 177,191 (with W), 198, 201 (with Ni), 218, 238 (with Au) and 243. Elevated Pb concentrations (Pb> 150) occur in drill holes CBAC14, 16,44, 47, 60, 198, and 218 (with Au). The highest Pb anomaly (Pb = 1010 ppm) was detected from drill hole CBAC198 (Figure 6.16, Appendix 7).

6.3.3.2 ANOMALIES IN THE REGOLITH CARBONATE FACIES

The regolith carbonate facies is characterised by elevated Au contents (≥ 0.01) observed in drill holes CBAC41, CBAC64, CBAC188 and CBAC204. In CBAC41 and CBAC64 elevated Au is associated with Sb anomalies, whereas in CBAC188 Au is associated with elevated Pb and W values, and in CBAC204 Au is associated with Cr and Mo anomalies. Anomalous Cu values range from 50 ppm to 283 ppm. Significant Cu anomalies of 277 ppm and 283 ppm were observed in drill hole CBAC6 and CBAC85 respectively, where elevated Cu is not associated with anomalies in any other element. Anomalous Cu is associated with elevated Pb and As in drill hole CBAC2. Major concentrations of Zn were observed in drill holes 69 (with Cu), 81, 121 (partly with Co), 167 (with W), 169 (with Sb) and 198 (Figure 6.17, Appendix 7).

6.3.3.3 ANOMALIES OF THE IRON-RICH REGOLITH FACIES

Anomalies in the Fe-rich saprolite facies are summarised in Figure 6.18 and Appendix 7. Elevated Au is associated with As and Mo in drill hole CBAC204. Arsenic is also accompanied by elevated Cr, Pb, Sb and V in drill hole CBAC237 and with elevated Cu in drill hole CBAC243. Another elevated Cu value was observed in drill hole CBAC246 (62-63 m) and is associated with high Ni and Zn contents. The anomalous association between Cu, Ni, Cr and V was also observed in drill hole CBAC16. Elevated Zn values are associated with elevated Ni in drill holes CBAC27 and CBAC246, and with high Pb contents in dill holes CBAC104 and CBAC205 (with Sb). Chromium anomalies occur in drill holes CBAC65 and CBAC 231 (with Mo, Sb, V).

6.3.3.4 ANOMALIES IN THE MANGANESE-RICH FACIES

In the Mn-rich facies of the *in situ* regolith (Figure 6.19, Appendix 7), Anomalous As was observed in drill holes CBAC174 and 167. In CBAC174, As is associated with elevated Zn. Elevated Au values range from 0.022 ppm to 0.077 ppm and occur in drill holes CBAC122 (3-5m) associated in the upper part with Co (287 ppm), Cu (129 ppm)

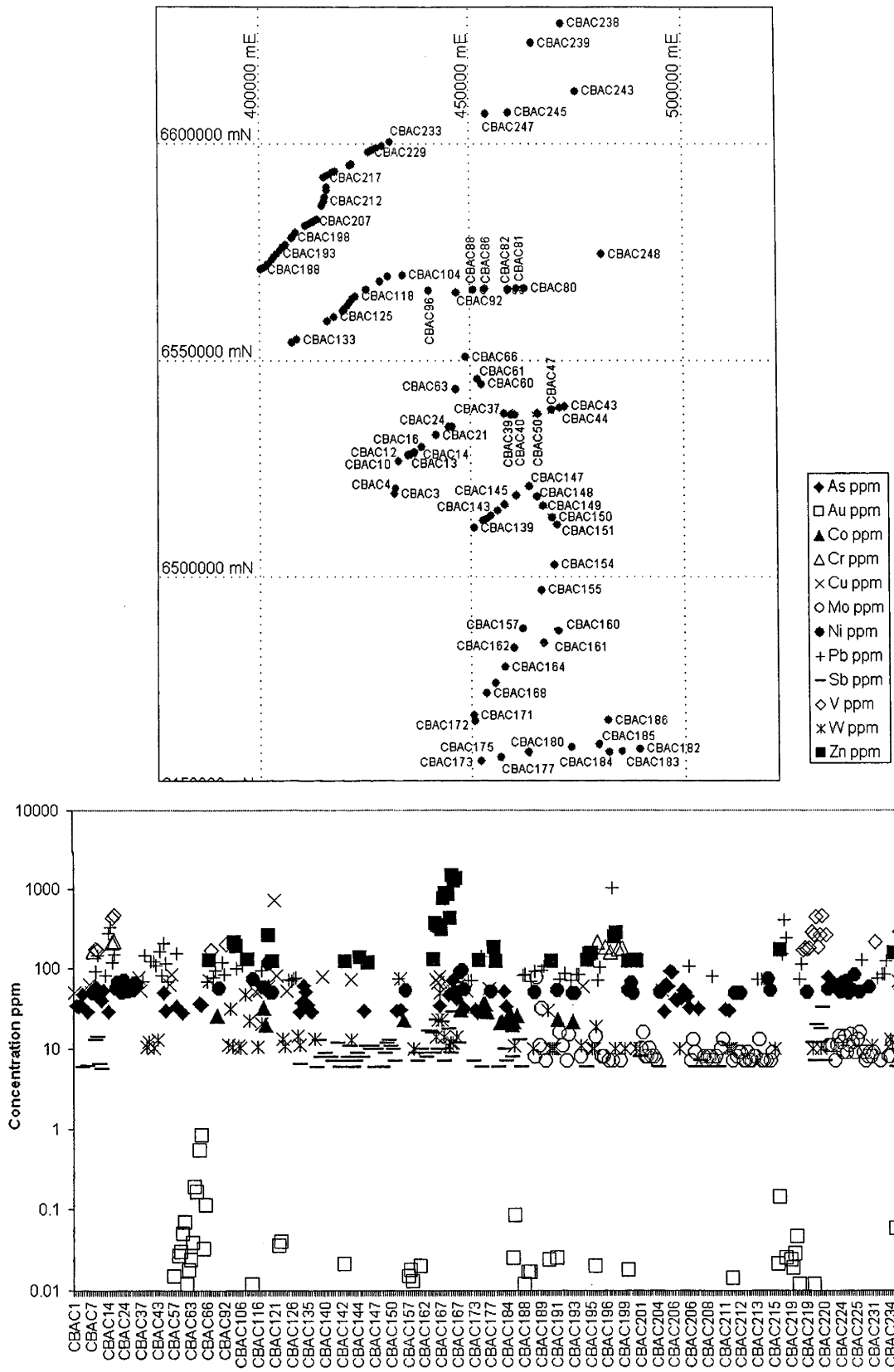

Figure 6.16 Anomalies of As, Au, Co, Cr, Cu, Ni, Pb, Sb, V and Zn in the *in situ* clay-silt-gravel facies. Data for this figure are in Appendix 7.

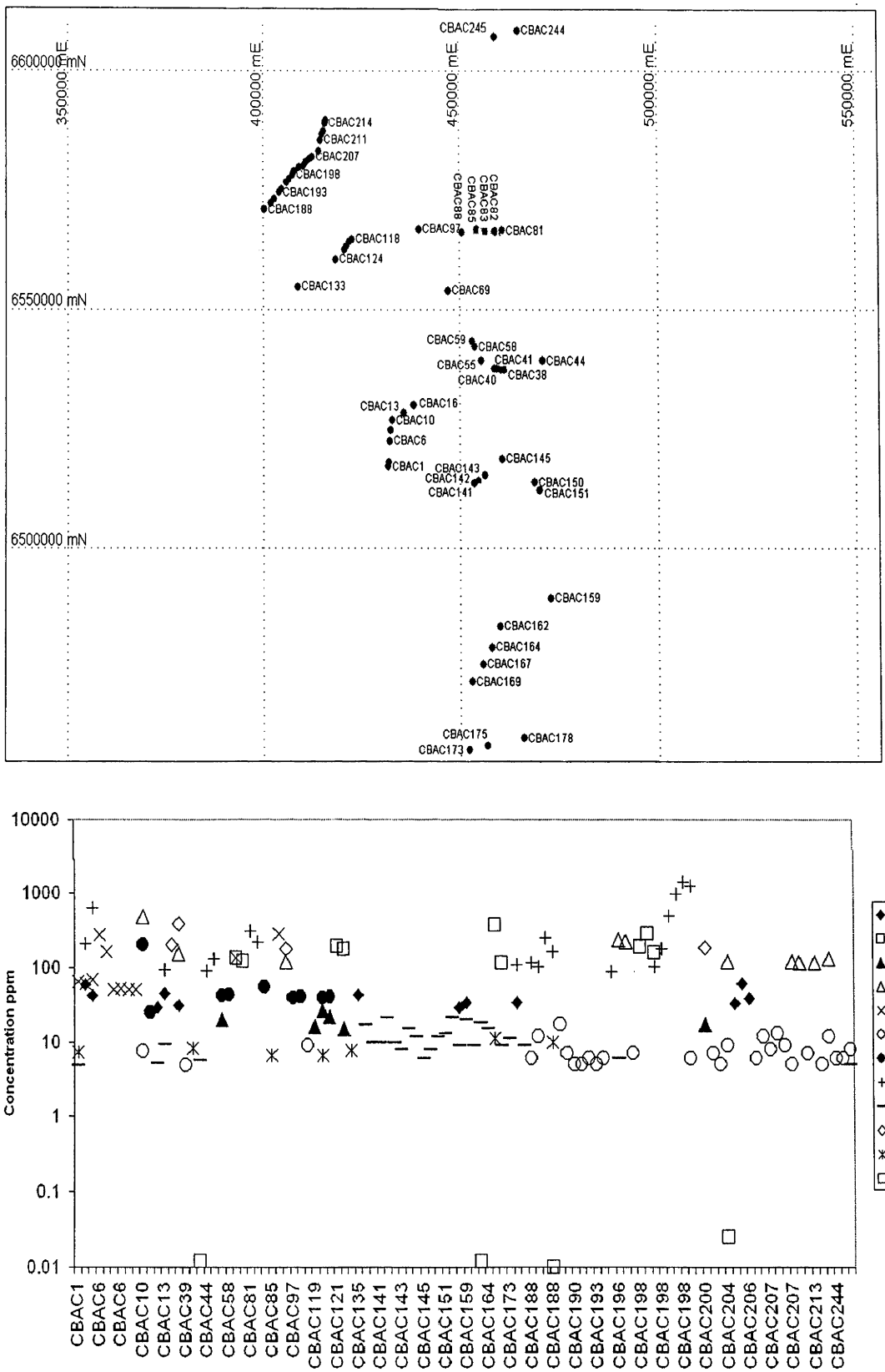

Figure 6.17 Anomalies of As, Au, Co, Cr, Cu, Mo, Ni, Pb, Sb, V, W and Zn in the regolith carbonate facies of the *in situ* regolith. Data for this figure are in Appendix 7.

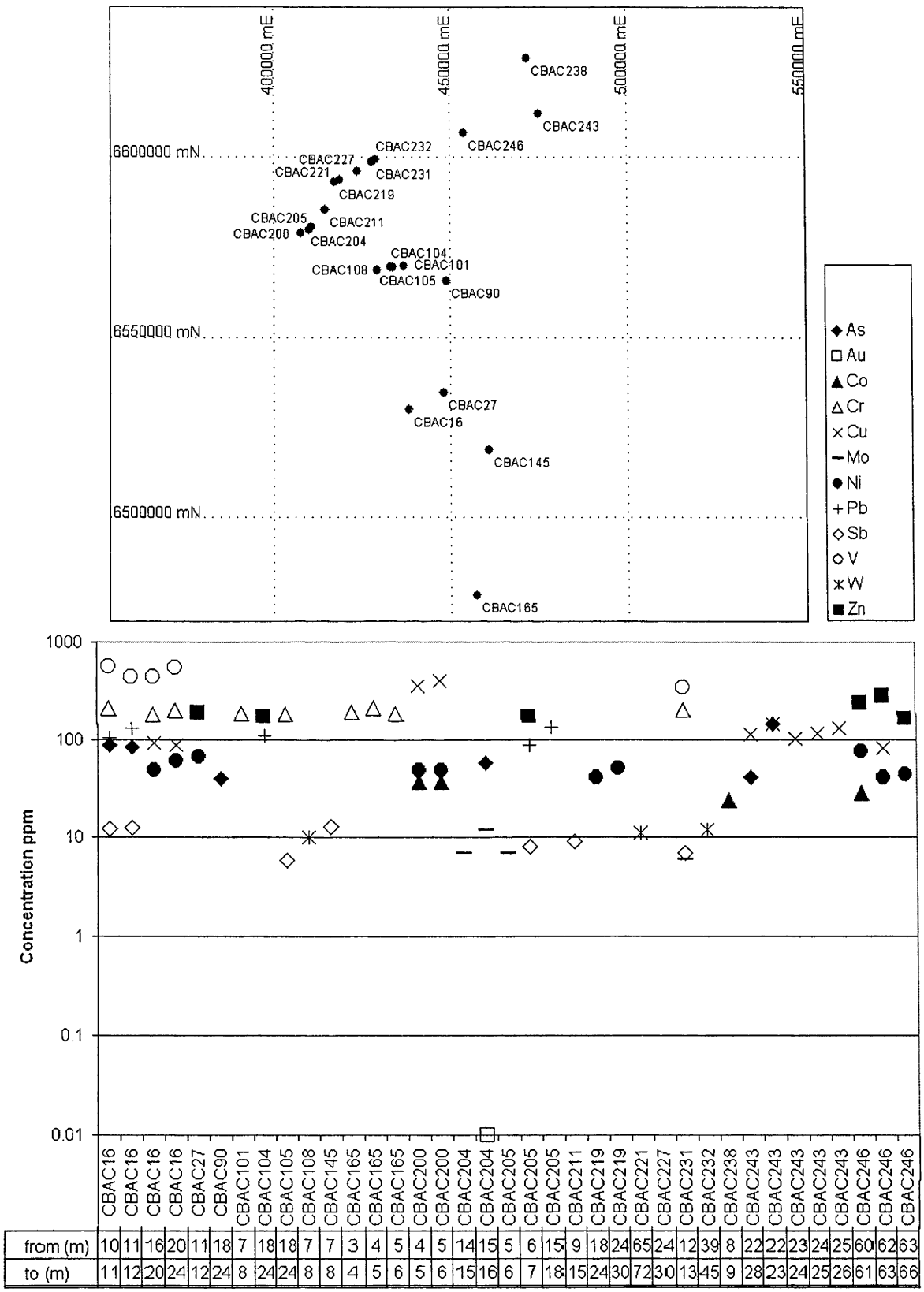

Figure 6.18 Anomalies of As, Au, Co, Cr, Cu, Ni, Pb, Sb, W and Zn in the Fe-rich facies of the *in situ* regolith.

and Ni (190 ppm) anomalies; CBAC123 (1-2 m), CBAC191 (20-21 m), CBAC195 (31 - 32 m) and CBAC198 (15-17 m) associated in the upper part with Co (674 ppm), Cu (155 ppm), Ni (126 ppm) and Pb (212 ppm). Cobalt anomalies range from 182 ppm to 674 ppm. In addition to the previously mentioned anomalies of Co with Au, elevated Co values of 254 ppm, 259 ppm and 415 ppm occur in drill holes CBAC 211, CBAC191 and 177 (associated with Cu and Ni) respectively. A chromium anomaly (155 ppm) is present in drill hole CBAC195 (27-33 m). Anomalies of Cu closely correlated with elevated Ni occur in drill holes CBAC 122, 177 and 198 (as mentioned above). A Ni anomaly (161 ppm) occurs in drill hole CBAC201 (27-33 m). Two anomalous Pb values (78 ppm and 86 ppm) were observed in drill holes CBAC 118 (5-6 m) and CBAC 119 (0-1 m) respectively. Other elevated Pb values were found in drill hole CBAC198 (15-71 m). Zinc anomalies occur in drill holes CBAC167 associated with elevated As, CBAC174, CBAC176 and CBAC198 (Figure 6.19, Appendix 7).

6.4 ELEMENT ASSOCIATIONS

Cluster analysis (CA) was used to explore the relationships between As, Au, Ba, Co, Cr, Cu, Mo, Ni, Pb, Sb, V and Zn in addition to major elements Ca, Fe, Mg and Mn. Elements were excluded from the analysis when more than 30% of their records are below detection limits (i.e., Au, As, Bi, Sb and W). Aluminium and K values were also excluded because of potential errors for these elements in the analytical technique, particularly at high concentration (Chan *et al* 2001). As explained in the data analysis chapter, cluster analysis is an explorative technique that provides a reduction in the dimensions of the data by classifying them into groups.

Dendrograms of the inter-elemental relationships in the top metre, transported and *in situ* regolith facies are shown in Figures 6.20 and 6.21. Groups (Clusters) of elements at selected Similarity Distance Levels (SDL=10) represent element associations at that level. For more detailed investigations, such as element-to-element relationship, the clustering needs to be decided on high similarity level (low SDL).

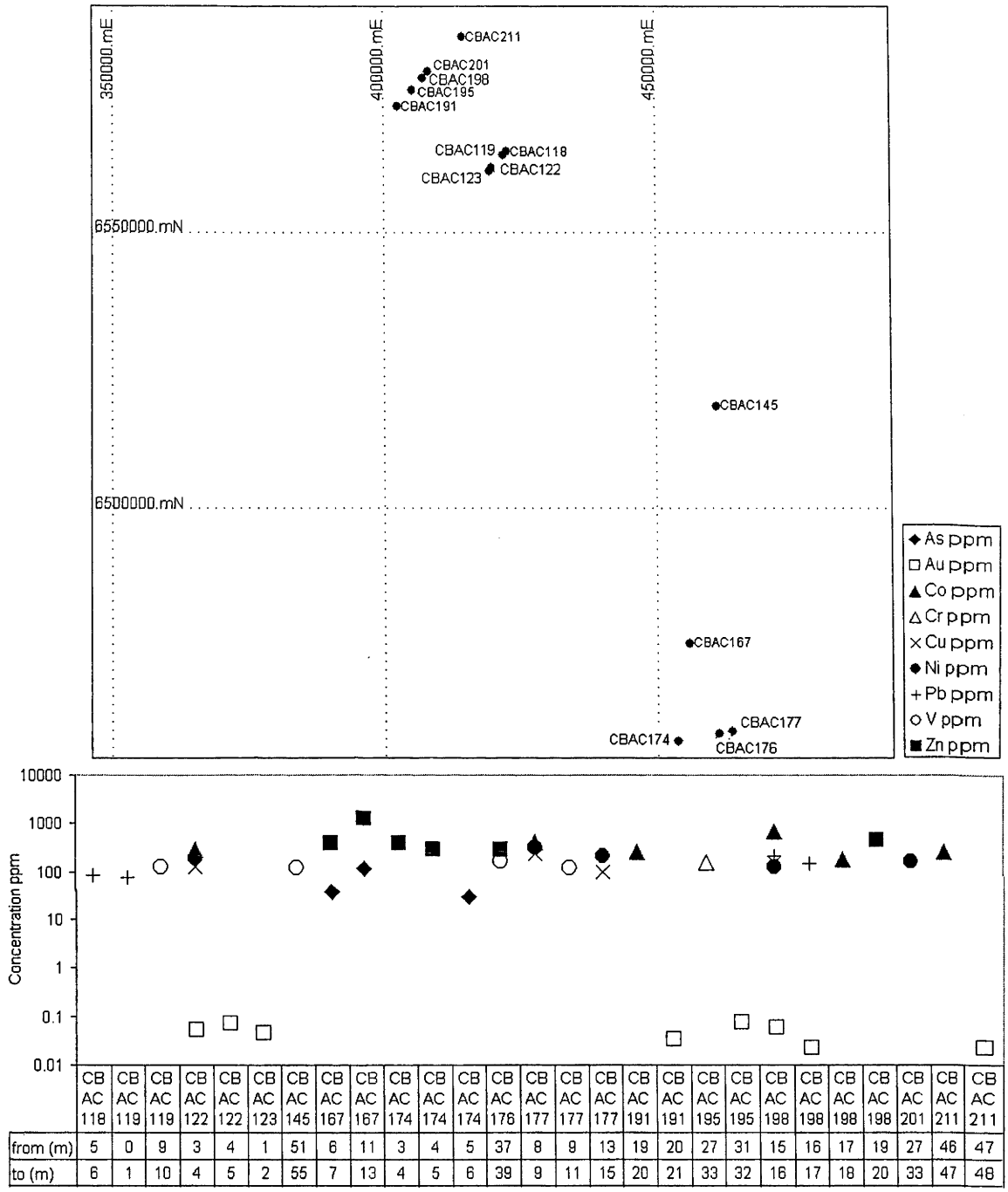

	CBAC118	CBAC119	CBAC119	CBAC122	CBAC122	CBAC123	CBAC145	CBAC167	CBAC167	CBAC174	CBAC174	CBAC174	CBAC176	CBAC177	CBAC177	CBAC177	CBAC191	CBAC191	CBAC195	CBAC195	CBAC198	CBAC198	CBAC198	CBAC198	CBAC201	CBAC211	CBAC211
from (m)	5	0	9	3	4	1	51	6	11	3	4	5	37	8	9	13	19	20	27	31	15	16	17	19	27	46	47
to (m)	6	1	10	4	5	2	55	7	13	4	5	6	39	9	11	15	20	21	33	32	16	17	18	20	33	47	48

Figure 6.19 Anomalies of As, Au, Co, Cr, Cu, Ni, Pb and Zn in the *in situ* Mn- rich facies.

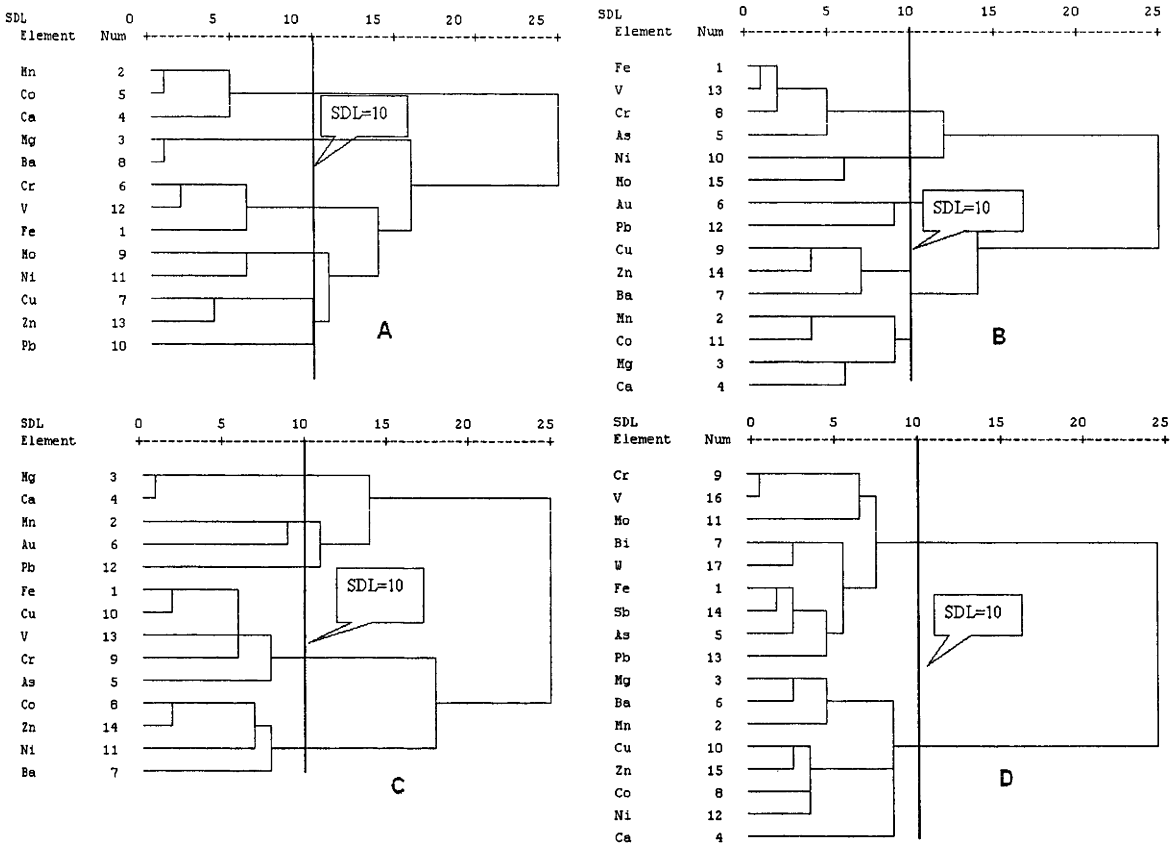

Figure 6.20 Elements cluster dendrograms of the clay-silt-gravel facies of the top metre regolith unit (A) and the transported regolith unit clay-silt-gravel facies (B), regolith carbonate facies (C) and (D) Fe-rich facies. SDL represents similarity distance level (see the text)

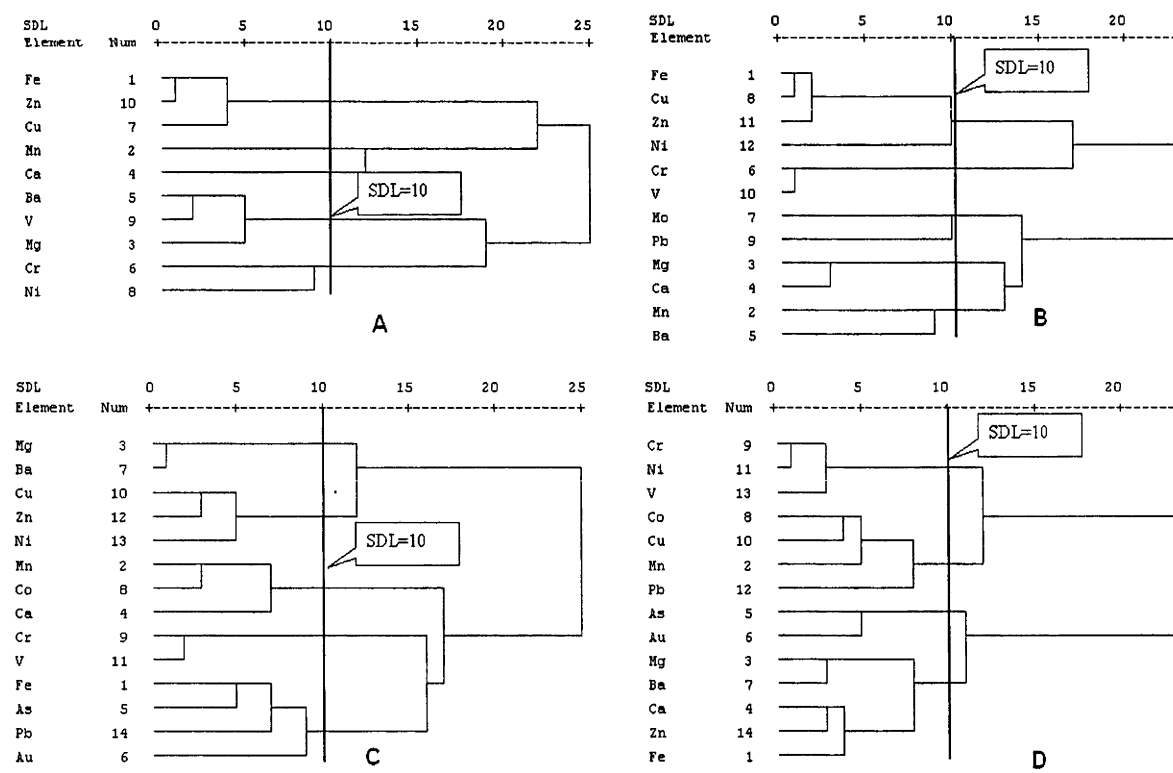

Figure 6.21 Elements cluster dendrograms of the *in situ* regolith unit. (A) Clay-silt-gravel facies, (B) regolith carbonate facies, (C) Fe-rich facies and (D) Mn-rich facies. DSL represents similarity distance level (see the text).

Principal component analysis (PCA) is also applied to determine the main geological components (processes) that control the suggested element associations. Significant components were determined based on total variance explanations. The statistical stages in calculating the total explained variance, component (factor) statistics table and extracting the desired number of components using SPSS statistical software have been described by Coakes and Steed (2001). The final rotated factor matrices [loadings of variables (elements) on components (processes)] for the regolith facies are displayed in Tables 6.4 and 6.5. These variables have a loading of 0.3 or greater on at least one component and they explain ≥69% of total variance (except in clay-rich *in situ* regolith = 61). Complex variables may have high loadings on more than one component.

The element associations of the regolith facies in the Girilambone region are summarised in Table 6.6. In the top meter it was only possible to analyse the clay-silt-gravel facies because of the small number of samples with regolith carbonate and Fe-rich facies (< 10 samples). Utilizing cluster and principal component analyses to determine element association shows that the pathfinder elements in the regolith environment are mainly associated with Fe, Mn or Ca-Mg, in addition to a few single element clusters or components. These associations are:

- Iron in the clay-silt-gravel facies of the top metre unit, and generally in all transported regolith units, is mainly associated with Cr-V ± Ni ± As ± Cu ± Zn ± Pb ± Sb. Part of this association (Fe-V-Cr) probably reflects association of these elements in iron oxide minerals (particularly hematite) and/or to lesser extent the influence of intrusive mafic and ultramafic rocks.

- In the *in situ* regolith clay-gravel and regolith carbonate facies Fe is significantly associated with Cu and Zn whereas in the Fe- and Mn- rich facies it associates with As-Pb-Au and As, Zn, Ca, Ba, Mg and V respectively. PCA generally shows that Fe enrichment is possibly controlling the dispersion of Cu+ Zn +V± Pb ± As in all *in situ* facies. The significant associations of Cu and Zn with Fe and Mn are possibly related to absorption of these metals by Fe and Mn oxide/oxyhydroxide minerals.

- Manganese is associated with Ca-Co ± Cu in the clay-gravel facies of the top metre and transported regolith, transported regolith carbonate facies and Mn-rich *in situ* facies. This association reflects Mn oxide/oxyhydroxide minerals (e.g., lithiophorite, todorokite, birnessite) that can accommodate Co and Ca in their structures. Energy dispersive X-ray Analysis (EDXA) of Mn minerals explored this

Table 6.4 The rotated factor matrices with loading of elements on each component of the principal component analysis. Table A represents clay-silt-gravel faces of the top metre. B, C and D represent clay-silt and gravel, Ca-Mg and Fe rich facies of the transported regolith, respectively.

	Component				
	1	2	3	4	5
Cr	.879				
V	.876				
Fe	.814	-.331			
Ca		.789	-.315		
Co		.685	.363		
Mn	-.458	.685			
Pb	-.509	-.583			
Zn			.944		
Cu			.716		.506
Ni			.622	-.348	.341
Mg				.933	
Ba		-.495		.758	
Mo					.946

A

	Component				
	1	2	3	4	5
Fe	.898				
V	.772			.309	
Cr	.769			.396	
As	.696	-.307			
Cu	.578	.544	.326		
Co		.789			
Zn		.656	.558		
Mn	-.369	.593			.342
Mg			.740		
Ba			.651		
Mo			-.571	.433	
Au				-.800	
Ni		.340		.720	
Pb					-.829
Ca					.717

B

	Component				
	1	2	3	4	5
Fe	.822		.311		
V	.778				
Cr	.675				-.327
Cu	.641		.577		
As	.602				
Mg		.923			
Ca		.820			
Ni		-.811			
Co		-.308	.827		
Zn			.801		
Mn			.637		
Pb				-.876	
Ba			.387	.671	
Au					.882

C

	Component					
	1	2	3	4	5	6
V	.877					
Cr	.859					
Pb		.793				
As		.675				
Fe	.581	.657				
Sb		.634				
Bi	.324		.716			
Cu			-.707	.301		
W			.660	.326		
Co	-.426		-.540			
Ni		-.301		.817		
Ca			-.421	-.766		
Mn					.727	
Mg		-.332			.697	.397
Ba					.641	
Mo						-.852
Zn				.605		.663

D

Table 6.5 The rotated factor matrices with loading of elements on each component of the principal component analysis. Tables A, B, C and D represent clay-silt and gravel facies, regolith carbonate facies, Fe- rich facies and Mn- rich facies of the *in situ* regolith, respectively.

	Component		
	1	2	3
V	.85		
Ba	.69		.39
Cr	.68		-
Mn	-		
Zn		.85	
Fe		.84	
Cu		.73	
Ni			-
Mg	.42		.67
Ca	-		.57

A

	Component			
	1	2	3	4
Fe	.901			
Cu	.875			
Zn	.870			
Ni	.506			
V		.904		
Cr		.903		
Ca	-.371		.732	
Pb		-.328	-.686	
Mg	-.504		.626	
Mo				-.747
Ba				.736
Mn			.458	.522

B

	Component				
	1	2	3	4	5
V	-.838				
Cr	-.805				
Cu	.658		.375	-.331	
Ni	.654				
Au		-.896			
Zn	.613	.661			
Ba		.637	-.544		
Fe			.784		
Mg		.421	-.704		
As			.670		
Mn				.898	
Co		.315		.694	.427
Pb					-.780
Ca		-.318			.700

C

	Component				
	1	2	3	4	5
Cr	.892		-.321		
V	.874			.330	
Ni	.778			-.322	.341
Ca	-.608	-.335	.512		
Cu		.843			
Mg		-.817		.437	
Mn	-.403	.587			.445
Zn	-.336		.866		
Fe			.730	.480	
Co		.556	-.593		.324
Pb				-.772	
Ba	-.363	-.448		.614	
As				.362	-.765
Au			-.345		-.746

D

Table 6.6 Elemental groups as are suggested by cluster analysis (CA) and principal component analyses (PCA) from the top metre, transported and *in situ* regolith facies. Bolded elements are variables with secondary loading on components.

Regolith unit		Clay-silt-gravel rich facies element associations	Regolith carbonate facies element associations	Fe-rich facies element associations	Mn-rich facies element associations
Topmetre	CA	• Mn-Co-Ca • Mg-Ba • Cr-V-Fe • Mo-Ni • Cu-Zn-Pb			
	PCA	1. Cr-V-Fe 2. Ca-Co-Mn 3. Zn-Cu-Ni-**Co** 4. Mg-Ba 5. Mo-Cu-Ni			
Transported	CA	• Fe- V- Cr-As • Ni- Mo • Cu-Zn-Ba • Mn-Co • Ca-Mg • Au-Pb	• Mg-Ba • Cu-Zn-Ni • Mn-Co-Ca • Cr-V • Fe-As-Pb-Au	• Cr-V- Mo • Bi-W • Fe-Sb-As-Pb • Mg- Ba- Mn • Cu-Zn-Co-Ni • Ca	
	PCA	1. Fe-Cr-V-As-Cu 2. Co-Zn-Mn-**Cu**-Ni 3. Mg-Ba-**Zn-Cu** 4. Ni-Mo-**Cr-V** 5. Ca-**Mn**	1. Fe-V-Cr-Cu-As 2. Mg-Ca 3. Co-Zn-Mn-Cu-**Ba-Fe** 4. Ba 5. Au	1. V-Cr-**Fe**-Bi 2. Pb-As-Fe-Sb 3. Bi-W 4. Ni-**Zn**-**W**-Cu 5. Mn-Mg-Ba 6. Zn-**Mg**	
In situ	CA	• Fe-Zn-Cu • Ba-V- Mg • Cr-Ni • Mn • Ca	• Fe-Cu-Zn • Cr-V • Mg-Ca • Mn-Ba • Ni • Mo • Pb	• Mg-Ba • Cu-Zn-Ni • Mn-Co-Ca • Cr-Vi • Fe-As-Pb-Au	• Cr-Ni-V • Co-Cu-Mn • As-Au • Mg-Ba • Ca-Zn-Fe • Pb
	PCA	1. V-Ba-Cr-Mg 2. Zn-Fe-Cu 3. Mg-Ca-**Ba**	1. Fe-Cu-Zn-Ni 2. V-Cr 3. Mg-Ca-**Mn** 4. Ba-Mn	1. Fe-V-Cr-Cu-As 2. Mg-Ca 3. Co-Zn-Mn-Ba-**Fe** **4. Ba** 5. Au	1. Cr-V-Ni 2. Cu-Mn-Co 3. Zn-Fe-Ca 4. Ba-Mg-Fe-As-V 5. **Mn**-Ni-Co

association between Mn and Co and to some extent Ca (Chapter 9). Manganese is associated with Ba in the Fe-rich facies of the transported and *in situ* regolith and in the *in situ* carbonate facies. This association represents the typical hollandite composition, which is also observed in this study (Chapter 9).

- The magnesium-Ca association is predominantly observed in the regolith carbonate facies. However, this association is not significantly correlated with any element, which means that the Ca-Mg enrichment process has limited influence on dispersion of the elements. A magnesium-Ba association is noticed in the *in situ* facies and in the transported Fe-rich and regolith carbonate facies. This association possibly reflects occurrences of Ba as barite or within Mg-clay minerals (see Chapter 9).

- Gold and to some extent Pb and Mo are not associated with any of the Fe, Mn and Ca-Mg enrichment facies, which generally indicates the independent behaviour. Lead is associated with As, Sb and Fe particularly in the Fe-rich facies.

6.5 SUMMARY AND CONCLUSIONS

The regolith of the Girilambone region can be subdivided into the top metre (as a general representative of soil), transported and *in situ* regolith based on visual field, petrographic and chemical analysis. These units also can be further classified based on clay-gravel, carbonate, iron and manganese enrichment, using the boundaries of Ca & Mg $\geq$ 1 %, Fe $\geq$ 8.5 % and Mn $\geq$ 0.1 %. These boundaries are based on comparison between chemical composition and visual and petrographic examination. The clay facies represents samples that do not include any Ca, Mg, Fe and Mn enrichment.

To understand the processes that affected element distribution, accumulation and association, the thresholds and anomalies of the elements were calculated in each regolith facies and only for element values above the detection limits. Element thresholds can be calculated using two methods of estimation (MAD+2Median and boxplot). Generally the boxplot estimation of the threshold is higher than that from the MAD method. The results showed significant enrichment of Au, Cu, Zn and to some extent Pb in a profile extending from drill hole CBAC119 to drill hole CBAC125 in the

northwest Sussex area. The regional background values of Au, Cu, Pb and Zn are higher in the in-situ facies, which possibly relates to parent material enrichment. Arsenic, Cr and V showed higher background values within the Fe facies. This relates to adsorption or incorporation by secondary Fe oxides (hematite and goethite).

Major and trace element contents determined in clay- carbonate- Fe- and Mn-rich facies were subjected to cluster and principal component analyses. Cluster analysis generally revealed four element associations, which are Ca and Mg (carbonate group) association, MnO (manganese oxides) association, Fe_2O_3 (iron oxides) association and Ni and Cr (mafic group) association. Principal component analysis generally showed similar groups, representing association with calcrete (Ca+Mg), adsorption (Fe-Mn oxides) and bedrock influences.

Cluster analysis and principal component analysis were used to show the main factors controlling the trace element associations. The association of base metals with Fe and Mn is clear in the *in situ* facies. An association of mafic group element (i.e., Cr, V) with Fe is common in the top metre clay and transported facies. No significant association between regolith carbonates facies and Au was observed.

7. CHAPTER SEVEN: GROUNDWATER CHEMISTRY AND HYDROGEOLOGY

7.1 INTRODUCTION

Groundwater is a potentially useful sampling medium for successful mineral exploration (e.g., Gray, 1991; Giblin and Dickson, 1992; Gray, 2001; Jeong, 2001; Giblin and Rutherford, 2003; Cameron *et al.*, 2004; Caritat and Kirste, 2004; Phipps *et al.*, 2004; Pirlo and Giblin, 2004; Cameron and Leybourne, 2005). It is also one of the agents important in weathering processes and the geochemical evolution of the regolith, given its reactive nature and ability to transport elements and dissolved gases (Giblin and Rutherford, 2003). An aim of the study was to investigate potential geochemical signatures in groundwater from background and weakly mineralised sites. This would also assist in understanding the geochemical controls on groundwater compositions.

This chapter examines the hydrogeology of the area, the likely hydrogeochemical processes, water types and water-rock interaction, using observations of the groundwater major and trace element compositions. It also includes interpretation of $^{36}Cl/Cl$ isotope ratios and calculated mineral saturation indices of potential aquifer minerals in the area.

7.2 SITE DESCRIPTIONS

Groundwater samples were collected from drill holes CBAC217, CBAC218, CBAC219, CBAC227, CBAC231, CBAC235, CBAC242, CBAC243 and CBAC248 in the Byrock area and CBAC150, CBAC154, CBAC158, CBAC160 and CBAC173 from the Hermidale area (Figure 7.1).

A digital elevation model and the present drainage pattern in the Byrock area show a northwest trending ridge separating the Byrock catchment from the Bogan River (Figure 7.2). In the Byrock area the Bogan River and Mulga Creek are flowing north whereas Tindarey Creek is flowing north-northeast (Figure 7.2).

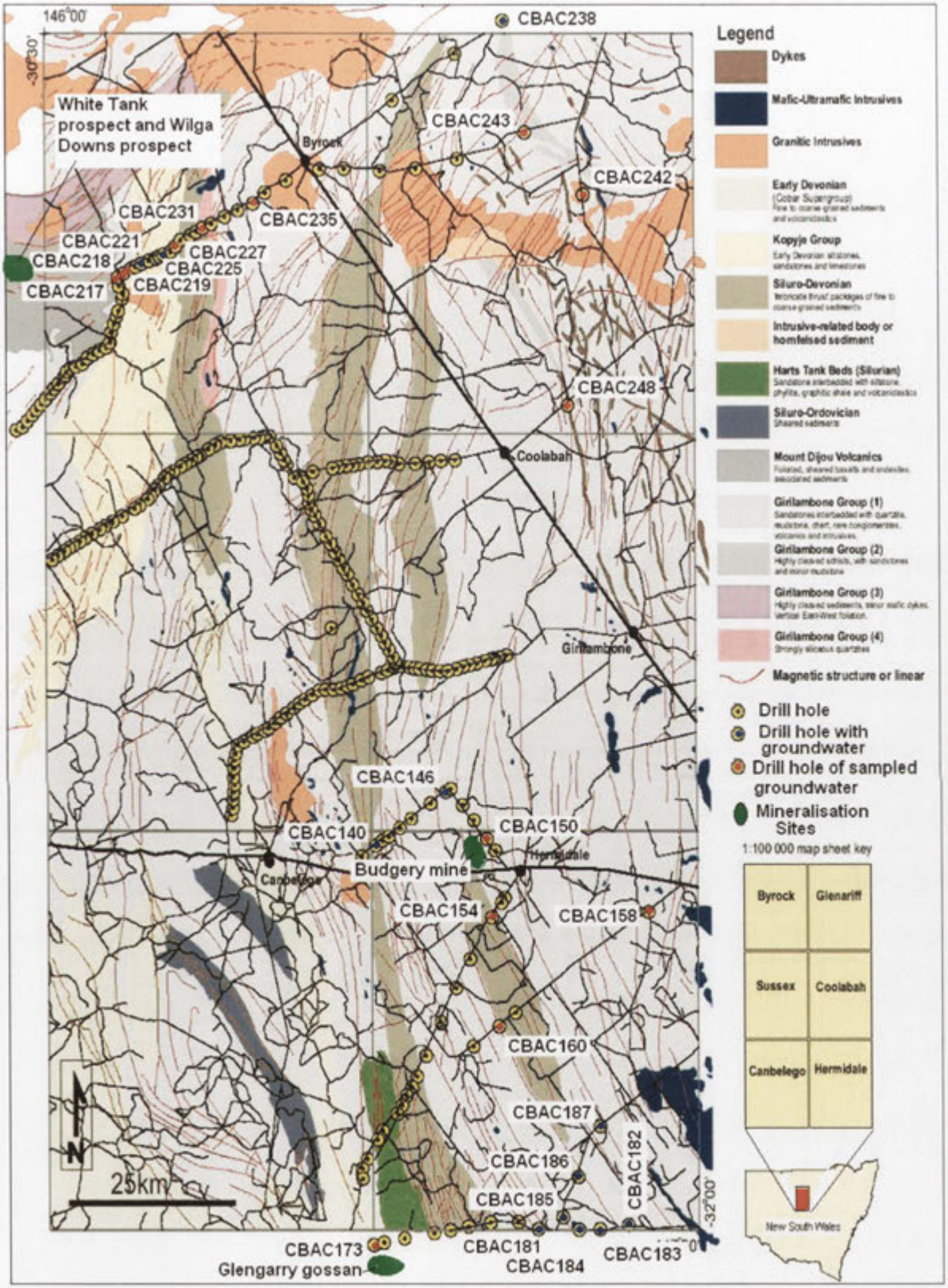

Figure 7.1. Geologic map of the Girilambone region showing some known mineralisation sites, drill hole locations, drill holes (CBAC) that intersected groundwater (blue dots) and drill holes from which the groundwaters were sampled (red dots).

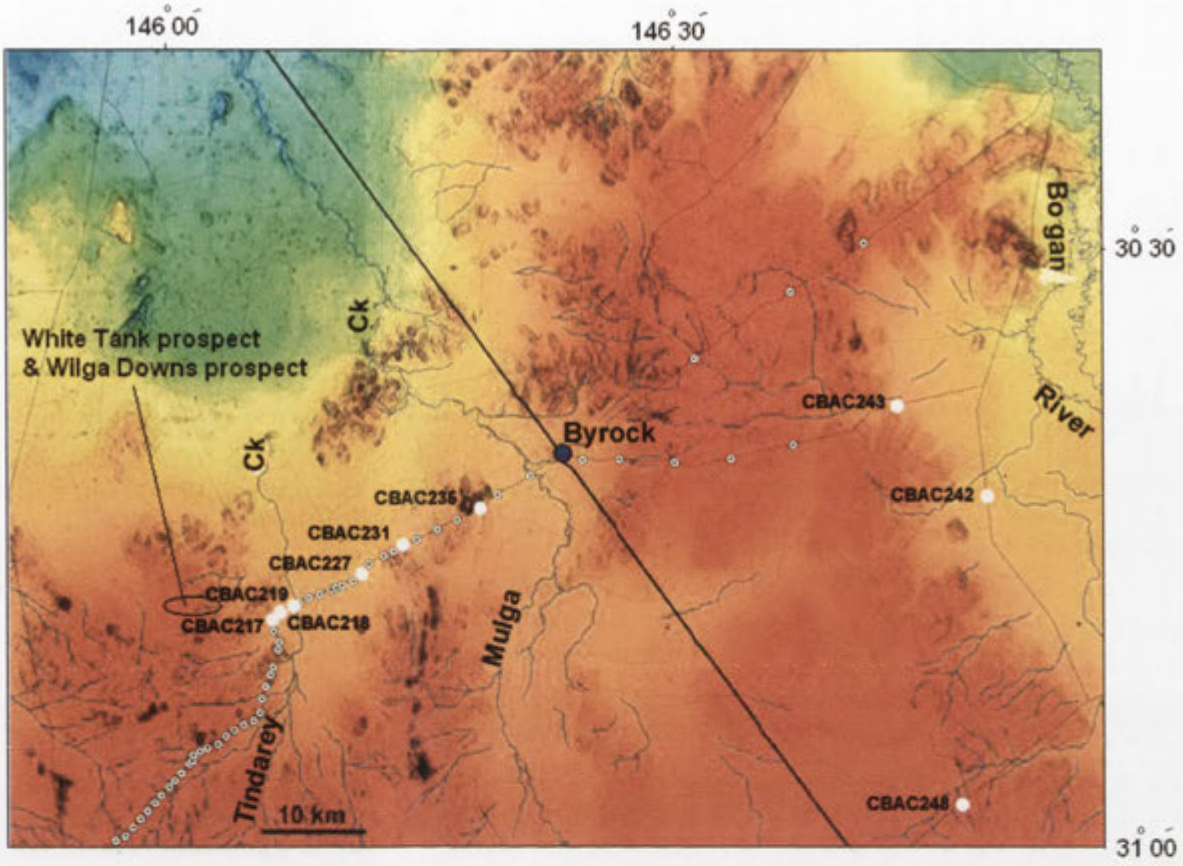

Figure 7.2 Digital elevation model of the Byrock area with present drainage, roads and the drill holes sampled for groundwater. Red and blue represent high and low elevated areas respectively. Modified from Chan *et al.* (2004).

In the Hermidale area, Whitbarrow and Pangee Creeks generally flow to the north and northeast (Figure 7.3). Palaeodrainage systems in the Byrock and Hermidale areas identified on magnetic imagery show roughly the same patterns as the present-day drainage (Figures 7.4, 5).

The landscape in the Byrock area represents a transitional environment between eroded colluvial domains and depositional fluvial domains (Chan *et al.*, 2004). Zones of strongly weathered bedrock in the central portion of the area are flanked by the Darling and Bogan River systems. A prominent hill and ridge of leucitite dominate the landscape west of Byrock (Glanville *et al.*, 2003). These Miocene volcanics are relatively unweathered and mostly well exposed. In some areas they sub-crop within creeks, roadside drains and borrow pits. In the Hermidale area the landscape consists of thick alluvial depositional plains in the east and colluvial erosional plains, rises and low hills in the western and southwestern parts of the area (Chan *et al.*, 2002).

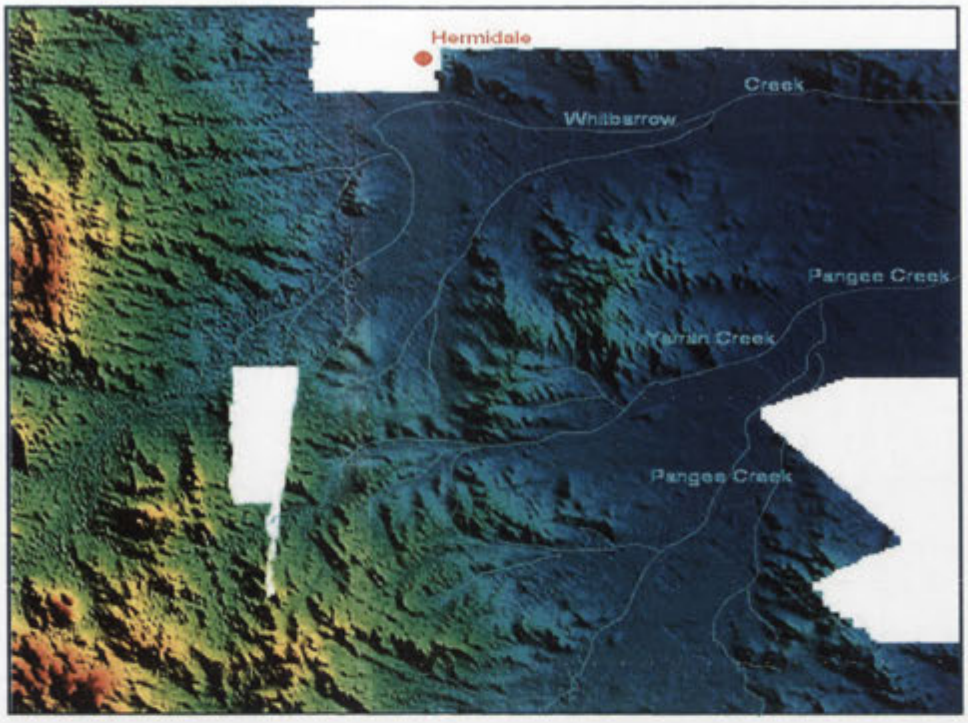

Figure 7.3 Digital elevation model of the Hermidale area with present drainage. Red and blue represent high and low elevated areas respectively. Modified from Chan *et al.* (2002). Gaps in data due to mining lease restriction.

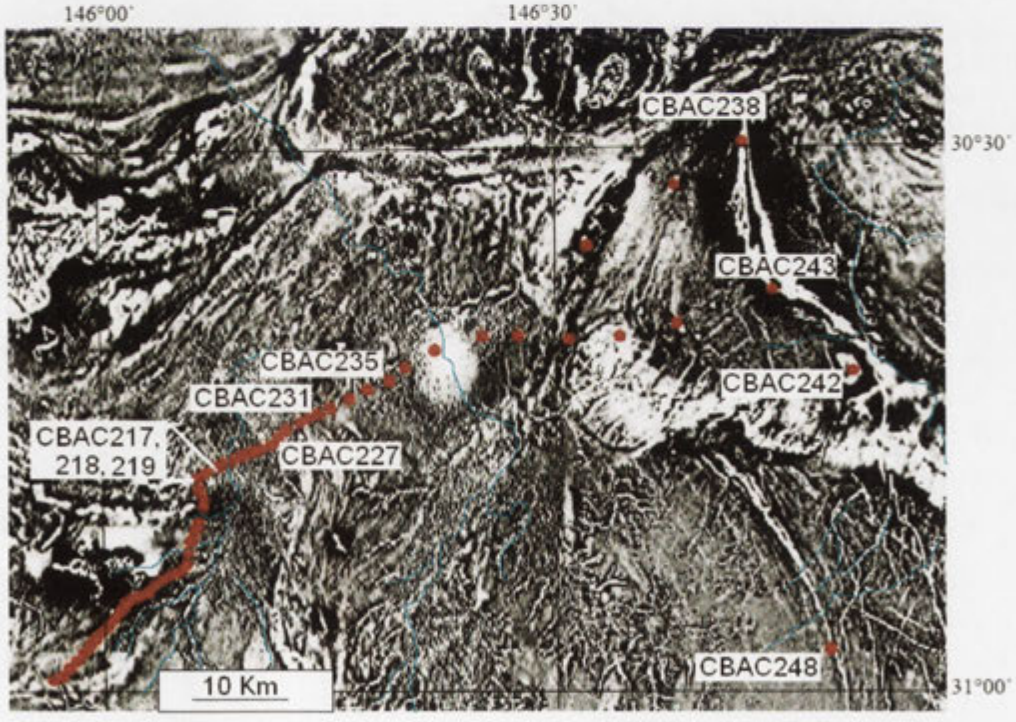

Figure 7.4 Magnetics imagery (1.5 vertical derivative) of the Byrock area showing magnetic drainage lines (paleodrainage), magnetic basement and the groundwater drill holes. Present day drainage is in blue. Modified from Chan *et al.* (2004).

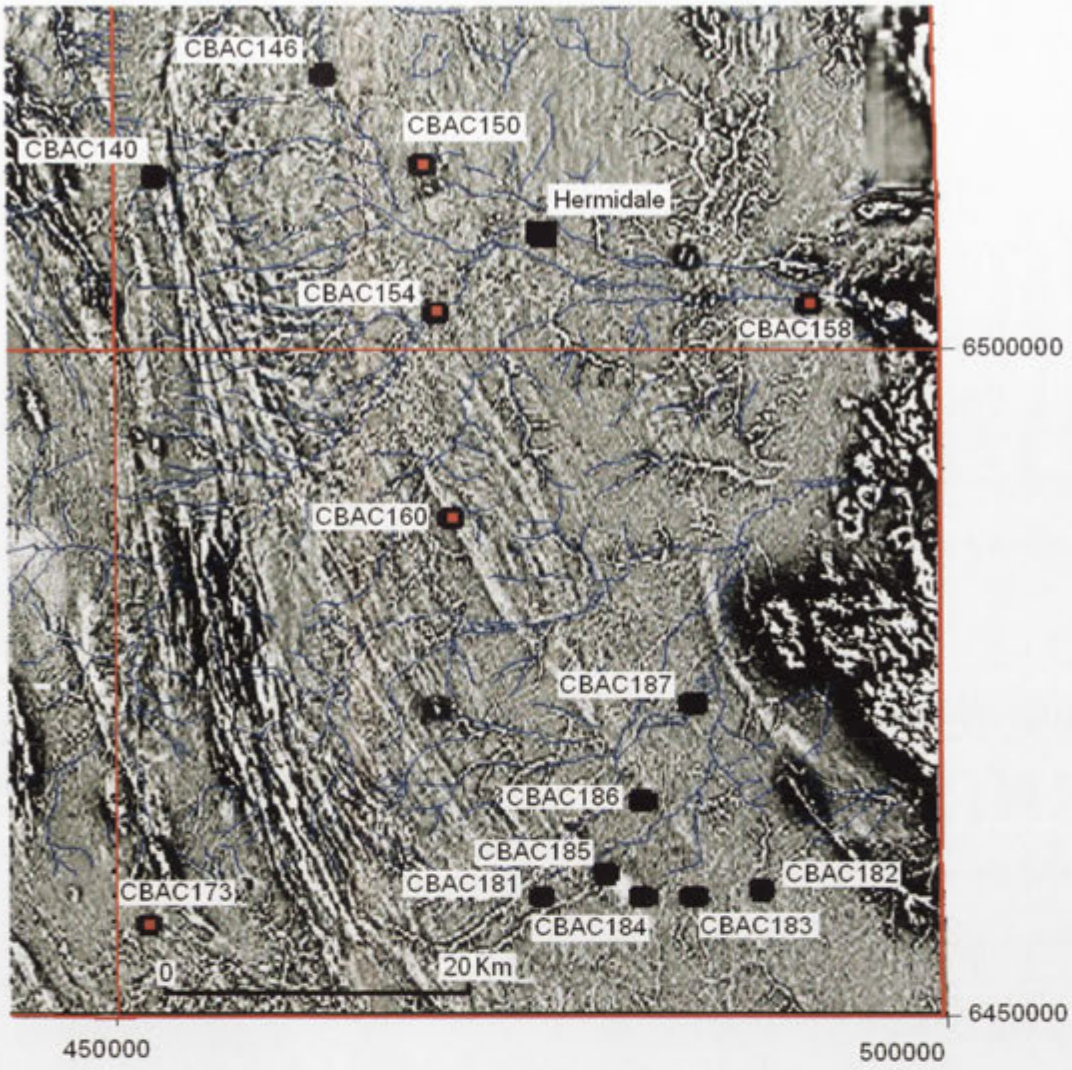

Figure 7.5 Magnetics imagery (1.5 vertical derivative) of the Hermidale area showing magnetic drainage lines (paleodrainage), magnetic basement, the drill holes that intersected groundwater (black dots) and the drill holes from which the groundwaters were sampled (red dots). Present day drainage is in blue. Modified from Chan *et al.* (2004).

7.3 HYDROGEOLOGY

The groundwater in the Byrock area was intersected within weathered silty sandstones interbedded with phyllite, felsic volcanic and siltstone with breccia (Figure 7.6). In the Hermidale area it was detected within weathered phyllitic siltstones sandstones (Figures 7.7,8). The first appearance of groundwater in the drill hole was recorded as the water table depth (Chan *et al.*, 2002; 2004). These depths were used to identify the groundwater flow directions and to calculate the hydraulic gradients along the flow

path. The water table mirrors topography suggesting that the aquifers are unconfined. The general flow directions in the Byrock and Hermidale areas are from southwest to northeast (Figures 7.9,10). The hydraulic gradients are low (≤ 0.0035), which suggest slow groundwater flow.

7.4 ELECTRICAL CONDUCTIVITY, pH/Eh AND TEMPERATURE

Groundwater compositions are tabulated in Appendix 3. Electrical conductivity (EC) ranges from 843µS/cm to 31600 µS/cm. In the Byrock area the EC is significantly variable and the lowest value (843µS/cm) was recorded to the west of Byrock (CBAC235). In this area the aquifer is mainly in weakly weathered leucitite rocks (Glanville et al., 2003). These rocks form Byrock Hill and are covered by very thin transported sediments. Therefore the fresh groundwater is possibly a result of minimal water-rock interaction between rainwater and the weakly weathered aquifer rocks. Low

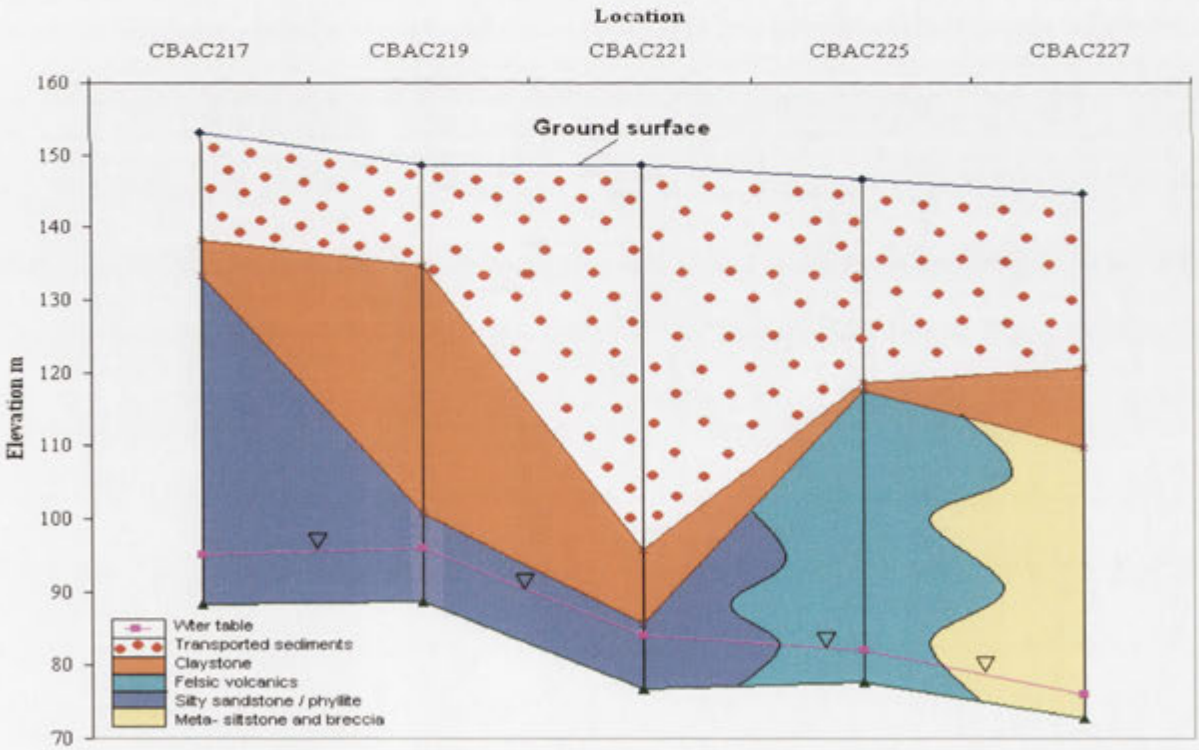

Figure 7.6 Cross-section showing how the water table mirrors topography along the groundwater flow between and CBAC217 and CBAC227 in the western part of the Byrock area (see Figure 7.9 for location).

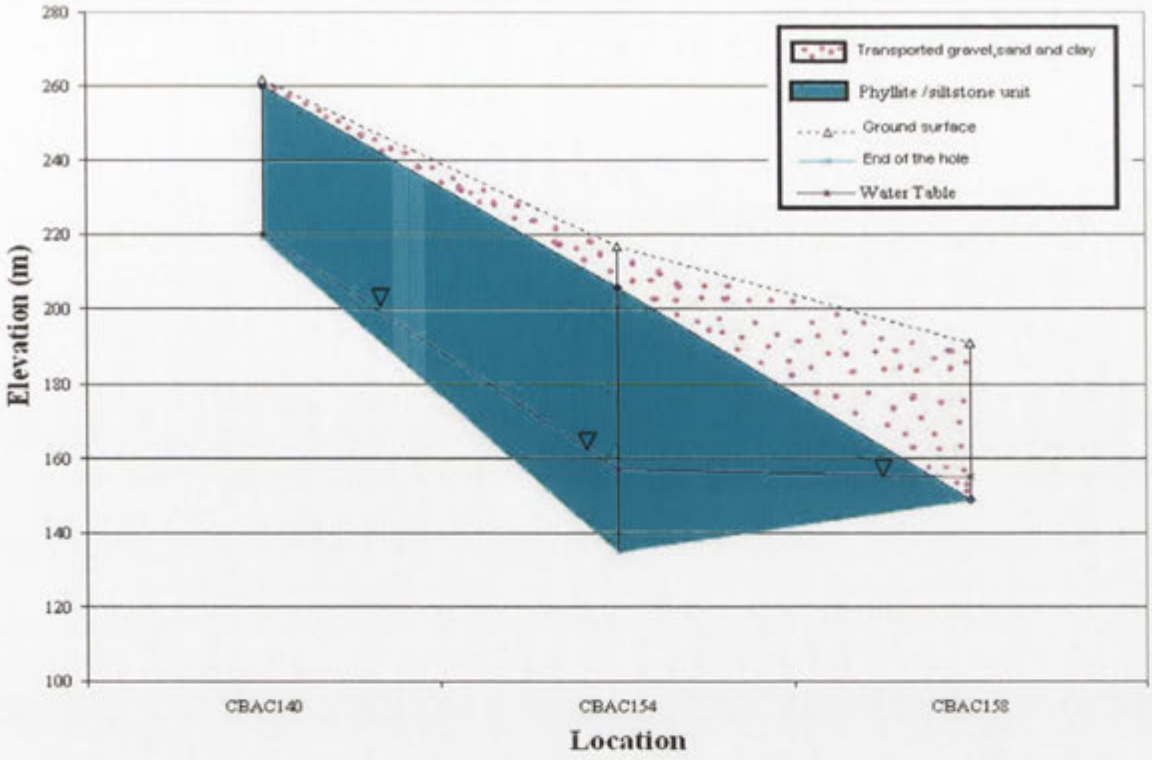

Figure 7.7 Lithologic cross-section showing how the water table mirrors topography along the groundwater flow between CBAC140 and CBAC158 in the northern part of the Hermidale area (see Figure 7.10 for location).

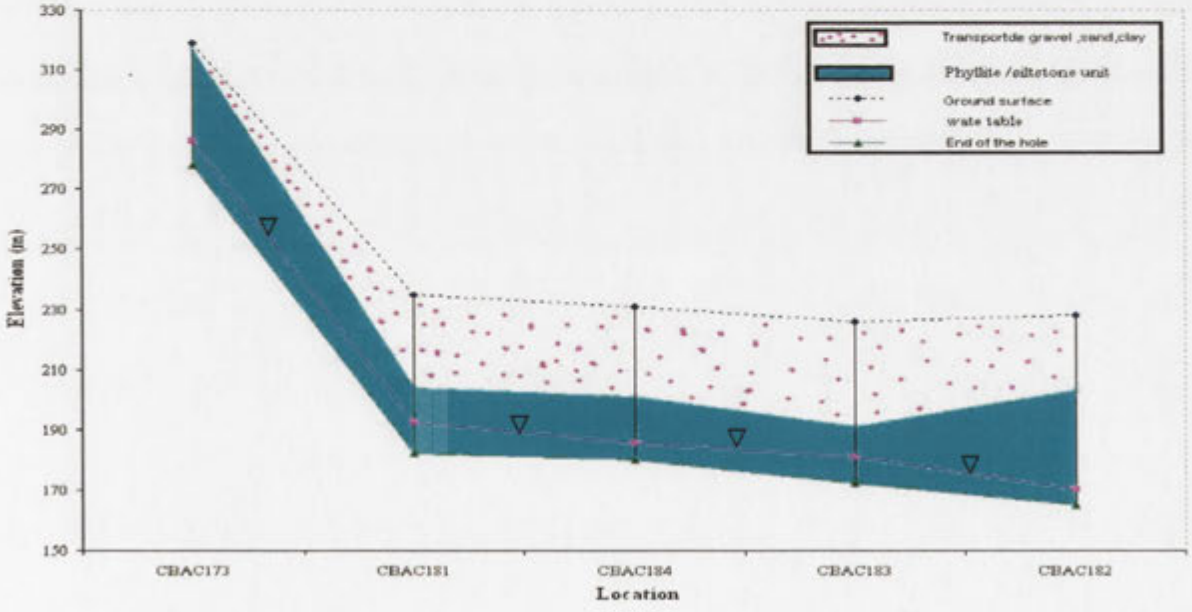

Figure 7.8 Lithologic cross-section showing how the water table mirrors topography along the groundwater flow between CBAC173 and CBAC182 in the southern part of Hermidale area (see Figure 7.10 for location).

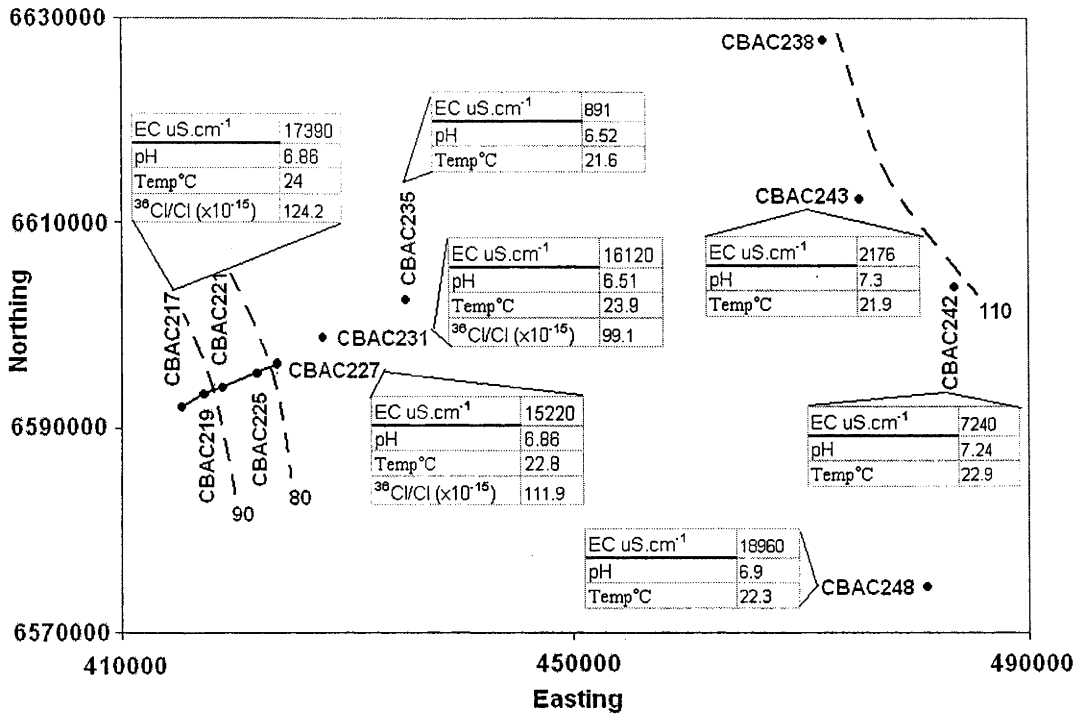

Figure 7.9 General hydraulic contours (m) in the Byrock area (dashed lines) and measured water chemistry parameters. Solid lines indicate locations of the cross-sections in Figures 7.6.

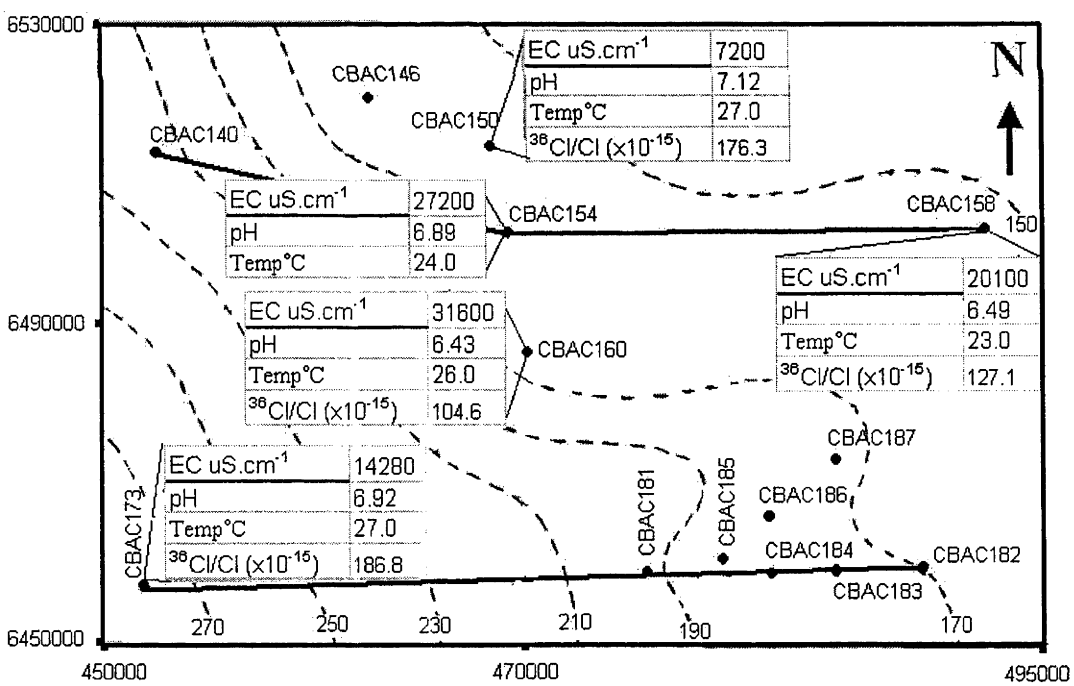

Figure 7.10 General hydraulic contours (m) in the Hermidale area (dashed lines) and measured water chemistry parameters. Solid lines indicate locations of the cross-sections in Figures 7.7 and 7.8.

EC was also recorded in CBAC242 and CBAC243, east of Byrock and this area possibly represents a recharge zone. EC decreases along the inferred flow path from 17390 µS/cm in CBAC217 to 15220 µS/cm in CBAC227 (Figure 7.9). This may relate to mixing with less saline water along the flow path.

In the Hermidale area, the EC is lowest in the southwest and north, suggesting proximity to recharge areas, as those samples are from holes in the highest parts of the landscape. The EC is higher in the samples inferred to be downstream of the lower-EC samples, which may indicate mixing with higher salinity water or evaporation, both of which are consistent with the observed element ratios (e.g., Na/Cl, Cl/Br; Khider, 2004). The easternmost sample (CBAC158; Figure 7.10) has an intermediate salinity, but it comes from the overlying gravel layer and is probably not downstream of the other samples, and is therefore unrelated to them. It is possible that it has a lower salinity than the other samples taken from approximately the same depth and in the phyllitic material because of mixing with recharging fresher water.

The pH and temperature decrease along the flow path in both areas (Figures 7.9,10), but differences are small and probably not significant. The pH ranges from 6.4 to 7.3 and the temperature ranges from 21.6°C to 27°C (Table 7.1). Due to the difficulty of measuring *in situ* Eh of groundwater it was only possible to measure the redox (Eh) values in the Byrock samples, where the Eh ranges from 305 to 407 mV. To identify the environment of groundwater, Eh and pH values are plotted on an Eh-pH diagram (Sato, 1960; Figure 7.11). In this diagram the groundwater environment is divided into depth, transitional and weathering environments. All the studied water samples from the Byrock area plot in the weathering environment (Figure 7.11) indicating oxidised groundwaters.

7.5 ALKALINITY

In this study the measured alkalinity represents total alkalinity (in term of $CaCO_3$ mg/L) using the standard potentiometric titration method (Eaton *et al.*, 1995). About 94.8% of the measured carbonate species in neutralised water (pH around 7) at temperature of 20°C represents the bicarbonate ion (Fetter, 2001). The alkalinity in the studied groundwater samples ranges from 196 to 801.2 mg/L (Table 7.1). Assuming that all the

alkalinity in these samples is a result of inorganic carbon species, the concentration of bicarbonate and carbonate can be calculated using eqs.1 and 2 (Deutsch, 1997).

Table 7.1 Sample depth, Electrical conductivity (EC), pH, Eh, temperature and alkalinity of the groundwater samples from the Byrock and Hermidale areas.

Source	Drill hole	Sample depth (m)	EC uS.cm^{-1}	pH	Eh mV	Temp C	ALK mg/L
Byrock	CBAC 217	47.3	17390	6.9	350	24	654.2
Byrock	CBAC 217a	47.1	17300	6.8	355	23.6	648.7
Byrock	CBAC218	46.2	14820	6.7	344	22.3	543.9
Byrock	CBAC219	43.4	14960	7.1	344	21.7	445.9
Byrock	CBAC227	39.2	15220	6.9	350	22.8	373.6
Byrock	CBAC 227a	39.0	15178	6.9	348	22.6	662.5
Byrock	CBAC231	38.6	16120	6.5	340	23.9	294.0
Byrock	CBAC235	18.6	891	6.5	407	21.6	434.9
Byrock	CBAC 235a	18.3	843	6.7	400	22.4	451.5
Byrock	CBAC242	11.8	7240	7.2	305	22.9	801.2
Byrock	CBAC243	28.0	2176	7.3	354	21.9	632.1
Byrock	CBAC248	34.0	18960	6.9	383	22.3	557.4
Hermidale	CBAC 150	50.0	7200	7.1		27.0	494.9
Hermidale	CBAC 154	55.0	27200	6.9		24.0	240.1
Hermidale	CBAC 158	30.0	20100	6.5		23.0	247.5
Hermidale	CBAC 160	65.0	31600	6.4		26.0	196.0
Hermidale	CBAC 173	18.0	14280	6.9		27.0	485.1

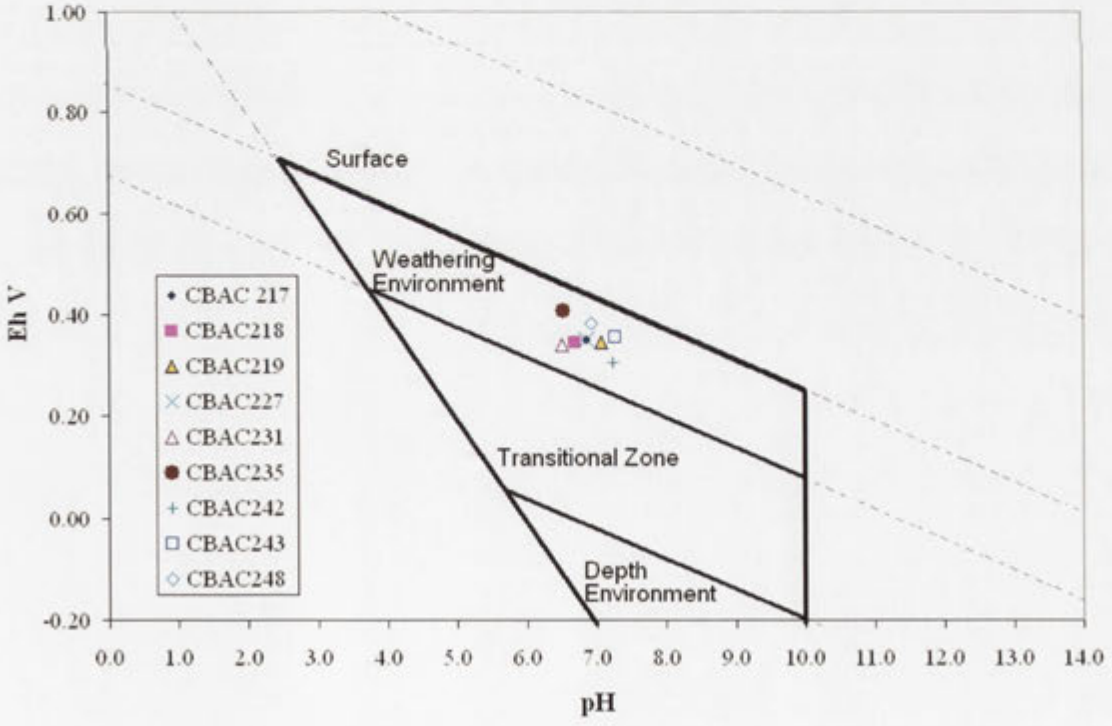

Figure 7.11 Eh-pH diagram (Sato, 1960) showing water stability of Byrock water samples.

HCO_3^- (mg/L)= [alkalinity(mg/L)/ {1+ ($2\times10^{-10.3}/10^{-pH}$)}×50] ×61.....(1)

CO_3^{-2} (mg/L)= [alkalinity(mg/L)/ {2+ ($10^{-pH}/10^{-10.3}$)}×50] ×60.....(2)

The calculated concentrations of HCO_3^- for the studied groundwater samples are tabulated in Appendix 3.

7.6 MAJOR IONS GEOCHEMISTRY

Analysis of how major ions and compounds are distributed in the aquifers assists the interpretation of the aquifer mechanics and reveals flow paths and potential recharge areas. For example HCO_3^- concentration was used as an indicator of flow direction, preferential permeability and possible mixing (Herczeg *et al.*, 1991; Wolfgang and White, 2000).

The distributions of HCO_3^- in the Girilambone area (Appendix 3) show higher values (> 590 mg/L) towards the southeastern part of the Byrock area, and the HCO_3^- concentration decreases along the flow path from CBAC217 to CBAC231. A high concentration of HCO_3^- was also recorded from the highland area (possible recharge area) of the Bogan River catchment east and northeast of Byrock. In the Hermidale region, the likely recharge areas are in the southeast (CBAC173) and north (CBAC150) of the region and generally characterised by high concentrations of HCO_3^-. Similarly Na/Cl (in mmol/L) shows a general increase in values moving towards the southeast, east and northeast in the Byrock area and from north to southwest in the Hermidale area. The northeastern portion of the Hermidale area (CBAC158) shows a relatively high Na/Cl value.

Calcium, Mg and K distributions all increase along the inferred flow path. In the Byrock area Ca, Mg and K change from 316 mg/L, 697mg/L and 131(mg/L) respectively in CBAC217 to 342, 752 and 162 in CBAC227 within 8 km. Correspondingly the concentrations of Ca, Mg and K in the recharge area of the Hermidale region (CBAC173) are 168, 276 and 16.2 and they change along the inferred flow path to 531,1297 and 109 respectively in CBAC160. In other words these cations

are increasing in the studied drill holes (except CBAC158) down the flow path, indicating mineralogical changes and/or an increase in weathered material in the aquifer rocks. Low concentration of Ca, Mg and K in CBAC158 are possibly related to mixing of fresh water from surface.

7.7 GROUNDWATER TYPE AND ORIGIN OF DISSOLVED IONS

Based on the major ion contents, three water types are identified (Figure 7.12). This Piper diagram shows that the groundwater compositions at the studied sites of the Girilambone region vary, but are generally Na-Cl dominant. The different patterns may reflect the evolutionary stages of the water, mixing of waters or mineralogical changes in the aquifer composition. The waters in this region can be classified as follows:

- Chloride type, where the anion is chloride and the cation is mainly sodium and /or potassium. This type of water occurs in almost all the studied sites (except CBAC235 and CBAC243) in the Byrock and Hermidale areas (Figure 7.12). The EC measurements showed that the majority of the waters are over the 5000 µS/cm level of conductivity (Table 7.1) and this is mostly related to predominant occurrence of sodium chloride.
- Calcium-bicarbonate type. This type of water is reported only from CBAC235 (Byrock area). It is characterised by high Ca, Mg and HCO_3^- contents, alkalinity of 434.87 mg/L and EC of 891 µS/cm (Table 7.1). Bicarbonate is possibly generated by the reaction of water with $CaCO_3$. The abundance of calcium and magnesium probably indicates interaction of the water with the leucitite rocks at this site.
- Bicarbonate and chloride type. This type of water occurs in CBAC243 (Byrock area) and includes high contents of HCO_3^-, Cl^- and Na^+ with high alkalinity (632.1 mg/L) and EC (2176 µS/cm).

The dissolved ions in groundwater are mainly derived from two main processes (e.g., Rabemanana *et al.*, 2005). These are:

1. Water- rock interaction

The most common water-rock interaction processes (weathering of silicates and carbonates) tend to release base cations (particularly Na^+ and Ca^{2+}) and alkalinity

(HCO_3^-), whilst raising the pH (Freeze and Cherry, 1979; Hem, 1985). The metamorphic and igneous nature of the bedrocks in the study area (Chapter 3) precludes primary evaporite minerals such as gypsum or halite, which could be possible sources of chloride, sulphate, sodium and calcium. Subsequent ion exchange may modify the chemistry (ratios of Ca^{2+} and Na^+) whereas reactions such as oxidation of pyrite may prove to be a source of sulphate (Rabemanana *et al.*, 2005).

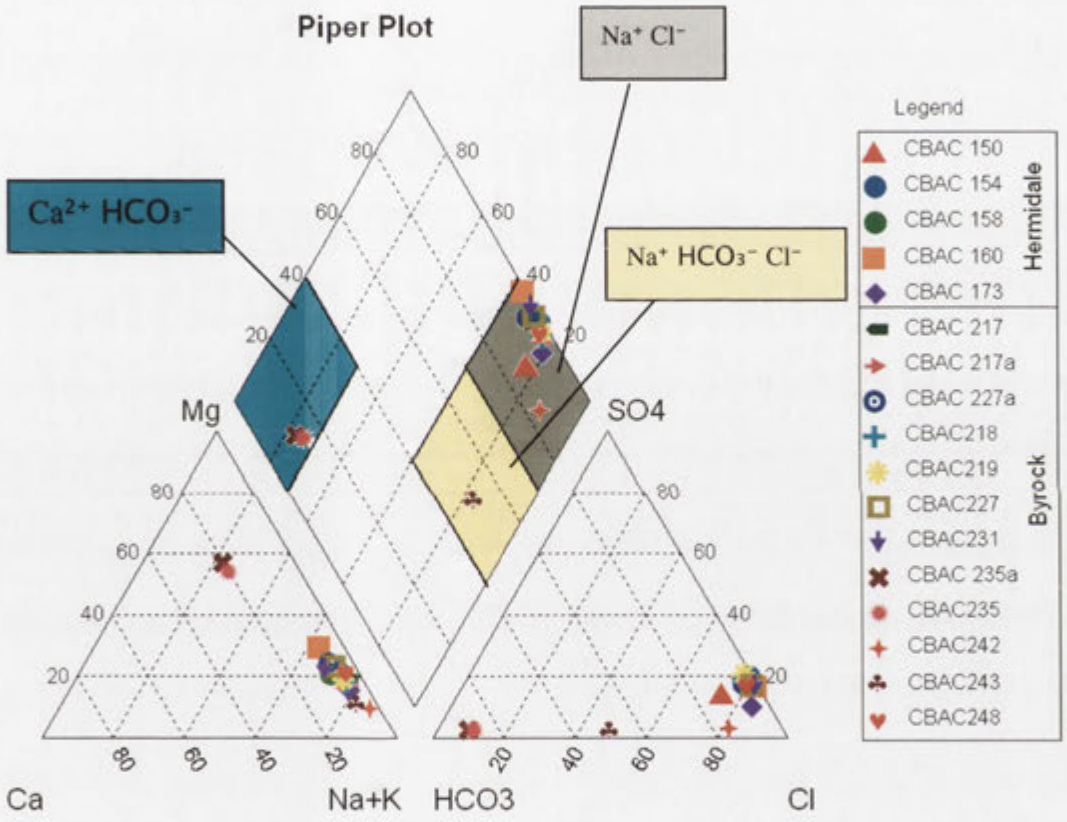

Figure 7.12 Piper plots illustrating different types of groundwater in the study area.

The plot of alkalinity with Na+K+Ca+Mg shows that all the water samples fall below the 1:1 line (Figure 7.13). This suggests another source of cations in addition to water-rock interaction process. The observed excess of Na^+ over K^+ in all the studied waters (except the water in CBAC235) reflects occurrences of clay materials within the weathered aquifer rocks. High concentrations of Ca^{2+}, Fe^{2+}, Mg^{2+} can be attributed mainly to weathering of feldspar and mafic minerals. The relationship between K^++

Na^+ and $Ca^{2+}+Mg^{2+}$ suggests a predominant felsic component in nearly all the studied sites, except CBAC235 (Figure 7.14). Water in the latter has more likely been in contact with carbonate and/or mafic rocks. However, the occurrence of leucitite in the aquifer of CBAC235 (Glanville *et al.*, 2003) supports the mafic origin.

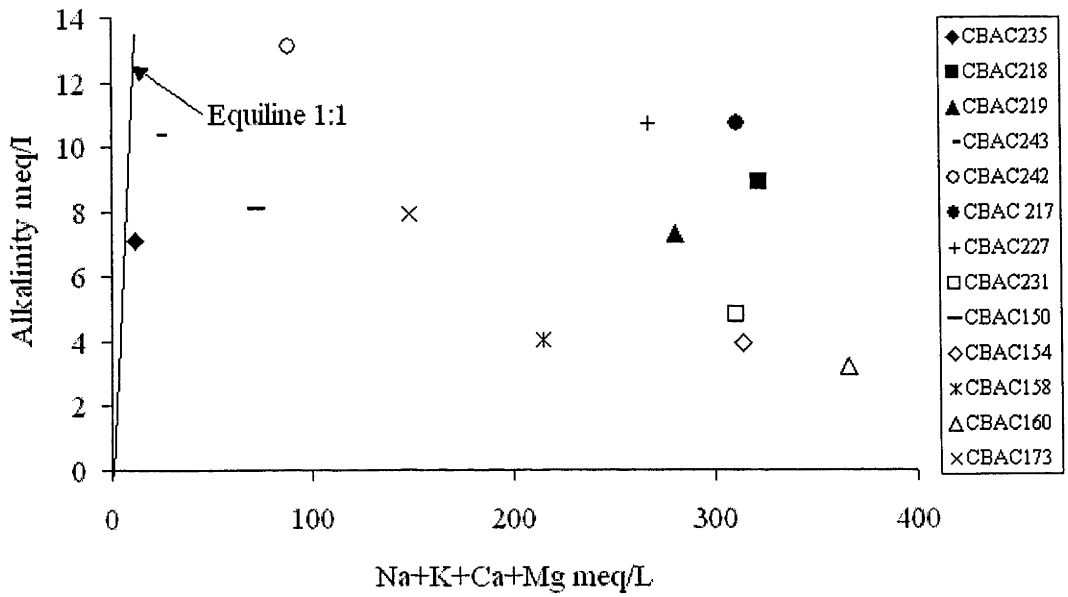

Figure 7.13 Scatterplots of alkalinity vs (Na+K+Ca+Mg) for the Byrock and Hermidale groundwater samples.

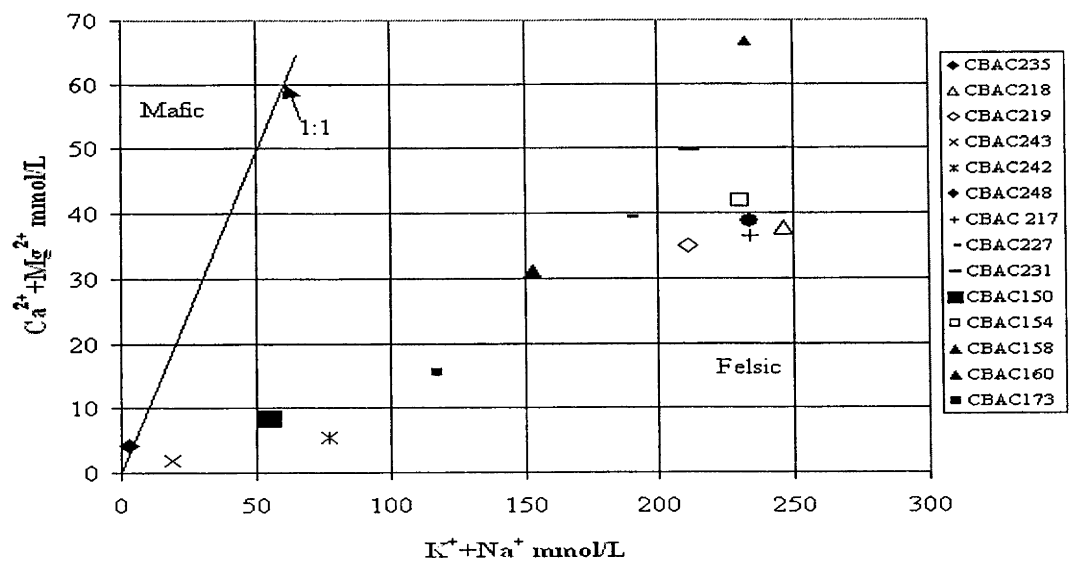

Figure 7.14 Scatterplots of $(Ca^{2+}+Mg^{2+})$ vs $(K^+ + Na^+)$ showing possible aquifer rock types in the Byrock and Hermidale areas.

2. Salinisation

The increase in salinity essentially describes the evaporative concentration of solutes at the surface or in the shallow subsurface (e.g., Thomas *et al.*, 1989; Nativ *et al.*, 1997). This may include evaporative concentration at the surface, concentration of solutes by evapotranspiration in the subsurface, precipitation and subsequent re-dissolution of secondary evaporite minerals in the unsaturated zone from evapo-concentrated waters. The solutes that are subject to this process are possibly derived from water-rock /regolith interaction (Na^+, $Ca^{2+}$and HCO_3^-) or from external sources, such as marine salts (Na^+, Cl^- and SO_4^{2-}) arriving in the rainfall recharge (Rabemanana *et al.*, 2005).

The significant correlation between the Na^+ and Cl^- ions indicates that the major part of the salinity in the groundwater is a result of NaCl (Figure 7.15). Na/Br-Cl/Br relationships for Byrock and Hermidale groundwaters generally show three groups of samples (Figure 7.16):

- samples approximately parallel to 1:1 line (i.e. CBAC150, 154, 173, 218, 219, 242) in which both Na/Br and Cl/Br are comparable, possibly showing the influence of evaporation;
- samples with high Na/Br and low Cl/Br. This group (i.e. CBAC235, 243) has excess of Na^+, which likely reflects cation exchange and/or silicates weathering (i.e., albite dissolution) due to water-rock interaction; and
- samples with increased Cl^-, high Cl/Br and low Na/Br (e.g., CBAC227, 231 and 260), which indicates mixing with higher salinity water.

There is a strong correlation between SO_4^{2-} and Cl^- suggesting that their accumulation in the groundwater is the result of a common process (evapo-concentration or dissolution of secondary evaporite mineral; Figure 7.17). Chloride-SO_4^{2-} data diverge from the seawater (SW)-rainwater (RW) line, indicating addition of SO_4^{2-}, which possibly related to oxidative weathering of pyrite and/or the dissolution of anhydrite (Dogramaci *et al.*, 2001; Rabemanana *et al.*, 2005).

The Ca^{2+} and SO_4^{2-} contents at two sites (CBAC150 and 227; Figure 7.18) approximates the seawater trend, which suggests concentration by evaporation or dissolution of gypsum. Some of the samples show relative enrichment in SO_4^{2-}

(CBAC154, 217, 219, 248), which possibly relates to oxidation of sulphides and/or precipitation of Ca^{2+} as carbonate. Similarly some other samples show Ca^{2+} enrichment (CBAC173, 242 and 243 in addition to CBAC235 and CBAC158). The elevated Ca^{2+} concentration can be related to leaching of carbonate minerals by unsaturated water-rock interaction and mobilisation of Ca^{2+} as a result of cation exchange in the soil and regolith.

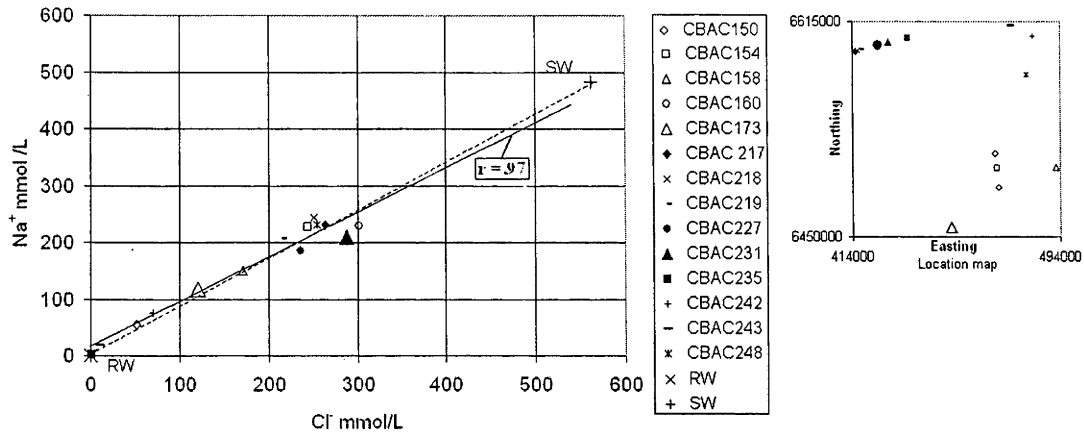

Figure 7.15 Scatterplot of Na^+ vs Cl^- for groundwater samples of the Byrock and Hermidale areas. Sold line represents regression line with correlation coefficient (r = 0.97) and the dashed line represents seawater dilution.

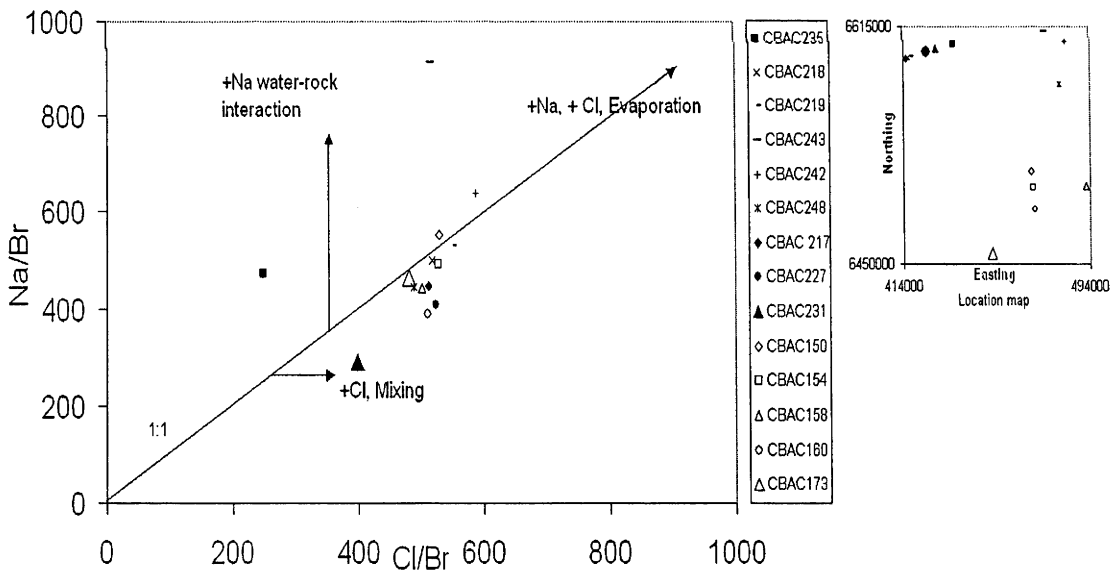

Figure 7.16 Scatterplot of Na/Br vs Cl/Br for the Byrock and Hermidale groundwater samples showing trends of evaporation (equiline 1:1) and increasing of Cl^- and Na^+ as arrows parallel to X and Y axes respectively.

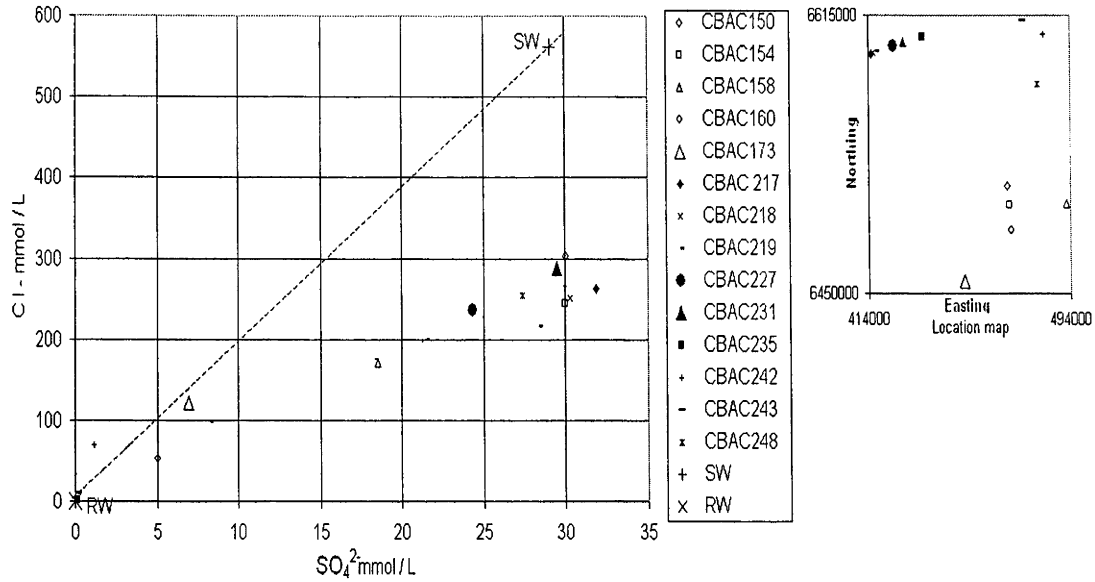

Figure 7.17 Scatterplot of Cl^- vs SO_4^{2-} for the Byrock and Hermidale groundwaters. The dashed line represents seawater dilution.

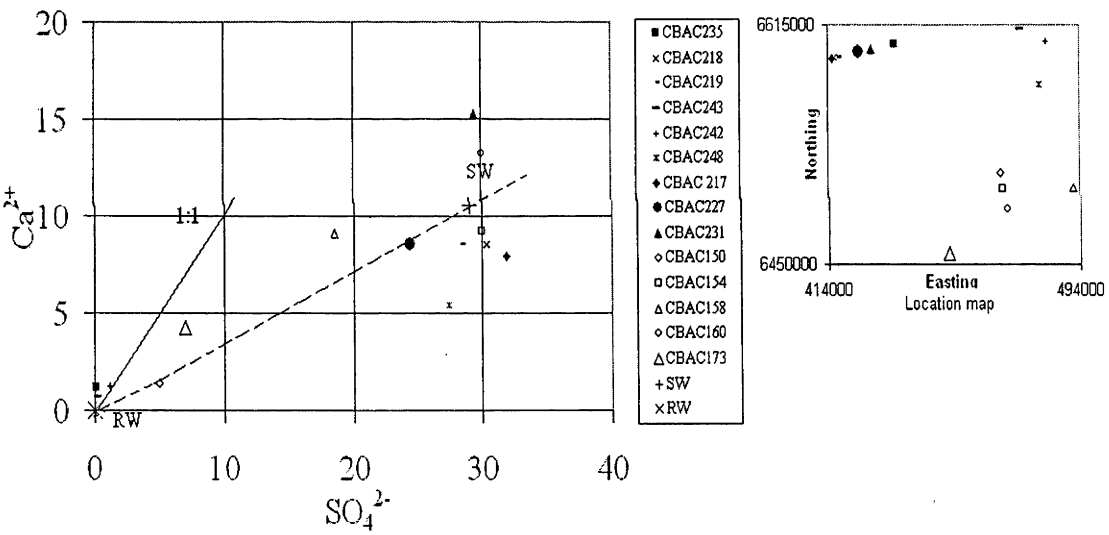

Figure 7.18 Scatterplot of Ca^{2+} vs SO_4^{2-} for the Byrock and Hermidale groundwaters. Sold line represents equiline (1:1) and the dashed line represents seawater dilution.

7.8 CHLORIDE–36

^{36}Cl is a radioactive isotope with a half-life of 301,000 yrs (e.g., Phillips et al., 1991). As chloride is hydrophilic, this isotope has the potential to be used as a groundwater-dating tool or tracer as reported in a number of Australian studies (e.g., Bently et al., 1986; Davie et al., 1989; Torgersen *et al.*, 1991; Cresswell et al., 1999; Love *et al.*,

2000; Lehmann et al., 2003, Wischusen *et al.*, 2004). These studies, along with ^{36}Cl groundwater studies elsewhere (Phillips *et al.*, 1986) and more general atmospheric ^{36}Cl studies (Bird *et al.*, 1991; Keywood, 1995; Phillips *et al.*, 1986) give background information on the formation of ^{36}Cl in the atmosphere and its likely behaviour in groundwater systems, including epigene and hypogene production effects.

^{36}Cl is produced in the atmosphere, in near-surface rocks, and in the deep subsurface. Atmospheric fallout is derived from cosmic-ray interaction, mainly with argon in the stratosphere and shows a strong latitudinal dependence, with greatest fallout at mid-latitude (Wischusen et al., 2004). Chloride –36 is also produced in the deep subsurface through neutron-capture on ^{35}Cl, supplying ^{36}Cl to groundwater systems (Bentley *et al.*, 1986).

The atmosphere also contains stable chloride derived from sea-spray, and from remobilised terrestrial salts. This stable chloride combines with ^{36}Cl. The $^{36}Cl/Cl$ ratio can be measured readily on a few milligrams of chloride using accelerator mass spectrometry (Elmore *et al.*, 1979) and varies in natural systems from several hundred parts in 10^{15} of total chloride, down to a background of a few parts in 10^{15} (e.g., Cresswell, *et al.*, 1999).

The $^{36}Cl/Cl$ ratio may be used to estimate ages of groundwaters if three assumptions are made. These are: the only sink for ^{36}Cl in the aquifer is radioactive decay; the only source for additional ^{36}Cl is normal deep subsurface production, or that additional sources can be identified; and, quantified; and the production rate for ^{36}Cl is the same now as at the time of recharge (Andrews and Fontes, 1991). The groundwater may then be dated using the following standard decay equation:

$$t = -1/\lambda \, (\ln A_t/A_0) \quad \text{.......................................(3)}$$

Where A_t is the $^{36}Cl/Cl$ ratio for the groundwater sample, A_0 is the $^{36}Cl/Cl$ ratio for the recharge (or input function) and $1/\lambda$ is the mean life of ^{36}Cl: 434,251yr (Cresswell *et al.*, 1999).

Seven Byrock and Hermidale water samples were analysed for ^{36}Cl by the Nuclear Physics Department of the Australian National University (Table 7.2). Details of the method of analysis and a description of the Accelerator Mass Spectrometer used are outlined by Fifield *et al.* (1987). The plotted ratio of $^{36}Cl/Cl$ against total chloride content in the Hermidale area together with representative trends for the processes indicated, showed that the $^{36}Cl/Cl$ ratios are relatively high in CBAC173 and CBAC150, lowest in CBAC160 and intermediate in CBAC158 (Figure 7.19). The ratio decreases along the inferred flow path, although the easternmost sample (CBAC158) has a higher ratio. The high values indicate the water is proximal to recharge, and the lowest value in CBAC160 is probably a result of evaporation and mixing of groundwaters along the flow path. The intermediate ratio at CBAC158 could be a result of mixing with a less saline and lower chlorine ratio water. Alternatively the groundwater is from a different source than to that in the east. For example, the groundwater from CBAC158 could be from the transported gravel layer (Figure 7.7). Similarly, plotting $^{36}Cl/Cl$ along the flow path from the drill hole CBAC217 to CBAC231 in the Byrock area showed an increase in $^{36}Cl/Cl$ ratio in CBAC227 that possibly relates to dilution of groundwater as a result of mixing with lower salinity (fresh) water (Figure 7.20).

To estimate the age of groundwater in the study area the ^{36}Cl content of the rainfall needs to be known. These data are not available for the study area. However, the $^{36}Cl/Cl$ ratio in rainfall for central Australia has been calculated as 325×10^{-15} (Keywood, 1995; Keywood *et al.*, 1997). If this value of $^{36}Cl/Cl$ is used as input for the Girilambone region then the value seems to be reduced during recharge by additional chloride input from local salts in the unsaturated zone or from aerosols and dust wind-blown from local playa lakes. Consequently if the assumptions pertaining to Eq. 3 are assumed valid, and an input ratio of 325×10^{-15} is used, calculated groundwater ages range from 241,000 to 492,000 years in the Hermidale area and from 418,00 to 516,000 years in the Byrock area (Table 7.2).

7.9 IDENTIFICATION OF AQUIFER MINERALS

In environments where ore minerals have been preserved for long periods of time, it is reasonable to assume that either the groundwater-aquifer rock system is at equilibrium,

or that rates of chemical reactions are so slow that a steady state, or locally equilibrated state exists. Aquifer minerals that can be calculated from groundwater composition are those that either formed out of constituents carried in the groundwater, or are minerals formed from chemical interaction between the groundwater and minerals within rock units that predated groundwater flows. In order to understand the changes in the

Table 7.2 ^{36}Cl determinations for the Byrock and Hermidale groundwaters.

Sample	Location	$^{36}Cl/Cl$ ($x10^{-15}$)	Error	^{36}Cl age(years)
CBAC150	Hermidale	176.3	8.9	265527
CBAC158	Hermidale	127.1	6.5	407698
CBAC160	Hermidale	104.6	5.8	492428
CBAC173	Hermidale	186.8	8.6	240564
CBAC217	Byrock	124.2	6.8	417561
CBAC227	Byrock	111.9	6.2	463006
CBAC231	Byrock	99.1	5.8	515913

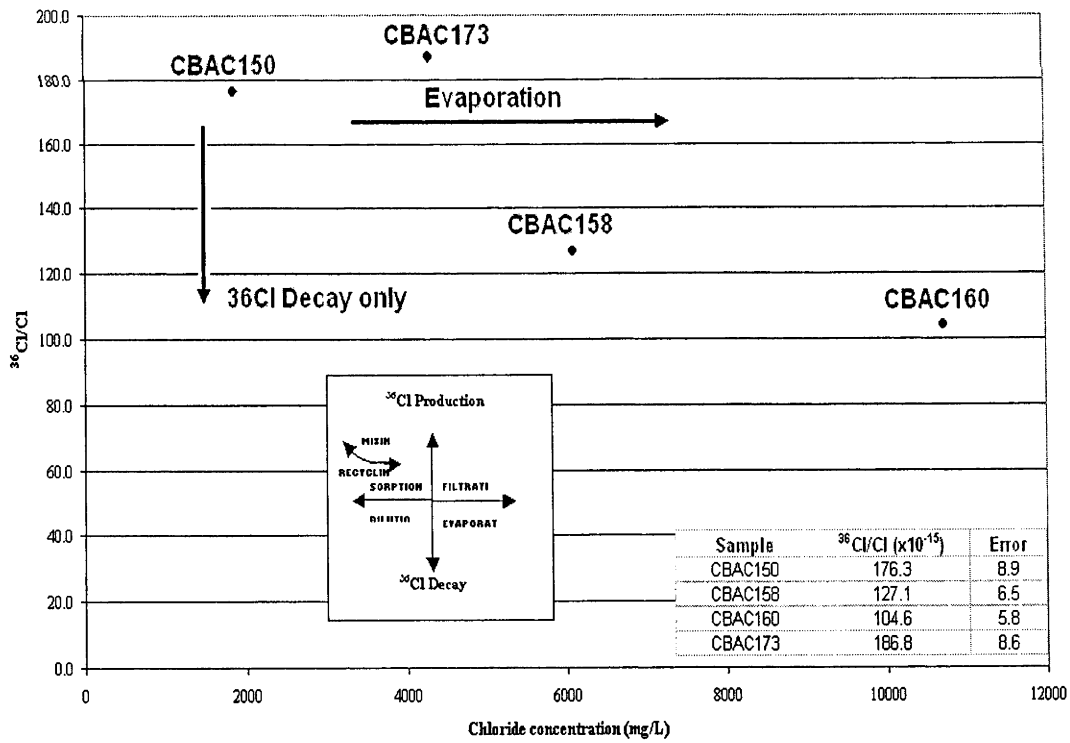

Figure 7.19 ^{36}Cl /Cl versus chloride for the Byrock groundwater samples. Process trends are shown by arrows (Bird *et al.*, 1991).

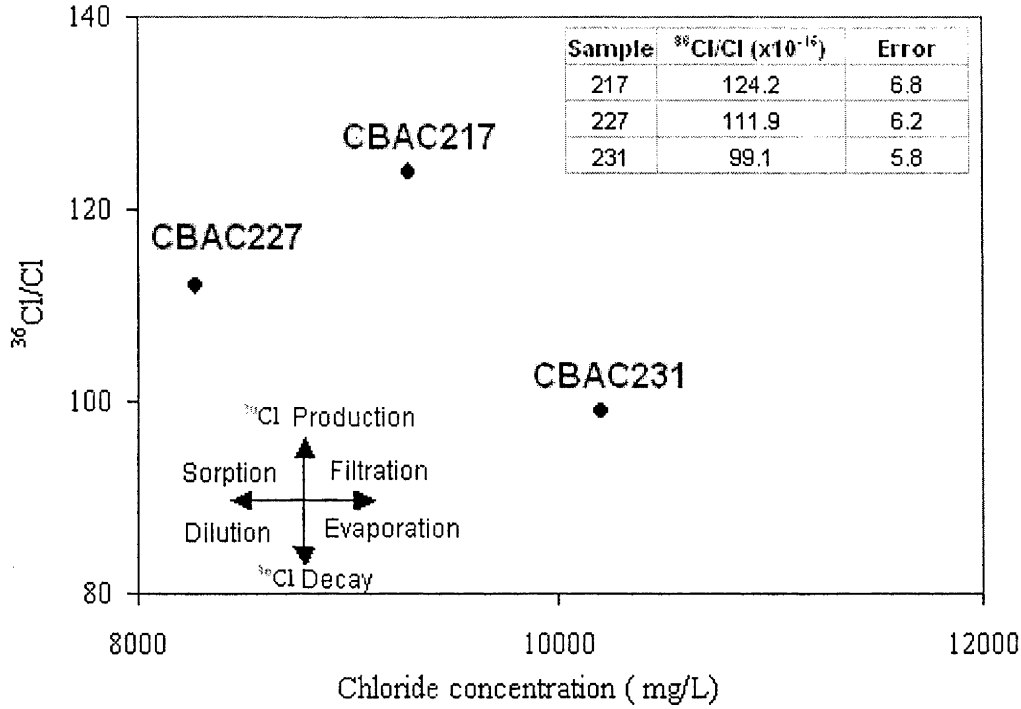

Sample	^{36}Cl/Cl (x10^{-15})	Error
217	124.2	6.8
227	111.9	6.2
231	99.1	5.8

Figure 7.20 ^{36}Cl /Cl versus chloride for the Hermidale groundwater samples. Process trends are shown by arrows (Bird *et al.*, 1991).

hydrogeochemistry and the interaction between groundwater and regolith, the measured element concentrations in the groundwater were plotted on activity-activity diagrams and mineral saturation indices for all samples were calculated. The Geochemist's Workbench Release 6.0 (Bethke, 2005) with the associated thermo.dat database of thermodynamic properties was used for all calculations.

7.9.1 WEATHERING OF SILICATE MINERALS

The concentrations (activities) of the major cations and anions can be employed to understand solution-silicate mineral equilibria in terms of pH. Depending upon the relative concentrations of major cations, it is possible to identify the chemical weathering stage and type of source rock. The suite of silicates with which each groundwater sample is saturated can be used as another type of signature for classifying aquifer lithology (Giblin, 2001). The initial weathering product of silicate minerals in which the groundwater is saturated is gibbsite and as the weathering process continues more silica is dissolved into the groundwater and the next principal saturated mineral will be kaolinite (Helgeson *et al.*, 1969). Depending upon the concentrations of major

cations, continued interaction with groundwater causes the principal saturated mineral to change from kaolinite to K-mica or K-feldspar or in the case of Na or Ca to smectite.

All the water samples (except CBAC173) plot in the muscovite stability field on a log a K^+/H^+ (as representative of K-Feldspar, K-mica, kaolinite) versus log a Mg^{++}/H^+ (representative of Mg-silicate, Mg-smectite, chlorite) diagram indicating stability of these waters with respect to muscovite (Figure 7.21). The water sample from drill hole CBAC173 plots close to the kaolinite- muscovite stability boundary. There are two apparent distribution trends: the CBAC235-CBAC243-CBAC242 trend and the CBAC173-CBAC219 trend (Figure 7.21). These trends show that the groundwaters are associated with variously weathered versions of K-Mg mica. The XRD results showed dominant occurrence of muscovite (K source) within the aquifer minerals in drill holes CBAC217 (22.9 wt %), CBAC 219 (41.2 wt %) CBAC227 (29.5 wt %) and CBAC248 (42.8 wt %; Appendix 4). Occurrence of Mg is possibly relates to the Mg principal isomorphous replacement for octahedral Al of muscovite (Deer et al., 1992) and /or occurrence of Mg-rich clay minerals. This illustrates how groundwaters can reflect the mineral species in the underlying regolith and bedrock.

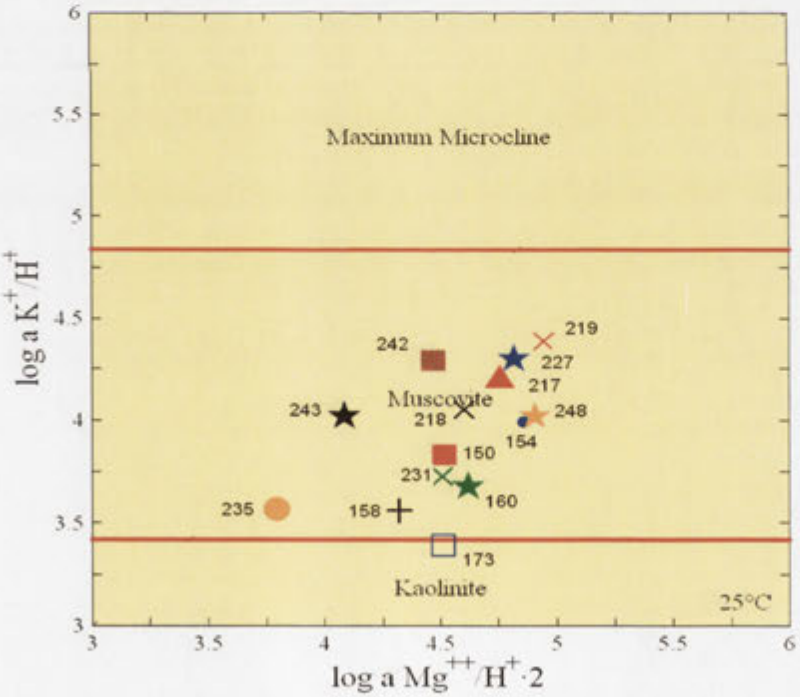

Figure 7.21 Hermidale and Byrock groundwaters plotted on a portion of the log a K^+/H^+ versus log a Mg^{++}/H^+*2 diagram which covers the stability fields of kaolinite, muscovite and maximum microcline in equilibrium with quartz and water at 25°C and 1 bar.

muscovite and maximum microcline in equilibrium with quartz and water at 25°C and 1 bar.

7.9.2 SATURATION INDICES

Saturation index calculations can be useful in examining groundwater composition for the stability of a mineral of interest in an aquifer system (Jeong, 2001). The spatial distribution of saturation indices is possibly useful in vectoring to mineralisation (Khider and McPhail, 2005). The geochemical program PHREEQC (Parkhurst and Appelo, 1999) with Minteq database was used to calculate saturation indices for the groundwaters. In order to predict the saturation state of common primary and secondary minerals, dissolved concentrations of Ca, Al, Fe, K, Mg, Si, SO_4^{2-}, HCO_3^-, Cl^-, pH, Eh and temperature of groundwaters were required in the input file. The output file of PHREEQC displays the saturation state of all the possible minerals (based on the chemical system and database) as positive or negative index values. Positive values indicate supersaturation of minerals, zero value indicates that the solution is in equilibrium with a mineral, and negative values indicate undersaturation of a mineral. However, these results only specify possible reactions, as kinetic constraints may limit reactions that are thermodynamically indicated. For example, waters are commonly in equilibrium with calcite, but may become over-saturated with respect to dolomite as a result of slow solution equilibration with this mineral (Drever, 1997).

The SI for a number of relevant phases (generally the least soluble mineral phase for each element tested) is shown in Appendix 6. Figure 7.22 shows examples of $ZnSiO_3$ (chosen to avoid the measurement uncertainty and complications of variables such as Eh and CO_2, which may affected by atmospheric interaction during measurement), malachite ($Cu_2(OH)_2CO_3$) and tenorite (CuO) for the Hermidale groundwaters. In general, the saturation index for all these minerals increases from south to north, with the exception of drill hole CBAC173. Known mineralisation at the Budgery mine lies to the northwest of drill hole CBAC150, so the slight change in SI appears to indicate the position of the mineralisation, even though the inferred flow paths are from southwest to northeast (Figure 7.10). Similarly the increasing SI for these minerals in drill hole CBAC173 is possibly related to mineralisation at the Glengarry gossan (see Chapter 3, Figure 3.7).

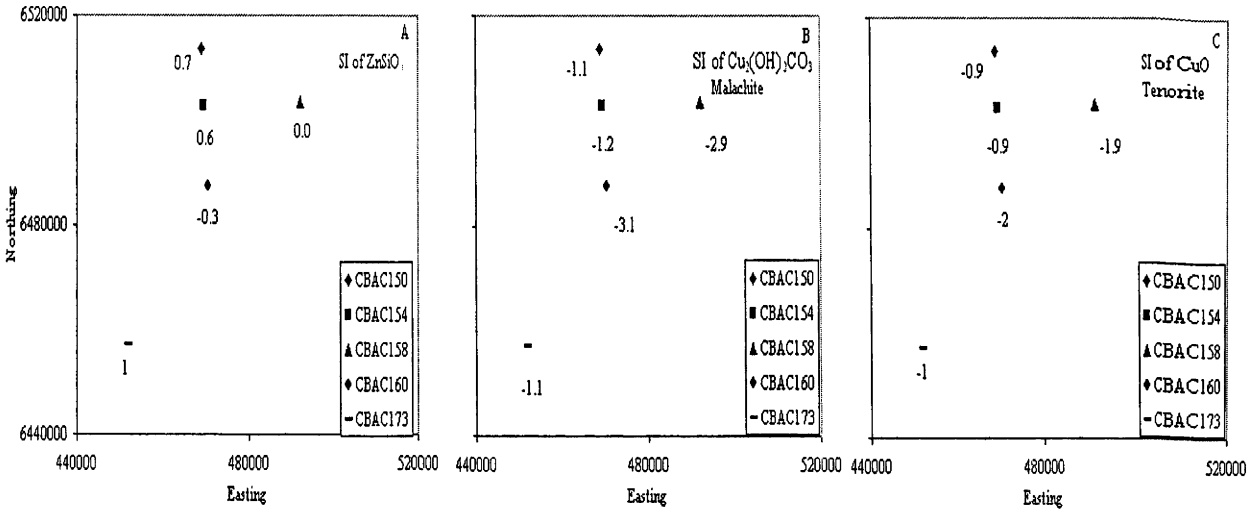

Figure 7.22 Calculated saturation indices of $ZnSiO_3$ (A), malachite (B), and tenorite (C) in Hermidale groundwaters.

7.10 IMPLICATIONS FOR EXPLORATION

Groundwater field and laboratory measurements, in addition to data on the regional geology, groundwater flow and spatial distribution of rock units, are important resources for exploration. Groundwater geochemical exploration procedures are based on comprehensive chemical analyses of groundwater parameters to identify the components of rocks and minerals that have interacted with water, especially those that host ore deposits (Giblin, 2001; Phipps *et al.*, 2004).

It is important to understand regolith-water interactions that alter groundwater composition because these interactions may include mineral dissolution, incongruent aqueous alteration of minerals or dissolution of salts in the unsaturated zone of local regolith and/or by downward moving surface waters or upward moving groundwaters. Therefore, depending on how long a groundwater has been in contact with the minerals, the solutes it contains could potentially reflect the geochemistry of an extensive volume of crustal (regolith) materials. A groundwater that is sampled at a specific location and depth below the water table potentially represents the solute content of all aquifers in

hydraulic contact with that location and the closer to a specific unit a sample is collected, the greater will be the proportion of its total solutes derived from that unit (Giblin, 2001).

This study has investigated the anomalous occurrences of base metals (particularly Cu and Zn) in groundwater using the geochemical parameters of groundwater (i.e., Eh, pH, salinity) and correlated these with the concentration of these metals in the regolith of the aquifers. The concentrations of the base metals in the groundwater depend on the quantity of the base metal minerals in the regolith and solvent capacity of the contacting groundwater. This capacity varies with temperature, Eh, pH and groundwater composition (Drever, 1997).

In the Girilambone region the waters were found to be generally undersaturated with respect to oxidised copper and zinc minerals, assuming all the copper and zinc are oxidised (dissolved and solid). Although Eh was not measured in the Hermidale samples, other samples from the area had an average Eh of 350 mV. At these conditions, plotting of the groundwater samples on pH-pe diagram show that the all water compositions plot in the undersaturated zones for Cu and Zn on (Figure 7.23).

The spatial distribution pattern of Cu and Zn in the groundwater shows significant association between Cu and Zn particularly in a number of drill holes (CBAC150, CBAC154, CBAC158, CBAC160 and CBAC173) in the Hermidale area. The pattern also displays a high concentration of Cu (0.33 mg/L) in drill holes CBAC217 and elevated concentration of Zn (0.35 mg/L) and (0.29 mg/L) in CBAC219 and CBAC248, respectively (Figure 7.24). It is important to note that Cu and Zn anomalies in these drill holes are not associated, as commonly observed in the regolith as a result of accommodation of these metals by Fe- and/or Mn- oxides/oxyhydroxide (Chapter 9). Enrichments of Cu and Zn in the groundwater are not correlated with the Cu and Zn values in the immediate regolith aquifers of CBAC217 and CBAC219 (Figure 7.25). This, in addition to the location of these drill holes near known mineralisation at the White Tank prospect and the Wilga Downs prospect (Figure 7.2) suggests the groundwaters are carrying a geochemical signature from mineralisation. Elevated concentration of Zn is also observed in the groundwater of drill hole CBAC248,

The distribution pattern of groundwater electrical conductivity, and contents of SO_4^{2-}, Cl^-, Cu^{2+} and Zn^{2+} show remarkable correlation between Cu^{2+} and the salinity parameters (EC, SO_4^{2-} and Cl^-), which indicate significant influence of salinisation on Cu concentration and solubility (Figure 7.26). It has been reported (Giblin, 2001) that under equivalent Eh, pH conditions Cu solubility proportionally increases with chloride concentration of groundwater.

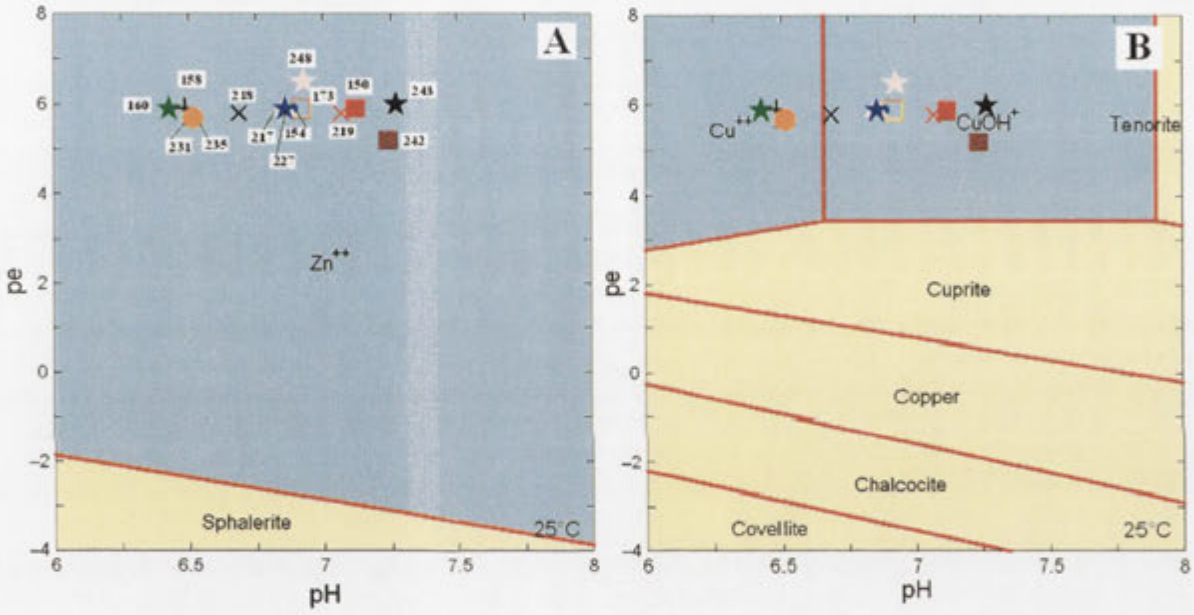

Figure 7.23. The Hermidale and Byrock groundwater compositions, mineral stability fields and aqueous species predominance areas. Diagrams are calculated assuming representative conditions of the samples: (A) a $_{Zn\ species} = 8.7 \times 10^{-7}$ (B) a $_{Cu\ species} = 1.3 \times 10^{-7}$ with a $SO_4^{2-} = 4.1 \times 10^{-3}$ and a $HCO_3^- = 9.9 \times 10^{-3}$. Sample labels in B are as in A.

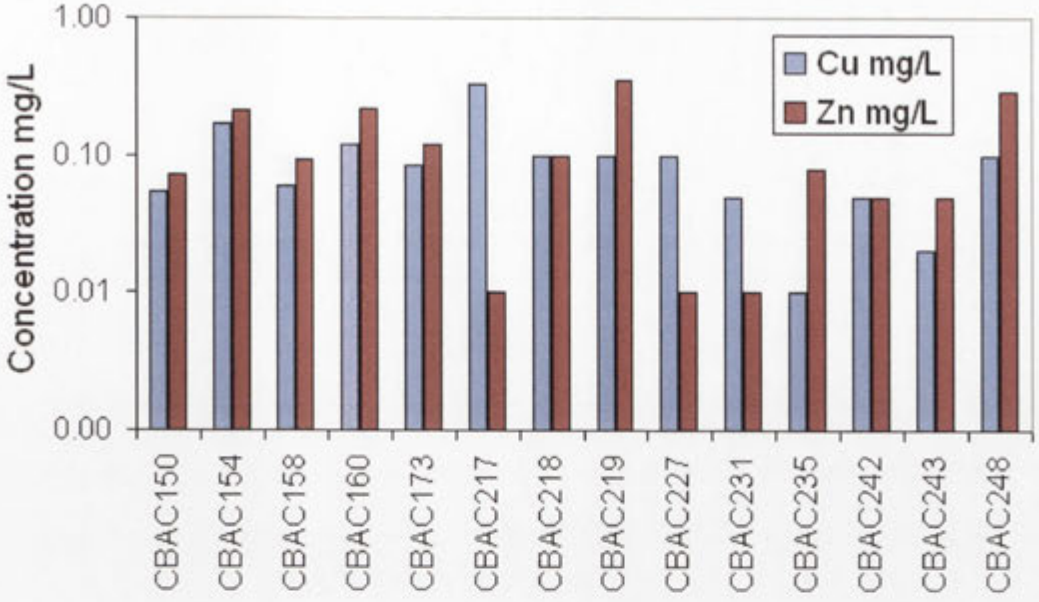

Figure 7.24. The distribution pattern of Cu and Zn in the groundwater of the Byrock and Hermidale drill holes.

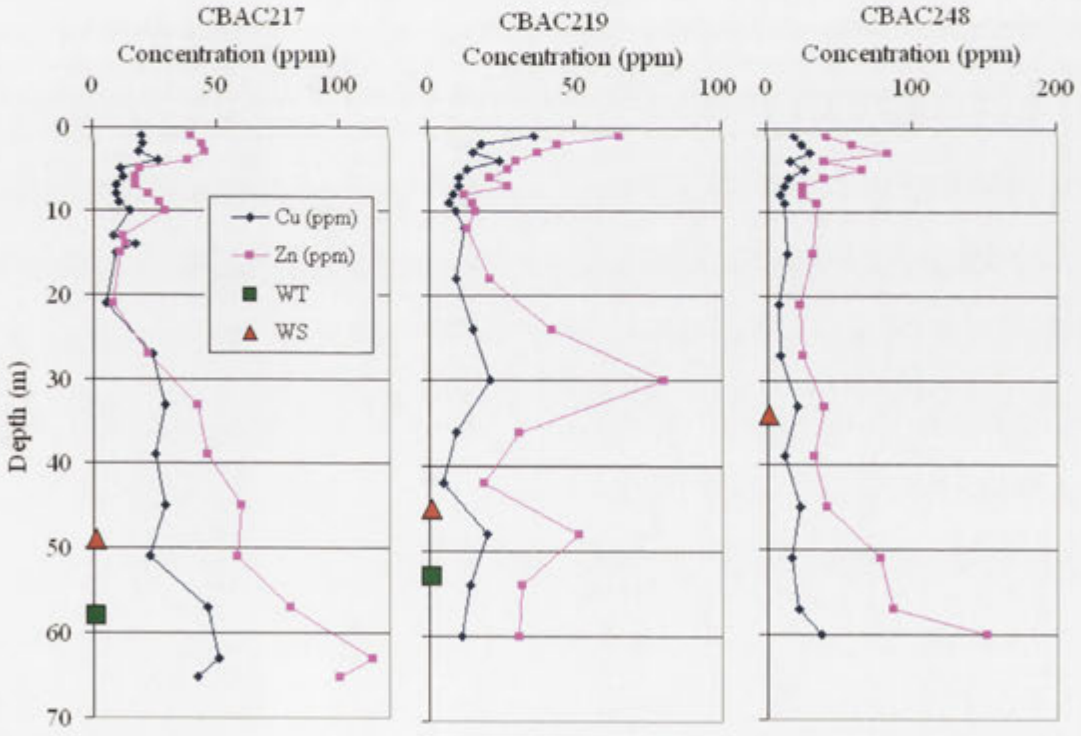

Figure 7.25 Distribution profiles of Cu and Zn in the regolith of the Byrock drill holes CBAC217, CBAC219 and CBAC248 with water table (green square) and sample (red triangle) levels.

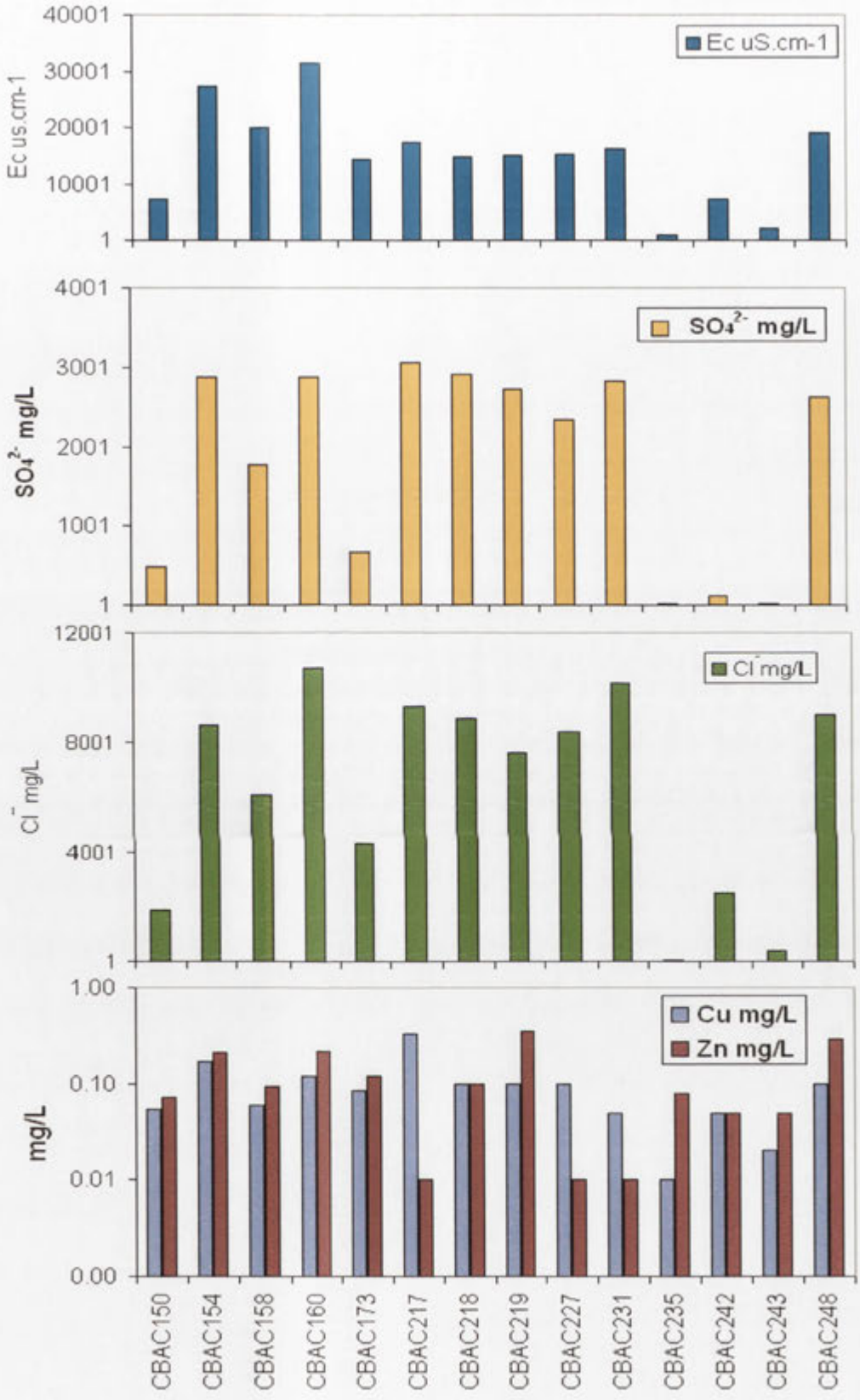

Figure 7.26 Distribution patterns of EC, SO_4^{2-}, Cl^-, Cu and Zn in groundwater of the Byrock and Hermidale drill holes.

7.11 SUMMARY AND CONCLUSIONS

Analysis of groundwater samples from the Byrock and Hermidale areas showed that the groundwater is moving slowly through the regionally extensive weathered phyllitic siltstone-sandstone layer of the *in situ* regolith. Water levels mirror topography, indicating an unconfined aquifer system, and groundwater is flowing in general to the northeast in the Hermidale area and similarly in part of the Byrock area. The groundwater in the region is mainly of chloride type, rich in Na, Cl and SO_4 .The other calcium-bicarbonate and bicarbonate-chloride types are less common. The correlation between Br/Cl and Na/Cl shows three processes affected the groundwater composition. These are evaporation, in which both ratios increase; water-rock interaction; and water mixing, in which Na/Br and Cl/Br increase respectively. Salinity and $^{36}Cl/Cl$ values indicate that mixing of groundwater is likely. Calculation of groundwater ages based on $^{36}Cl/Cl$ showed that the ages range from 241,000 to 492,000 years in the Hermidale area and from 418,000 to 516,000 years in the Byrock area. The waters are undersaturated with respect to oxidised copper and zinc minerals. Calculated saturation indices of $ZnSiO_3$, malachite and tenorite appear to show a vector towards known mineralisation at some sites in the area. The correlation between the groundwater and regolith composition suggests at least two sites (drill holes 217 and 219) of potential mineralisation.

8. CHAPTER EIGHT: WEATHERING PROCESSES AND PROVENANCE

8.1 INTRODUCTION

Clastic sedimentary rocks contain a record of their provenance and of the processes that have operated during weathering, erosion, sedimentation, and after deposition. In most cases, the geochemical "signals" from both provenance and processes are intermingled and complex (McLennan *et al.*, 2003), and accordingly this record can be difficult to understand. In the last thirty years major developments in petrography and geochemistry have greatly advanced our ability to evaluate the detailed sources and history of sedimentary rocks and in turn use this information to recognise parental material, tectonic association, diagenesis and climate (Gu *et al.*, 2002; Lentz, 2003).

Different weathering and erosional regimes can produce regolith with different mineralogical and chemical characteristics. In this way landscape evolution leaves a geochemical signature. Geochemical data from regolith can be used to: differentiate regolith materials with different regolith histories (e.g., Robertson *et al., 1997;* McQueen, 2006); determine the parent rock type and provenance (e.g., Hallberg, 1984; Roser and Korsch, 1988; 1999; Roser *et al.*, 2002; Khider and McQueen, 2005) and to identify geochemical alteration/dispersion haloes of mineral deposits (e.g., Whitbread and Moore, 2004).

This chapter examines the significance of geochemical parameters (i.e., elemental ratios) and indices (e.g., Chemical Alteration Index (CIA)) to understand how geochemistry can be used to evaluate the provenance and weathering history of terrigenous regolith materials in the Girilambone region. Data from this study are compared with available geochemical analyses of felsic and mafic igneous intrusives and identified sedimentary rock units (Girilambone and Cobar Groups) from the Cobar-Girilambone region. In this study, 190 bottom of the hole samples of saprolite and saprock (compared to saprock, saprolite has more than 20% of weatherable minerals altered, Eggleton, 2001) from the Byrock, Sussex and Hermidale areas were analysed (Appendix 2).

The main stratigraphic units in the Girilambone region are the Girilambone Group (Cambro-Ordovician) and Kopyje Group (Late Silurian-Early Devonian; Chan *et al.*, 2001; 2002; 2004). Stratigraphy and bedrock geology of the study area were discussed in detail in Chapter 3.

8.2 GEOCHEMICAL APPROACHES TO EVALUATE SEDIMENTARY PROCESSES

A dominant control on the chemical composition of clastic sediments is the composition of the source rocks or provenance (McLennan *et al.*, 2003). Typically these sources comprise a complex mixture of upper crustal igneous/metamorphic lithologies, volcanic arc-related lithologies and recycled sedimentary rocks (McLennan *et al.*, 1990; Johnsson, 1993; McLennan *et al.*, 1993). A variety of other sources such as localised volcanic and mafic intrusives may also be locally important. Chemical analyses of the main rock-forming minerals and representative Australian rock types (parent material) in each category have been reviewed in a number of studies (e.g., Joplin, 1963; 1965; Taylor and McLennan, 1985; Gray and Murphy, 1999; 2002). These analyses can be use for broad comparisons with saprolith.

A variety of sedimentary processes, including weathering, transport (sorting) and diagenesis can cause profound changes to compositions (McLennan *et al.*, 2003); however, the potential influences exerted on sediment geochemistry by these processes are reasonably well understood (Fralick, 2003). Source rock composition will, to a large degree, control the amount and type of framework grains, in contrast to finer material capable of being generated elsewhere (Heins, 1993; Palomares and Arribas, 1993).

The presence of more than one unknown variable (weathering rate, sorting, climate, metasomatic and metamorphic influences) in the equation relating sediment composition to its controlling factors makes a linear solution to the problem of determining sources area composition from sediment composition impossible (Fralick, 2003). A partial solution can be obtained if all variables but one are constant. For example, in the saprolith the sediments are adjacent to source area and on the local scale these sediments have undergone similar weathering and diagenetic processes.

Thus the chemical differences could be ascribed to differences in chemical composition of the source rock.

An alternative approach is to identify elements in the geochemical data set whose concentration depends only on the parent material or other factors (i.e., sorting, climate, etc.), which can be determined and quantified. The major problem in using sediment geochemistry to infer source area composition is in establishing which elements are immobile (Fralick, 2003). MacLean (1990) has developed a technique for determining elemental mobility during alteration of volcanics, including a continuously fractionated series, and suggests that sedimentary rocks with primary continuity of chemical composition are amenable to the procedure. The basic tenet of the technique is that immobile elements will increase or decrease in concentration as mobile elements are lost from, or gained by, the rock. The technique of plotting immobile-immobile, mobile-immobile and mobile-mobile element ratios can be used to identify the source rock composition and hydrodynamic influence or sorting (Barrett and MacLean, 1991).

Additional information can be obtained on the alteration history of a data set by employing a second technique. This technique rests on the premise that chemical weathering acts, over time to destroy all major primary mineral phases except quartz as a framework constituent of sand. Given that quartz-rich (high SiO_2%) sands are more mature, this assumption seems to be generally tenable (Fralick, 2003). Therefore plotting element concentration in contrast to SiO_2 provides further information about relative mobility, sorting and source rocks as discussed below.

8.2.1 TESTING ELEMENT IMMOBILITY

One method of testing element immobility involves plotting pairs of elements that are suspected of being immobile, e.g., Al, Ti, Zr, Nb, Y, Sc, La, Ce and Th (Bhatia and Crook, 1986; Condie and Sinha, 1996; Fralick, 2003; Niu, 2004).

In this study, and for saprolith after sedimentary rocks, saprolith sediment element pairs involving Al_2O_3, TiO_2, Nb, Sc, La, Ce and Th form the strongest correlation (R^2 ranges from 0.4 to 0.8) with linear arrays along lines extending through the origin (Figure 8.1). Thorium displayed an insignificant (R^2 =0.1) linear pattern with Al_2O_3 (Figure 8.1 H).

The distribution of points in Figure 8.1 requires that Al_2O_3, TiO_2, Nb, Sc, Ce and La were immobile and hydraulically fractionated in a similar manner. Deviations from linearity may be caused by the main mineral phases containing these elements. Zirconium and La (except La vs. Ce Figure 8.2B) are not significantly correlated with the other elements (Figures 8.1- 2). The patterns produced by Zr when plotted against chemically immobile elements show a broad indirect correlation with Al_2O_3 (Figure 8. 1 D) whereas its correlation with TiO_2 is not significant.

Plotting Al_2O_3, TiO_2, Nb, Sc, Zr and Th against SiO_2 concentrations in the saprolith provides further insight into chemical and hydrodynamic behaviour of their major mineral phases (Figure 8.2 F-K). Trends in Zr data indicate that Zr is proportionally increasing with SiO_2, which suggests that Zr is preferentially concentrated in the quartz-rich (high SiO_2) relatively coarse fraction (Figure 8.2 J). However, deviation from this trend may be related to a variation in source composition or recycling processes (see below). Figures 8.2 (A, B, C) clearly indicate that Ti, Al and Nb are concentrated in the clay (low SiO_2) fraction.

8.2.2 WEATHERING AND CHEMICAL INDEX OF ALTERATION (CIA)

Weathering is the process that most significantly influences the geochemistry of terrigenous sedimentary rocks. Geochemical relationships associated with weathering phenomena are discussed in Chapter 9. Typical weathering of the upper continental crust is dominated by the alteration of feldspar, and during weathering and transport plagioclase is less stable than K-feldspar leading to an increase in K-feldspar/ plagioclase and K_2O/Na_2O ratios (Nesbitt, 2003). If the relatively resistant mineral quartz is neglected the average of the feldspar group of minerals composes approximately 70% of the upper crust (Nesbitt and Young, 1984; Taylor and McLennan, 1985). Thus, much of the effect on major-element compositions can be evaluated in the geochemical system using the relative mole fractions of Al_2O_3-(CaO*+Na_2O)-K_2O (coded as A-CN-K diagram; Nesbitt and Young, 1984).

A weathering index (CIA) can be formulated using these components such that:
CIA= 100* [Al_2O_3 / (Al_2O_3+CaO*+ Na_2O+K_2O)] (Nesbitt and Young, 1982; 1984; 1996) where CaO* refers only to the calcium associated with silicate minerals.

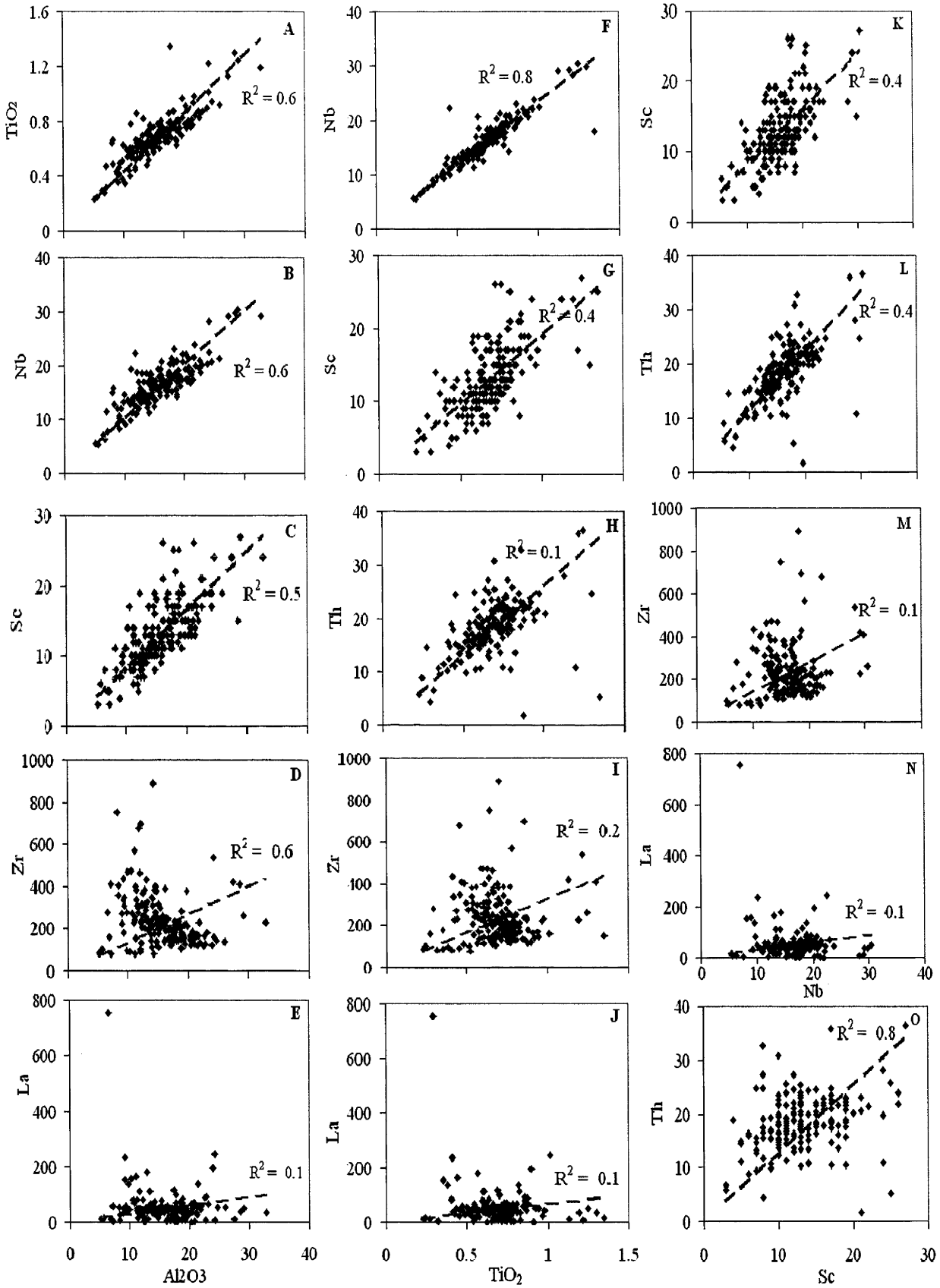

Figure 8.1 Scattergrams showing correlations between likely immobile elements: Al, Ti, Nb, Sc, Zr, La and Th. Dashed line represents the best linear regression through the origin.

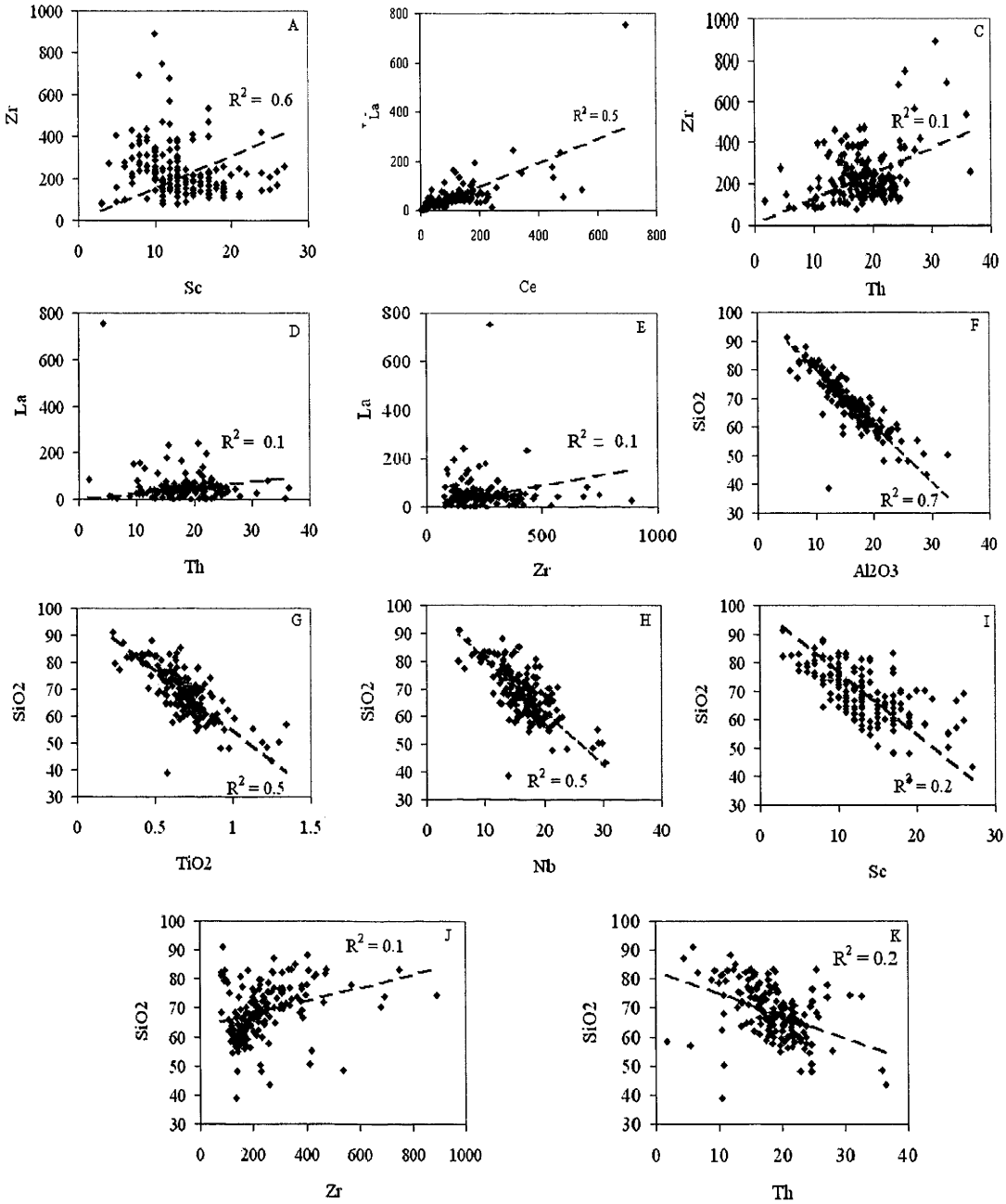

Figure 8.2 Scattergrams showing immobility test correlations of Zr, Sc, La, Ce and Th, also plots for Al, Ti, Nb, Sc, Zr and Th against SiO_2 (Dashed lines represent best linear regression fit).

In the Girilambone region the CaO values are generally low (<0.2 wt %). The positive correlation of high CaO values (<3%) and Al_2O_3 (Figure 8.3) suggests that the high content of CaO in the saprolith samples compared with that in the Post-Archaean Australian Shale (PAAS, Taylor and McLennan, 1985) is not due to a high amount of calcium carbonate. High CaO values are associated with high values of mafic related

elements (i.e., Ni, Cr, Co, Appendix 2). These associations together with the observed absence of carbonate minerals in these samples (Chan *et al.*, 2001; 2002; 2004) strongly support a silicate related origin for the Ca.

Sodium is commonly the most useful dissolved indicator of silicate weathering. This is because it is easy to measure and it is derived almost entirely from the hydrolysis of a single dominant mineral (plagioclase). It is also the most nearly conservative of the major cations (ranked last in both soil exchange preference and biological utilization; Staufer 1990). However, high Na values in the regolith may also be related to occurrences of added salts (e.g., NaCl), therefore it might be necessary to correct for Na_2O using Cl analysis (McLennan *et al.*, 2003). This correction for sodium concentration (Na* = Na - 0.86Cl Staufer, 1990) reflects the conventional understanding that Na:Cl in wet and dry deposition follows the marine ratio and that both ions behave conservatively once in solution (Staufer, 1990).

The samples in this study generally have low Na_2O contents (<1 wt%; Appendix 2) and applying the correction to high values (>1%) of Na_2O showed that the amount of additional Na that is probably derived from the salt source is insignificant (Appendix 2).

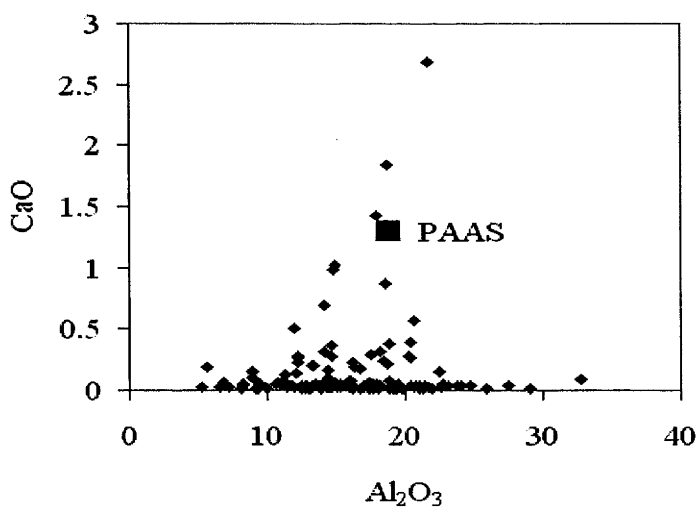

Figure 8.3 Scattergram showing correlation between Al_2O_3 and high CaO concentration values in base of the hole saprolith samples from the Girilambone region. Post-Archaean Australian Shale (PAAS) is from Taylor and McLennan (1985).

Weathering trends can be displayed on the A-CN-K triangular plot (Figure 8.4A). On this diagram the initial stages of weathering form a trend parallel to the $(CaO+Na_2O)$-Al_2O_3 side of the diagram, whereas advanced weathering shows a marked loss in K_2O as compositions move towards the Al_2O_3 apex (Figure 8.4 A). The trends follow mixing lines representing the removal of alkalies and Ca in solution during the breakdown of first plagioclase and then potassium feldspar and ferromagnesian silicates (McLennan *et al.*, 2003).

The CIA and weathering trends on triangular plots have been used in two different ways (Rollinson, 1993). Firstly, chemical changes in a recent weathering profile such as that illustrated in Figure 8.4A are used as a template to evaluate the chemical history of ancient profiles. Deviations from such trends can be used to infer chemical changes resulting from diagenesis or metasomatism (Nesbitt and Young, 1984; 1989). The second is that the A-CN-K diagram was based on the relationship between feldspar weathering and Al concentration of modern muds (silt, clay). While it has been successfully used to understand the chemical composition and weathering history of ancient muds, it is not so readily applied to sandstone particularly when the sands are not well sorted (Nesbitt, 2003). It is also important to remember that when dealing with weathering of sedimentary rocks, the sediment forming the rock has already gone through previous cycles of weathering and that this is part of the overall geochemical composition.

CIA values typically range from about 50 or less for most unweathered igneous and metamorphic rocks to 100 for pure aluminosilicate residues such as kaolinite (McLennan *et al.*, 2003). The CIA scale is shown to the left on Figure 8.4.

To identify the effect of weathering, all the bottom of hole saprolith samples from this study were plotted onto the A-CN-K diagram, including samples characterised by apparent igneous (mafic-intermediate) composition, and the CIA was calculated (Figure 8.4B). Slightly weathered sediments as characterised by CIA value, show a range from 50 to 70. They plot adjacent to the weathering trends of andesitic - granitic igneous rocks (Figure 8.4B). The deeply weathered samples plot along the muscovite-illite trend close to the Al-K boundary with high Al content. It has been observed that high

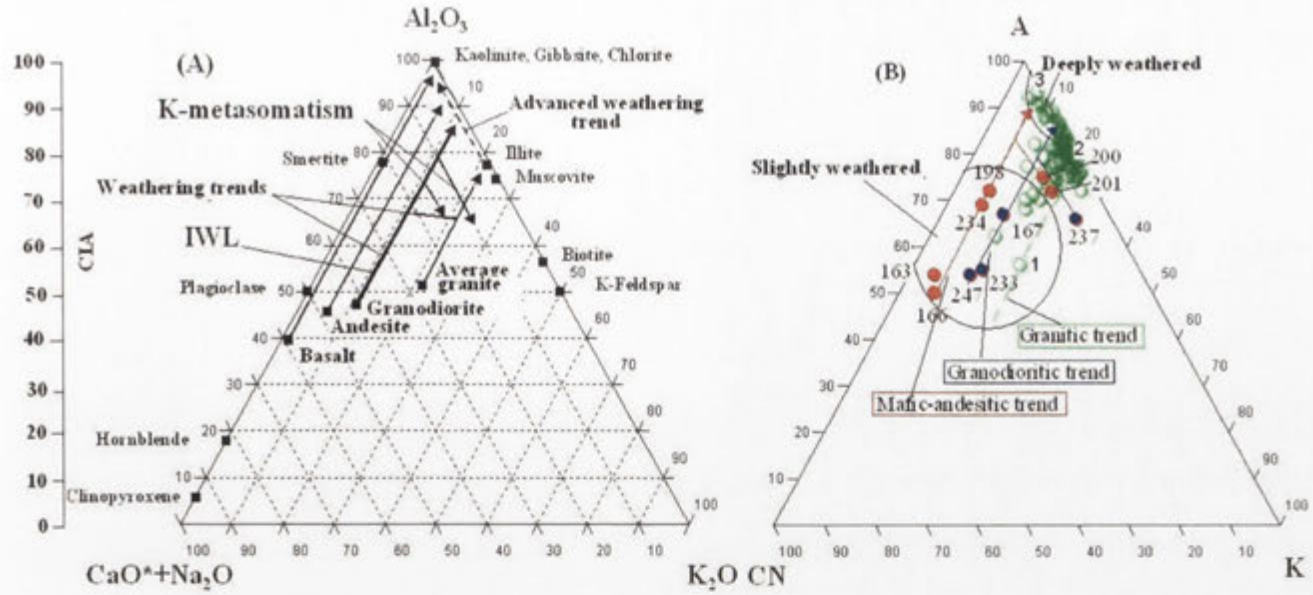

Figure 8.4 Ternary plots of molecular proportions of Al_2O_3- (Na_2O+CaO*)-K_2O with the Chemical Index of Alteration (CIA) scale shown on the left modified from McLennan and Murray (1999). (A) Shows selected idealized igneous and sedimentary minerals and weathering trends for selected upper crustal igneous lithologies. (B) Shows bottom of the hole saprolith samples from the Girilambone region for slightly and deeply weathered zones and the suggested weathering trends. IWL represents the ideal feldspar weathering line.

Al concentration in marine sediments relates to fine-grained aluminosilicate detrital fractions (Calverts, 1976). Potassium is mostly associated with potassium feldspar ($K AlSi_3O_8$) and illite ($(K, H_3O) Al_2 [(OH)_2 Si_3AlO_{10}]$) (Shimmield and Mowbray, 1991; Martinez *et al.*, 1999; Yarincik *et al.*, 2000). High Al values in these samples (CIA >75) indicate a significant amount of potassium-rich clay, probably produced by advanced weathering processes.

On the A-CN-K diagram the chemical compositions of the slightly weathered igneous rocks show mafic-andesitic and granodioritic weathering trends. The data also display remarkable clustering of points at the muscovite-illite weathering zone parallel to a general weathering trend of granite (Figure 8.4B). These trends are parallel to the ideal feldspar weathering line (IWL) indicating that weathering was the (only) dominant process (McLennan *et al.*, 2003). However leaching of Ca, Na and K during weathering causes a change to bulk composition of the residual weathering products along these

lines from granite to illite (Figure 8.4A, Nesbitt, 2003). Three arbitrarily chosen bulk compositions of the weathering residues labelled 1, 2 and 3 (Figure 8.4B) represent gradual leaching of Ca, Na and K along the granitic weathering trend. The CIA of residue 1 is about 55 and the weathering trend of granite intersects the A-K boundary at residue 2 where the CIA value is about 80. Along or parallel to the A-K boundary the bulk compositions of the samples from sample 2 to sample 3 contain no Ca or Na, hence all plagioclase of the initial granitic material has been weathered to clay (primarily kaolinite but others as well). Illite is likely to have formed after K-feldspar and mica (Nesbitt, 2003). A depletion of K is typically used as an index for maturity of sediments (Zabel *et al.*, 2001); hence K/Al would be a useful proxy for the intensity of weathering.

8.2.3 METASOMATISM

Recognition of metasomatism is important when evaluating the chemical characteristics of the original sediments prior to interpreting the effects of weathering (Fedo *et al.*, 1997; Nesbitt and Young, 1997). Potassium- Na-, and Mg- metasomatism have been studied in paleosols (Nesbitt and Young, 1989; Rainbird et al., 1990). The effects of K-metasomatism are readily discerned in paleosol profiles produced on igneous rocks because their weathering trends can be accurately predicted; they are sub-parallel to the CN-Al boundary of A-CN-K diagram (Nesbitt, 2003). Addition of potassium to partially weathered samples, for example, results in systematic increase in K therefore the metasomatized samples diverge systematically from the weathering trend toward the K apex (Figure 8.4A). Similarly, the weathering trend towards illite diverges from IWL (Figure 8.4A) due to syn- or post-depositional K-enrichment in the clay fraction (Fedo *et al.*, 1995), which suggests significant K- metasomatism of clay minerals (Roser *et al.*, 2002; Nesbitt, 2003).

In this study a significant deviation from the ideal weathering trend is generally observed in some of the saprolith samples. This deviation coincides with the K-metasomatism trend (Nesbitt, 2003, Figure 8.4A), which possibly diverged from the weathering trend of mafic-andesitic and granodioritic sources. The mafic-andesitic weathering trend is identified for samples numbered 166-163-234-198 (Figure 8.4B). Some samples (i.e., 200, 201) diverge from this trend toward K enrichment suggesting that these samples were derived from K-metasomatised mafic source rocks

K-metasomatism was also detected in granodioritic and /or granitic weathering trends. Strong K-enrichment in sample numbered 237 is most probably due to K-metasomatism, which diverted the composition from the granodioritic weathering trend, defined by samples 247- 167 (Figure 8.4B) or from the inferred granitic trend. These two trends overlap because of the gradual composition changes between granodiorite and granite.

8.2.4 SEDIMENTARY RECYCLING

The sedimentary recycling (derivation from older sedimentary rocks) of sediment tends to strongly enrich sands in heavy minerals (e.g. zircon, monazite, rutile and tourmaline) and thus in trace elements associated with those minerals (McLennan *et al.*, 1993, 2003). This relationship can be monitored by a plot of Th/Sc against Zr/Sc (Figure 8.5) for most igneous rock compositions. In this diagram both Th and Zr are incompatible and typically become more enriched relative to the more compatible element Sc. Although both Th and Zr are enriched in heavy minerals (monazite (Ce, La, Th, U) PO_4 and zircon ($ZrSiO_4$) respectively), zircon is typically far more abundant than monazite. Therefore, during sedimentary recycling processes, Zr/Sc tends to become increasingly higher almost independent of changes in Th/Sc (McLennan *et al.*, 2003). First-order sediments show a simple positive correlation between these ratios (Th/Sc and Zr/Sc) whereas recycled sediments show a substantial increase in Zr/Sc with far smaller increase in Th/Sc.

The plotted saprolith data on the Zr/Sc and Th/Sc diagram (Figure 8.5) display a significant increase of Zr/Sc with insignificant or no increase in Th/Sc, suggesting significant recycling. The slightly weathered igneous rocks plot below (more mafic) and above (more felsic) the Th/Sc ratio level (Th/Sc=1) of upper continental crust, indicating that the sources of these sediments are from a wide range of igneous compositions.

8.2.5 SEDIMENTARY SORTING

Although source composition plays a major role in controlling the composition of sediments, other factors such as chemical weathering, mechanical disaggregation and hydrodynamic sorting can also affect the sediment composition to various degrees, according to the transportation system and depositional environments (Johnsson, 1993).

During sediment transport, whether in air or water, minerals begin to separate according to size, density and shape. For the major mineralogical components (and thus major elements) the processes of weathering and sorting may be difficult to differentiate because weathering processes continue during the sediment transport process (Johnsson, 1993).

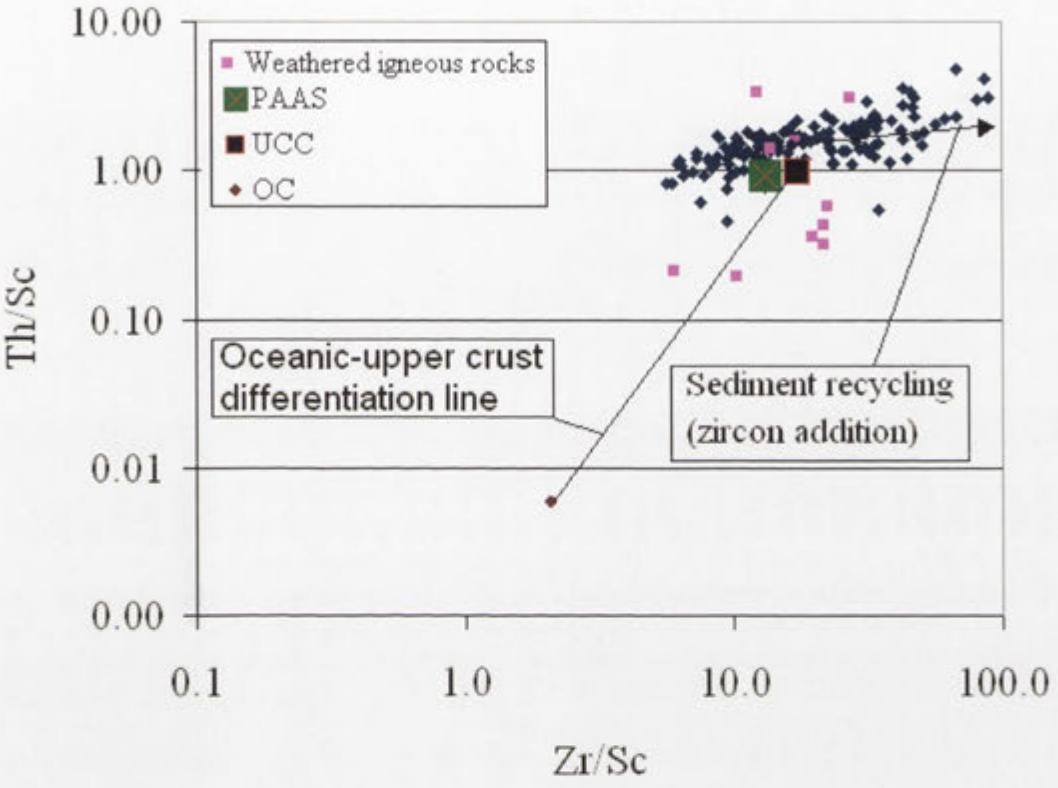

Figure 8.5 Plot of Th/Sc versus Zr/Sc for saprolith of the Girilambone region showing both the oceanic-upper crustal differentiation line and the trend of sediment recycling. Data for the PAAS, upper continental crust (UCC) and oceanic crusts (OC) are from Taylor and McLennan (1985). The Th/Sc ratio of 1 marks the boundary of upper continental crust.

Sedimentary sorting produces alternating shales and sandstones with complementary chemistries. The preferential partitioning of quartz and zircon in the coarse-grained fraction of the sediments results in a strong fractionation between SiO_2, Zr and other components (e.g., Al_2O_3, TiO_2). In other words, the sedimentary sorting causes a systematic fractionation between SiO_2 (quartz) and Al_2O_3 (clay) and also between Zr (zircon) and other minor or trace elements that are preferentially retained in the fine-grained fraction. As a consequence, shales may be defined chemically as having higher Al_2O_3/SiO_2 and TiO_2/Zr ratios than sandstone (Garcia *et al.*, 1994).

The fine scale turbiditic interbedding and high degree of mixing of the air core samples (see Chan *et al.*, 2001; 2002; 2004), meant it was difficult to separate many of the saprolith samples into different grain sizes based on field and petrographic examinations. To minimise the influence of sorting as a masking factor of source composition signature it was important to separate the analysed composite saprolith sediments into sand-dominant sediments and shale (clay)-dominant sediments, based on a geochemical compositional model proposed by Garcia *et al.* (1994). Sediments with TiO_2/Zr and Al_2O_3/TiO_2 ratios higher than 0.33 and 0.23 were considered as shale-dominant and the complementary ones ($TiO_2/Zr < 0.33$ and $Al_2O_3/TiO_2 < 0.23$) as sandstone-dominant (Figure 8.6, Appendix 2).

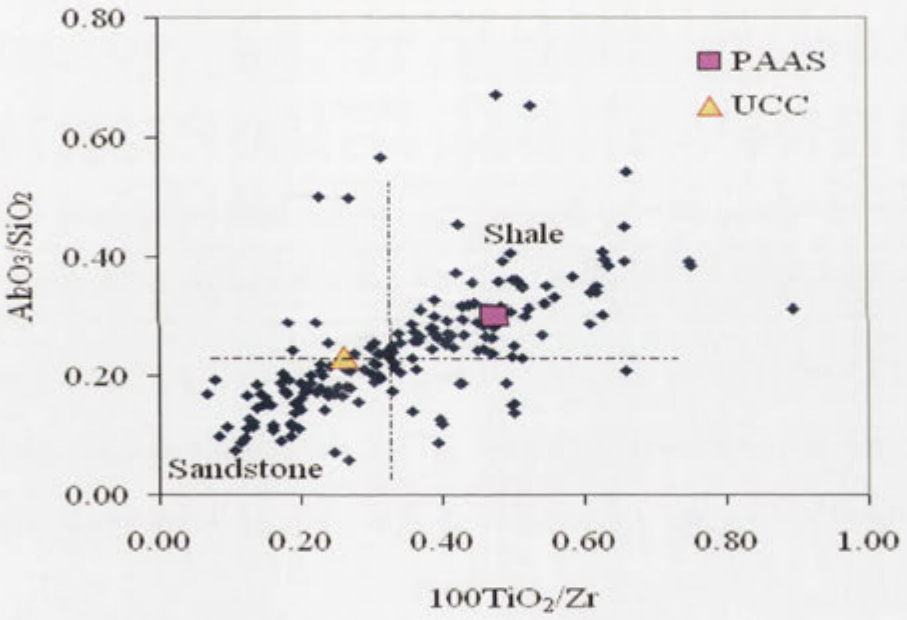

Figure 8.6 $Al2O3/SiO_2$ -$100TiO_2/Zr$ diagram for base of the hole saprolith samples from the Girilambone region. PAAS and UCC data are from Taylor and McLennan (1985).

The relationship between Al and Ti/Zr (as shown on a Al-Ti-Zr ternary diagram; Figure 8.7) was also used to characterise the effect of sorting processes. This diagram is based on the following considerations: sedimentation involves weathering, transport, mixing from different sources and sorting (Sawyer, 1986). In the first three processes, the total contents of typically insoluble elements such as Al, Ti and Zr may vary in response to

leaching of the soluble elements, but their relative proportions are transferred from the source area into bulk sediment without any or with little modification (Zhang *et al.*, 1998). This material is then sorted according to the hydraulic properties of its mineral components and the mechanical and chemical fractionations between complementary shales and sandstone are generated (Garcia *et al.*, 1994; Mongelli *et al.*, 1998). The centre of the Al-Ti-Zr diagram is proposed as the average of bulk sediment (ABS), which represents a conventional chemical boundary between shales and sandstones (Garcia *et al.*, 1994). The diagram also reflects the differentiation of igneous rocks. The Al_2O_3/TiO_2 ratio of igneous rocks is highly sensitive to magmatic differentiation and igneous and sedimentary trends crosscut on the Al-Ti-Zr diagram (Garcia *et al.*, 1994).

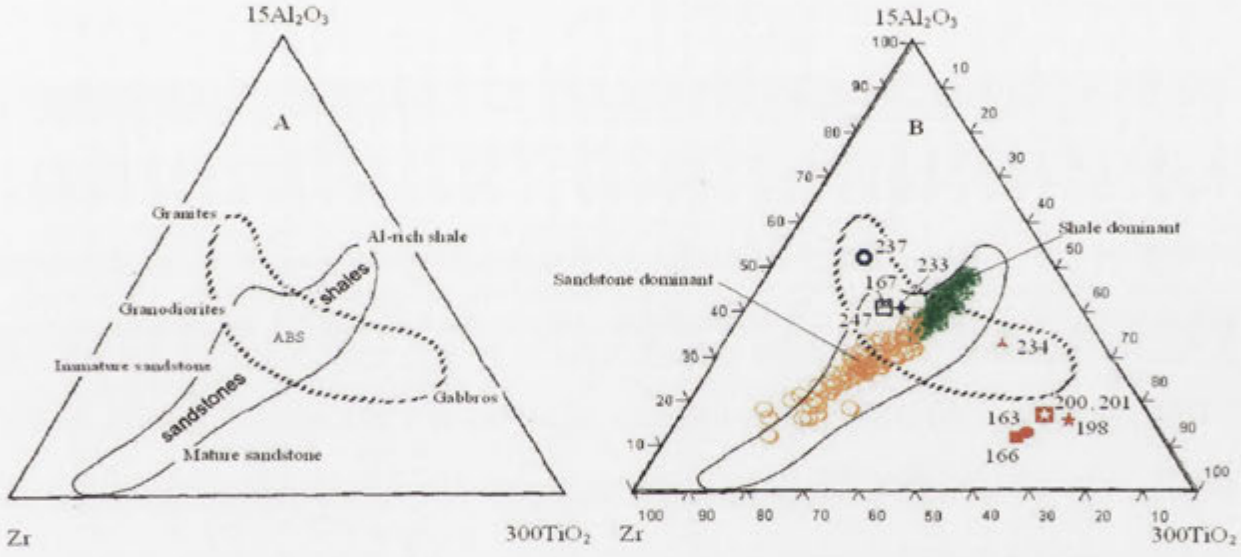

Figure 8.7 Ternary plot of $15Al_2O_3$-$300TiO_2$-Zr summarising the geochemical relations between common sedimentary (solid line boundary) and plutonic (dotted line boundary) trends (after Garcia *et al.*, 1994; A). The saprolith samples from the Girilambone region displays shale, immature sandstone, mafic and felsic igneous composition (B). Numbers represent drill holes.

Plotting the saprolith samples on the Al-Ti- Zr diagram showed a scatter of points along the shale-sandstone trend and the mafic–felsic igneous differentiation trend (Figure 8.7B). Chemical variation in the shale-dominant field is less than its sandstone-dominant counterpart. This is consistent with simple mass-balance considerations. As

quartz is abundant in sandstones, the absolute Al + Ti + Zr content is lower than complementary shales (Garcia *et al.*, 1994). Sandstone-dominant plots trend toward immature sandstone indicating a significant amount of silt and clay within these samples. The diagram also shows that bottom of the hole samples from drill holes CBAC163, 166, 198, 200, 201 and 234 plot adjacent to the mafic igneous field, and others (CBAC167, 233, 237 and 247) plot in the intermediate (granodioritic) igneous field (Figure 8.7.B).

8.3 BEDROCK, WEATHERING AND SEDIMENT COMPOSITIONS

8.3.1 WEATHERING ZONES

Chemical weathering of Al-silicates produces a new suite of minerals including clay minerals, secondary oxides, and hydroxides. The distribution of these constituents within an idealized profile is shown in Figure 8.8 (Nesbitt *et al.*, 1997; Nesbitt, 2003). Secondary minerals generally predominate near the top of weathering profiles whereas primary minerals and rock fragments are more abundant nearer the base. Softer portions of profiles are also likely to be eroded in preference to competent material. Therefore it is essential to identify whether the mineralogy of the derived sediments reflects the mineralogy of the eroded weathering products or the mineralogy of pristine bedrock. In this study, this was investigated as follows:

- identifying the original source composition using the A-CN- K diagram and weathering trends;
- recognising the zone and degree of weathering by calculating the CIA value for each and comparing that with the weathering zone model proposed by Nesbitt *et al.* (1997; Figure 8.8). The least weathered samples (lowest CIA value) are the closest to the original composition;
- calculating the CIA for all dominant lithologies (sand and shale). The studied saprolith materials were most probably derived from the underlying sedimentary bedrocks .The CIA represents the scale of weathering calculated relative to fresh feldspar concentration in the original composition from which the sedimentary bedrocks were produced; and

- classifying the samples based on their immobile geochemical signature (immobile elemental ratios). Samples from the same source composition and different weathering zones (which have undergone different degrees of weathering) will display similar immobile ratios and various CIA values.

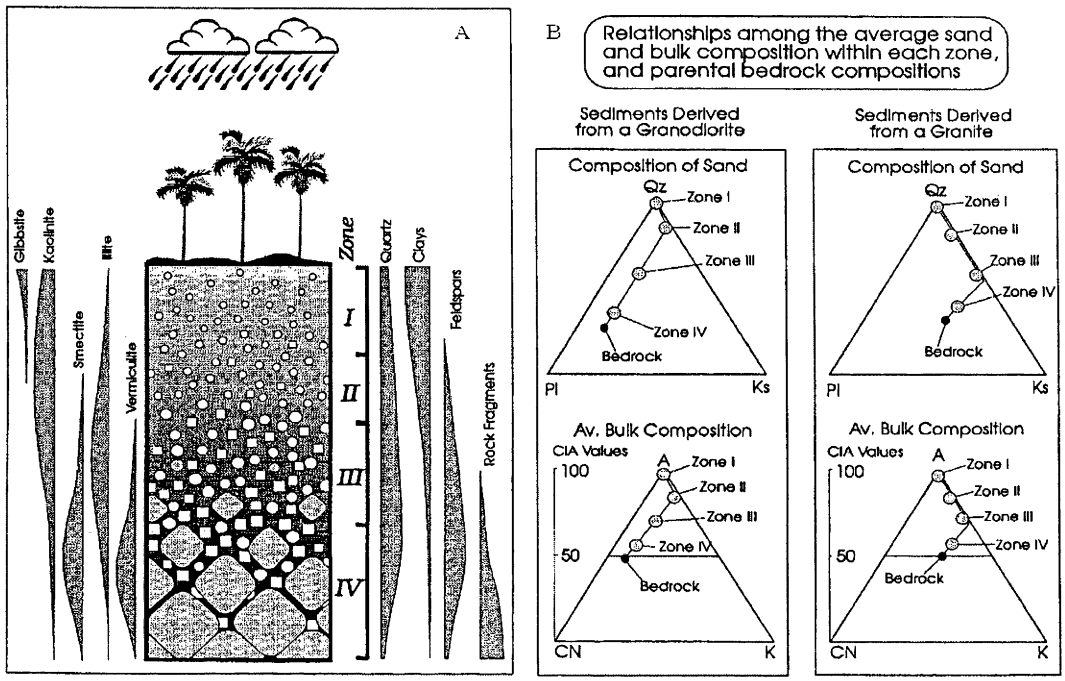

Figure 8.8 An idealized weathering profile developed on granitic bedrock after Nesbitt *et al.* (1997). Qualitative changes in the proportions of clay minerals are plotted to the left of the profile, and qualitative changes in quartz, total clay minerals, total feldspars and rock fragment proportions are plotted to the right of the profile (A). Four weathering zones are shown (I-IV) on Quartz-Plagioclase-K-feldspar (Qz -Pl-Ks) and A-CN-K diagrams illustrate qualitatively the mineralogy and bulk composition of the four weathering zones in sediments derived from granite and granodiorite (B).

As previously discussed, the A-CN-K diagram and the identified weathering trends strongly suggest granite- and granodiorite-type compositions as the main primary source of the sedimentary rocks, now weathered to saprolith in the Girilambone region (Figure 8.4). The saprolith materials are classified based on CIA values using the classification of the weathering zone (Nesbitt *et al.*, 1997) into Zone I (CIA>85), Zone II (85≥CIA>75), Zone III (75≥CIA > 55) Zone IV (CIA ≤55). The original source composition, weathering trend and chemical composition of the saprolith materials in these zones are displayed in Figure 8.9. According to this model, Zone IV and Zone III

are the least weathered, which is consistent with the definition of saprolith (saprock and early stage of saprolite). However, if the sediments were not directly derived from the original (igneous) rocks the chemical composition of the saprolith possibly represents a higher (Zone II or Zone I) weathering zone. Immobile element ratios used to identify the compositional signature of source materials in the weathering zones showed that variations in theses ratios are insignificant compared to the CIA values. This means that the source compositional signature could be maintained by these elements in the saprolith, material despite the intensity of weathering.

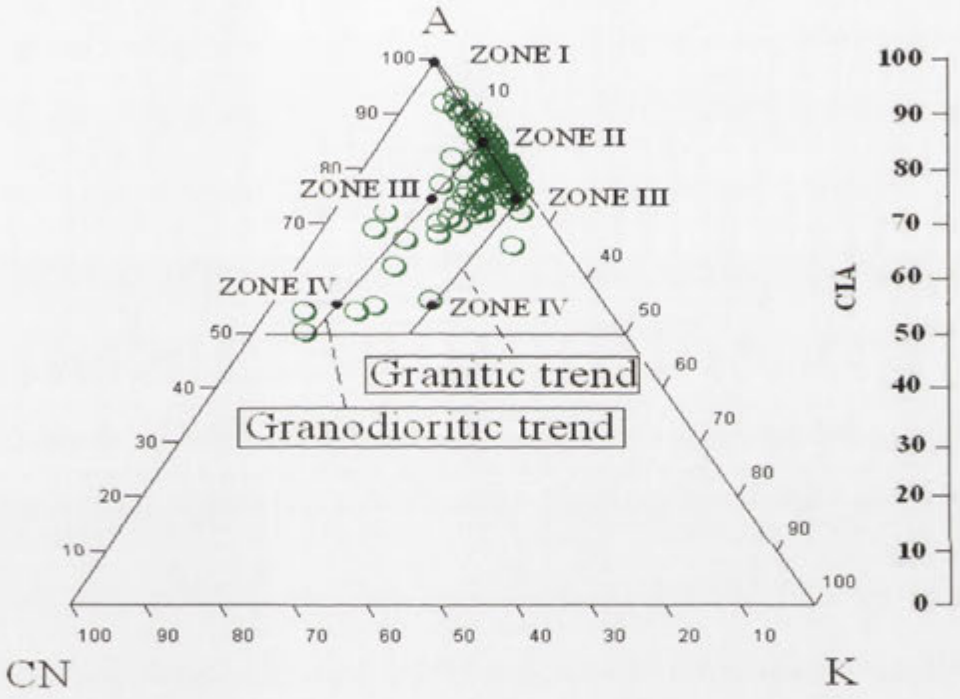

Figure 8.9 A-CN-K diagram shows the weathering zones (I-IV) for saprolith materials of the Girilambone region derived from granitic and granodioritic sources. CIA and Zones composition are calculated from Nesbitt *et al.* (1996; 1997).

8.3.2 BEDROCK IDENTIFICATION

This study has identified mafic and felsic igneous rock composition for some of the regolith samples. An attempt was also made to assess the compositions of the saprolith developed on sedimentary and metasedimentary bedrock. The chemical composition of these saprolith samples are compared with those of fresh rocks from bedrock units suspected to be present (i.e., Cobar Supergroup and Girilambone Group). The data for the Cobar Supergroup (Whitbread, 2004) are for sand and shale units from

unmineralised sites in the Elura area. Those for the Girilambone Group are from Ackerman (2005).

To minimise the effects of weathering processes the comparison between the data sets is based on likely immobile element associations. Conservative elements (Ti, Al, Ce, La) are reported to be relatively immobile in both sand and shale units of the Cobar Supergroup (Whitbread, 2004). Rare Earth Element (REE) distributions are widely used to characterize source composition of detrital sediments (Taylor and Mclennan, 1985; Cullers, *et al.*, 1987; Zhang *et al.*, 1998). Linear correlation and mass balance consideration indicate that clays are more important than zircon (or other heavy minerals) in hosting both light and heavy REE in cratonic shales (Condie, 1991). Trace element behaviour is also reported to be largely controlled by the dominant clay or the degree of weathering (Kronberg *et al.*, 1979).

Aluminium and Ti are relatively immobile and significantly correlated in the saprolith samples (Figure 8.1). However the TiO_2/Al_2O_3 ratio is susceptible to sorting because TiO_2 significantly concentrates in the sand fraction, (as detrital rutile and ilmenite) whereas Al_2O_3 concentrates in the clay fraction. Therefore the TiO_2/Al_2O_3 ratio combined with any conserved element (i.e., Ce or La) was used to cover all the chemical compositional changes including that caused by sedimentary sorting.

Plotting $30TiO_2/ Al_2O_3$ against Ce and La showed a clustering of the majority of the data in limited concentration ranges for Ce (46-119 ppm) and La (22-51 ppm) in comparison with the relatively wide range of $30TiO_2/Al_2O_3$ ratios (Figure 8.10,11). Plotting fresh sandstone and shale data from the Cobar Supergroup (Whitbread, 2004) indicates that portions of the saprolith are possibly weathered from rock units similar to the Cobar Supergroup in composition. Various saprolith materials (sandstone, shale) from different weathering zones are grouped together on the Ti/Th - Ce/La diagram (Figure 8.12) indicating that they have similar chemical composition and were therefore derived from similar sources. In this context saprolith materials that are related to the Cobar Supergroup are clustered in limited ranges of Ti/Th ($0.039 \geq$ Ti/Th ≥ 0.03) and Ce/La ($2.2 \geq$ Ce/La ≥ 1.9) ratios, whereas the Girilambone group is characterised by relatively small range of Ti/Th ($0.03 \geq$ Ti/Th ≥ 0.005) and Ce/La ($2.3 \geq$ Ce/La ≥ 1.8; Figure 8.11).

In order to identify the weathering influences on the La/Ce ratio, Ce and La were normalised to chondrite (Taylor and McLennan, 1985) and the normalised $(La/Ce)_N$ is plotted against the CIA in Figure 8.13. The saprolith materials showed a wide range of change in $(La/Ce)_N$ within the most weathered zone (Zone II, CIA= 75-85) and no correlation was observed between $(La/Ce)_N$ and CIA. On the other hand La/Ce ratios show a limited range (1-1.5) from the least weathered samples. This indicates that the $(La/Ce)_N$ values can be used reliably as a geochemical signature to identify the underlying bedrock in less weathered saprolith samples (with CIA value up to 75).

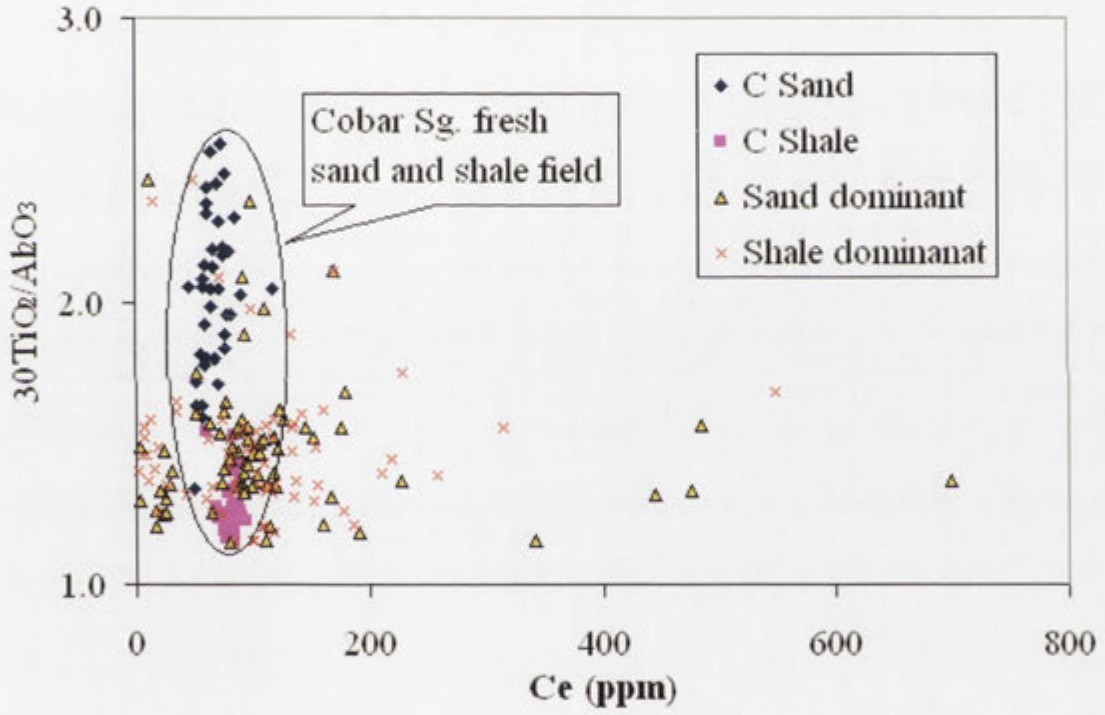

Figure 8.10 Scattergram of $30TiO_2/Al_2O_3$ and Ce showing the correlation between Cobar Supergroup fresh rock compositions and the saprolith of the Girilambone region. Data of Cobar Supergroup (Sg) are from Whitbread (2004).

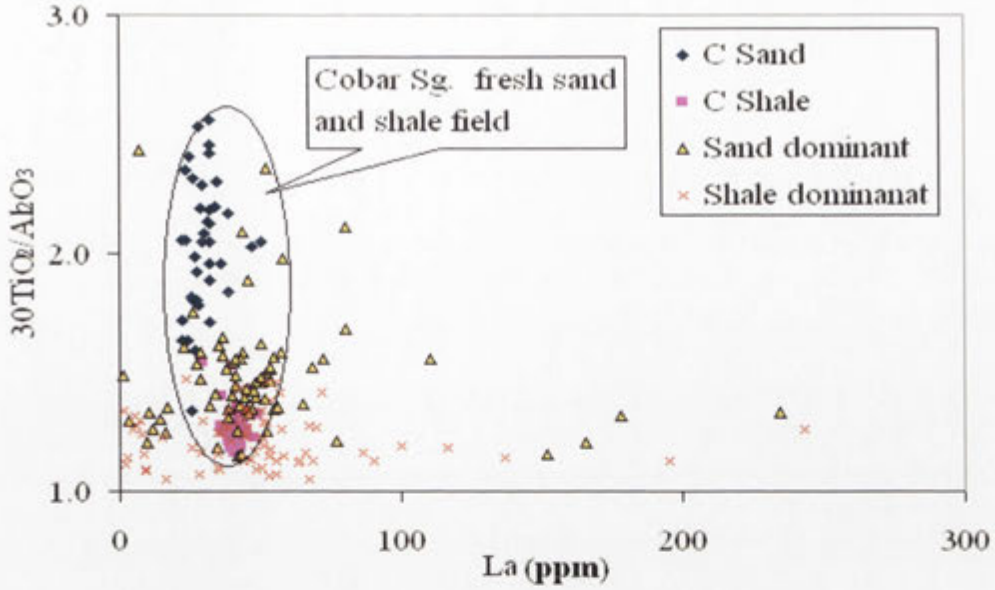

Figure 8.11 Scattergram of $30TiO_2/Al_2O_3$ and La showing the correlation between the Cobar Supergroup (Sg) fresh rock compositions and the saprolith of the Girilambone region. Data of Cobar Supergroup are from Whitbread (2004).

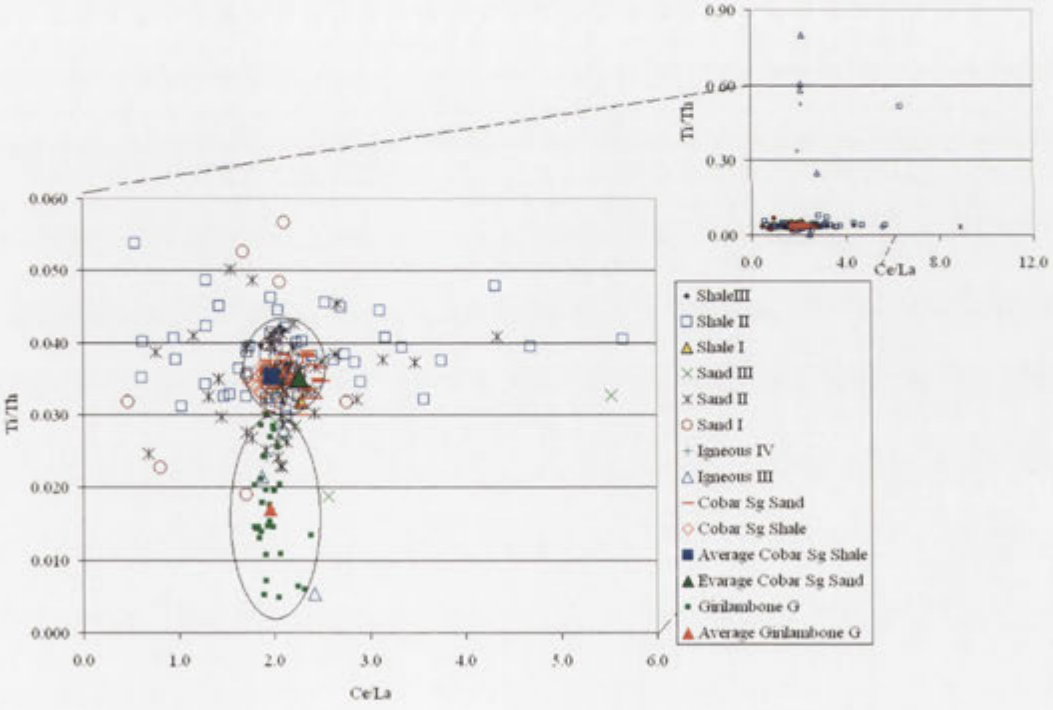

Figure 8.12 Ti/Th - Ce/La diagram of saprolith materials from the Girilambone region. Samples that are comparable with the Cobar Supergroup (Sg) data are identified by a circle. Numbers (I-IV) are related to materials (sand, shale and weathered igneous rock) from different weathering zones explained in Figures 8.8-9. Cobar Supergroup data are from Whitbread (2004) and the Girilambone data are from Ackerman (2005).

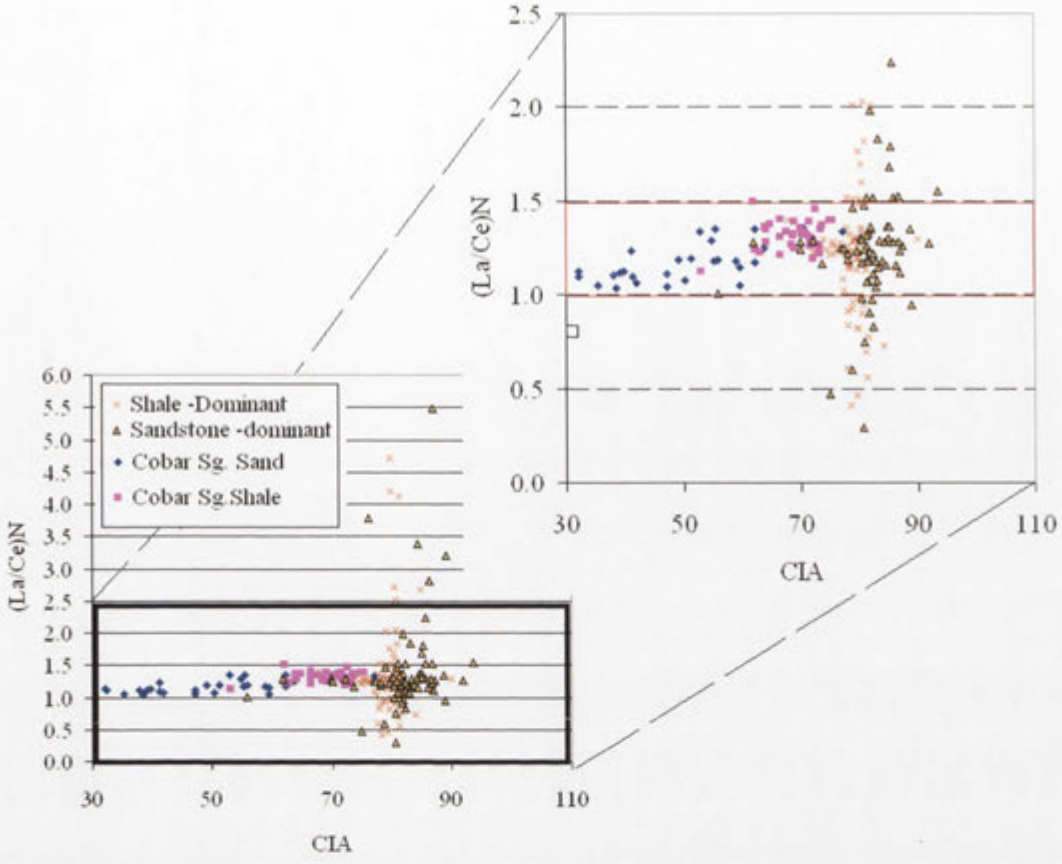

Figure 8.13 CIA – $(Ce/La)_N$ diagram of saprolith materials from the Girilambone region showing $(Ce/La)_N$ of the Cobar Supergroup data range (1.0- to 1.5). Cobar Supergroup (Sg) data are from Whitbread (2004). Ce and La were normalised to chondrite (Taylor and McLennan, 1985).

8.4 SUMMARY AND CONCLUSIONS

Analysis of the least weathered regolith present in bottom of the hole samples has shown that elemental ratios and the CIA index are useful for identifying the parent rock of weathered samples.

A-CN-K plots have identified the effect of weathering, showing that some of the samples are slightly weathered (CIA=50-70) with andesitic-granitic igneous rock composition. The deeply weathered (>70 CIA) samples plot adjacent to muscovite-illite weathering zone parallel to a general weathering trend of granite. A significant deviation from the ideal granodioritic and/ or granitic weathering trends was observed on the A-CN-K diagram associated with K enrichment. This K enrichment is possibly due to K-metasomatism or alternatively it indicates high K granitic source rocks.

Ratios of Zr/Sc and Th/Sc diagram indicate that some of the least weathered samples are mafic (relatively low Zr/Sc and Th/Sc). The deeply weathered samples showed an independent increase in Zn/Sc, which indicates significant recycling.

The ratios of Al_2O_3/SiO_2 vs 100 TiO_2/Zr and $15Al_2O_3$-Zr-$300TiO_2$ reveal the effect of sedimentary sorting. These ratios also show that sandstone-dominant samples approximate immature sandstones indicating significant amounts of silt and clay, whereas the shale- dominant field is relatively limited. Mafic intermediate and felsic igneous compositions are also identified.

Saprolith materials (after sandstone and shale) from the less weathered zones are grouped together on the Ti/Th and Ce/La diagram, indicating that they have similar chemical composition and are therefore derived from similar sources. The majority of saprolith samples show Ti/Th and Ce/La ratios within the range found in fresh Cobar Supergroup or Girilambone turbidites. Some show depletion in Ce and La and some enrichment suggesting these samples were derived from different source rocks or that Ce and La have been mobilised in the most weathered regolith.

9. CHAPTER NINE: ELEMENT DISPERSION IN CALCRETE- MANGANESE- IRON-DOMINANT REGOLITH

9.1 INTRODUCTION

Element distributions in the regolith are determined by:

- the mineralogy of the regolith and the stability of their primary host minerals;
- the influence of ground and surface waters; and
- the influence of biota (Lewis et al., 1987; Butt *et al.*, 1998; Britt *et al.*, 2001; Anand and Paine, 2002). These factors are all affected by the prevailing climatic regimes (Koinig *et al.*, 2003). In general, only processes related to past regimes of long duration, to extreme climates or to recent regimes leave a significant imprint. Thus, in much of Australia many of the dominant geochemical (and mineralogical) characteristics of the regolith are related to weathering under humid climates with high water tables and generally acid conditions, whereas others are due to later, possibly still active, events related to arid, alkaline environments with lower water tables. The features produced by these later events appear as modifications of the pre-existing regolith and tend to be reflected by the concentrations of minor components (Ollier and Pain, 1996; Taylor and Shirtliff, 2003).

This chapter explores the relationships between weathering-controlled element dispersion and regolith accumulations of carbonate (Ca- and Mg- rich), iron oxides/ oxyhydroxides (Fe-rich) and manganese oxides/oxyhydroxides (Mn-rich). This subdivision of regolith is based on knowledge of the regolith materials in the Girilambone region and the observed element associations. A better understanding of host phases for the various trace elements can help predict regolith-related background variations in element abundances and advise the most appropriate regolith sampling media for particular elements. This in turn should improve geochemical exploration in the region.

9.2 ELEMENT ASSOCIATIONS AND DISPERSION IN REGOLITH CARBONATE ZONES.

9.2.1 INTRODUCTION

Regolith carbonate (commonly called calcrete) is defined by Wright & Tucker (1991) as near-surface, terrestrial, accumulations of predominantly calcium carbonate, which occurs in a variety of forms from powdery to nodular to highly indurated. Calcrete is widely distributed in semi-arid regions (e.g., Goudie, 1983; Nahon, 1991; Wright and Tucker, 1991; Hema and Navin, 2004; Durand *et al.*, 2006) and has been used as a sampling medium in geochemical exploration for gold and some base metals (e.g., Lintern and Butt, 1993; 1998; Hill *et al.*, 1999; McQueen *et al.*, 1999; Chen *et al.*, 2002). Calcrete forms by cementation and displacive and replacive precipitation of predominantly calcium-rich carbonate into soil profiles, transported and *in situ* regolith and bedrocks, in areas where pore water and groundwater become saturated with respect to calcium carbonate (Durand *et al.*, 2006). Calcrete composition varies from calcite–dominant to dolomite–dominant (Chen *et al.*, 2002).

9.2.2 NATURE AND REGIONAL DISTRIBUTION OF REGOLITH CARBONATE

There are many types of regolith carbonates and classification schemes. Wright and Tucker (1991) proposed a morphological classification (Table 9.1). Various forms that have genetic implications are not defined in this classification. Calcretes can also be classified by their hydrological setting. Wright and Tucker (1991; Figure 9.1) genetically classified the regolith carbonates based on hydrological setting into:

- phreatic (valley) or groundwater non-pedogenic calcrete-forms in areas around the groundwater table;
- capillary fringe non-pedogenic calcrete-forms in the capillary fringe of phreatic zone;
- gravitational zone non-pedogenic calcrete develops in the gravitational water zone of the vadose zone;
- pedogenic calcrete developed in the soil moisture vadose zone; and
- superficial non-pedogenic calcrete which forms on the regolith surface .

Table 9.1 Morphological classification of calcrete (from Wright and Tucker, 1991).

Type	Description
Calcareous soil	Very weakly cemented or uncemented soil with small accumulations as grain coatings, patches of powdery carbonate including needle-fibre calcite, carbonate filled fractures and small nodules
Calcified soil	A firmly cemented soil, just friable; few nodules.10-50% carbonate
Powder calcrete	A fine, usually loose powder of calcium carbonate as a continuous body with little or no nodule development
Pseudotubule calcrete	All, or nearly all, the secondary carbonate forms encrustations around roots or fills root or other tubes
Nodular calcrete	Discrete soft to very hard concretions of carbonate cemented and/or replaced soil. Concretions may occur with laminated coatings to form pisoids
Honeycomb calcrete	Partly coalesced nodules with interstitial areas of less indurated material between
Hardpan calcrete	An indurated horizon, sheet-like, typically with a complex internal fabric, with sharp upper surface, gradational lower surface
Laminar calcrete	Indurated sheet of carbonate, typically undulose. Usually, but not always, over hardpans or indurated substrate
Boulder/cobble calcrete	Disrupted hardpans due to fracturing, dissolution and rhizobrecciation including tree heave). Not always boulder grade (clasts are rounded due to dissolution)

Generally in semi-arid systems the alluvial deposits are characterised by three major carbonate sinks: groundwater calcretes, pedogenic calcretes and calcrete conglomerates (Khadkikar *et al.*, 1998; Gomez-Gras and Zarza, 2003; Durand *et al.*, 2006). Groundwater calcretes originate from carbonate-saturated waters travelling preferentially along stratification planes. Pedogenic calcretes form through soil-forming processes typically in extra-channel areas. Calcrete conglomerates occur as ribbons, sheets and lenses due to the reworking of both pedogenic and groundwater calcretes.

Nash and McLaren (2003) studied a Late Quaternary-Holocene non-pedogenic valley calcrete and concluded that the development of non-pedogenic calcretes is less closely linked to climatic regime, given their independence from a pedogenic mechanism of carbonate precipitation.

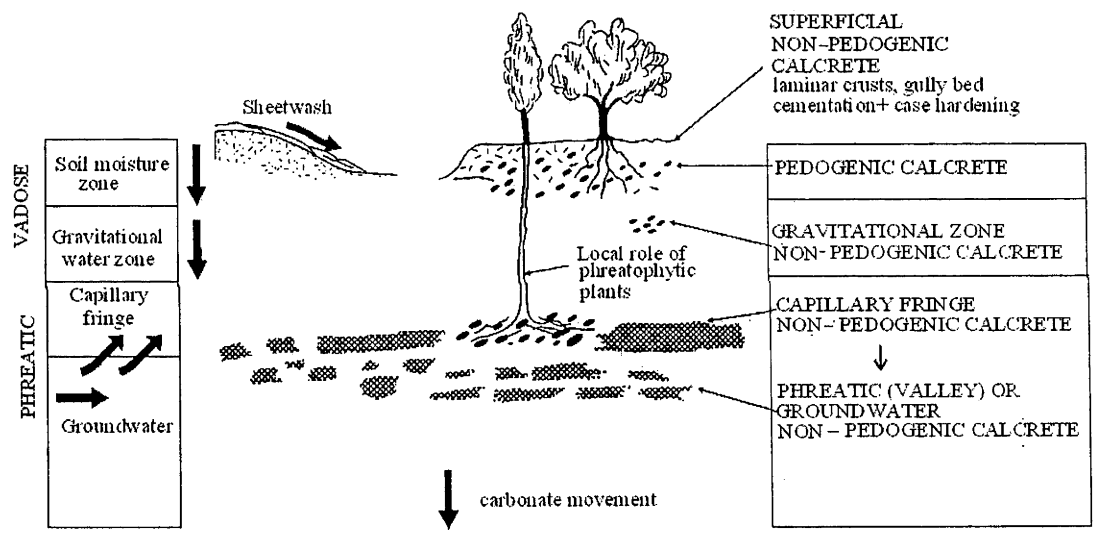

Figure 9.1 Classification of calcrete by hydrological setting (after Wright and Tucker, 1991).

In Australia, calcrete occurs over about 21% of the land surface (Figure 9.2) due to the large proportion of arid and semi-arid lands (Chen *et al.*, 2002). Their regional distribution is largely controlled by a fundamental relationship between:

- the availability of carbonate (CO_3^{2-}) and required cations (Ca^{2+}, Mg^{2+}) that are derived from bedrock (primary carbonate and mafic rocks), aeolian materials and rain water or older regolith carbonate accumulations; and

- the environmental factors such as landscape setting, rainfall rate and chemistry, groundwater depth and chemistry (Chen *et al*, 2002).

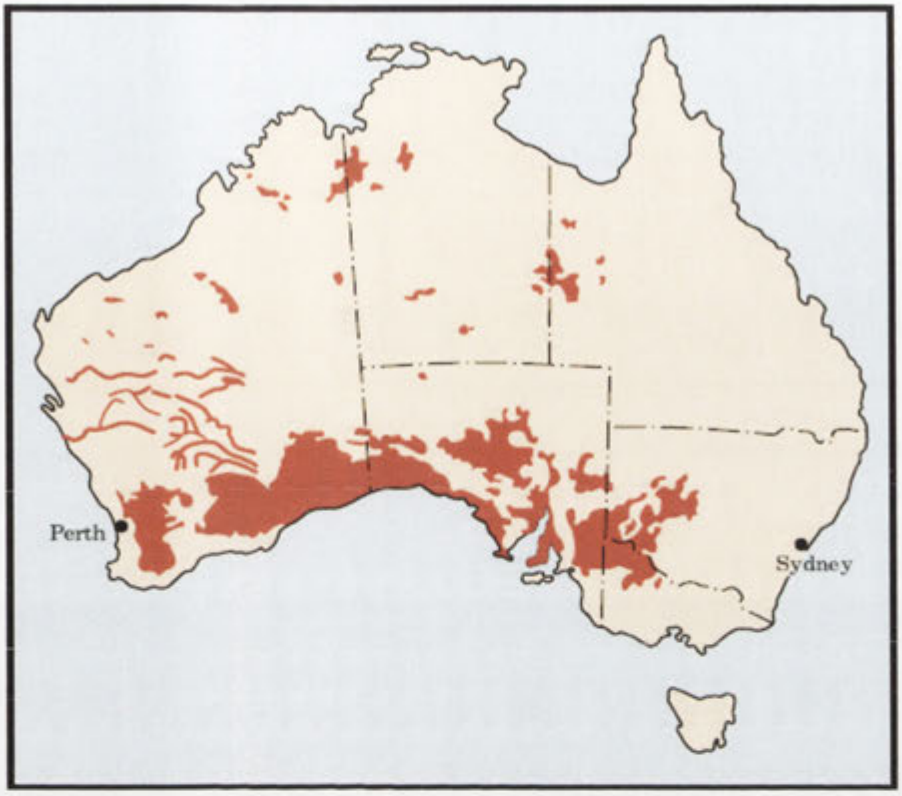

Figure 9.2 Distribution of calcrete and associated soils in Australia (after Northcote, 1975).

Carbonate occurrences in soil or regolith profiles range in thickness from tens of centimetres to tens of meters. Within such profiles, there can be more than one morphologic type of calcrete, either within a layer or as separate layers. In southern Australia calcrete occurs in association with coastal calcarenite dune complexes and further inland with a wide range of geological and landscape settings (McQueen *et al.*, 1999).

Based on morphology, Hill *et al.* (1999) broadly subdivided the calcrete into nodular carbonate facies and coated grains, carbonate rhizoliths, carbonate hardpan facies, boulder carbonate facies, powder carbonate facies, tabular massive carbonate facies and septarian magnesite accumulations. The occurrences of nodular carbonates, carbonate hardpans (as massive and laminated layers, coatings and veinings on bedrock), and powder carbonate in the Cobar-Girilambone region were reported by McQueen (2006).

The distribution of calcrete in southeastern Australia appears to be similar to that observed in Western Australia (Lintern and Butt, 1998) with the widespread pedogenic groundwater types occurring south of about latitude 30°S (i.e., an extension of a feature equivalent to the Menzies Line in Western Australia). North of this zone groundwater-related valley calcrete and red-brown hardpans are more common (Hill *et al.*, 1999).

In this study it was difficult to recognise the morphological characteristics of most of the calcrete in the pulverised composite samples, but observations of exposed calcrete throughout the region indicate at least four calcrete facies in regolith with elevated values of CaO (≥1.0 wt %) and MgO (≥1.0 wt%). These facies are: i) coated grains and nodular carbonate; ii) powdery carbonates; iii) massive or laminated carbonate hardpans; and iv) filling carbonate that occur as veins (see also Khider and McQueen, 2006; McQueen, 2006). The first two are weakly consolidated carbonate and generally associated with carbonate hardpan, which is common within soil and alluvial/colluvial sediments. The third facies occurs in regolith profiles where carbonate-bearing solutions have ponded, typically within *in situ* regolith or along the boundary between the transported and *in situ* regolith (the T/I boundary). The fourth facies forms filling along cracks in transported and *in situ* regolith and fracture-fillings in saprock/ bedrock (Figure 9.3).

The regolith profiles and regolith-landform toposequences indicate that the regolith carbonate (calcrete) facies vary both vertically within a profile and laterally across the landscape. The number and thickness of carbonate-rich "horizons' varies widely, possibly due to multiple episodes of calcrete precipitation and re-dissolution (Figures 9.4-9). In the *in situ* regolith the carbonate horizon is 1-8 m thick and generally associated with the T/I boundary (Figures 9.7-9), whereas in the transported regolith the carbonate is a single near-surface layer, approximately 1 to 3 m thick (Figures 9.4-6). Generally, the carbonate-rich layers are within the top 10 m of the regolith (Figures 9.4-9).

9.2.3 CALCRETE COMPOSITION

Compositional variability of carbonate-bearing regolith can be shown using the components MgO, CaO and the major non- carbonate component Al_2O_3 (Figure 9.10). The proportion of carbonate in the samples varies from several wt% to nearly pure

carbonate. Most samples have a significant non-carbonate component, as reflected by the concentration of compositions towards the Al_2O_3 apex of the ternary plot. All the data show a significant MgO content reflecting both the common presence of dolomite (Figures 9.11-12) and a non-carbonate contribution of MgO from clay minerals. X-ray

1

CBAC 40 (1-2 m)
Sandy silty mudstone with carbonate veinlet

2

CBAC 85 (1-2m)
Laminated mudstone with carbonate veinlet

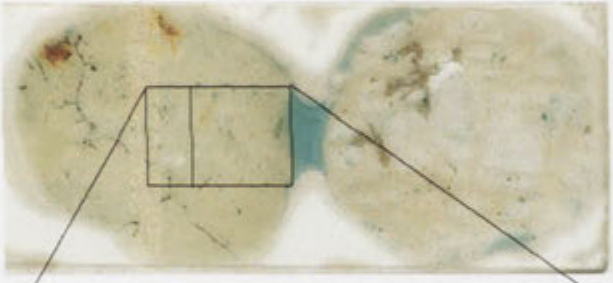

3

CBAC 88 (4-5 m)
White quartz lode showing vermicular quartz chlorite intergrowth, broken and invaded by calcrete

Figure 9.3 Examples of calcrete from the Girilambone region showing carbonate filling cracks (1-3) and replacing pre-existing materials (3)(samples from aircore drilling, Fleming *et al.*, 2001).

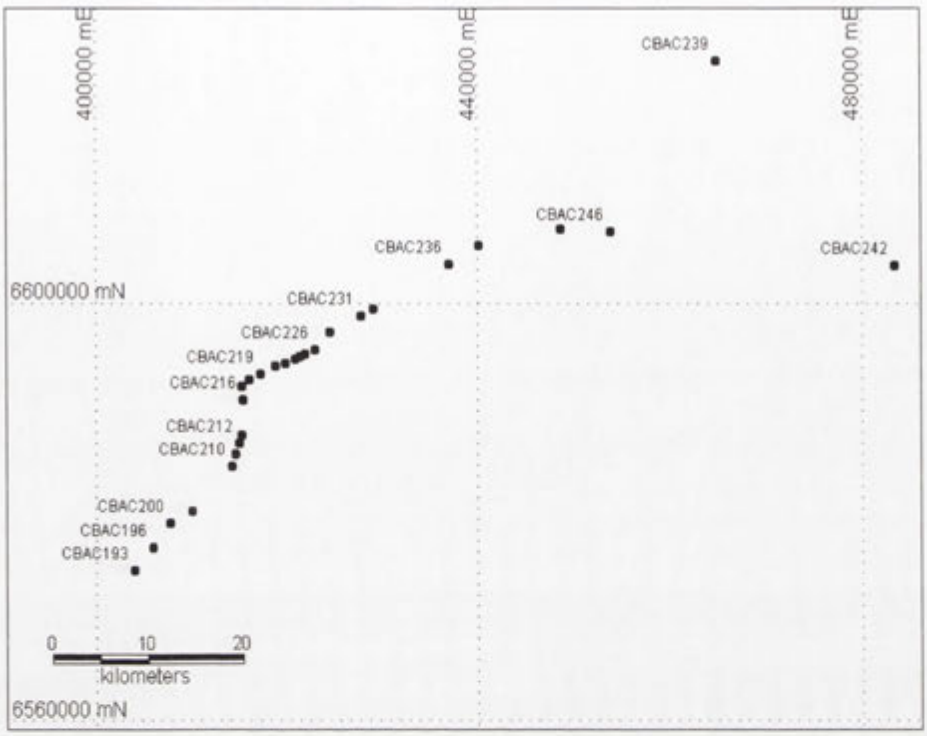

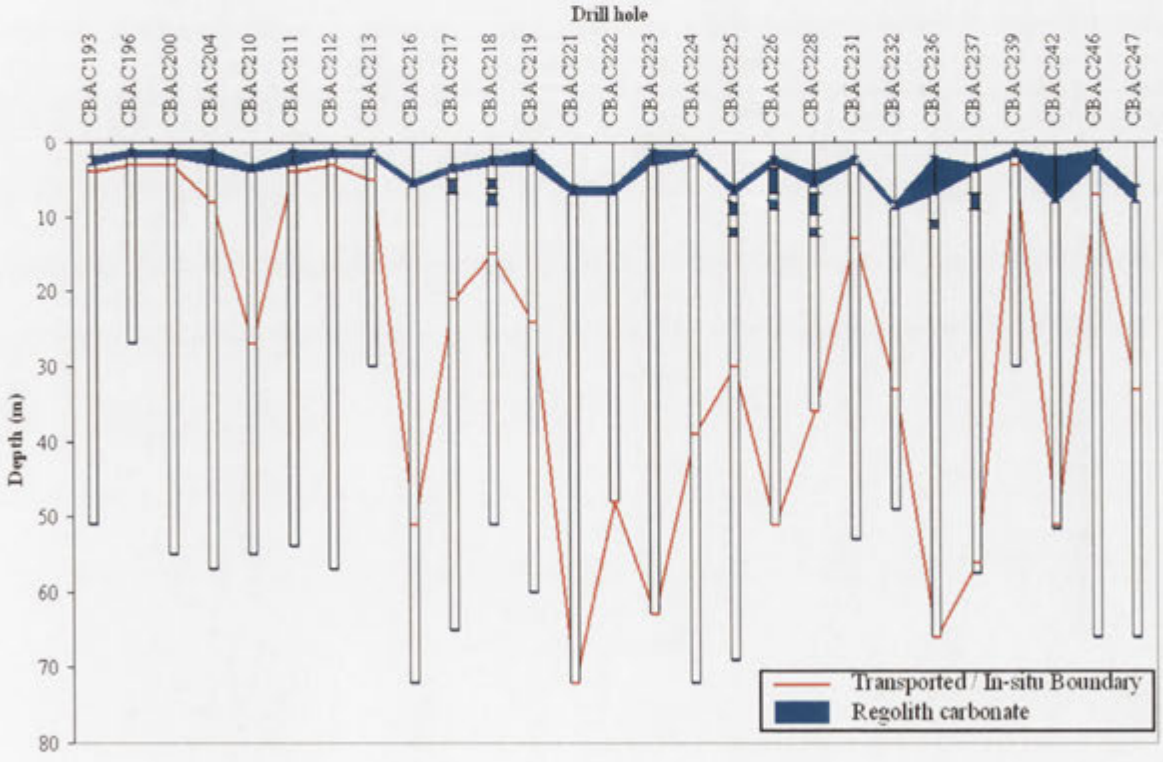

Figure 9.4 Drill hole plots showing the transported/*in situ* boundary and distribution of calcrete-bearing zones in the transported regolith of the Byrock area from the Girilambone region. Drill hole locations are shown on the associated map.

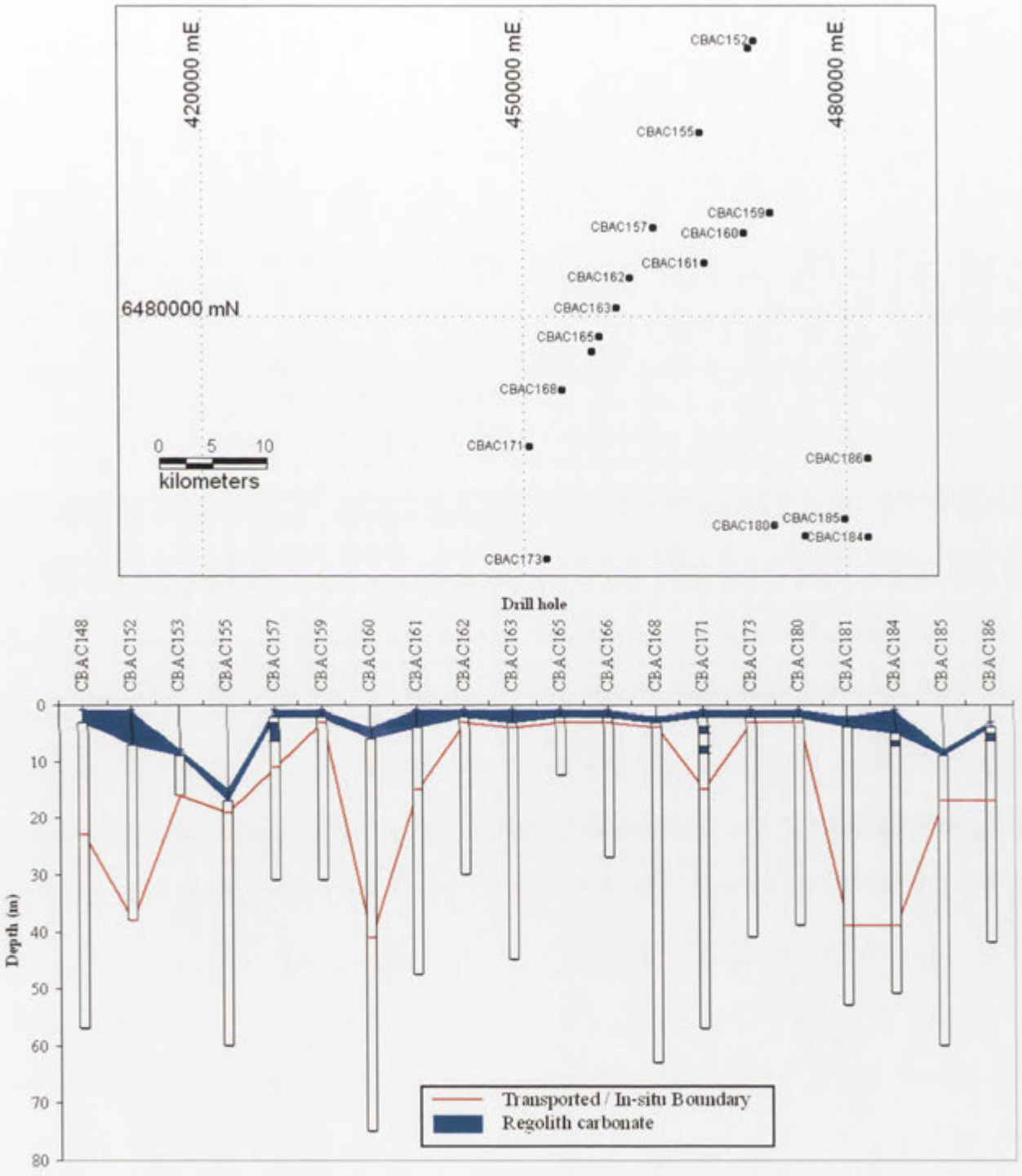

Figure 9.5 Drill hole plots showing the transported/*in situ* boundary and distribution of calcrete-bearing zones in the transported regolith of the Hermidale area from the Girilambone region. Drill hole locations are shown on the associated map.

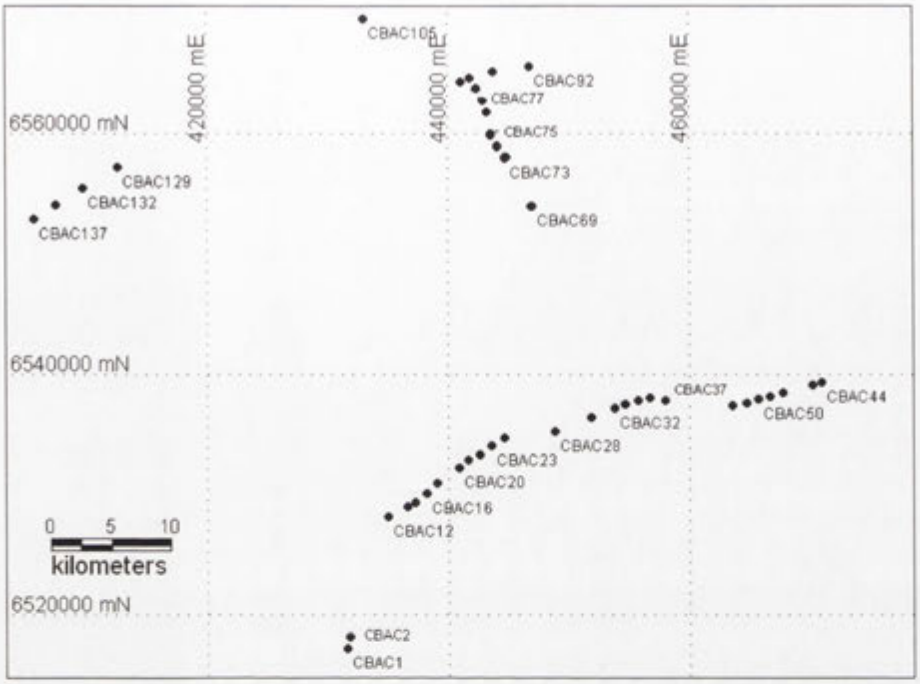

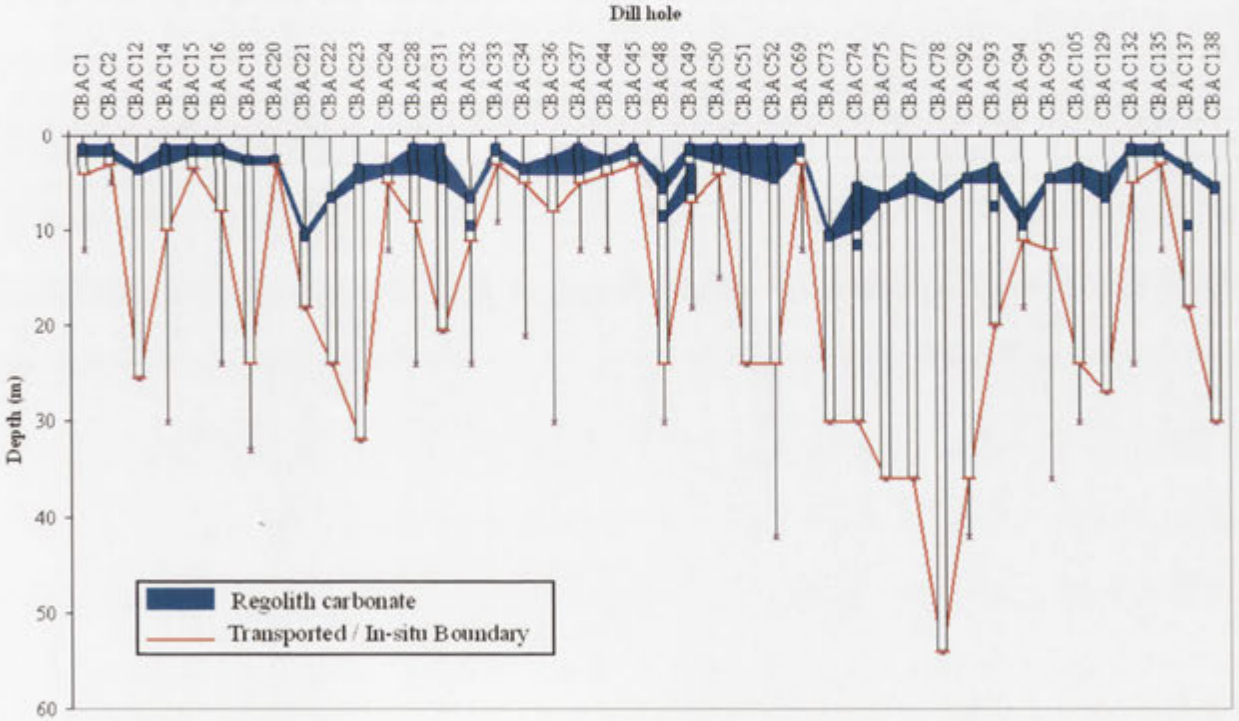

Figure 9.6 Drill hole plots showing the transported/*in situ* boundary and distribution of calcrete-bearing zones in the transported regolith of the Sussex area from the Girilambone region. Drill hole locations are shown on the associated map.

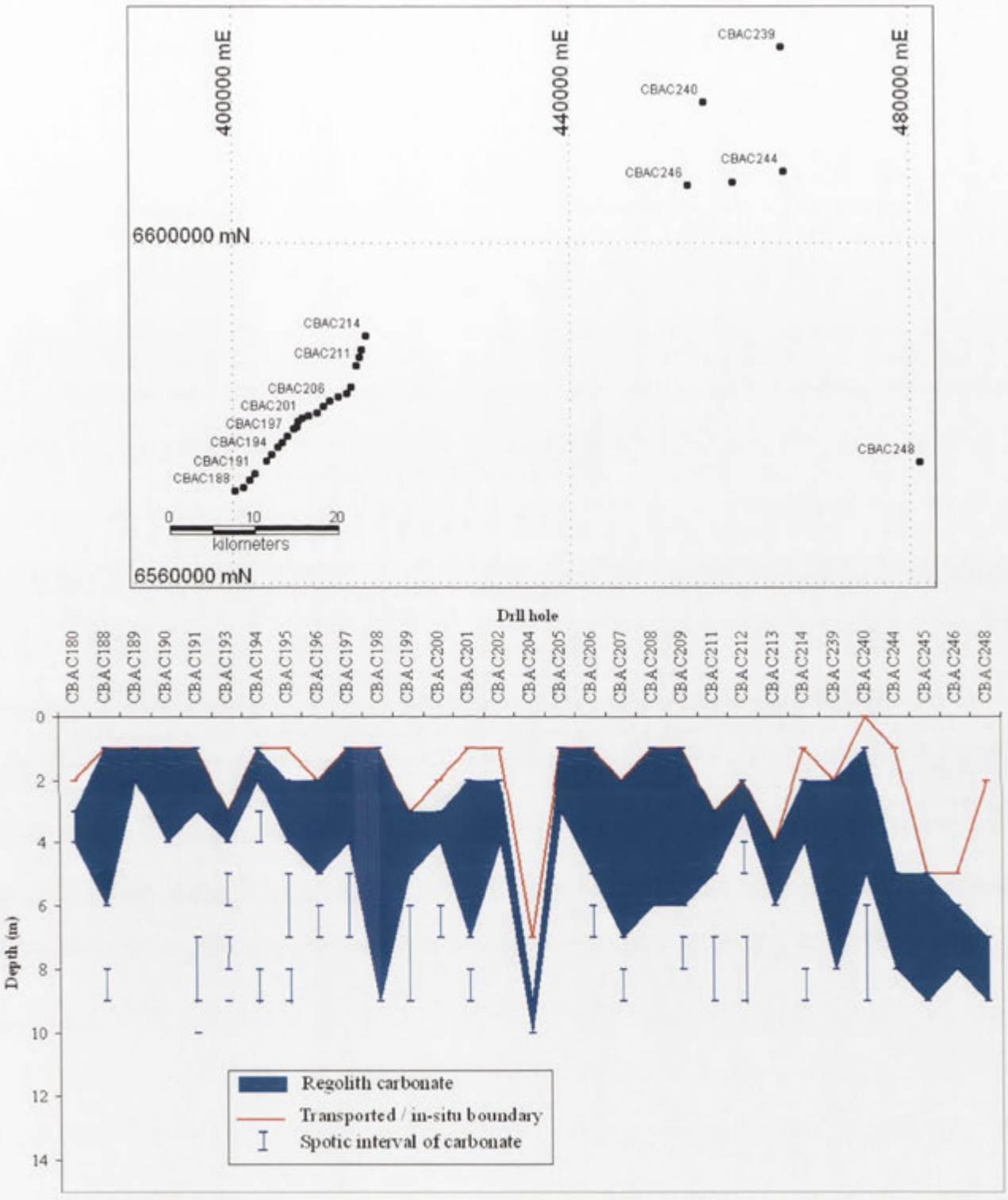

Figure 9.7 Drill hole plots showing the transported/*in situ* boundary and distribution of calcrete-bearing zones in the *in situ* regolith of the Byrock area from the Girilambone region. Drill hole locations are shown on the associated map.

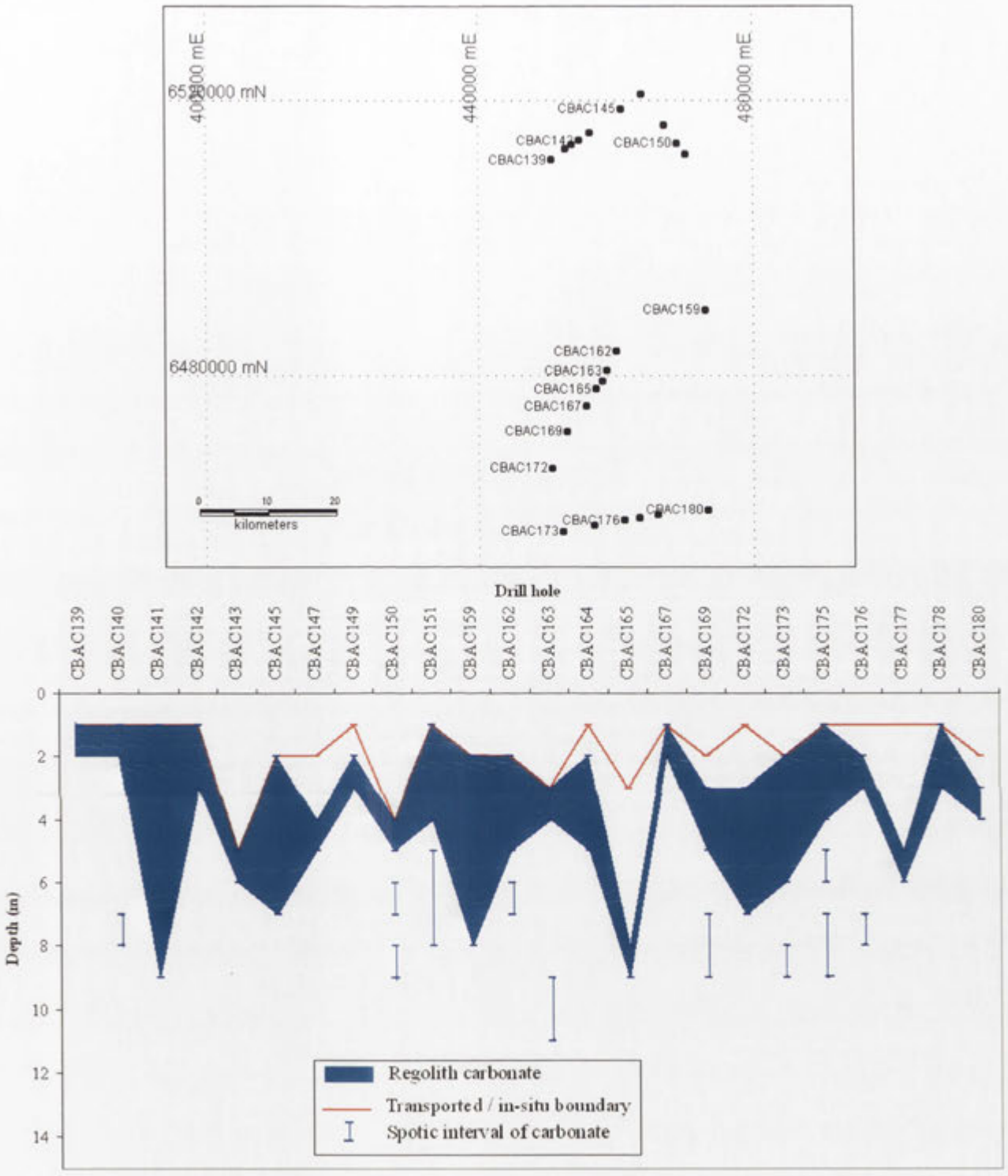

Figure 9.8 Drill hole plots showing the transported/*in situ* boundary and distribution of calcrete-bearing zones in the *in situ* regolith of the Hermidale area from the Girilambone region. Drill hole locations are shown on the associated map.

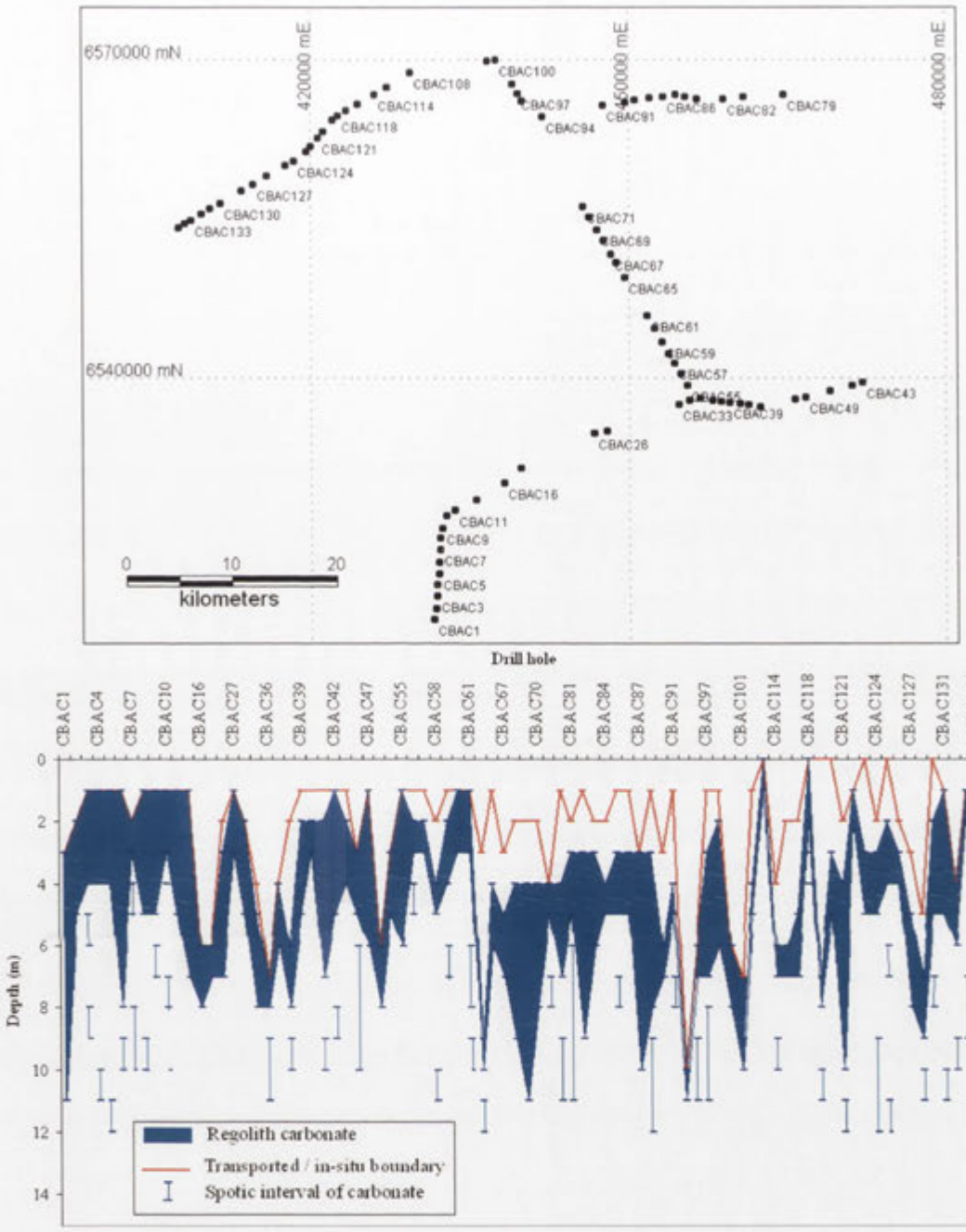

Figure 9.9 Drill hole plots showing the transported/*in situ* boundary and distribution of calcrete-bearing zones in the *in situ* regolith of the Sussex area from the Girilambone region. Drill hole locations are shown on the associated map.

diffraction analysis on a suite of calcrete-bearing samples indicates that there is no magnesite in the carbonate. There does not appear to be any systematic differences between compositions for calcrete from transported versus *in situ* regolith (Figures 9.11-12).

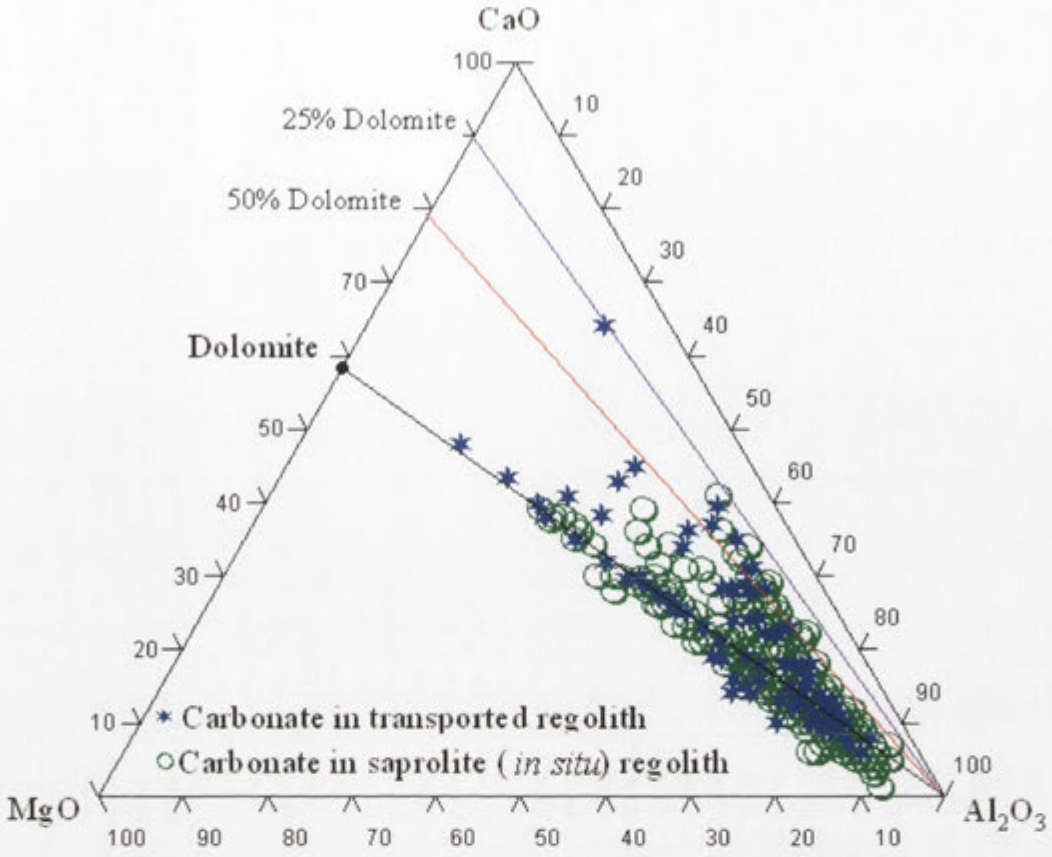

Figure 9.10 Triangular (MgO-CaO-Al_2O_3) compositional diagram of the transported and in-situ regolith from the Girilambone region.

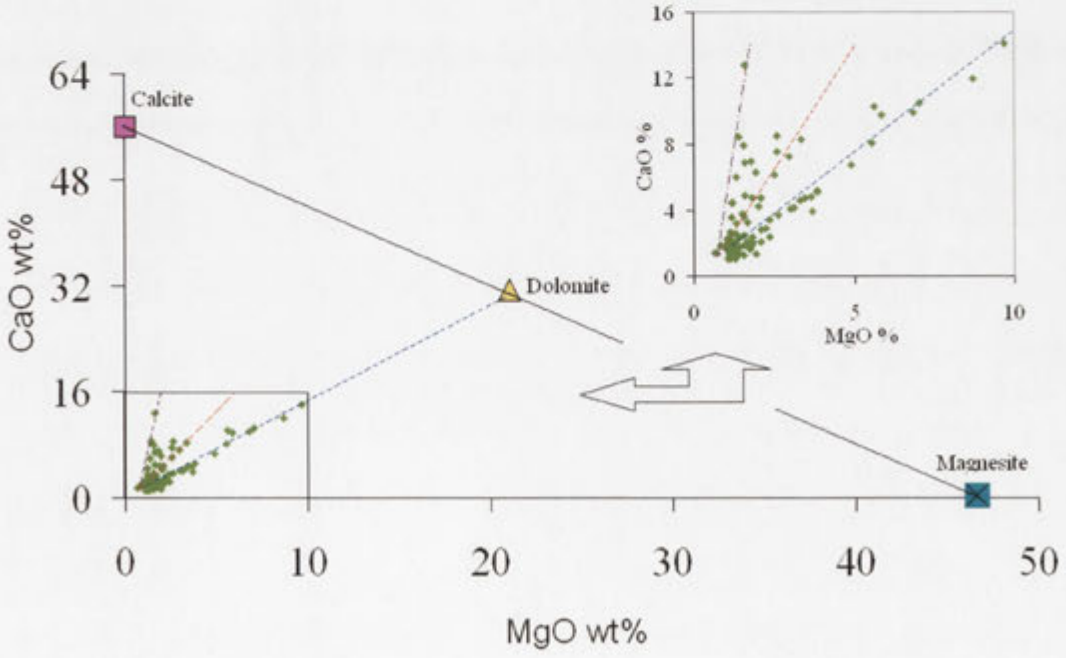

Figure 9.11 Bivariate MgO-CaO diagram of the transported calcrete–bearing regolith from the Girilambone region.

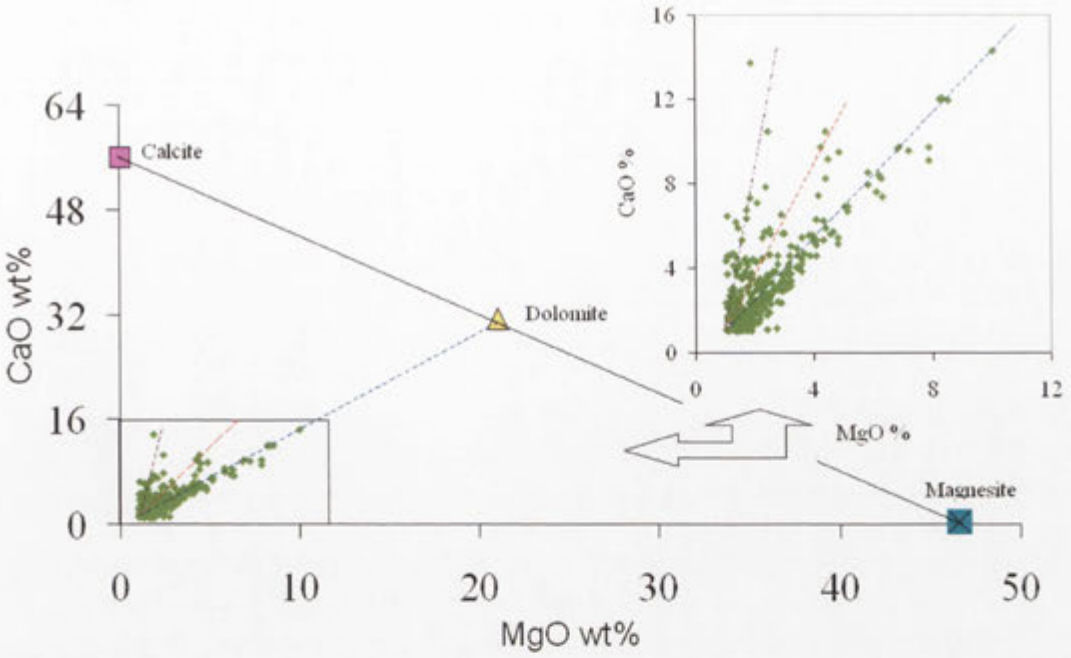

Figure 9.12 Bivariate MgO-CaO diagram of the *in situ* calcrete-bearing from the Girilambone region.

Potassium and Al contents in the regolith carbonate commonly represent the composition of relict muscovite and clay minerals. The distribution pattern of regolith carbonate compositions on the K_2O-Al_2O_3 diagram shows a trend toward the illite-muscovite composition (Figure 9.13 A). A small number of samples plot close to the kaolinite composition, which indicates more advanced weathered or reworked components of clay. There was no significant correlation of CaO or MgO with Al_2O_3, K_2O or Fe_2O_3 (Figure 9.13).

Fe_2O_3 in the regolith carbonate samples ranges from 0.74 % to 8.4 %. In gold-enriched horizons (see below), there appears to be an antipathetic relationship between Ca, Mg and Fe. This suggests that Fe is not significantly present in the carbonate but most likely present as iron oxide/oxyhydroxide impurities.

9.2.4. GOLD CONCENTRATION IN CALCRETE

Previous investigation of exposed calcrete in the Cobar-Girilambone region has indicated a clear association of Au with calcrete (McQueen *et al.* 1999; McQueen 2006). In areas away from known mineralisation calcrete generally contains less than 0.001 ppm Au (the detection limit). Detectable Au is found in calcrete at sites close to

or down drainage from known gold mineralisation, with 0.004 ppm considered a regional threshold and 0.012 ppm a local (deposit) threshold (McQueen, 2006).

In this study, the calculated thresholds of gold are 0.006 ppm and 0.009 ppm in the regolith carbonate (calcrete) of the transported and *in situ* regolith respectively. There is no direct correlation between the carbonate content (CaO and MgO concentrations) and Au concentration in calcrete-bearing regolith zones. To understand the distribution of Au in the calcrete zone selected profiles of high-Au content from the calcrete of the *in situ* and transported regolith were examined.

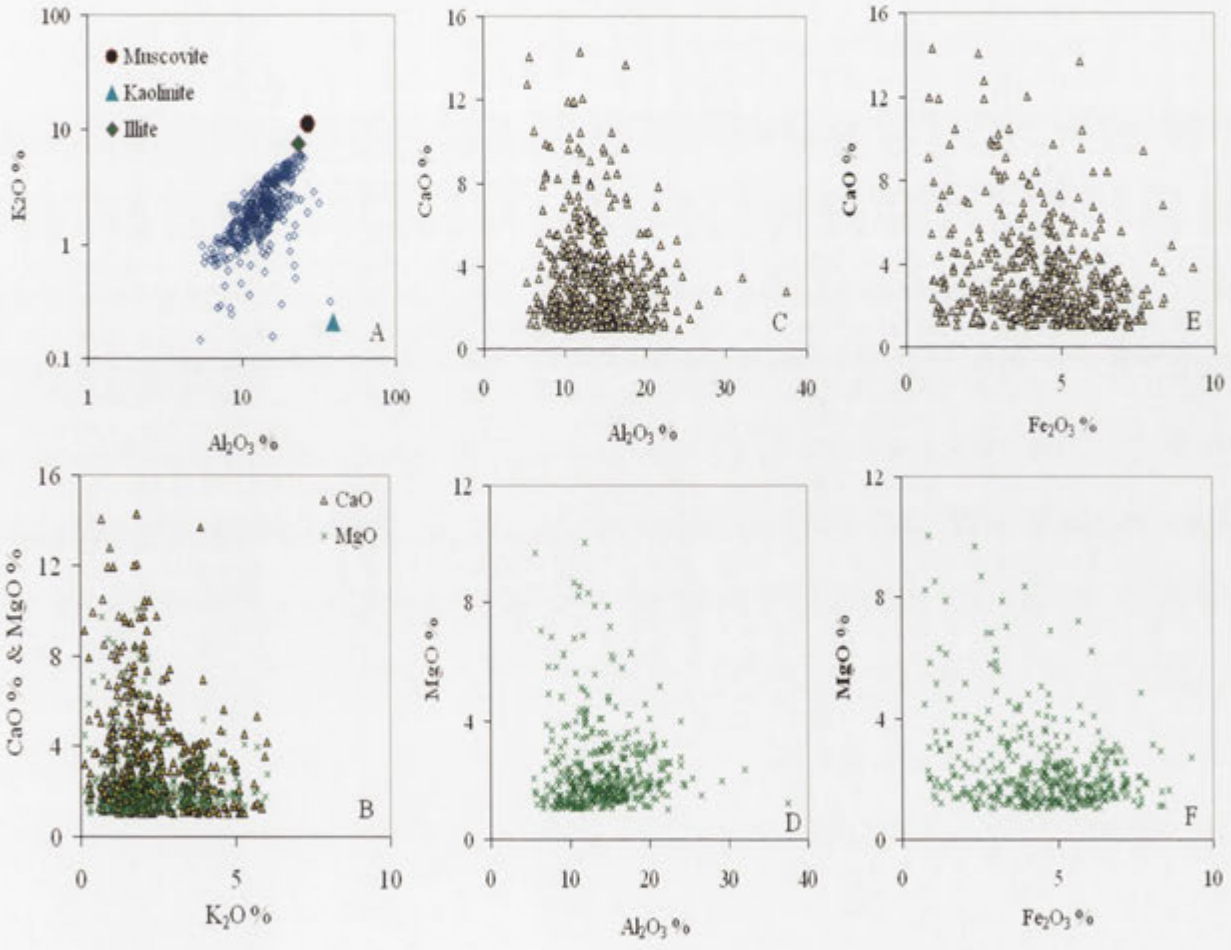

Figure 9.13 Scattergrams of major components in the regolith carbonate zones of the Girilambone region.

9.2.4.1 ASSOCIATION OF AU WITH CALCRETE IN THE *IN SITU* REGOLITH

Elevated Au values associated with calcrete from *in situ* regolith range from 0.005 ppm to 0.025 ppm (Appendix 7). Four examples occur in drill holes CBAC2, CBAC41, CBAC188 and CBAC204.

In CBAC2 and CBAC188 calcrete has accumulated along and just below the T/I boundary (Figures 9.14, 15). The highest Au values in these drill holes do not coincide with the highest Ca or Mg contents, suggesting that the calcrete is not directly accumulating Au. Gold contents also vary within the regolith carbonate zone. In CBAC2 the highest Au content is in the middle of the regolith carbonate zone and is associated with elevated Bi and lower Fe contents (Figure 9.14). The compositional trends in CBAC2 show elevated Ca in the upper part of the profile decreasing more rapidly than Mg content with depth. This would be consistent with mixed calcite-dolomite in the upper part of the calcrete zone (1 m) and predominantly dolomite below (2 m; Appendix 4).

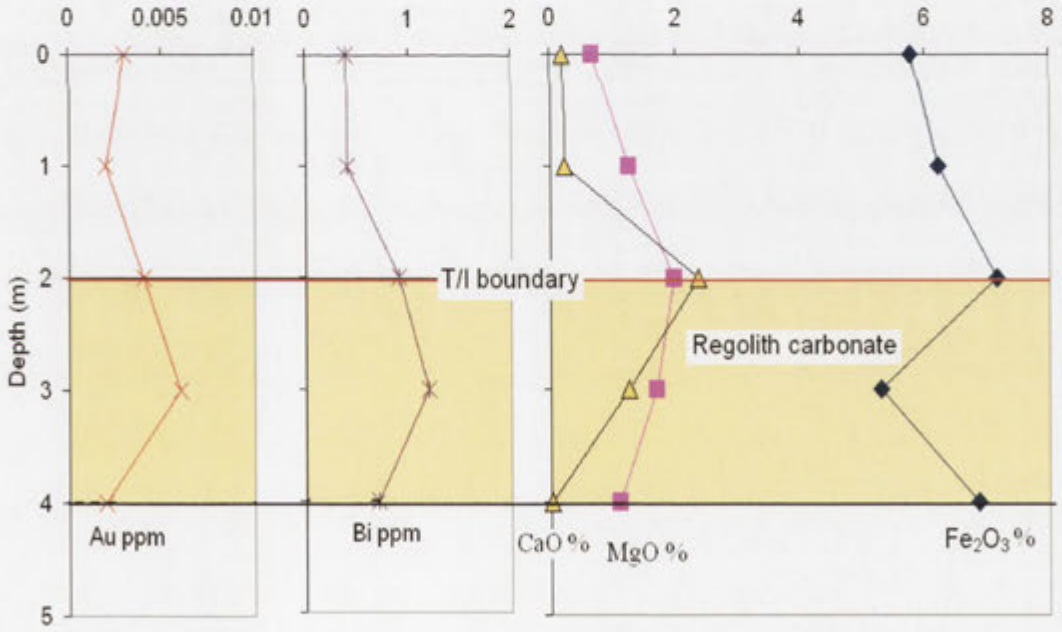

Figure 9.14 Distributions of Au, Bi, CaO, MgO and total Fe_2O_3 (wt %) through the regolith carbonate zone within *in situ* regolith in drill hole CBAC2.

There is also significant Ca enrichment near the top of the regolith carbonate zone in drill hole CBAC188. The Au content increases with depth through the carbonate zone

in association with increasing Fe content (Figure 9.15). This Au-Fe association possibly reflects remnant primary gold mineralisation in the saprolite (W and As are also elevated) or possibly the influence of a pH or redox boundary related to ferruginisation. Below the regolith carbonate zone at 8 m the gold content increases to 0.026 ppm in association with elevated W (10 ppm), As (31 ppm) and quartz veining. This is consistent with the presence of a remnant primary gold anomaly, possibly partly leached, within the saprolite underlying this site. The remnant Au may be adsorbed onto hematite/goethite, possibly formed by weathering of primary Fe sulphides associated with gold mineralisation.

In drill holes CBAC 41 and CBAC204 calcrete occurs within *in situ* regolith below the soil or T/I boundary. Elevated gold values in these profiles are strongly correlated with higher Ca and Mg contents, which are developed at the top of the regolith carbonate zone. This enrichment is associated with lower Fe content. The XRD analysis in drill holes CBAC41 and CBAC204 shows that the upper parts of these profiles are more calcite-rich than the other two examples (Figures 9.16-17, Appendix 4).

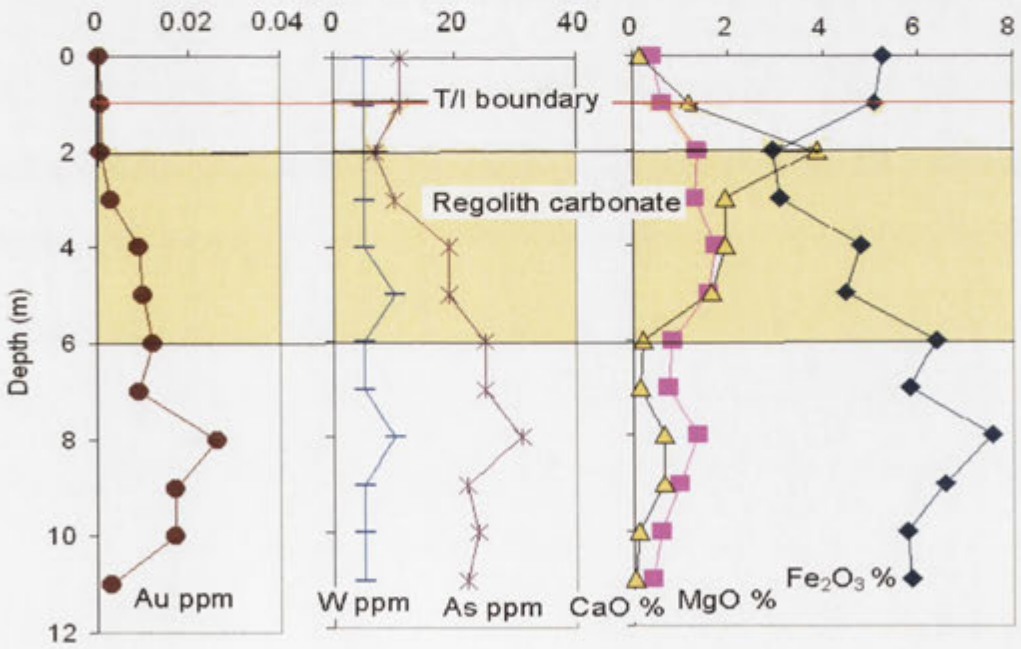

Figure 9.15 Distributions of Au, W, CaO, MgO and Fe_2O_3 (total) through the regolith carbonate zone in drill hole CBAC188.

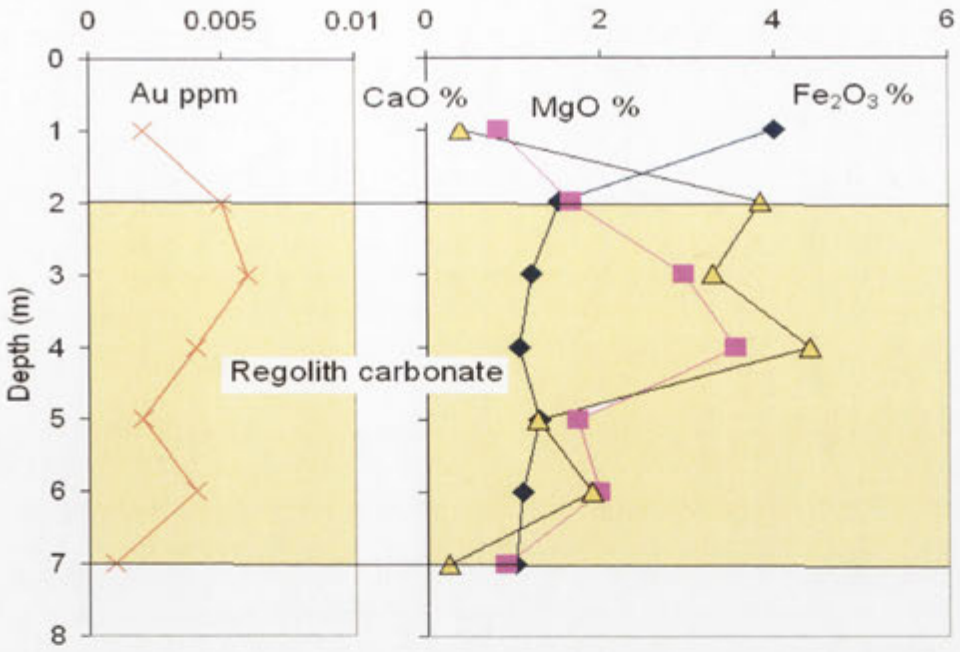

Figure 9.16 Distributions of Au, CaO, MgO and Fe_2O_3 (total) through the regolith carbonate zone within *in situ* regolith in drill hole CBAC41.

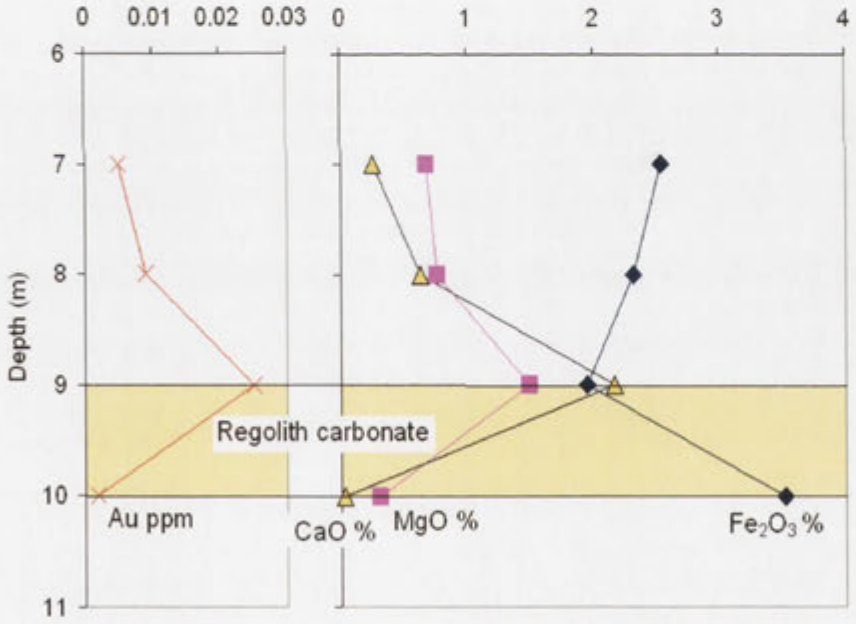

Figure 9.17 Distributions of Au (ppm), CaO, MgO and total Fe_2O_3 (wt %) through the regolith carbonate zone within *in situ* regolith in drill hole CBAC204.

9.2.4.2 ASSOCIATION OF AU WITH CALCRETE IN THE TRANSPORTED REGOLITH

Regolith carbonate zones in transported regolith are generally characterised by an upper layer or crust of calcrete. Two examples with elevated Au contents are in drill holes

CBAC78 and CBAC159 (Figure 9.18). In both these examples, the highest Au contents occur at the very top of the regolith carbonate zone. In drill hole CBAC78 the top of this zone is at 6 m depth within the transported regolith and has the highest carbonate content as indicated by slightly elevated CaO (1 wt%) and MgO (1.87 wt%) values. The Fe content is lowest in this part but increases at the base of the regolith carbonate zone (Figure 9.18A).

In drill hole CBAC159 the regolith carbonate zone extends across the T/I boundary. In the *in situ* part there are two levels of high carbonate (at 2 and 5 m depth) as indicated by Ca and Mg concentrations. The upper level coincides with T/I boundary. Neither of these levels coincides with the highest Au content in the profile, which is within transported regolith at the top of the regolith carbonate zone. The Au content decreases

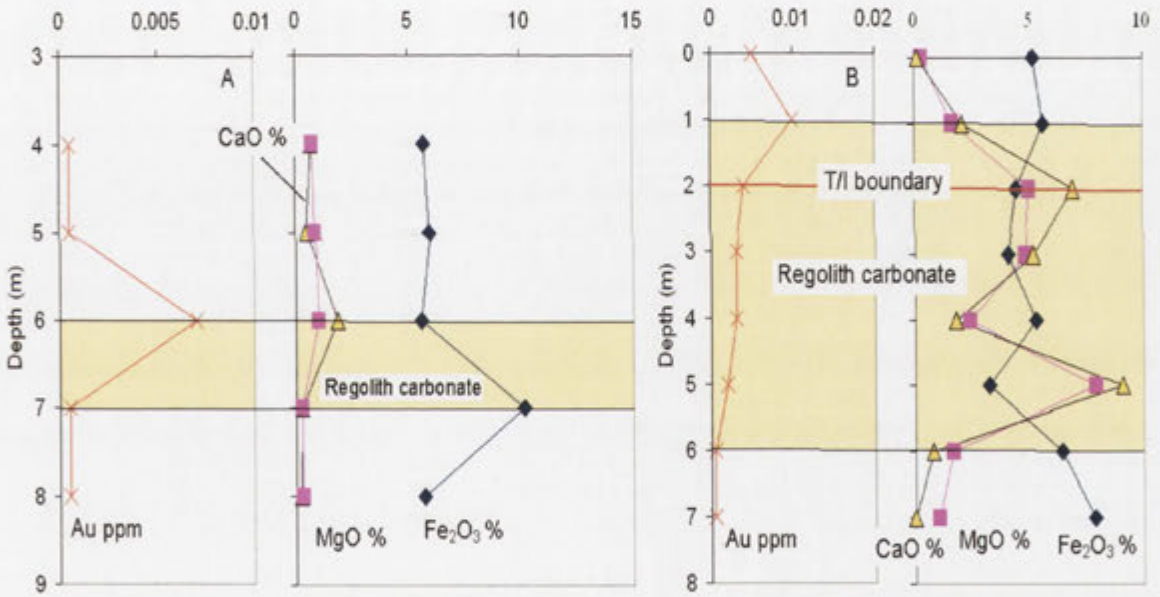

Figure 9.18 Distribution of Au (ppm), CaO, MgO and total Fe_2O_3 (wt %) through the regolith carbonate zone within transported regolith in drill hole CBAC78 (A) and across the transported/*in-situ* boundary in drill hole CBAC159 (B).

steadily down through the regolith carbonate in the *in situ* part of the profile. The overlying soil contains 0.005 ppm Au (Figure-9.18B). Again the Fe content is negatively correlated with Ca and Mg contents. X-ray diffraction analysis confirms that calcite is present in the upper part of the regolith carbonate zone, with dolomite dominating in the lower part (Appendix 4).

9.2.5 MINOR AND TRACE ELEMENT CHARACTERISTICS OF REGOLITH CARBONATE ZONES

Depending upon climate and local conditions, carbonates may be the dominant sink for some trace elements. The major control on trace element uptake by carbonate, commonly in metastable and polymorphic forms, is pH. Trace elements may be coprecipitated as their carbonates or replace Ca^{2+} in the lattice (Hall, 1998).

9.2.5.1 SILVER, ARSENIC, BISMUTH, ANTIMONY AND TUNGSTEN

The Ag content of the regolith carbonate bearing samples is generally low (89% of samples are below the detection limit 0.5 ppm). Elevated Ag values (> 0.5 ppm) are not significantly correlated with high CaO, MgO, Fe_2O_3 or MnO (Figure 9.19). One interval in drill hole CBAC188 (2-4 m) showed significant enrichment in Ag (2.9-16.2 ppm) associated with high Mo (8 ppm) content and slight enrichment in Mn (Figure 9.20). This may be related to association of Ag and Mo with minor co-precipitated manganese oxides/oxyhydroxides.

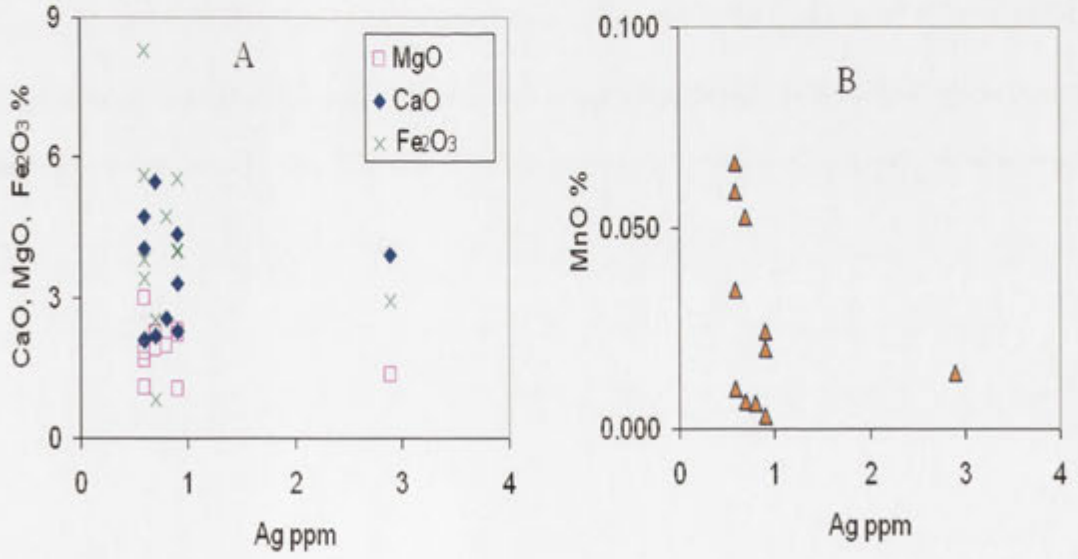

Figure 9.19 Scattergrams showing correlation of detectable Ag with major elements in calcrete-bearing regolith from the Girilambone region. (A) Ag plot against CaO, MgO and Fe_2O_3 (B) Ag verses MnO.

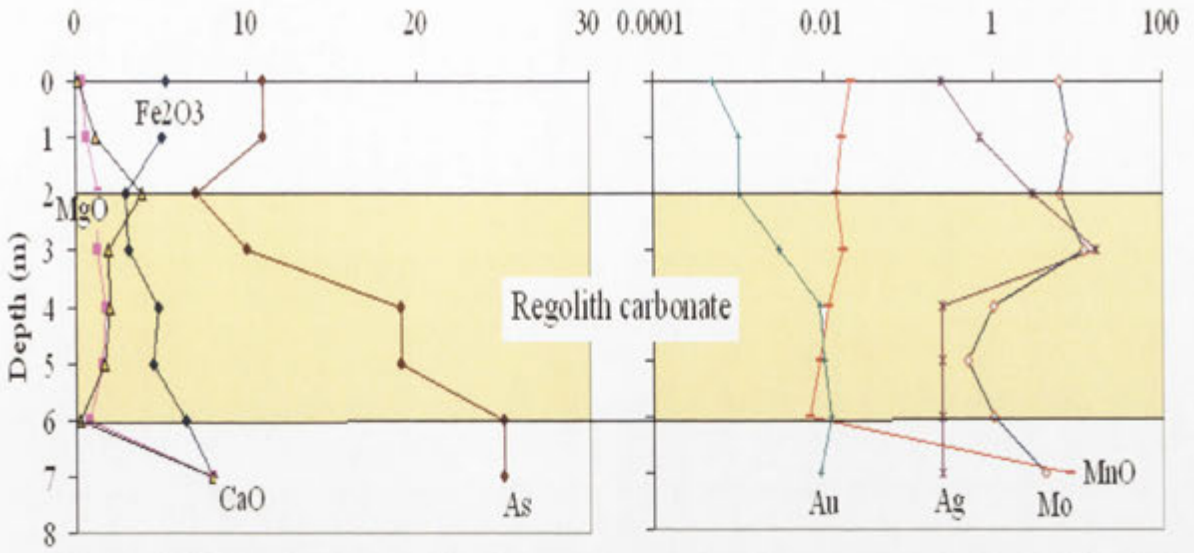

Figure 9.20 Distribution profile showing the relationships between Fe_2O_3, MnO, MgO, CaO (wt %), Ag, As, Au and Mo (ppm) in the regolith carbonate zone in drill hole CBAC188.

In the regolith carbonate zones there is no clear correlation between As and Fe, Mg, Ca and Mn, but the elevated As values (> 23 ppm) are accompanied by high Ca, Mg and/or high Fe concentration and enriched in the lower part of the carbonate horizons. Examples of such correlation between elevated As and Ca, Mg and Fe are found in drill holes CBAC13 and CBAC159 (Figure 9.21 A, B). The relationship of As with Fe in the regolith carbonate zone possibly reflects the presence of Fe oxide/oxyhydroxide impurities, containing As. This Fe-associated suite was also recognised in other regolith materials around the Cobar area (Scott and Taylor, 1989; McQueen and Munro, 2003; McQueen *et al.*, 2004) where As and other trace elements such as Sb, Cr and Bi were associated with hematite and/or goethite. In this study the As-Fe and Au association is observed in Fe-rich regolith (as discussed in section 9.3) with goethite and hematite enrichment. A small number of drill sections show enrichment of As in the upper part of the carbonate horizon associated with elevated Ca and Mn contents (Figure 9.21 B &C). However, this enrichment is not associated with high Au concentrations.

There is no correlation between Bi and Ca, Mg, Fe or Mn concentrations. About 70% of high Bi (Bi>6 ppm) samples are concentrated in the upper part of the regolith carbonate horizons. Distribution patterns of some of these elevated Bi values are mainly consistent with high Ca and to some extent with high Mg concentrations. However, these elevated values of Bi generally are not correlated with high Au values. There is

no correlation between Sb and Fe, Mn, Ca and Mg. Elevated Sb >10 ppm is also not correlated with high Au values.

Tungsten has a relatively homogeneous distribution in the regolith carbonate zones. Elevated W (>10 ppm) is not correlated with high Au contents except in drill hole CBAC188 where the enrichment of W coincides with consistent enrichment in Au down the hole (Figure 9.15). This enrichment in Au and W is not associated with the Fe pattern, which suggests the W and Au are hosted by mineral other than iron oxides/oxyhydroxides (e.g. they may be present as gold and W minerals in quartz-vein material).

9.2.5.2 BARIUM AND STRONTIUM

Barium is strongly enriched in the regolith carbonate zone (Appendix 7). Samples with high Ba content (> 1000ppm) are concentrated in the upper part of the carbonate accumulations (77% of high Ba samples). A small number of high Ba samples occur at the base and within the carbonate horizons (17 % and 8 % respectively). Typical host minerals for Ba are feldspar and barite. High Ba contents (particularly in feldspar) can give some indication of proximity to ore (Scott, 1992). In the presence of carbonate, a common alteration product of barite ($BaSO_4$) is witherite ($BaCO_3$; Deer *et al.*, 1992). Elevated concentrations of Ba (> 1000 ppm) have been previously reported with secondary carbonate minerals in soils (Kabata-Pendias and Pendias, 1984).

There is no close correlation between Ba, Ca and Mg in the regolith carbonate zone (Figure 9.22A, B). However, barium is significantly correlated with S in carbonate associated with transported regolith ($r^2 = 0.7$, Figure 9.22C). This suggest that the Ba is present as barite, rather than as a substituting for Ca in carbonate. Such a relationship between Ba and S in calcrete has been previously reported (e.g. Butt, 1991; McQueen, 2006). Barium is weakly correlated with S in the carbonate zones from *in situ* regolith (Figure 9.22 D), which probably indicates that barite is not the major host mineral. A very high concentration (1.88 %) of S was detected from the regolith carbonate horizon in drill hole CBAC213 (5-6 m depth). This enrichment is associated with relatively high Sr (Figure 9.23), which possibly indicates the presence of Sr-rich barite or Ba-bearing celestite ($SrSO_4$). However, there is not a direct correlation between Sr and Ba

in the regolith carbonate horizons (Figure 9.22 E, F). Barite with variable Sr content has been previously observed in weathered bedrock (siltstone) at the Elura deposit (Scott and Taylor, 1989).

Strontium is correlated with Ca and Mg in the regolith carbonate horizons from the transported and *in situ* regolith (Figure 9.22 G, H). The enrichment of Sr in regolith carbonates has been commonly observed in many regolith studies (e.g., Butt, 1991, McQueen, 2006) in which Sr probably occurs as a substitute for Ca in calcite (Butt, 1991).

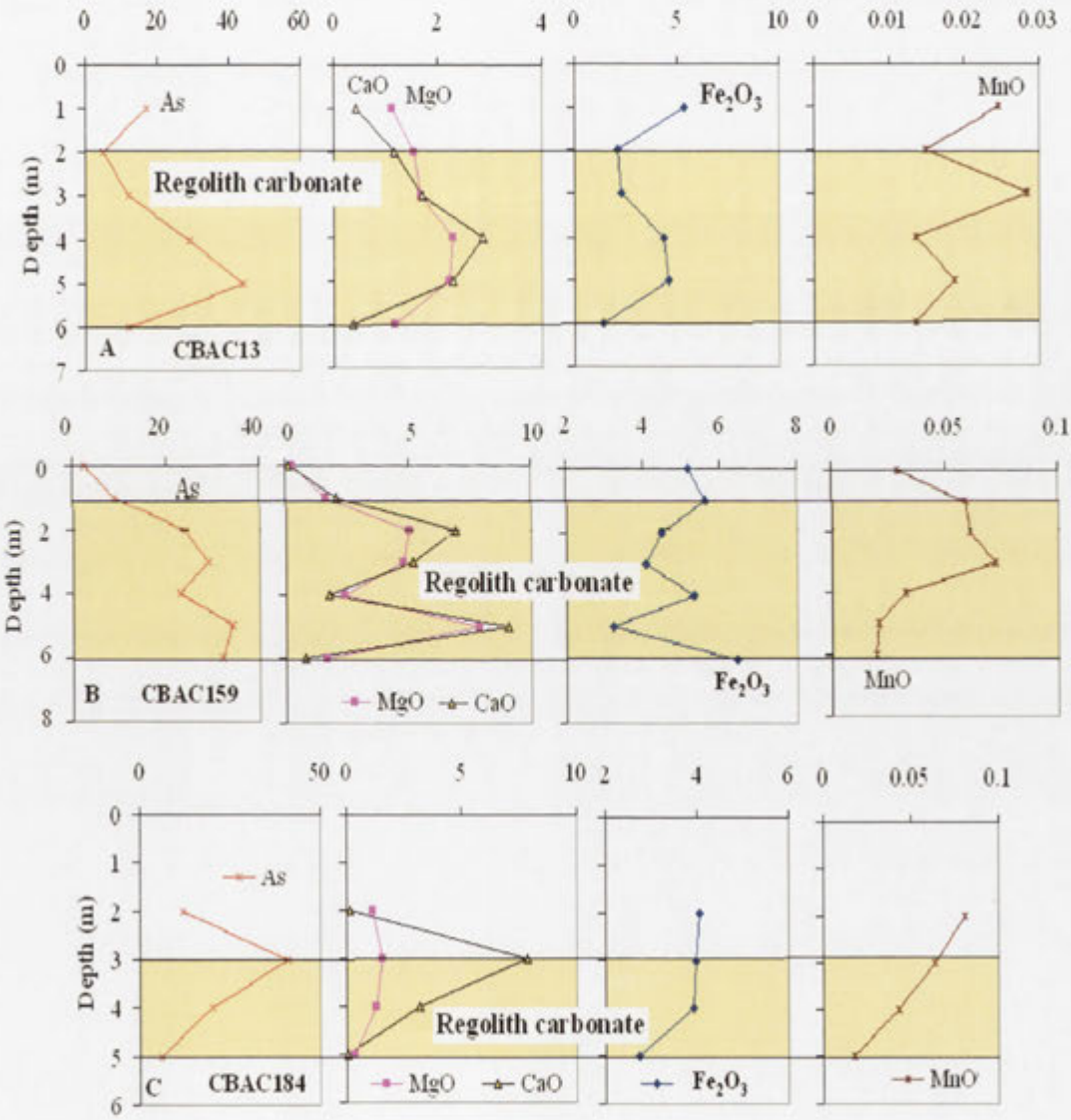

Figure 9.21 Arsenic distribution profiles showing the relationships between As (ppm) and MgO, CaO, Fe_2O_3, MnO (wt %), in the regolith carbonate in drill holes CBAC13 (A), CBAC159 (B) and CBAC184 (C).

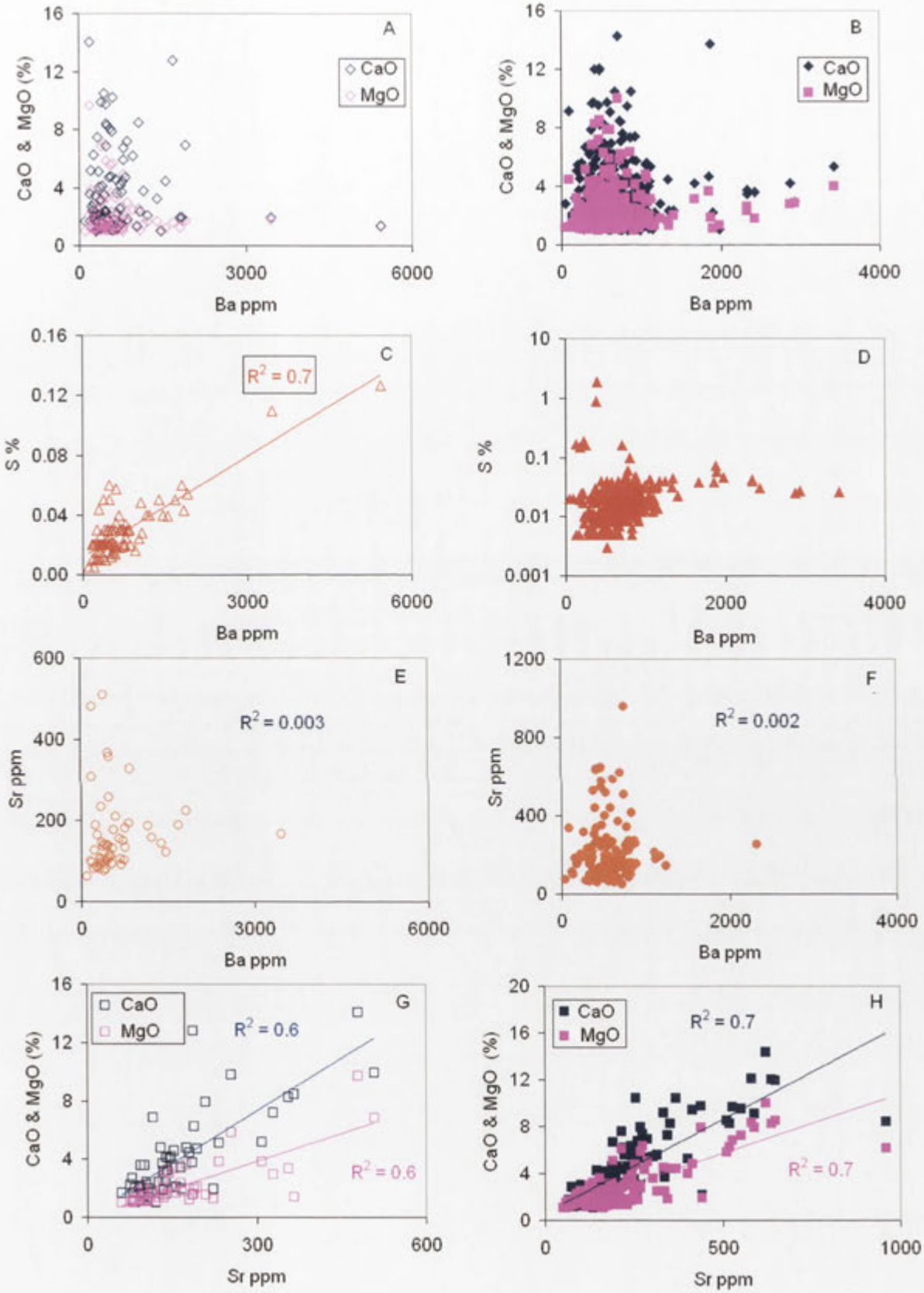

Figure 9.22 Scattergrams showing correlations between Sr and Ba and other elements in the regolith carbonates in the transported and *in situ* (solid symbols) regolith from the Girilambone region.

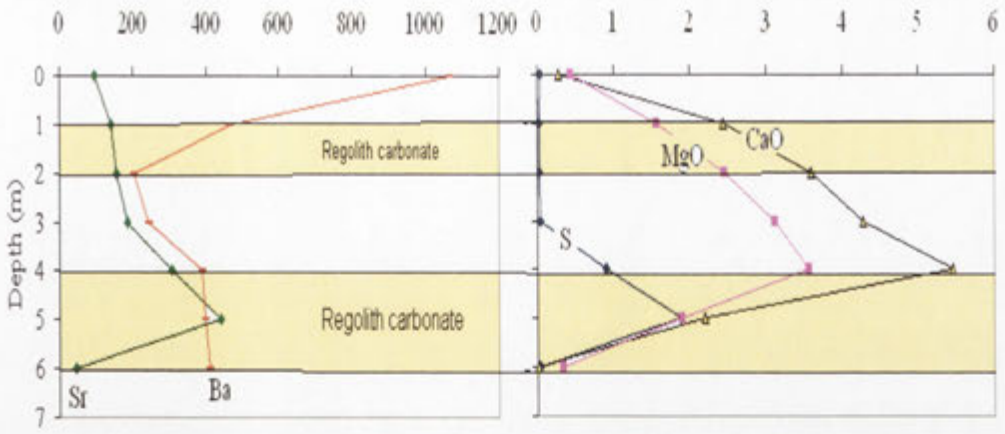

Figure 9.23 Showing distributions of Sr ppm, Ba ppm, S wt %, CaO wt % and MgO wt % in the calcrete bearing zone profile in drill hole CBAC213.

9.2.5.3 OTHER TRACE ELEMENTS

A number of trace elements analysed in the regolith carbonate zones (including Cu, Zn, Pb, Cr, Ni, Ti) show positive correlation with Fe and are negatively correlated with Ca and Mg, suggesting that these elements are contained within iron oxide/oxyhydroxide impurities in the carbonate zone. This Fe-associated suite of trace elements is recognised and discussed in detail in the Fe-rich facies (see below).

9.2.6 ORIGIN OF CARBONATE

A potential source of Ca and Mg and all other elements concentrated in regolith carbonate is the bedrock. Other sources include aeolian dust, marine aerosols, rainwater, groundwater and vegetation. In arid and semi-arid climates aeolian dust is probably the most significant source of Ca and Mg added to the regolith surfaces (Goudie, 1973; Taylor and Eggleton, 2001). Many playas contain significant Ca- and Mg-rich clay minerals and carbonates. During dry lake phases, these can be blown from the lake surfaces and deposited down-wind.

In the Cobar-Girilambone region most of the bedrocks have low contents of Ca and Mg (in the Cobar Supergroup rocks typically have <1.5% CaO wt % and < 3.2% MgO wt %, McQueen 2006; and the Girilambone Group rocks have <0.56 wt % CaO and < 2.45 wt % MgO, Ackerman, 2005). This suggests that the weathered bedrock is not a major source of these elements. Analysis of Sr^{87}/Sr^{86} ratios in calcrete from across the region has shown values ranging from 0.71195 to 0.71624, consistent with a predominantly

marine source for the Sr (McQueen, 2006). This suggests that the Sr and geochemically associated Ca have probably been introduced in dust, aerosols or rainwater from seawater or marine-derived carbonate accumulations (Dart *et al.*, 2005). Considerably elevated levels of many trace elements and gold in areas of known bedrock concentrations indicate the bedrock as a source of these elements.

9.2.7 SUMMARY AND CONCLUSIONS

In the Girilambone region, calcrete is widespread within a zone of variable thickness in the upper 10 m of the regolith. The calcrete typically consists of dispersed calcite-dolomite, generally with calcite predominating in the upper part of the zone and dolomite predominant towards the base. The highest Au contents in a profile are not necessary associated with the position of maximum calcrete development. Typically, the high Au concentration is at the top of the calcrete zone, but not all cases. There is generally a negative correlation between elevated Au and Fe_2O_3 content in this part of the regolith. Some *in situ* profile show an association of elevated gold with higher Fe_2O_3 content, but this is probably remnant primary Au in ferruginous saprolite.

The association of Au with calcrete in the Girilambone region appears to reflect a chemical environment within both transported and *in situ* regolith that is conducive to precipitation of both carbonate and mobilised gold rather than a direct control on gold fixation by calcrete.

There is no positive correlation between Cu, Zn, Pb, Cr, Ni and Ti concentration and CaO and MgO contents in the calcrete zone. However, these elements show positive correlation with Fe_2O_3 content suggesting that they are contained within iron oxide/oxyhydroxide impurities in the carbonate zone.

9.3 ELEMENT ASSOCIATIONS AND DISPERSION IN Mn-RICH REGOLITH

9.3.1 INTRODUCTION

Manganese-enriched zones are common in many deeply weathered terrains (e.g., Taylor and Ruxton, 1987). This section will describe the spatial distribution of Mn-rich

horizons, Mn oxide/oxyhydroxide minerals and the associated element concentrations. Their possible relationship with groundwater will also be investigated.

9.3.2 OCCURRENCE OF Mn-RICH HORIZONS

Manganese oxides occur in soils as deposits in cracks and veins, as coatings and stains on soil aggregates or as a cementing material. They may also be dispersed throughout the soil as microscopic accumulations, or concentrated as nodules up to about 2 cm in diameter (Taylor *et al.*, 1983).

In the Girilambone region Mn-enriched zones mainly occur within the *in situ* regolith (Figure 9.24). Manganese enrichment is highest in the west and south of the Hermidale area (e.g., drill hole CBAC174) and generally decreases toward the east. The Hermidale area is characterised by outcrops of saprolith that form rises and low hills (Chan *et al.*, 2002) partly developed on the Babinda Volcanics (Suppel and Gilligan, 1993). It is also thought to be a groundwater recharge area (Khider and McPhail, 2005). In the northern part of the region (Byrock area) the depth of Mn accumulation increases down the topographic slope to the northeast.

9.3.3 MANGANESE OXIDE/ OXYHYDROXIDE MINERALS

Manganese occurs in a number of valance states in nature (Day, 1963). A large number of oxides and oxyhydroxides exist, in which there is extensive substitution of Mn (II) and Mn (III) for Mn (IV), and of OH^- for O^{2-} (Taylor *et al.*, 1983). Manganese oxides also display a remarkable diversity of atomic architectures, many of which easily accommodate a wide assortment of other metal cations. In addition, Mn is abundant in most geological systems and forms minerals under a wide range of chemical and temperature conditions, and through biological interactions (Post, 1999).

The basic building block for most of the Mn oxide atomic structures is the MnO_6 octahedron. These octahedra can be assembled by sharing edges and/or corners into a large variety of different structural arrangements, most of which fall into one of two major groups: (i) chain, or tunnel, structures and (ii) layer structures. The tunnel Mn oxides are constructed of single, double, or triple chains of edge-sharing MnO_6 octahedra, and the chains share corners with each other to produce frameworks that have tunnels with square or rectangular cross sections. The larger tunnels are partially filled with water molecules and /or cations (Burns and Burns, 1975; Post, 1999).

Based on atomic structure, Post (1999) has described and classified the most common Mn oxide minerals into: Mn oxides with tunnel structures, which include pyrolusite, ramsdellite, nsutite, hollandite group (hollandite, cryptomelane, coronadite and manjiroite), romanechite and todorokite, and Mn oxide minerals with layer structures, which include lithiophorite, chalcophanite, birnessite, and vernadite. The chemical compositions of some of these minerals are summarised in Table 9.2.

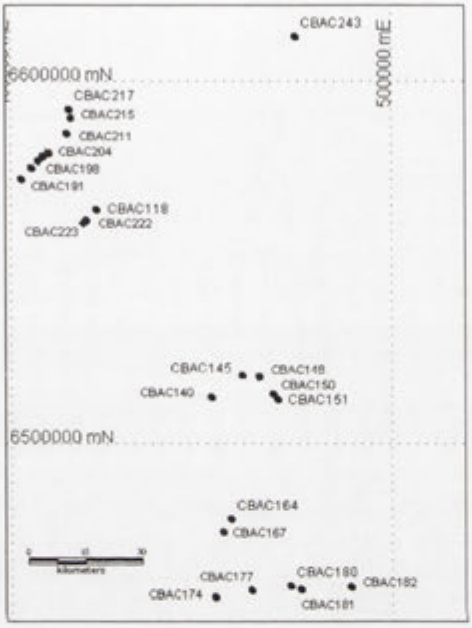

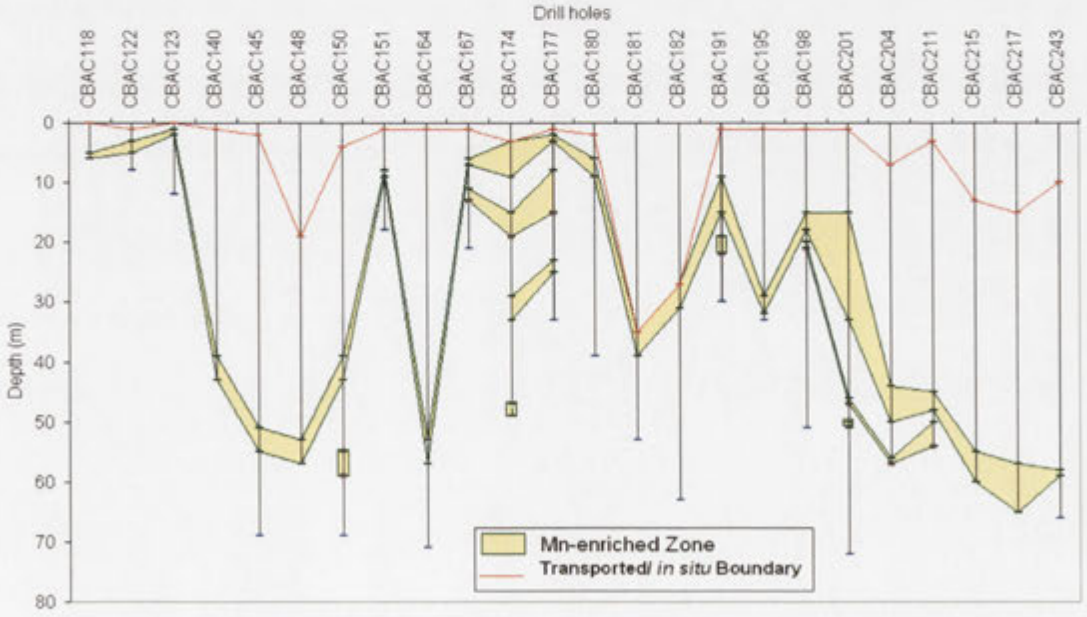

Figure 9.24 Drill hole plots showing the transported/*in situ* boundary and distribution of Mn-enriched zones in the *in situ* regolith of the Girilambone region. Drill hole locations are shown on the associated map.

The hollandite group minerals have the general formula A_{0-2} $(B+Mn^{4+})_8O_{16}$. xH_2O. The A site can be occupied by large cations such as K^+, Ba^{2+}, Na^+, Cu^+, Pb^{2+}, Rb^{2+}, Sr^{2+}, etc., whereas the B site includes Mn^{3+}, Mn^{4+}, Fe^{3+}, Si^{4+}, and Mg^{2+} (Burns and Burns, 1975). Cryptomelane, hollandite and coronadite are K, Ba and Pb end-members of a solid-solution series, respectively (Bystrom and Bystrom, 1950). Nicholson (1992) used a high Ba concentration as an indication of secondary enrichment of Mn during weathering. Nickel, Cu and Co are commonly reported in lithiophorite, where the Ni and Cu concentrate in the Al-OH sheets and Co in the Mn layers (Ostwald, 1984). Lithiophorite has been synthesized by substitution of aluminium and lithium into a birnessite-type mineral (Giovanoli *et al.*, 1973). Although lithiophorite generally contains a reasonable amount of Li (0.2-3 wt%, Post, 1999), no Li was detected by this technique, which probably needs further investigation.

In this study samples from Mn- enriched horizons were analysed to determine the morphology and chemical composition of Mn-oxide/oxyhydroxide minerals. Manganese-rich grains and Mn-coated dark coloured grains were collected from five Mn-dominant intervals in the drill holes CBAC 176 (37-39 m), CBAC177 (8-9 m, 13-15 m), and CBAC180 (6-7 m, 7-8 m). The samples were examined using scanning electron microscope (SEM) and energy dispersive X-ray analysis (EDXA).

The analysis showed that Mn-oxides/oxyhydroxides in these samples occur as microcrystalline masses and well-developed platy crystals (Figures 9.25, 27, 29, 31). The microcrystalline masses are commonly present as compact botryoidal aggregates, coating the clay particles and/or as clusters of Mn oxides/oxyhydroxides between clay crystals (Figures 9.25, 27, 29). Manganese oxides in soils in general were reported to be very fine grained, commonly poorly crystalline or amorphous (McKeague *et al.*, 1968; Childs, 1975). The energy dispersive X-ray analysis (EDXA) spectra of Mn microcrystalline masses showed that Mn oxides/oxyhydroxides are associated with K and Al and Si in addition to Co and Cu (Figures 9-25, 26). Occurrences of K and Si in association with Al are possibly related to muscovite and cryptomelane (Figures 9.25, 26 A), whereas the association of Mn, Al, Co and Cu in the absence of K and Si (Figure 9.26 B) suggests occurrence of lithiophorite. Chemical composition of the microcrystalline Mn minerals that coat clay and/or quartz crystals shown in Figure 9.27

confirmed occurrences of clay/mica with high Al and low K contents (possibly muscovite and kaolinite), quartz (high Si content) and lithiophorite with incorporated Co, Cu, Ni (Figure 9.28). The spectra of the microcrystalline Mn minerals that clustered between clay crystals shown in Figure 9.29 showed Mn associated with Al, Si, Na, Ca, Mg, P, Pb, K, Fe and Ba (Figure 9.30), where Al, Si, Na, Ca, Mg and K represent a common clay assemblage and Al, Mn, K, Ba, Pb and P possibly represent hollandite group minerals.

Table 9.2 Chemical compositions of the common Mn oxide minerals (from Post, 1999).

Mineral	Chemical formula
Pyrolusite	MnO_2
Ramsdellite	MnO_2
Nsutite	$Mn(O,OH)_2$
Hollandite	$Ba_x (Mn^{4+}, Mn^{3+})_8 O_{16}$
Cryptomelane	$K_x (Mn^{4+}, Mn^{3+})_8 O_{16}$
Manjiroite	$Na_x (Mn^{4+}, Mn^{3+})_8 O_{16}$
Coronadite	$Pb_x (Mn^{4+}, Mn^{3+})_8 O_{16}$
Romanechite	$Ba_{6.6}(Mn^{4+}, Mn^{3+})_5 O_{10}. 1.34H_2O$
Todorokite	$(Ca,Na, K)_x (Mn^{4+}, Mn^{3+})_6 O_{12}. 3.5 H_2O$
Lithiophorite	$LiAl_2(Mn_2^{4+} Mn^{3+}) O_6 (OH)_6$
Chalcophanite	$Zn Mn_3 O_7 3H_2O$
Birnessite	$(Na,Ca) Mn_7O_{14}. 2.8 H_2O$
Vernadite	$MnO_2.nH_2O$

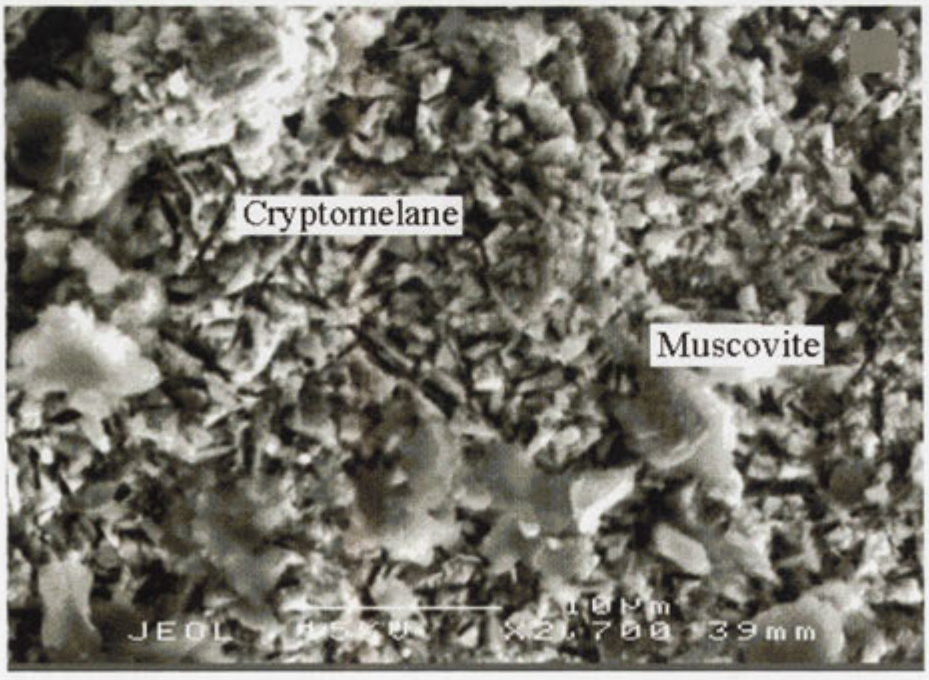

Figure 9.25 SEM photomicrograph showing large flakes of mica (muscovite) and microcrystalline Mn oxides (cryptomelane) in a sample from a Mn-enriched horizon (7-8 m depth) in drill hole CBAC180. Scale bar is 10 μm.

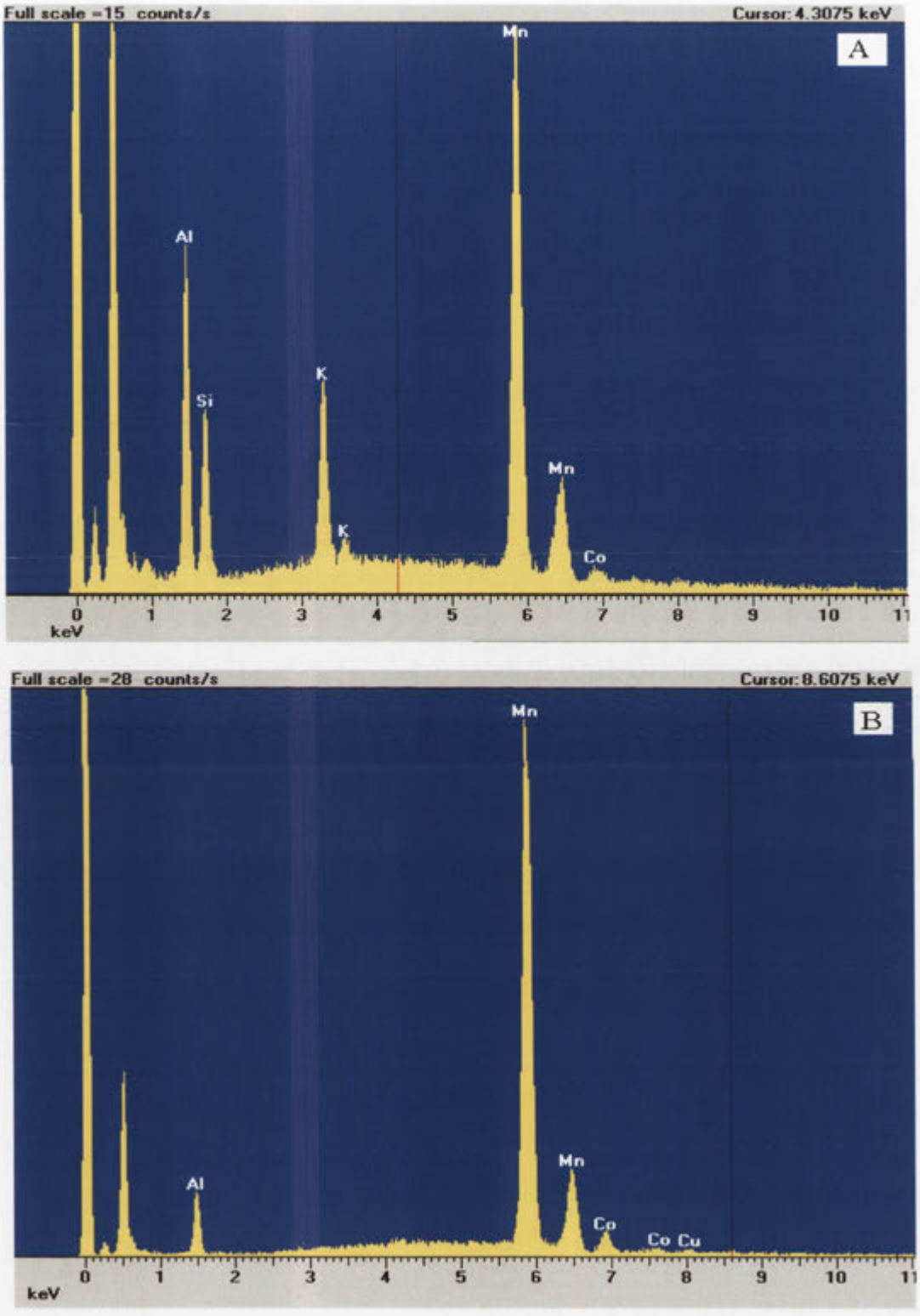

Figure 9.26 EDXA spectra showing the chemical compositions of (A) clay (Al-Si-K) with cryptomelane (Mn-K-Co-Cu) and (B) lithiophorite (Mn-Al-Co-Cu) for the sample described in Figure 9.25.

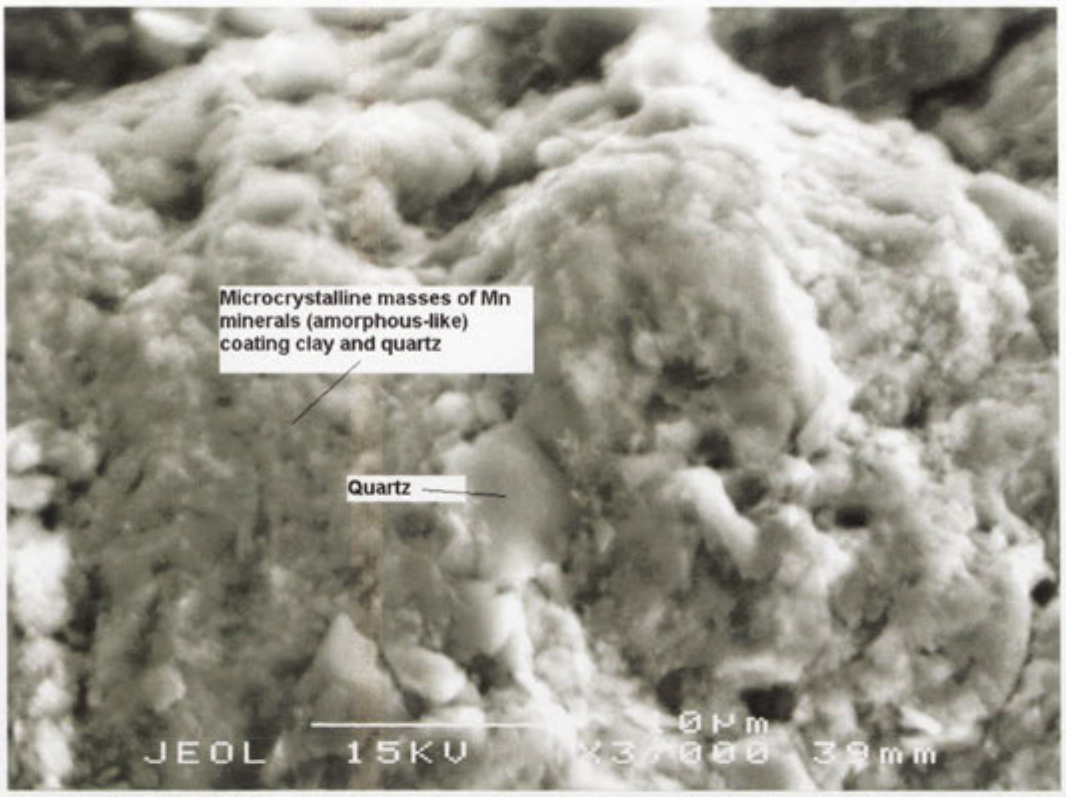

Figure 9.27 SEM photomicrograph showing a quartz crystal and microcrystalline Mn oxides including lithiophorite coating clay and quartz in a sample from a Mn-enriched horizon (13-15 m depth) in drill hole CBAC177. Scale bar is 10 μm.

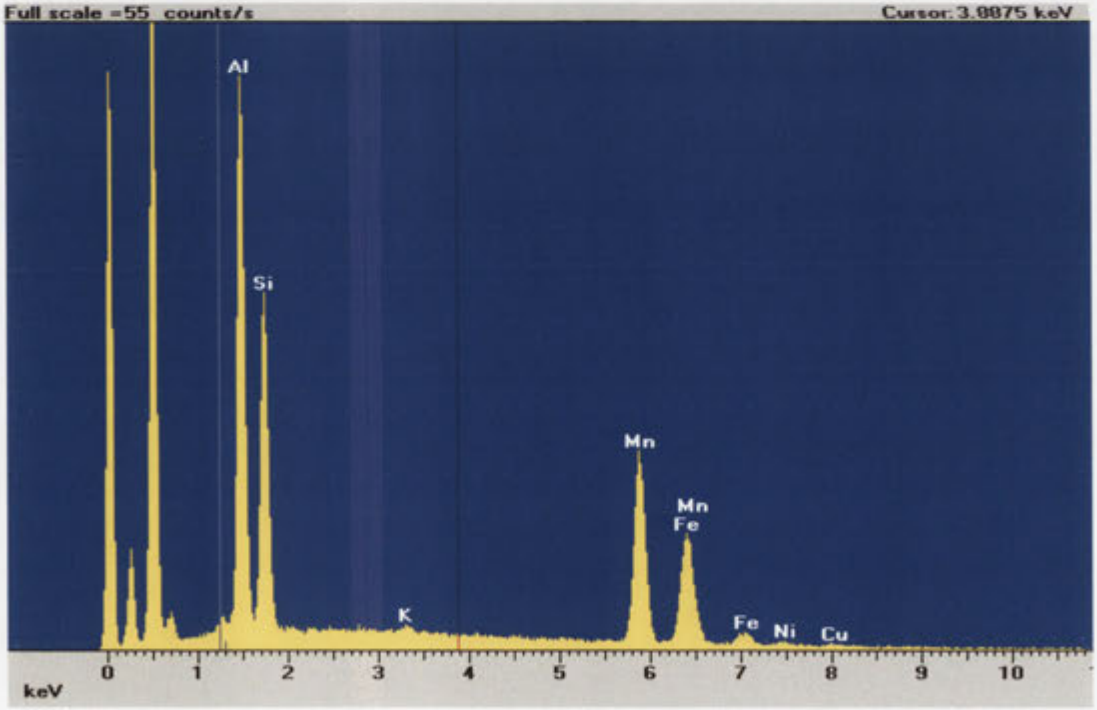

Figure 9.28 EDXA spectrum showing the chemical compositions of clay (Al-Si-K) with quartz (high Si) and lithiophorite (Mn-Al-Ni -Co-Cu) for the sample described in Figure 9.27.

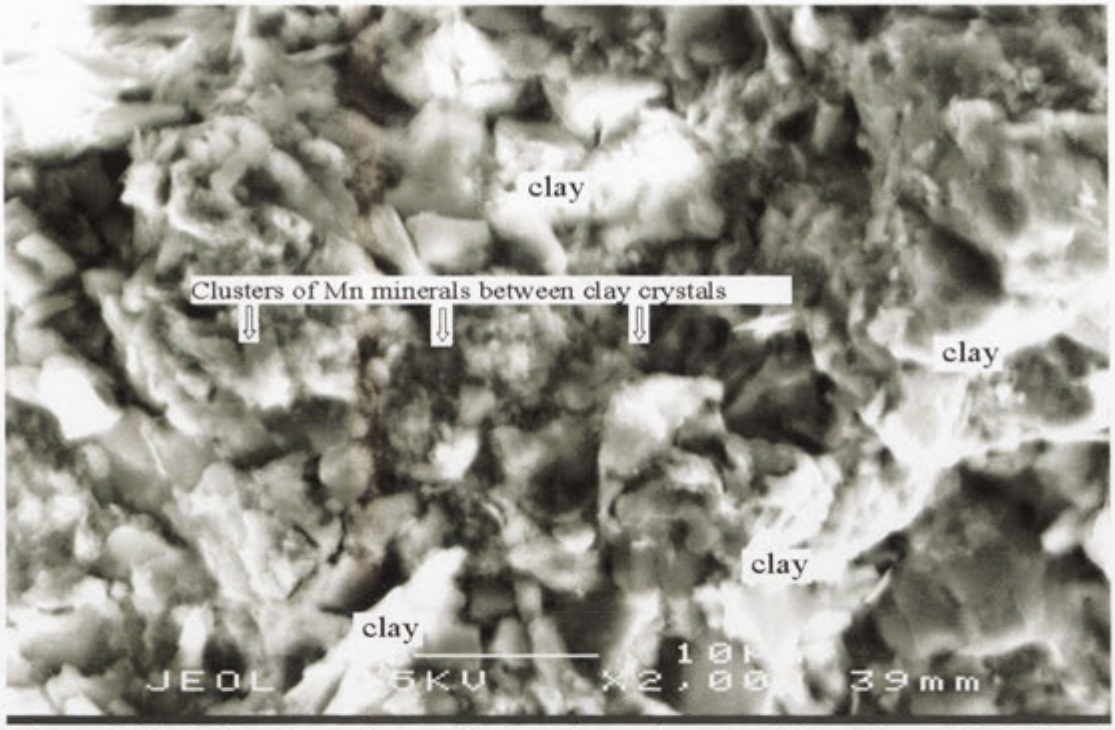

Figure 9.29 SEM photomicrograph showing microcrystalline Mn oxides clustered between clay crystals in a sample from Mn-enriched horizon (13-15 m depth) in drill hole CBAC177.Scale bar is 10 μm.

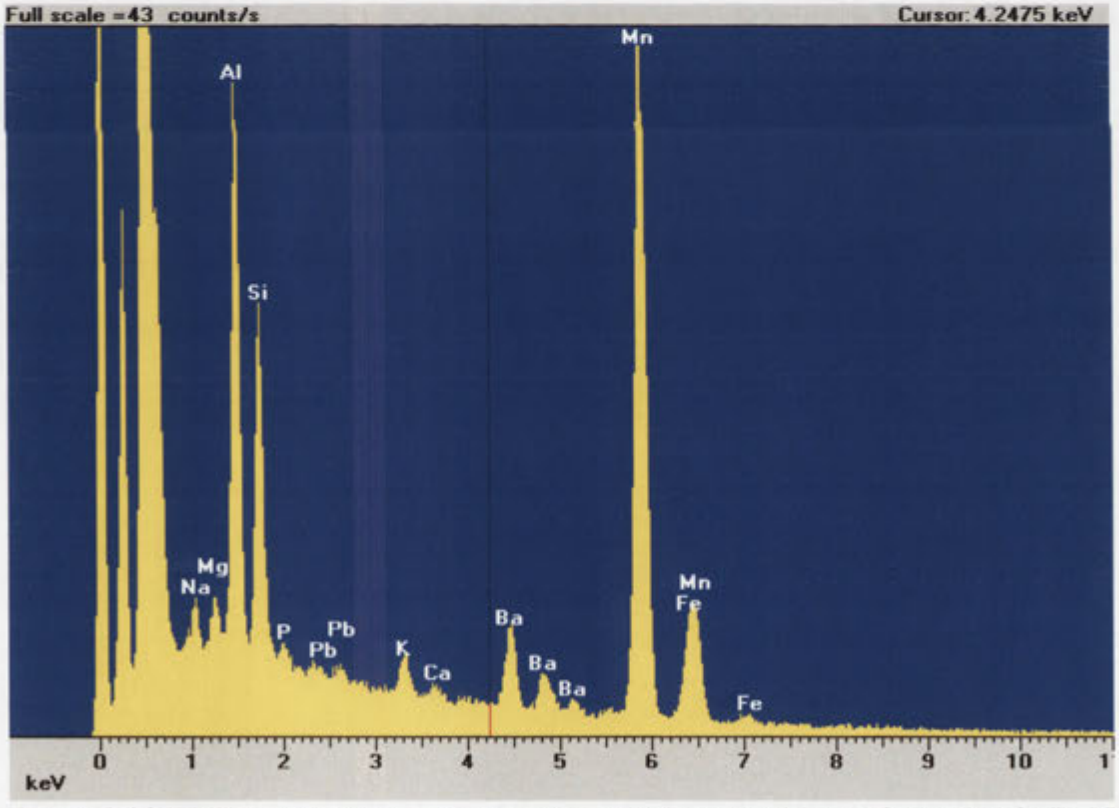

Figure 9.30 EDXA spectrum showing the chemical compositions of clay (Al-Si-K, Na, and Mg) and hollandite group (Mn- (Ba, K, Pb and Na) with some Fe for the sample described in Figure 9.29.

Well-developed manganese oxides/oxyhdroxides fill voids and cavities as sheaves of platy crystals (Figure 9.31), which probably indicate late-stage crystallisation. Another microcrystalline Mn mineral was also observed adjacent to lithiophorite, coating clay crystals (Figure 9.31). The EDXA spectra of the well-developed Mn oxides show that Mn is associated with Al, Si, Co and Cu, which suggest clay and lithiophorite (Figure 9.32), whereas the spectra of the microcrystalline massive Mn oxides show high Mn content associated with Al (Figure 9.33), which suggest the presence of pyrolusite or ramsdellite and mica.

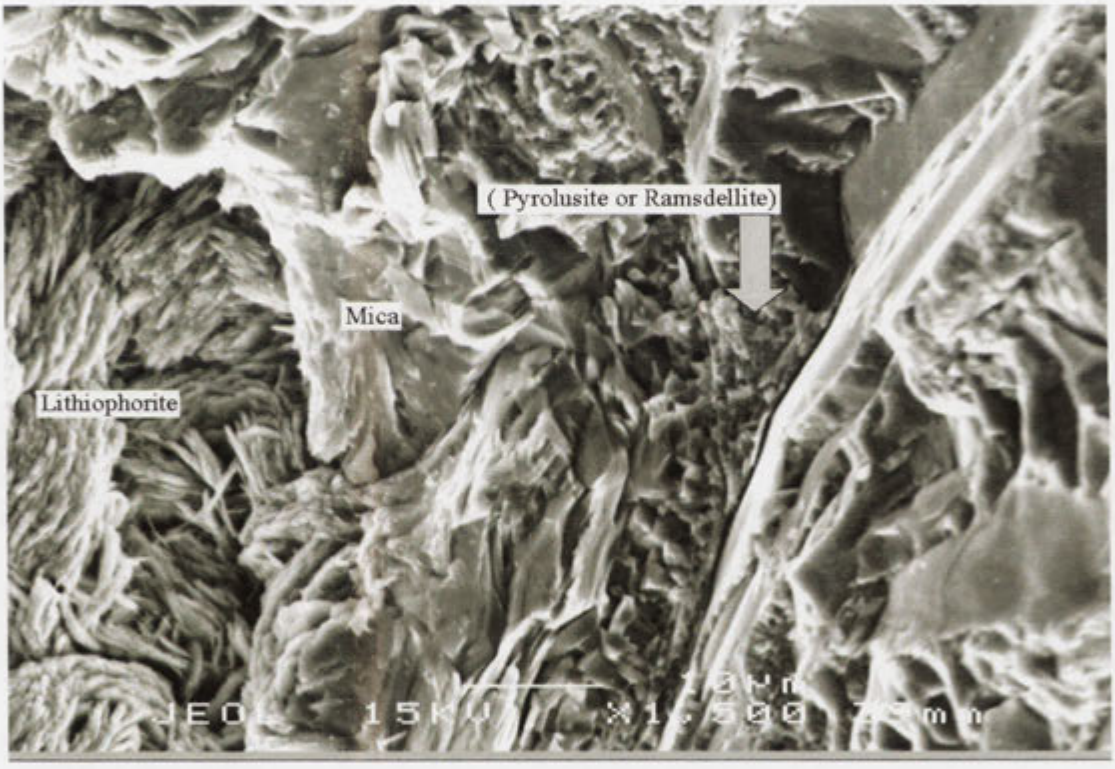

Figure 9.31 SEM photomicrograph showing well-developed Mn (lithiophorite) crystals forming sheaves in voids, mica crystals that formed the framework and microcrystalline Mn oxides (pyrolusite or ramsdellite) coating part of clay crystals in a sample from a Mn-enriched horizon (8-9 m depth) in drill hole CBAC177. Scale bar is 10 μm.

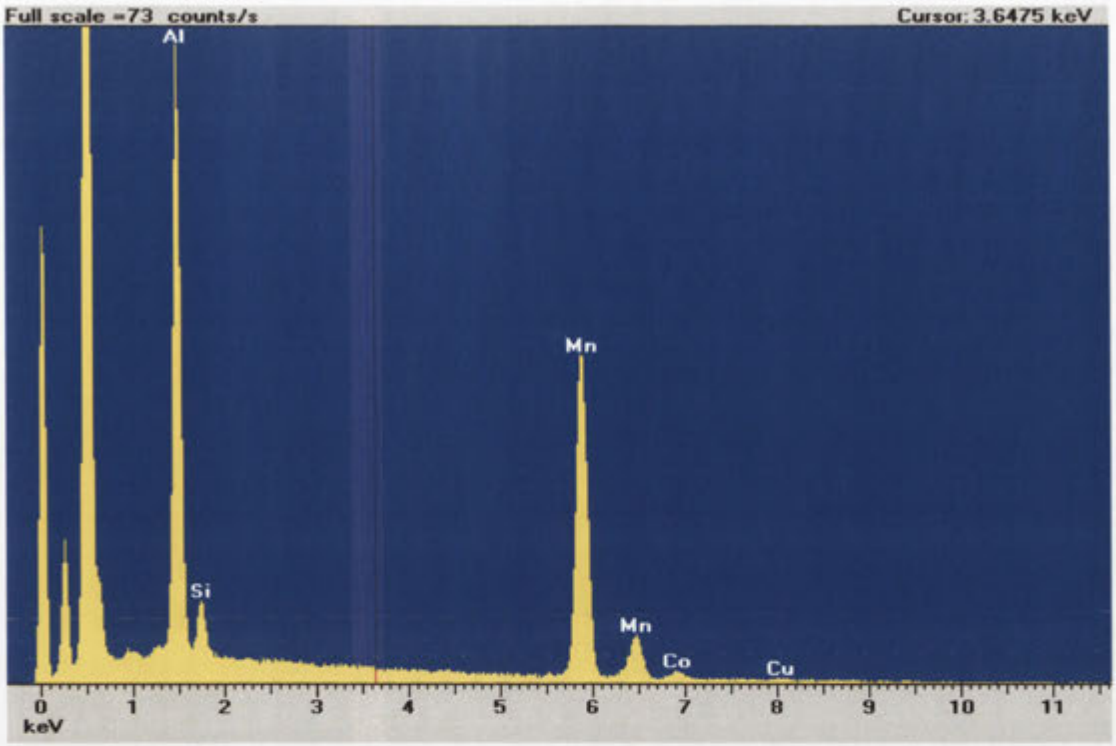

Figure 9.32 EDXA spectrum showing the chemical compositions of clay (Al-Si) and well-developed Mn oxides (lithiophorite, Mn-Al-Co-Cu) for the sample described in Figure 9.31.

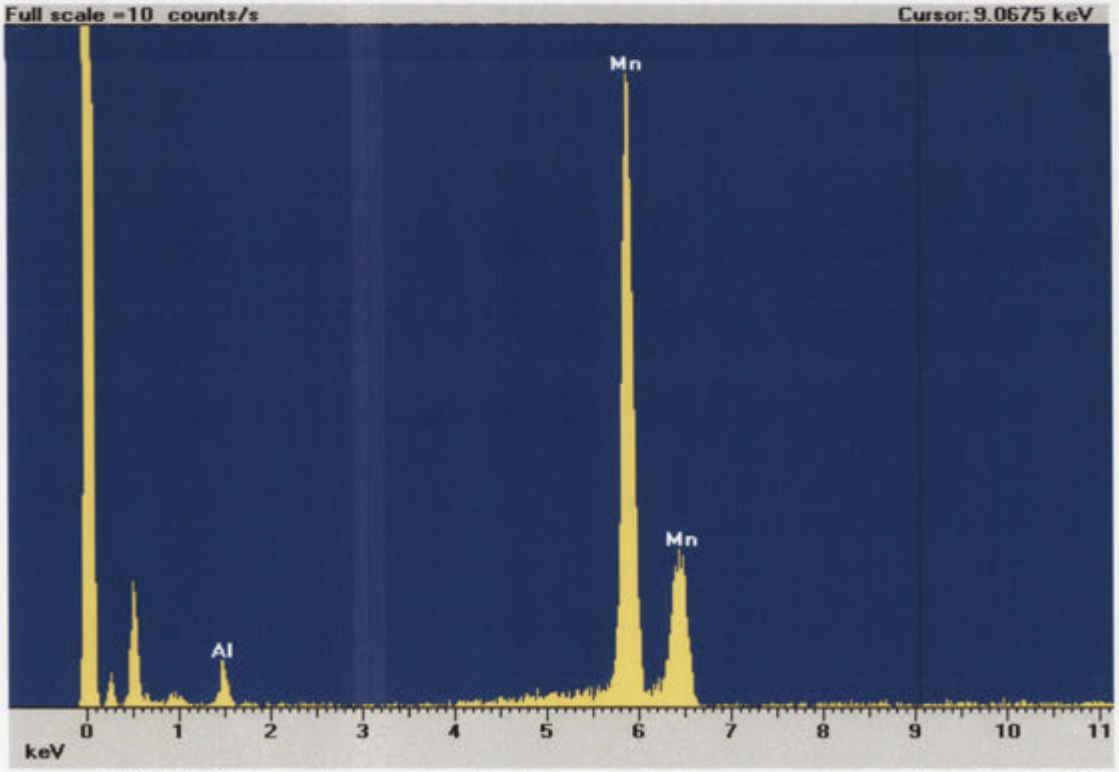

Figure 9.33 EDXA spectrum showing the chemical compositions of microcrystalline Mn oxides (pyrolusite) for the sample described in Figure 9.31.

9.3.4 ACCUMULATION OF MANGANESE OXIDES AND OXYHYDROXIDES

The relative importance of Mn and Fe oxides/oxyhydroxides as scavengers depends upon: pH-Eh conditions; degree of crystallinity of the oxides and therefore their reactivity; their relative abundances; and the presence of organic matter as a competing adsorbing and chelating fixing agent (Hall, 1998). Elements will show a preference for uptake by either Mn or Fe oxides depending on local conditions. Oxidation of manganese is catalysed by fine particles in soils (Morgan and Stumm, 1964). Hem (1964) reported that the oxidation is catalysed by MnO_2 at pH 7.8 or higher, but not at 7.2. He also discussed the oxidation of manganese by precipitated Fe $(OH)_3$, and concluded that it is the result of low activity of available Fe^{2+} in slightly acid solution.

It is difficult to present a typical weathering profile for Mn accumulation because it depends on the nature of the original parent rock and, particularly, on its structure (Nahon *et al.*, 1992). A general model of weathering for parent rocks consisting essentially of manganiferous silicates (Figure 9.34) was constructed by Nahon and Parc (1990) and Parc (1989). Hausmannite and manganite would not be expected to be present in the regolith because these minerals are unstable during weathering and they are either oxidised or disproportionated to give more oxidised Mn minerals under acid and alkaline conditions respectively (Taylor *et al.*, 1983).

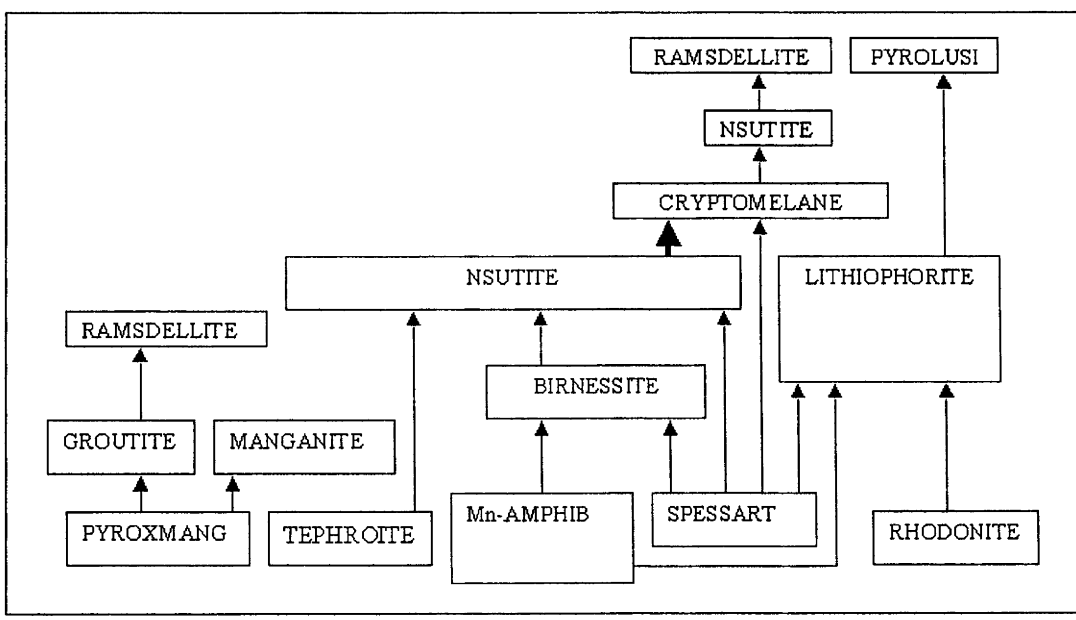

Figure 9.34 Mineral sequences in the weathering of Mn-bearing silicates. Heavy arrow indicates retromorphosis of oxides. (after Nahon *et al.*, 1992).

It is apparent that different minerals can generate the same oxidized weathering phase and that different minerals may generate, in the same horizon, different weathering minerals. Therefore it is common to observe in profiles a very oxidised manganiferous phase in shallow regolith grading into less oxidised phases at greater depth (Figure 9.34). Such a retromorphosis can be explained by late weathering of primary minerals in the profiles. For example, release of K by weathering of micaceous minerals allows the retromorphosis of nsutite ($Mn_{1-y}Mn_y\ O_{2-y}\ (OH)_y$) and even of pyrolusite (MnO_2) into cryptomelane($K_x(Mn^{4+}, Mn^{3+})_8\ O_{16}$; Nahon *et al.*, 1992). Similarly lithiophorite, which strongly develops toward the top of lateritic weathering profiles, shows modification of the valence of manganese due to incorporation in its structure of transition elements, particularly Ni^{2+} (Manceau *et al.*, 1987).

Formation of lithiophorite requires high Al, and this is possibly generated from the destruction of parent (alumino-manganifrous) minerals, or from weathering of kaolinite in the upper part of the profile. Nahon *et al.* (1989) showed that the relative concentration of manganese oxides could locally generate very acidic environments, allowing the release of aluminium by dissolution of kaolinite and its simultaneous incorporation into the structure of the precipitating lithiophorite.

The observed distribution of Mn minerals in a number of profiles (e.g., in drill hole CBAC177; Figure 9.35) suggests that microcrystalline lithiophorite changed through the weathering profile to well-developed recrystallised lithiophorite and pyrolusite. The change up the profile from lithiophorite to pyrolusite is consistent with the proposed weathering model of Mn-rich materials (Figure 9.34). In CBAC180, the cryptomelane and lithiophorite change to hollandite up the profile, probably as a result of significant incorporation of Ba in the Mn oxide structure.

9.3.5 MAJOR AND TRACE ELEMENTS CHARACTERISTICS OF MANGANESE OXIDES/OXYHYDROXIDES

There is no significant correlation between MnO and the major elements (Al_2O_3, CaO, MgO, Fe_2O_3, K_2O, Na_2O, P_2O_5, TiO_2) in the Mn-enriched regolith (Figure 9.36). This generally indicates that the distribution of these elements is not controlled by Mn oxide concentration. Similarly there is no correlation between Mn and typical pathfinder elements (Ag, As, Au, Bi, Mo, Sb, Figure 9.37) associated with Au mineralisation.

However these results must be cautiously interpreted because some of these elements have a large number of censored (BDL) values (Appendix 7).

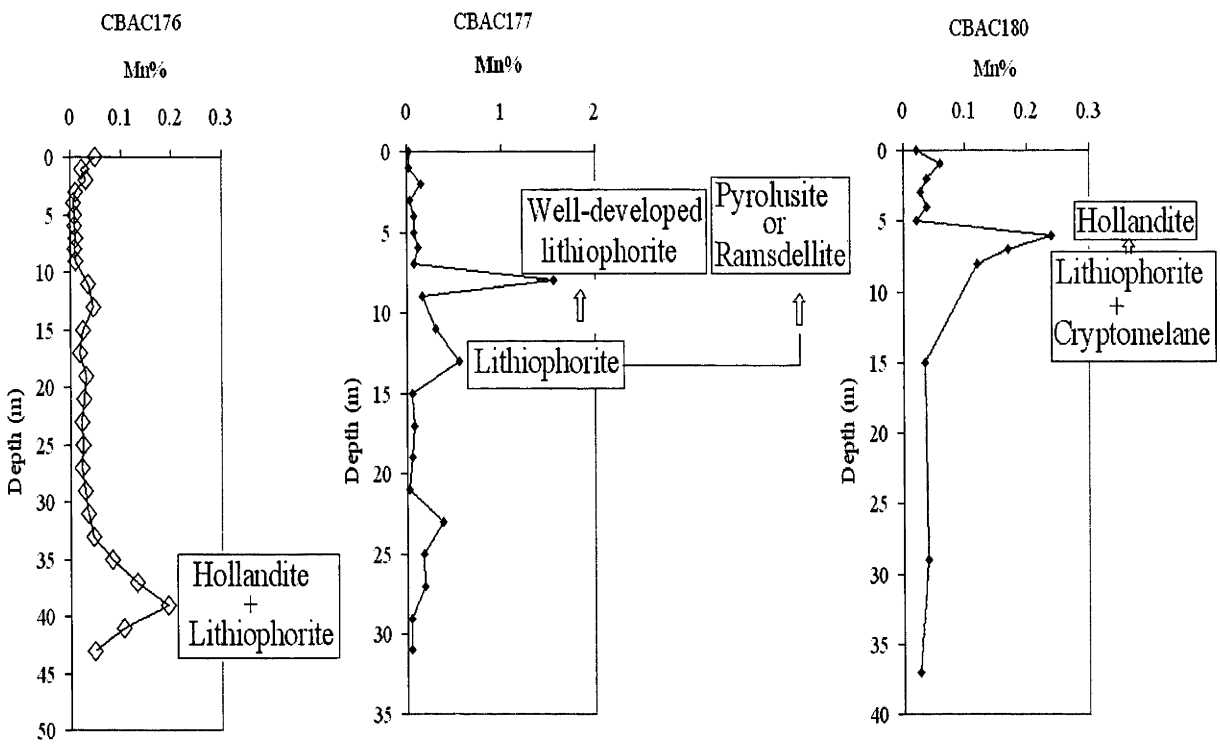

Figure 9.35 Distribution profile of Mn (wt %) and Mn-minerals in drill holes CBAC176, CBAC177 and CBAC180.

9.3.5.1 GOLD CONCENTRATION IN Mn-RICH REGOLITH

In the Mn-rich regolith Au contents range from <0.001 ppm to 0.077 ppm (Appendix 7) and Au shows noticeable concentration in some Mn- rich horizons. Therefore selected high-Au concentration profiles were examined to understand the relationship between Au and Mn–rich regolith. Significant enrichments of Au (Au > 0.01 ppm) were detected from drill holes CBAC 119, CBAC191, CBAC195, CBAC198, CBAC201 and CBAC211. Generally Au was enriched either at the top or at the base of the Mn-rich horizons (Figures 9.38, 40).

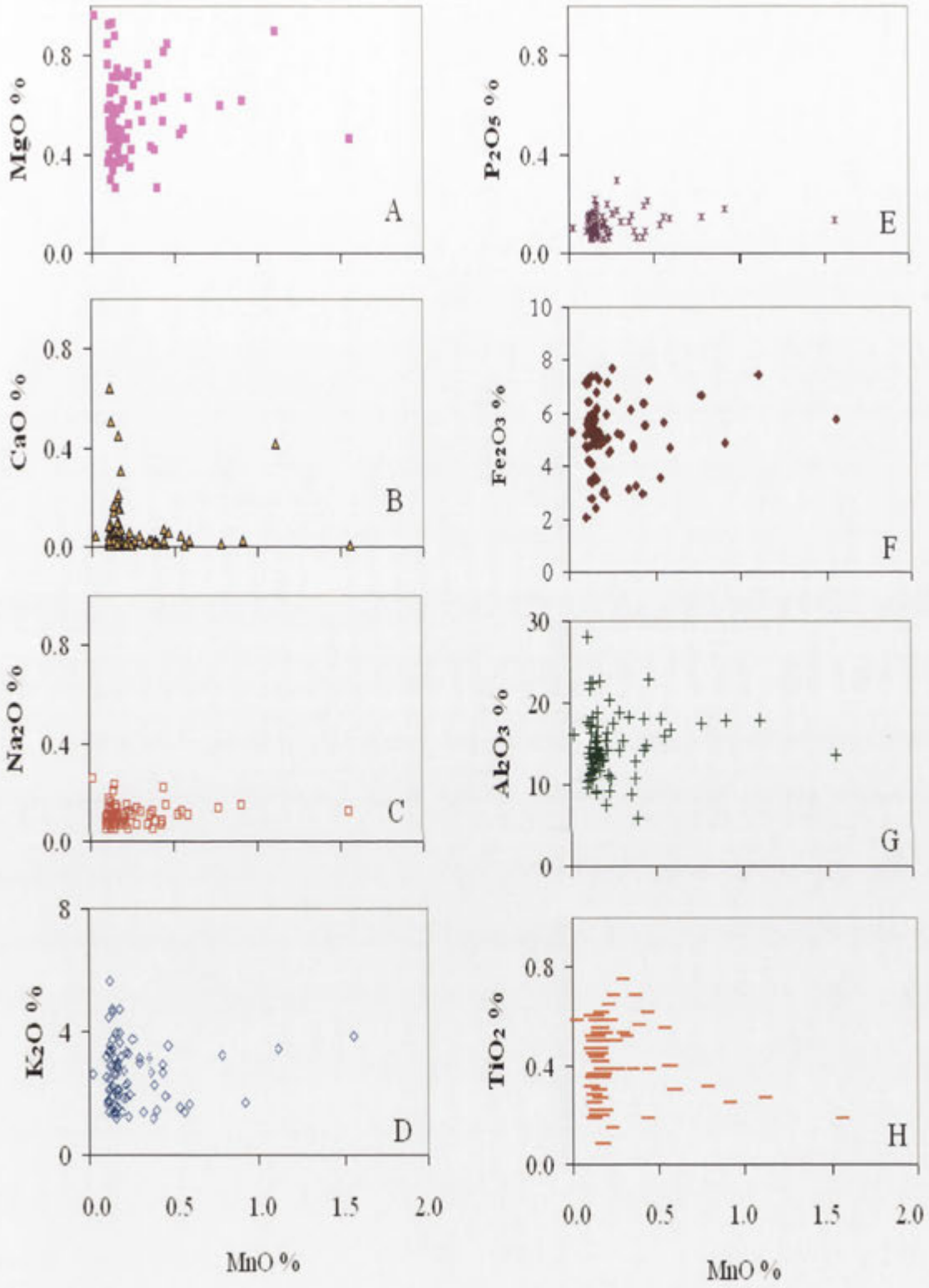

Figure 9.36 Scattergrams of major elements in the Mn-enriched regolith of the Girilambone region. MnO vs. MgO (A), CaO (B), Na_2O (C), K_2O (D), P_2O_5 (E), Fe_2O_3 (F), Al_2O_3 (G) and TiO_2 (H).

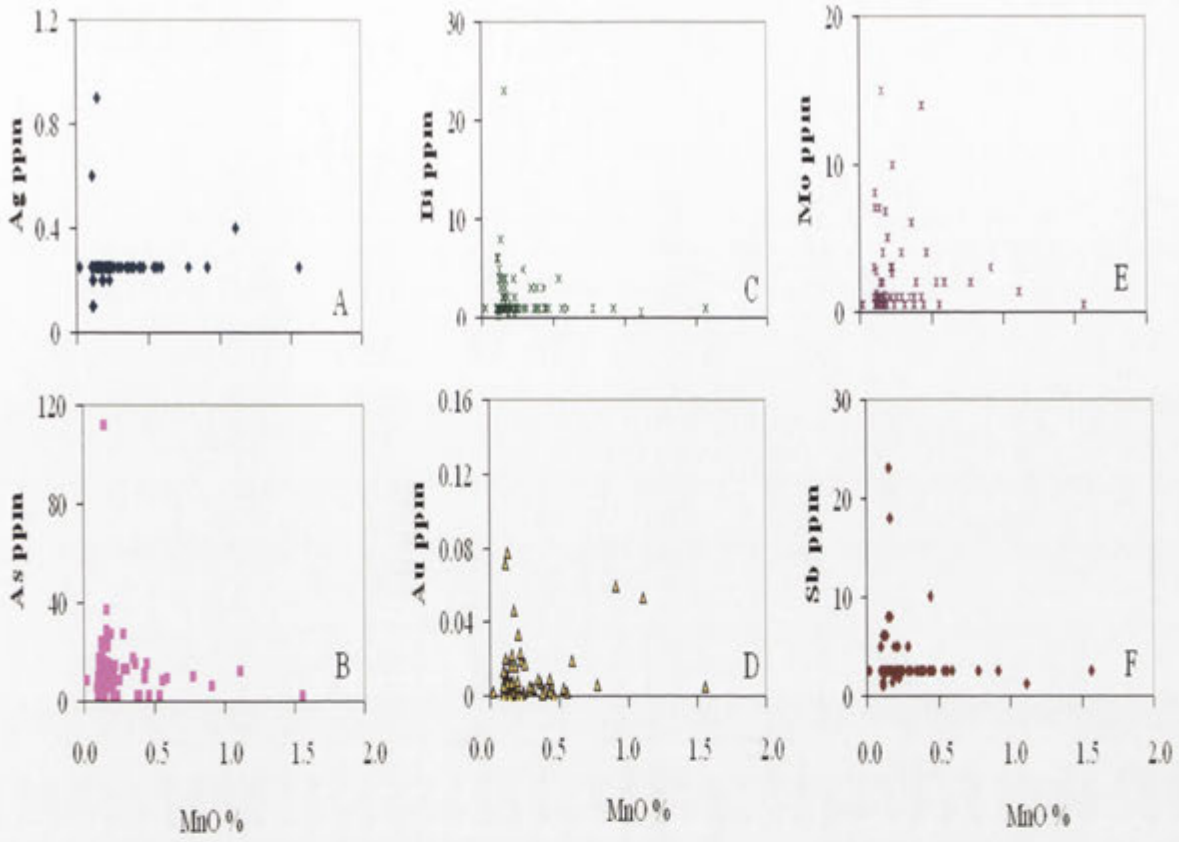

Figure 9.37 Scattergrams of trace elements in the Mn-enriched regolith of the Girilambone region. MnO vs. Ag (A), As (B), Bi (C), Au (D), Mo (E) and Sb (F).

In drill hole CBAC119 three Mn-enriched horizons were recognised. In the upper horizon (0-2 m depth) the elevated Mn concentration is associated with an anomalous range of Au values (0.012-0.019 ppm) and significant enrichment in Sb (Figure 9.38). This horizon also shows a slight enrichment in Fe. However, the distribution pattern of Au coincides with Mn, which possibly indicates co-precipitation and /or adsorption of Au on Mn oxides. In the middle Mn-rich horizon (4-6 m depth) increasing Mn content is associated with elevated As, Sb and to some extent with Au contents, particularly in the lower part of the horizon, but the distribution pattern of Au within the horizon is more comparable with Mg and Ca patterns (Figure 9.38). This possibly indicates that the calcification has a stronger influence on the Au dispersion than Mn scavenging processes, or that the accumulation of Mn in the upper part of the horizon occurred after Au-carbonate precipitation. In the lower horizon (9-10 m depth) the slight enrichment in Au (0.006 ppm) coincides with Mn enrichment; however, this horizon overlies a carbonate-rich layer at 10-11 m depth and therefore the elevated Au value

(0.006 ppm) across the Mn-carbonate boundary is possibly due to concentration of Au in the upper part of the carbonate layer (Figure 9.38).

Gold enrichment was also observed in drill holes CBAC 191, 195, 198, 201 and 211 (Appendix 7) but the highest Mn content does not coincide with the highest Au values. This suggests that the abundance of Mn is not controlling the amount of Au by substitution or adsorption on to Mn minerals. In CBAC 191, the highest enrichment of Mn coincides with enrichment of Fe, Mg, As, Co, Ni, Cu and Zn at the top of Mn-dominant horizon. This multi-element enrichment possibly reflects a mafic rock association. Gold is not associated with this upper level multi-element enrichment but is possibly slightly enriched in the middle of the Mn-rich horizon (Figure 9.39).

In drill hole CBAC195, Au content consistently increases with depth in the Mn horizon and the highest Au value (0.077 ppm) was observed at the base of the Mn horizon. The distribution pattern of Au in the Mn-dominant horizon in this hole is generally more compatible with Fe and Mg than Mn, which probably indicates that the enrichment of Au is controlled by Fe oxides and it is not related to abundance of Mn (Figure 9.40).

Two Mn-rich horizons occur in drill hole CBAC 198, where the highest concentrations of Au, Co, Cu, Zn and Ni are associated with elevated Mn and to some extent with elevated Fe values in the top of the upper Mn horizon (Figure 9.41). There is no significant change in the Au concentration in the lower Mn horizon; therefore the Au inter-elemental relationship is not clear. However the distribution pattern of the elements shows that the base metals are significantly influenced by Mn oxide development (as discussed below).

In drill hole CBAC201, there are three Mn-enriched horizons. Gold enrichment in the upper and lower horizons is associated with elevated Mn, As, Co, Ni, Cu, and Zn. Similarly in the middle horizon Mn enrichment is also associated with elevated Co, Ni Cu and Zn but not Au (Figure 9.42). The concentration patterns of associated elements are comparable with that of Mn and to some extent with that of Mg. Iron and CaO contents showed very little change down the profile. These patterns suggest that the enrichments of As, Au, Co, Cu, Ni and Zn are significantly controlled by the abundance and scavenging capacity of Mn oxides/oxyhydroxides and/or that the association

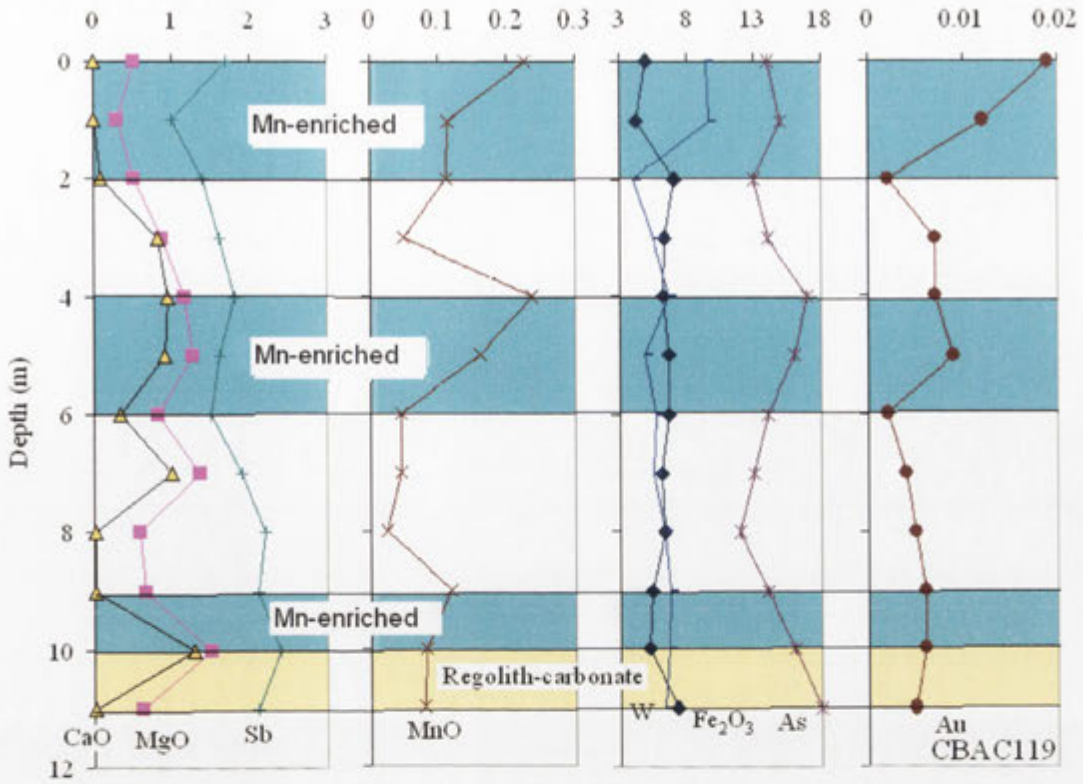

Figure 9.38 Distribution profiles of the trace elements Au, As, W, and Sb (ppm), and major elements Fe_2O_3 total, MnO, MgO and CaO (wt %) in the Mn-enriched horizon of drill hole CBAC119.

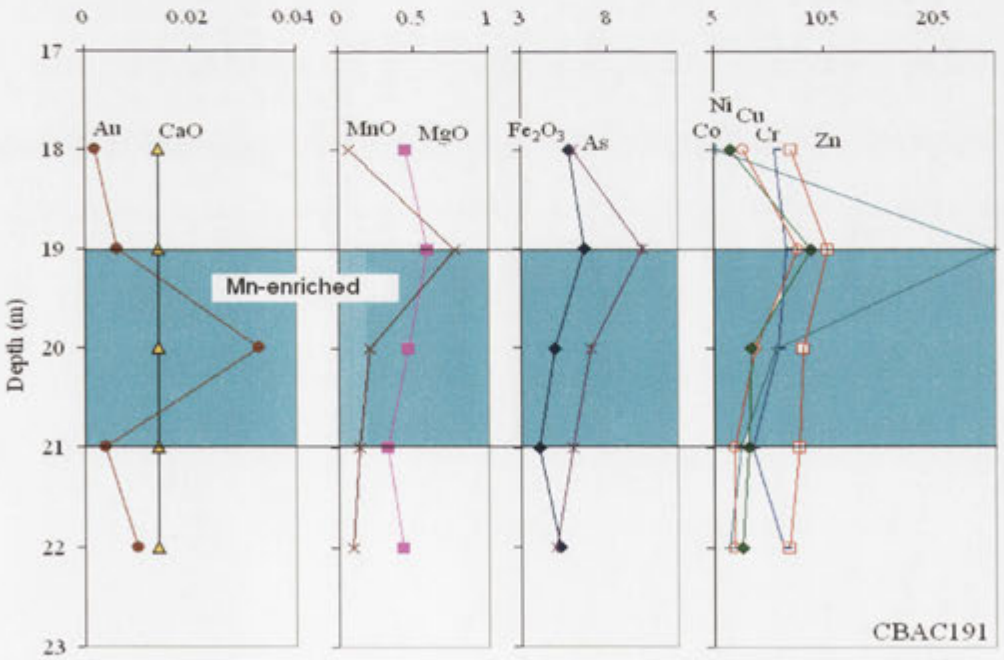

Figure 9.39 Distribution profiles of the trace elements Au, As, Co, Ni, Cu, Cr, and Zn (ppm), and major elements Fe_2O_3 total, MnO, MgO and CaO (wt %) in the Mn-enriched horizon of drill hole CBAC191.

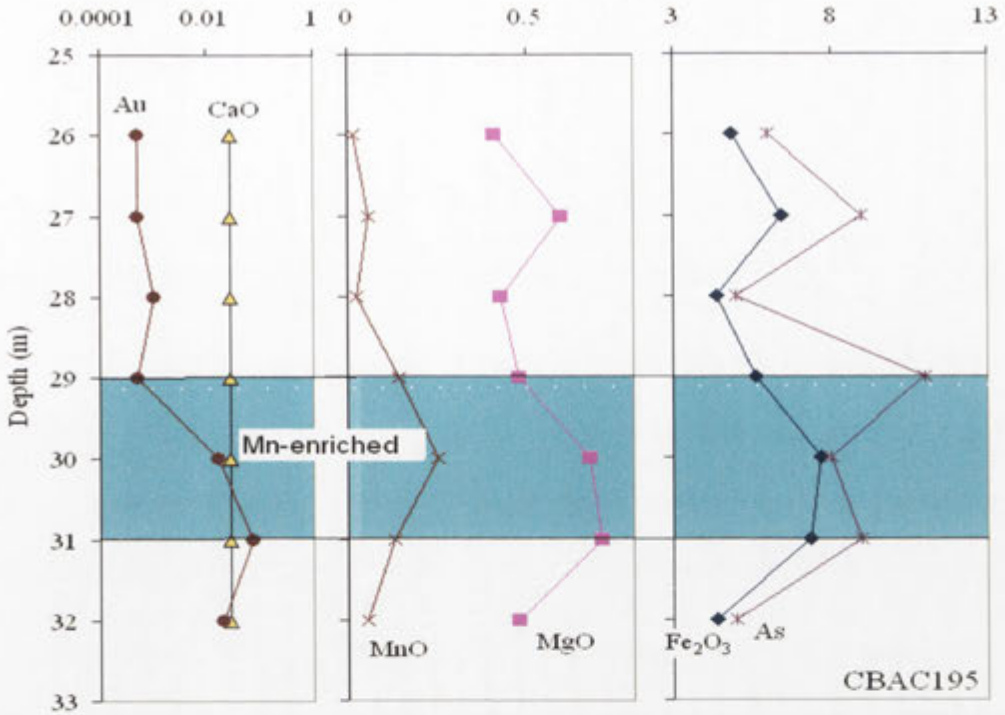

Figure 9.40 Distribution profiles of the trace elements Au and As (ppm), and major elements Fe_2O_3 total, MnO, MgO and CaO (wt %) in the Mn-enriched horizon of drill hole CBAC195.

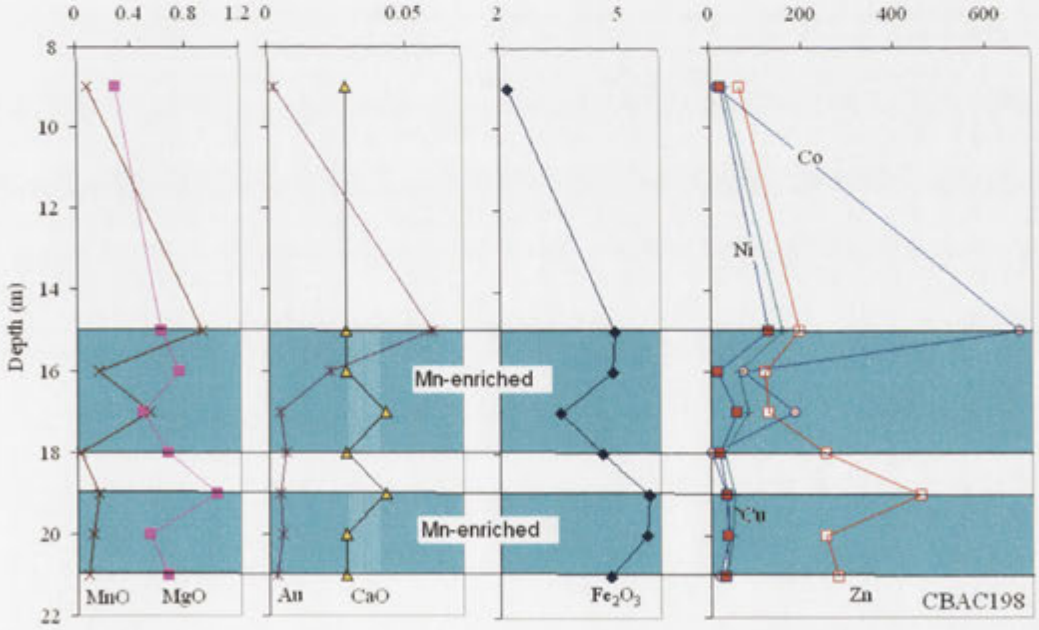

Figure 9.41 Distribution profiles of the trace elements Au, Ni, Cu, Co and Zn (ppm), and major elements Fe_2O_3 total, MnO, MgO and CaO (wt %) in the Mn-enriched horizon of drill hole CBAC198.

reflects the original source rock assemblages. Arsenic is dominantly adsorbed on to manganese- and/or iron- oxides/oxyhydroxides (e.g., Akai et al., 2004) and the internal structure of manganese oxides/oxyhydroxides may control the occurrence of some of these elements. For example, it has been found that uptake of Ag by poorly crystallised Mn oxides depends upon the amount of exchangeable of internal ions such as Na and K (Anderson et al., 1973).

Two Mn horizons were observed in drill hole CBAC211 (Figure 9.43). Distribution patterns of Ni, Cu and Zn significantly coincide with that of Mn. This association is commonly observed in saprolith containing mafic rocks. Elevated Au concentrations are noticed within the upper horizon and at the top of the lower horizon and the distribution pattern of Au particularly in the lower horizon does not match that of Ni, Cu and Zn. This suggests an independent enrichment of Au (probably transported). Iron and Ca show some enrichment in the lower horizon, but the distribution patterns of Fe and Ca are incomparable with the base metals, Au and Mn (Figure 9.43).

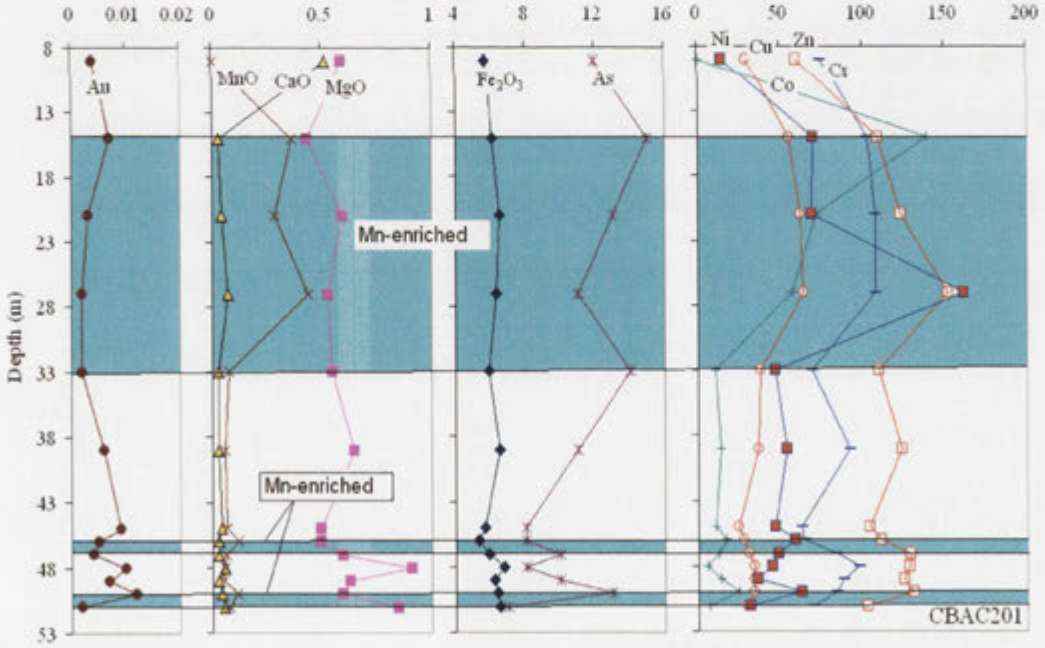

Figure 9.42 Distribution profiles of Au, As, Ni, Cu, Co, Cr and Zn (ppm), and major elements Fe_2O_3 total, MnO, MgO and CaO (wt %) in the Mn-enriched horizon of drill hole CBAC201.

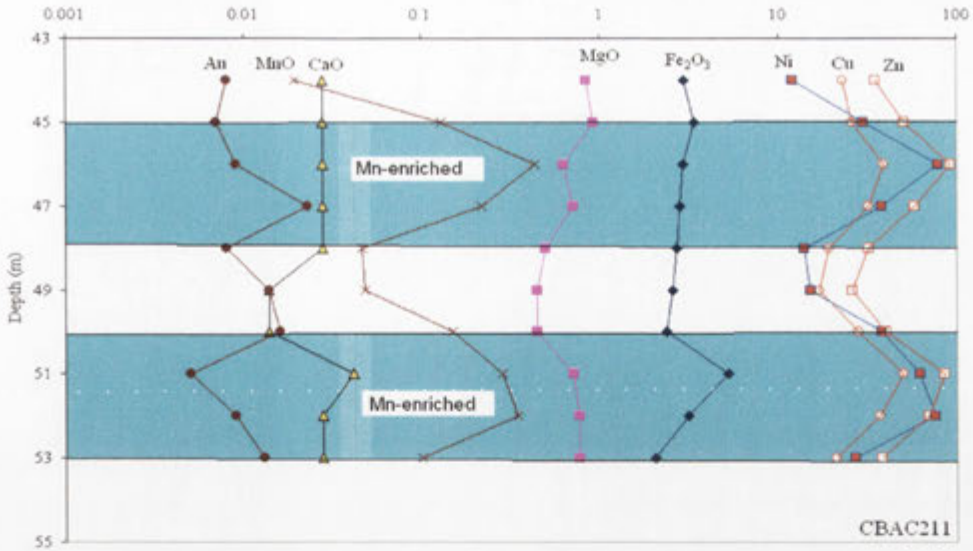

Figure 9.43 Distribution profiles of Au, Ni, Cu, and Zn (ppm), and major elements Fe_2O_3 total, MnO, MgO and CaO (wt %) in the Mn-enriched horizon of drill hole CBAC211.

9.3.5.2 MINOR AND TRACE ELEMENT CHARACTERISTICS

The distribution patterns of trace elements in the Mn-dominant samples showed significant correlation between Mn and Co (r^2=0.65), Cu (r^2=0.76) and Ni (r^2=0.7). A small number of samples show more marked positive correlation trends between these elements and Mn (Figure 9.44). The accumulation of Co in manganese oxides/oxyhydroxides in the soil has been studied extensively (McKenzie, 1975, 1970; Taylor, 1968). Chemical dissolution experiments showed that Co and to a lesser degree Ni are dominated by Mn redox cycling (Taylor et al., 2005). However, a small part of the Ni was reported to be associated with Co and Al in lithiophorite–asbolane mixed layer Mn-oxides (Manceau *et al.*, 2002; Quantin *et al.*, 2002). It has been found that an average of about 80 wt% of the total soil Co and part of the total Ni contents are associated with the manganese oxides. This possibly relates to the high sorptive capacities of manganese oxides, particularly for heavy metals. The adsorption capacities onto MnO_2 at pH 4.0 are 1.4 $mmolg^{-1}$ and 1.0 $mmolg^{-1}$ for Co and Zn respectively (Loganathan and Burau, 1973). Similarly, the adsorption capacity on MnO_2 for Cu at pH 5.0 is 1.8 $mmolg^{-1}$ (McKenzie, 1970). McLaren and Crawford (1973) showed that in a suite of soils the adsorption of copper by soil components followed the order Mn oxides > organic matter > Fe oxides > clay minerals. In synthetic hydrous Mn oxides with adsorbed of Co, Zn, Ca and Na, the Mn was released

to the solution during the adsorption of Co and Zn but not Ca and Na. It was deduced that Co interchanged with surface-bound H^+ and structural Mn^{2+}, and Mn^{3+}, Zn with H^+ and Mn^{2+}, and Ca only with H^+ (Loganathan and Burau, 1973).

Element distribution patterns for the Girilambone samples also show that some Mn enrichment is positively correlated with elevated Ba, Cr, Pb and Zn (Figure 9.44 A, C, E, G). The association of Co, Ba, Pb and Ni with Mn oxides is well documented in the geochemical literature (e.g. Taylor, 1968; Childs, 1975; Golden *et al.*, 1993; White and Dixon, 1996; Zaidelman and Nikiforova, 1998; Vaniman *et al.*, 2002; Neaman *et al.*, 2004). Barium behaviour is generally controlled by the biogenic precipitation and dissolution of barite and to a lesser degree by Mn redox cycling (Schenau, *et al.*, 2001; Cornu *et al.*, 2005; Taylor, *et al.*, 2005).

Observations show that the adsorption capacity of Pb on Mn oxides exceeds that of Fe oxides on a molar basis by approximately an order of magnitude (Dong and Hua, 2001; Dong *et al.*, 2003). Tan *et al.* (2006) showed that Ba, Co, Cu, Ni, Pb and Zn were significantly correlated with MnO_2 in iron-manganese nodules, whereas Cr is only correlated with Fe_2O_3 in the surrounding soil. Negra et al. (2005) studied the relation between Mn oxides and Cr in the soil and they concluded that soils with more total reducible Mn generally demonstrated greater net Cr content. This pattern was moderated by soil pH and relative Mn oxidation state. The greater Mn abundance and greater Mn^{4+}/ Mn^{3+} ratio in soil Mn oxides increase Cr oxidation

In this study a broad correlation between Mn and Cr and the general trends of Cr increasing with Fe_2O_3 content (Figure 9.44 H) probably reflect iron oxide control of Cr distribution. However the positive correlation between of Cr with Mn observed in some Mn-enriched samples (Figure 9.44 C) indicates that the relationship between these two elements is more complex.

The significant positive correlations between elevated Mn values and elevated Co, Ni Cu and Zn strongly suggest that these metals were preferably extracted and accommodated by Mn-oxides/oxyhydroxides. Examples from drill holes CBAC122, CBAC177, CBAC198 and CBAC211 show that the highest Mn value (the peak) coincides with the highest value of these metals (Figure 9.45). These enrichments are

consistent with the concentrations of Pb, Zn, Cu Co and Ni observed in Mn oxides from EDXA spectra (Figures 9.26, 9.28, 9.30, 9.32-33).

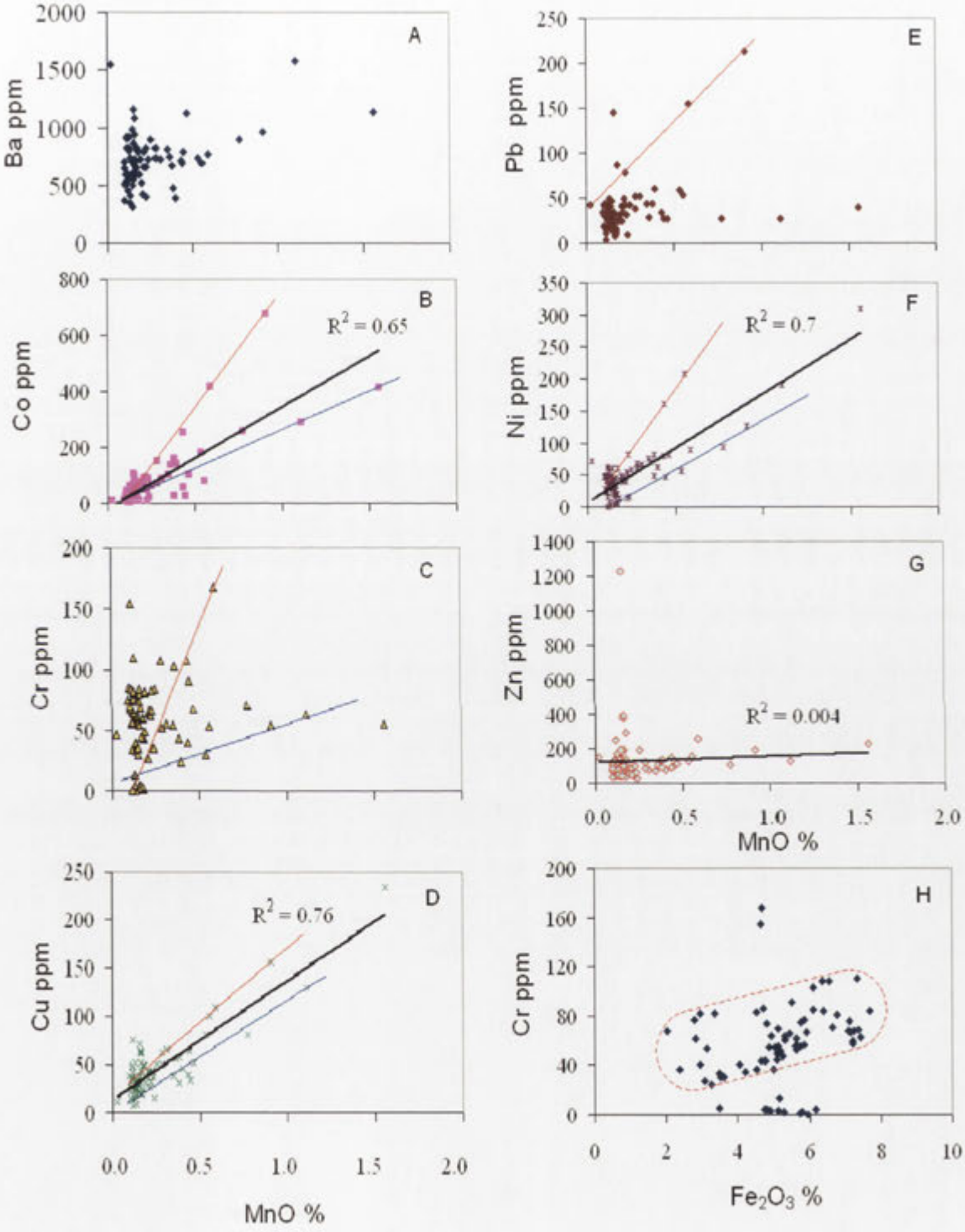

Figure 9.44 Scattergrams showing the correlation between Mn and Ba, Co, Cr, Pb, Ni and Zn (A-G respectively), and the correlation between Fe_2O_3 total and Cr (H) in the Mn-enriched regolith of the Girilambone region. Apparent additional correlations are represented by blue and red lines.

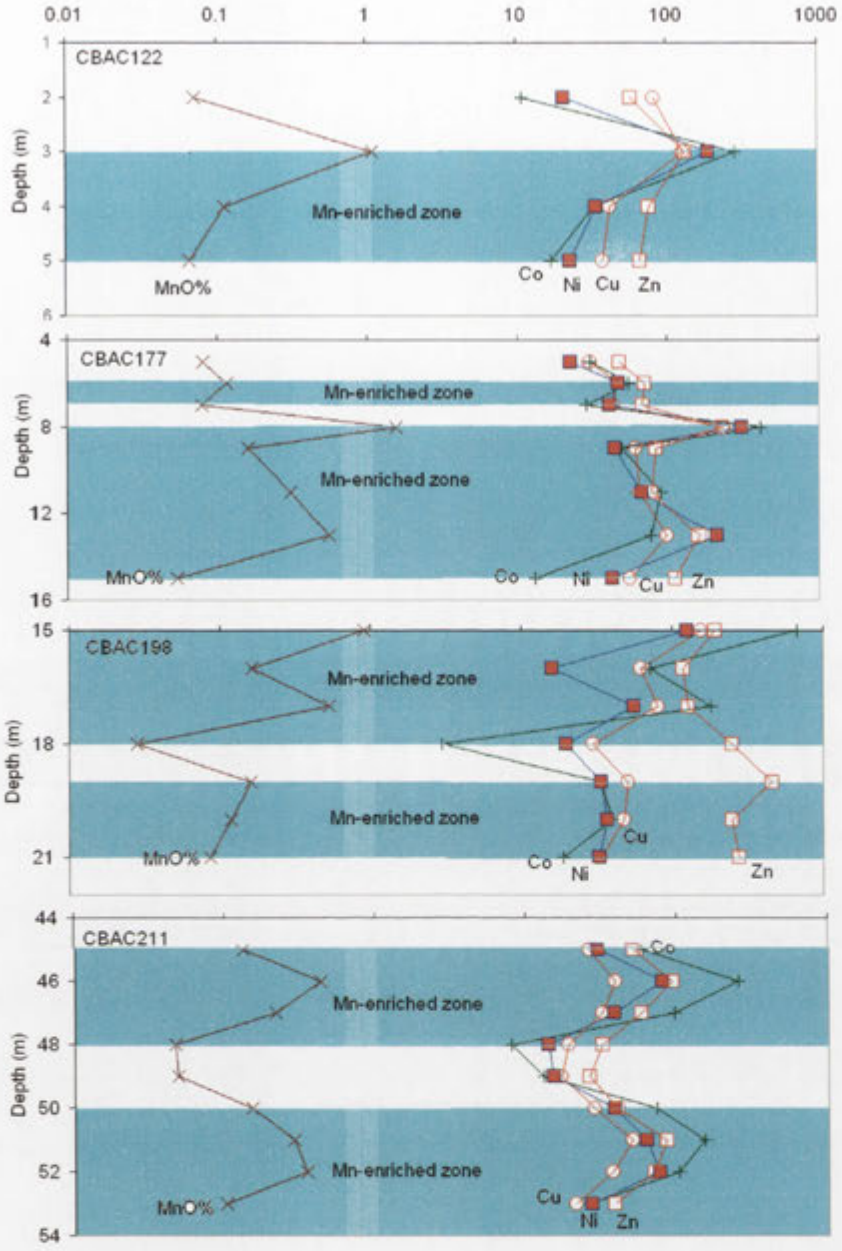

Figure 9.45 Distribution patterns of Mn (wt %) Co, Ni, Cu and Zn (ppm) in the Mn-dominant regolith of drill holes CBAC122, CBAC177, CBAC198, and CBAC211.

9.3.6 GROUNDWATER AND Mn-ENRICHED REGOLITH

Manganese oxides/oxyhydroxides commonly precipitate at the groundwater/regolith interface under suitable Eh-pH conditions. This process involves interaction between the groundwater and surrounding materials causing dissolution of Mn under reducing

precipitation of Mn-enriched materials can accumulate in the oxidised zone of the weathering front due to seasonal changes in groundwater level. The oxidised forms, Mn (III-IV), are present as hydroxides with low solubility (Burns and Burns, 1975; Murrey, 1979). This process is commonly associated with oxidation of Fe (II) to Fe (III), but it has been observed in marine sediments that the typical stratification for Fe (III) extends deeper than Mn (IV). The variation in Mn- and Fe-rich stratifications is related to differences in reaction kinetics and thermodynamics, i.e., slower oxidation rates of Mn^{2+} compared to Fe^{2+} and oxidation of Fe^{2+} by oxidized Mn (Stumm and Morgan, 1981; Lovely and Phillips, 1988) and differences in solubility of the reduced and oxidized forms of Mn and Fe (Froelich *et al.*, 1979; Aller, 1980).

Observations from this study have shown that the groundwater in the Hermidale area (southern part) flows east-northeast (Khider, 2004; Khider and McPhail, 2005; Chapter 7). The spatial distribution of Mn-horizons relative to the current water table shows that these horizons are precipitated in correlative intervals above the groundwater table (Figure 9.46). These Mn-rich zones are probably related to previous water table levels where the manganese oxides were precipitated due to changes in Eh and pH of the groundwater. In the Hermidale area the occurrence of Mn-enriched materials adjacent to the proposed recharge area (CBAC174) is consistent with the important role played by groundwater in concentration of Mn oxides in weathering profiles.

The abundance of MnO decreases along the established groundwater flow direction from 0.179% in CBAC173 to 0.09% in CBAC185 then it increases in CBAC182 to 0.15% (Figure 9.46). The distribution patterns of elements in CBAC 173 show that Mn and Fe are not correlated with Co, Cr, Cu, Ni, Pb and Zn (Figure 9.47), whereas in CBAC181 the distribution pattern of both Fe and Mn are consistent with the patterns of Mg, Co, Cu, Ni and Zn concentration but not Au, Ca and Pb (Figure 9.48), which indicates the influences of Mn and Fe on the dispersion/ fixation of these elements. In CBAC185 the Mn distribution pattern is only comparable with that of Co, except in the Mn-rich horizon where the Co pattern coincides with that of Fe. Iron content is significantly correlated with Mg, Cu, Cr, Ni and Zn contents (Figure 9.49), which possibly indicates that these elements are preferentially co-precipitated or adsorbed on iron oxides/oxyhydroxides. In drill hole CBAC182 only Mn shows significant association with the base metals, suggesting Mn-related accumulation. Magnesium is

association with the base metals, suggesting Mn-related accumulation. Magnesium is significantly enriched at the upper boundary of the Mn-enriched horizon in this drill hole. This enrichment is associated with elevated Co, Cu, Ni, Pb and Zn (Figure 9.50). No Au enrichment was observed in these profiles except in CBAC185, where an elevated value (0.85 ppm) was detected at 51 m depth associated with elevated Fe content (Figure 9.49). Along the groundwater path, element concentrations within the Mn-rich horizon show that the accommodation of the base metals changed from shared (Mn and Fe), to only Fe then to only Mn.

In the Byrock area there is no stratigraphic correlation between the current water table and Mn-rich regolith and this possibly relates to the saturation level of Mn in the groundwater and Eh-pH conditions. This aspect needs further investigation.

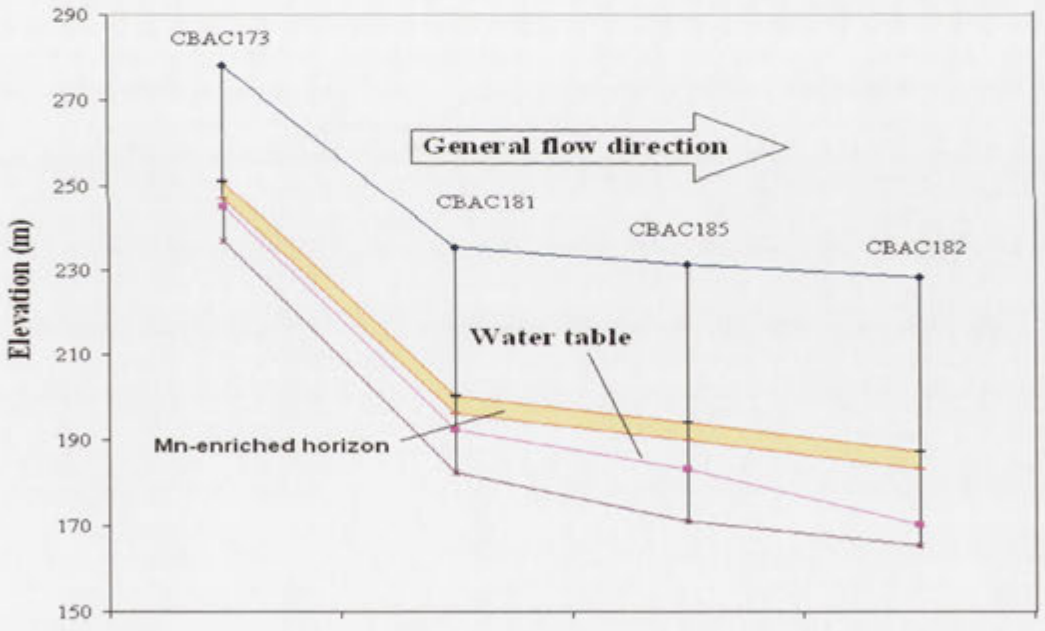

Figure 9.46 A cross section showing the Mn-enriched zone and watertable along the flow path of the groundwater from drill hole CBAC173 to CBAC182 in the southeastern-southern part of the Hermidale area.

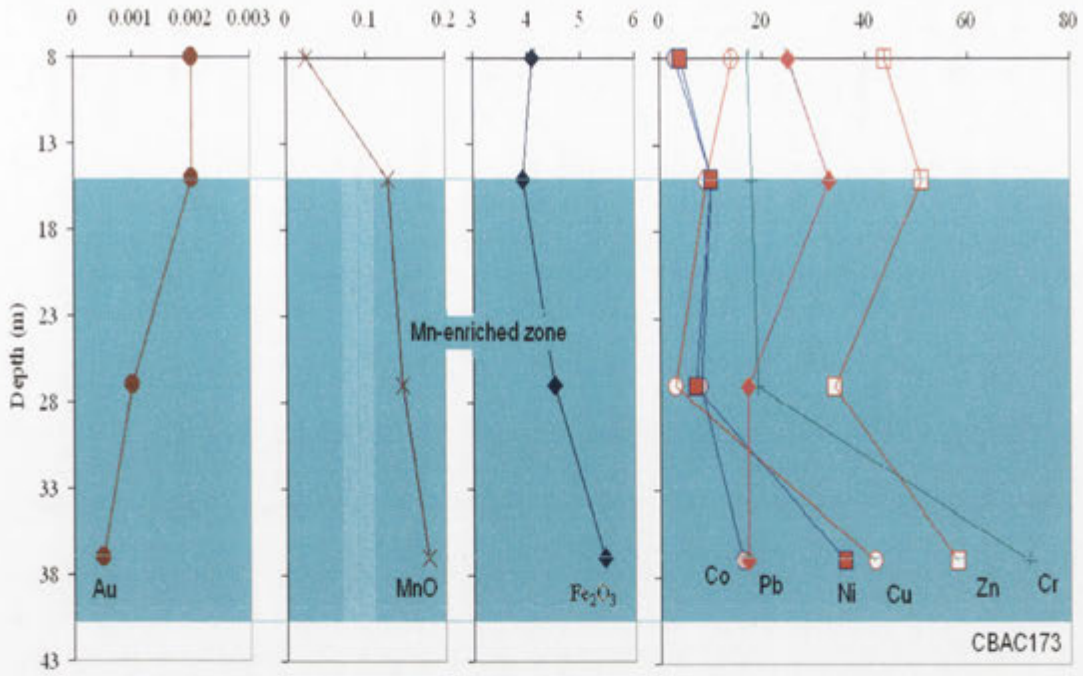

Figure 9.47 Showing the distribution patterns of the trace elements Au, Co, Pb, Ni, Cu, Zn and Cr (ppm) and their relationships with MnO and Fe_2O_3 total (wt %) in the Mn-enriched regolith in drill hole CBAC173.

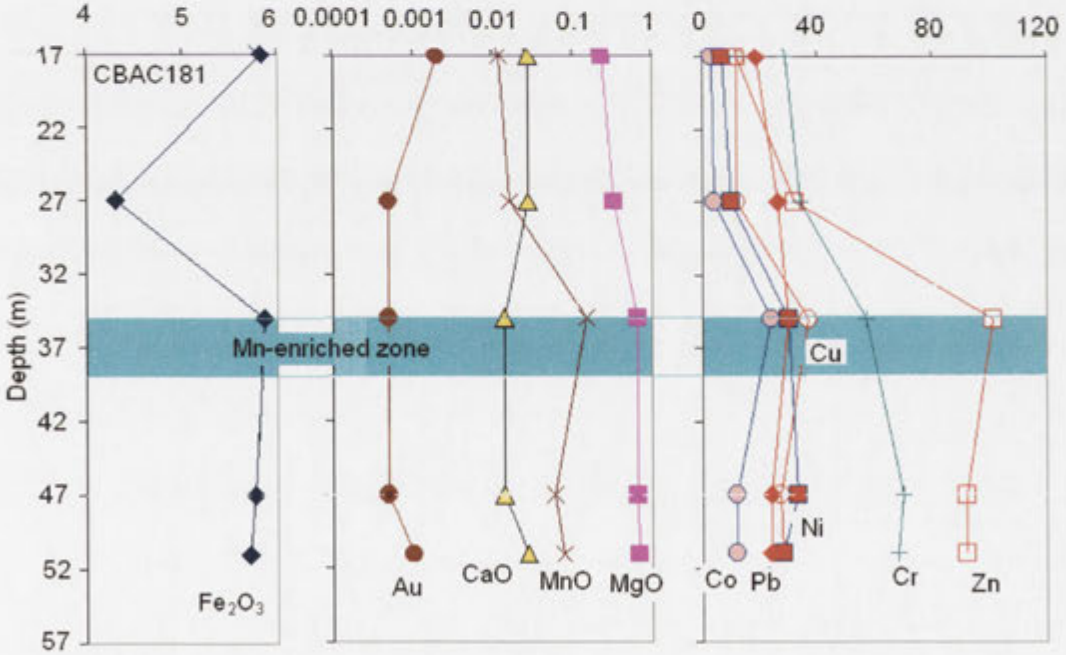

Figure 9.48 Showing the distribution patterns of the trace elements Au, Co, Pb, Ni, Cu, Zn and Cr (ppm) and their relationships with MnO, CaO, MgO and Fe_2O_3 total (wt %) in the Mn-enriched regolith of drill hole CBAC181.

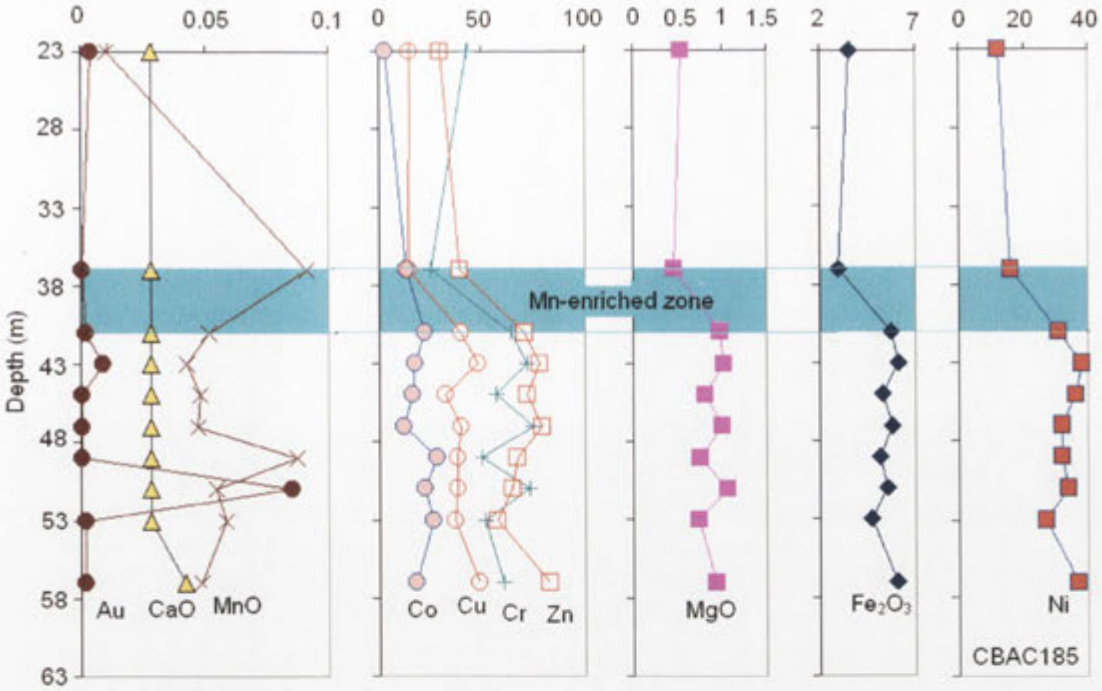

Figure 9.49 Showing the distribution patterns of the trace elements Au, Co, Ni, Cu, Cr and Zn (ppm) and their relationships with MnO, CaO, MgO and Fe_2O_3 total (wt %) in the Mn-enriched regolith of drill hole CBAC185.

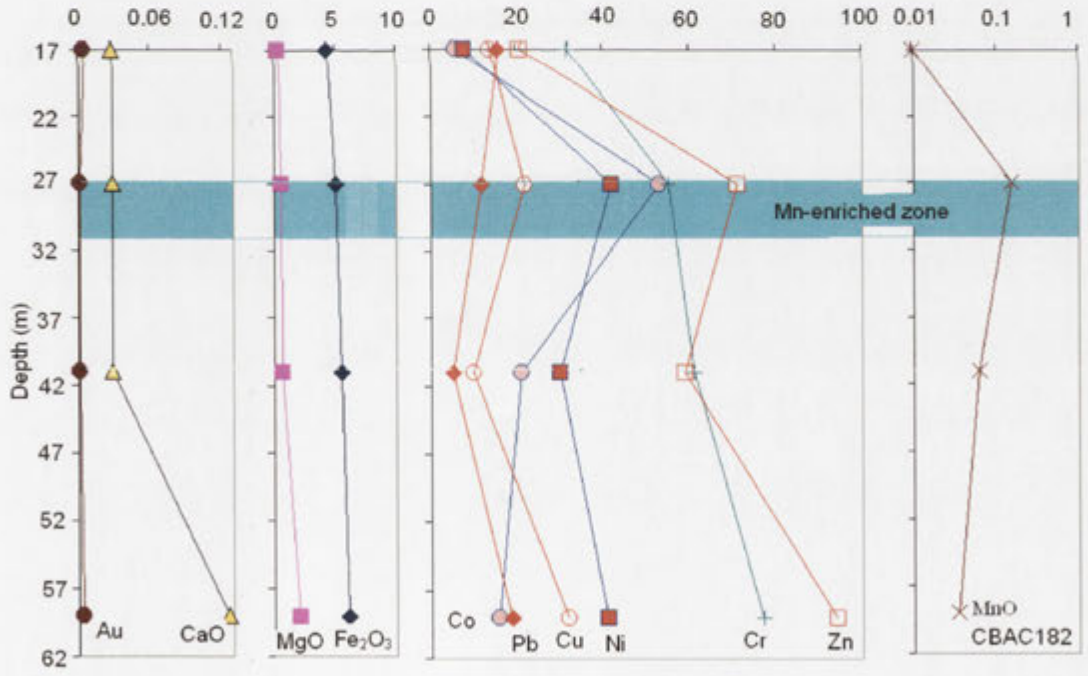

Figure 9.50 Showing the distribution patterns of the trace elements Au, Co, Pb, Cu, Ni, Cr and Zn (ppm) and their relationships with MnO, CaO, MgO and Fe_2O_3 total (wt %) in the Mn-enriched regolith of drill hole CBAC182.

9.3.7 SUMMARY AND CONCLUSIONS

In the Girilambone region Mn-enriched zones show a variable distribution in the regolith. Manganese enrichment is most noticeable in the *in situ* regolith. The highest MnO content is observed in the southwest of the Hermidale area and generally decreases toward the east. Lithiophorite, cryptomelane, pyrolusite and hollandite compositions have been identified by energy dispersive X-ray analysis (EDXA). The Mn-oxides/oxyhydroxides in these zones occur as microcrystalline masses or well-developed platy crystals.

Manganese oxide/oxyhydroxide content is generally correlated with that of Fe, Mg, As, Co, Ni, Cu and Zn. This is particularly the case in mafic rock dominant areas indicating that a mafic element suit released during weathering was accommodated by Mn oxide minerals. Gold enrichment is not associated with this multi-element enrichment nor is it correlated with the overall MnO abundance, which probably indicates its dispersion/fixation is not being controlled by incorporation or adsorption by manganese oxides/oxyhydroxides. The relative spatial distribution of Mn- rich horizons with respect to groundwater level shows stratified concentration of Mn oxides above the present water level along the groundwater flow path, indicating previous water table levels where the manganese oxides were precipitated due to chemical changes.

9.4 ELEMENT ASSOCIATION AND DISPERSION IN Fe-ENRICHED REGOLITH

9.4.1 INTRODUCTION

Iron is considered one of the most important elements in regolith geochemistry, because of its ability to undergo oxidation and reduction (ferric to ferrous), the high capacity for some Fe oxyhydroxides to adsorb large amounts of trace elements across broad pH ranges and its abundance in the crust. Iron oxide-rich zones are common in the regolith of the Girilambone region (Chan *et al.*, 2002; 2004).

Ferruginous regolith has potential as a sampling medium in mineral exploration in many deeply weathered terrains (Anand, 2001) and anomalies of geochemical pathfinders have been reported in ferruginous regolith in Australia (Anand *et al.*, 1993;

Anand, 2001) and around the world (Freyssinet *et al.*, 1989; Costa, 1993; Costa *et al.*, 1999).

In the Girilambone region Fe-enriched regolith (with > 8.5 wt% Fe_2O_3 as total Fe) shows variable distribution (Appendix 7). The greatest Fe enrichment is in the central part of the study area (Sussex area), where Fe is predominantly concentrated in the transported regolith particularly as ferruginous clasts (Figure 9.51). Toward the south (Hermidale area), the number and thickness of Fe-enriched horizons are significantly decreased (Figure 9.52). In the northern part (Byrock area) Fe-enrichment is observed in the *in situ* regolith in the west (where transported cover is thinner) and mainly in transported regolith in the east (Figure 9.53).

9.4.2 IRON OXIDE / OXYHYDROXIDE MINERALS

Iron oxides/oxyhydroxides can be distributed evenly throughout a weathering profile, or preferentially concentrated in particular horizons. Iron is mobile within a weathering profile because of its ease of reduction under anaerobic conditions and its susceptibility to be complexed (Taylor *et al.*, 1983). Iron oxides/oxyhydroxides can exist as concentrations in mottles, cemented aggregates, discrete fine particles and as coatings on grains and crack faces.

The most common soil iron oxides/oxyhydroxides are goethite (α-FeOOH), lepidocrocite (γ-FeOOH), hematite (α-Fe_2O_3), maghemite (γ-Fe_2O_3) ferrihydrite ($HFe_5O_8.4H_2O$) and magnetite (Fe_3O_4). With the exception of magnetite (which generally exists as a residual primary mineral), all are products of pedogenesis and derived either directly from primary sources of iron, or from the transformation of earlier pedogenic forms under new environmental conditions (Taylor *et al.*, 1983). Magnetite can also be oxidized in a solid-state transformation to maghemite; such a transformation is favoured by smaller particle size and a moist environment (Feitknecht, 1965).

As well as pH, Eh and temperature other local environmental variables can influence the precipitation of iron oxides/oxyhydroxides. These include for example, the inhibition of crystallization (eg. the effect of added silicate, phosphate etc.), change in

mineral species and the modification of crystal morphology (Schwertmann and Taylor, 1972; Taylor *et al.*, 1983).

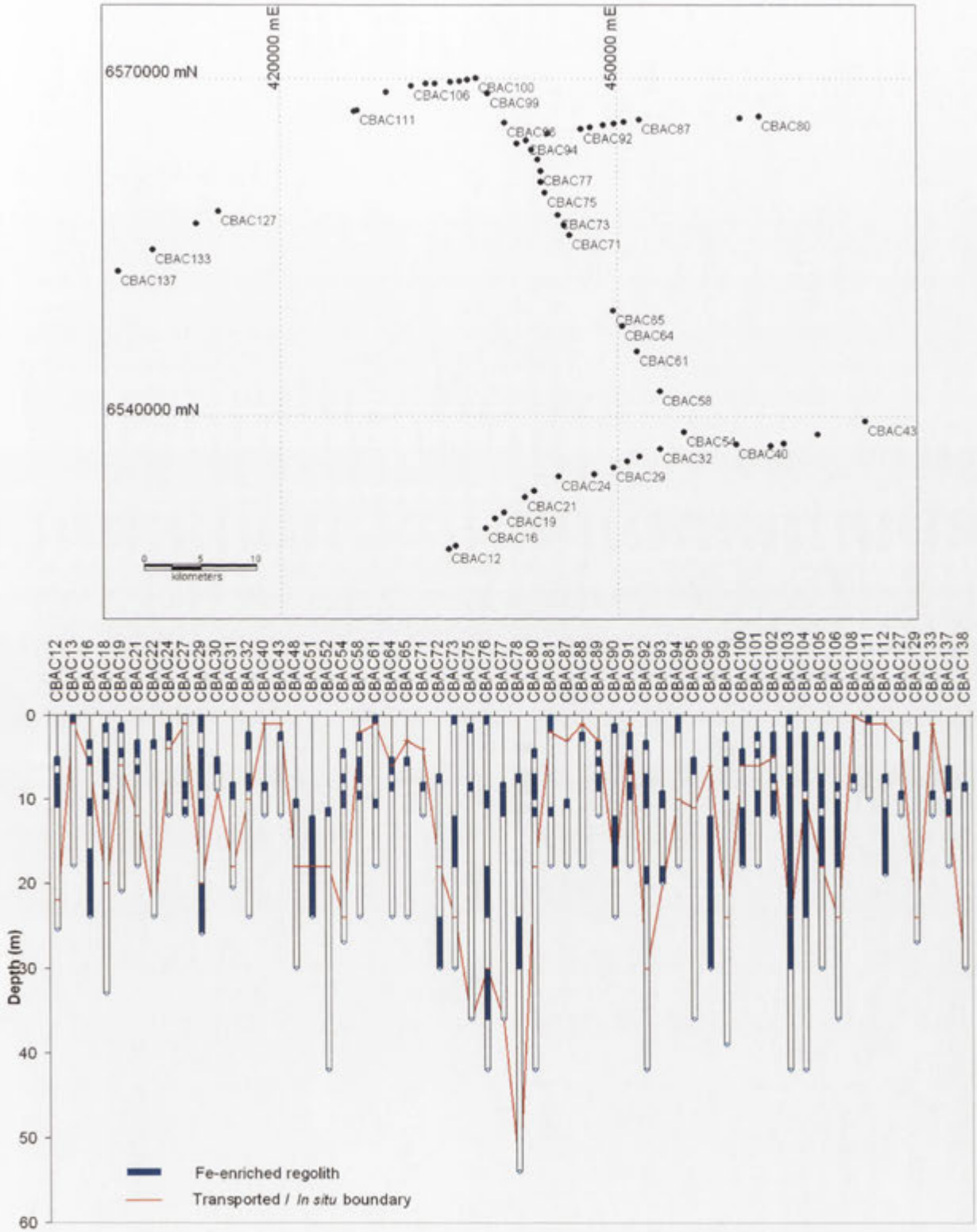

Figure 9.51 Plan showing the location of drill holes with observed Fe-enriched zones in the regolith from the Sussex area and profiles of these holes.

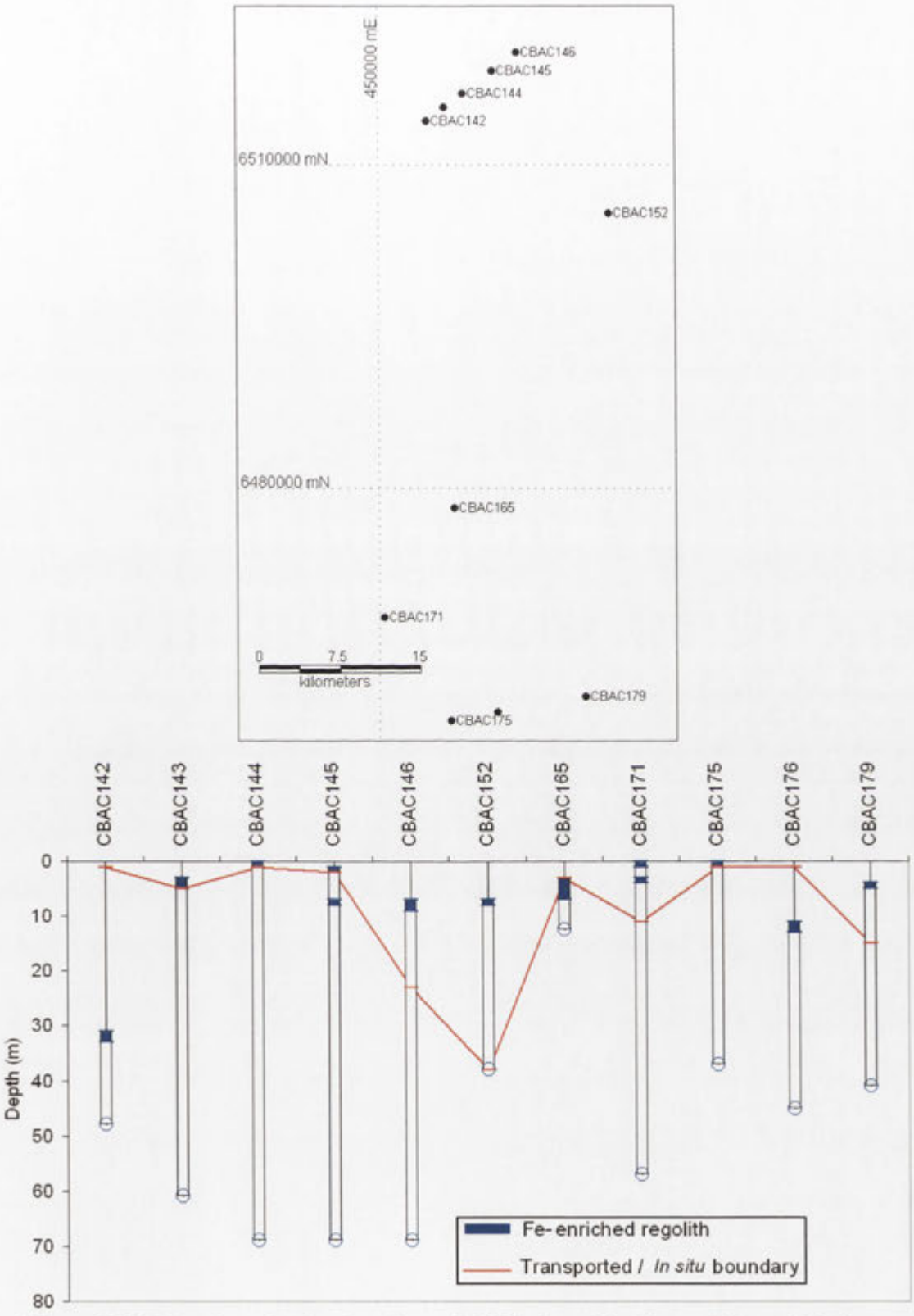

Figure 9.52 Plan showing the location of drill holes with observed Fe-enriched zones in the regolith from the Hermidale area and profiles of these holes.

.

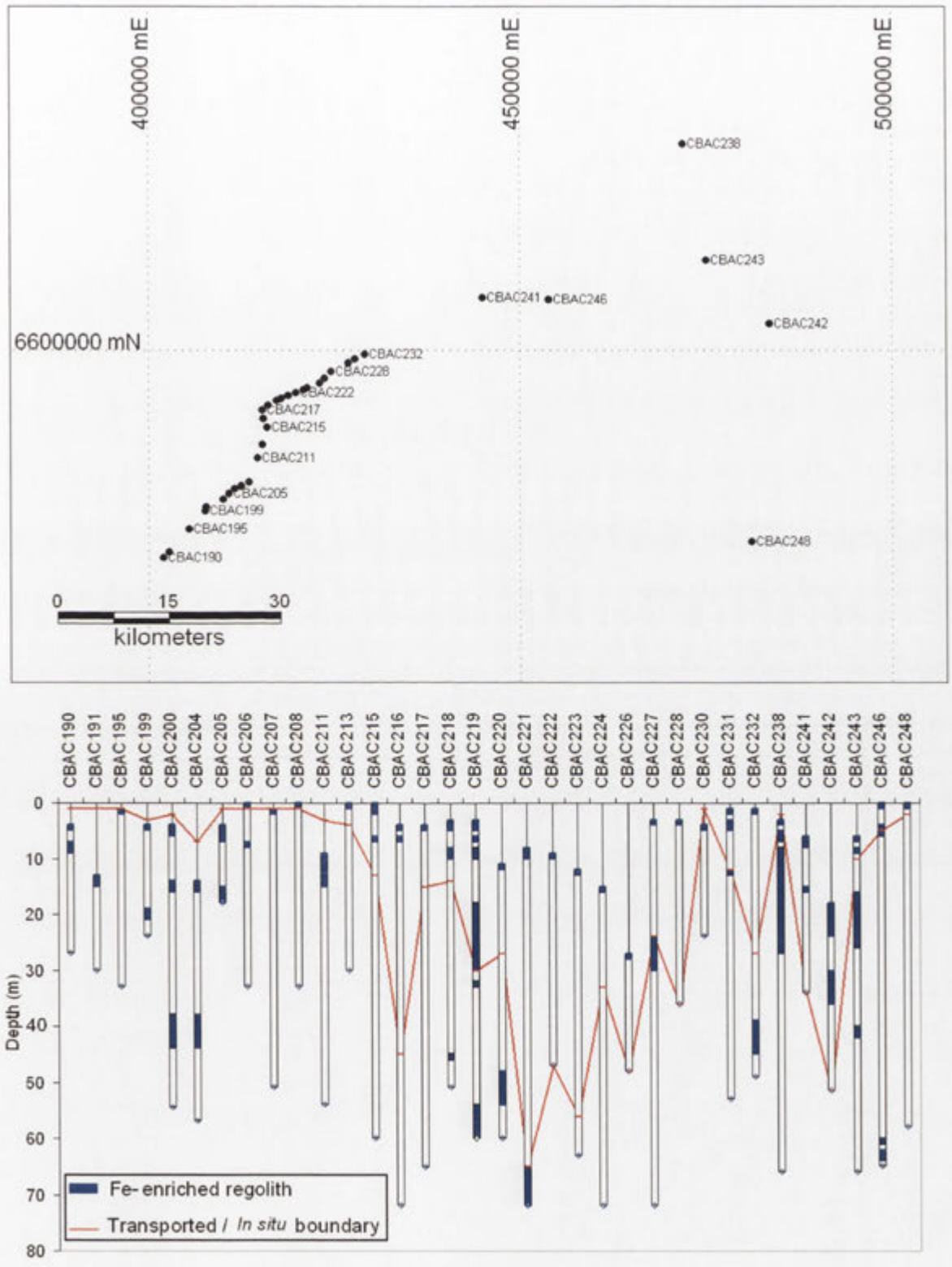

Figure 9.53 Plan showing the location of drill holes with observed Fe-enriched zones in the regolith from the Byrock area and profiles of these holes.

.

In this study hematite, goethite and maghemite were identified by X-ray diffraction in the Fe-enriched horizons. Some of these horizons (i.e. in drill holes CBAC215, CBAC243 and CBAC246) are characterised by the presence of only goethite, whereas in others (i.e. CBAC103 and CBAC224) hematite is the dominant iron oxide mineral. Maghemite is less abundant and it is only observed in a few Fe-enriched horizons (Appendix 4).

9.4.3 TRACE ELEMENT CHARACTERISTICS OF Fe-ENRICHED REGOLITH

Some *in situ* regolith samples shows apparent correlations between Fe, As and Cu contents (Figure 9.54 B, F). In the Fe-enriched transported regolith there is not a strong correlation between the content of total Fe_2O_3 and the trace elements except for As and Cr (Figure 9.54).

9.4.3.1 GOLD IN Fe-ENRICHED REGOLITH

Gold shows significant concentration in some of the Fe-rich horizons. However, there is no direct correlation between Au and Fe content (Figure 9.54 A). Enrichments of Au (> 0.009 ppm) were detected in samples from drill holes CBAC32, CBAC81, CBAC103, CBAC143, CBAC204 and CBAC219. Some of these drill holes (i.e. CBAC 103, CBAC204 and CBAC219) are selected to display the relationship between Au and Fe distribution in the regolith profile.

In drill hole CBAC103 there are three Fe-enriched horizons. The lower horizon extends across the T/I boundary. There are two levels of Au enrichment 0.026 ppm and 0.018 ppm recognised in the transported regolith at 7-8 m and 18-24 m depth respectively (Figure 9.55, Appendix 7). The upper Au enrichment zone is associated with significant enrichment in Fe and As. The drill hole log and field observations indicate a marked increase in ferruginous magnetic gravel and granules at this level. Mineralogical analysis shows high hematite content (21 wt%) with some goethite (1.2 wt%) and maghemite (4.4 wt%) at this level (Appendix 4). This possibly explains the enrichment of Au at this level as a result of mechanical accumulation of Au-bearing ferruginous sediments.

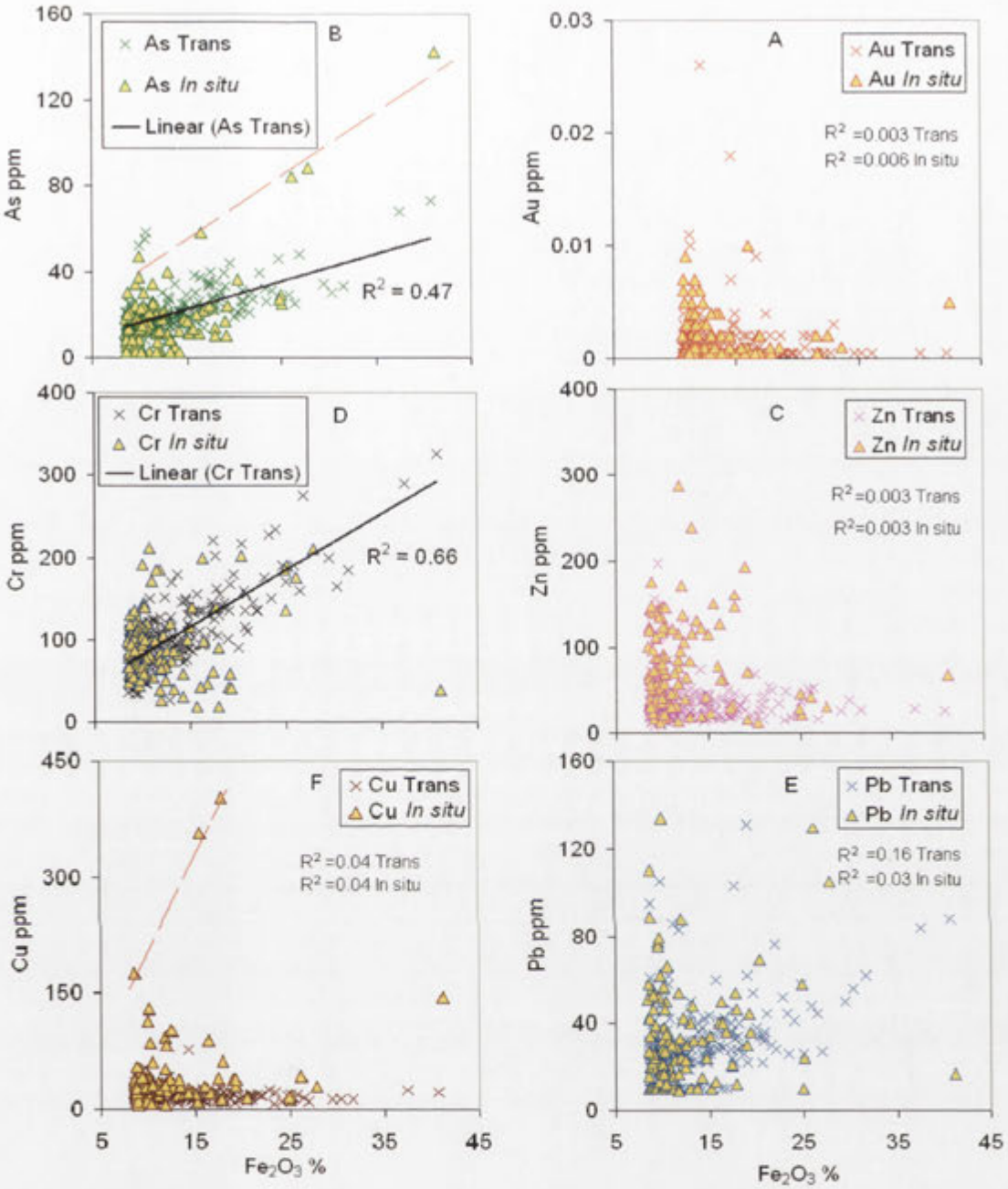

Figure 9.54 Scattergrams of trace elements in the Fe-enriched regolith of the Girilambone region. Fe_2O_3 % vs. Au (A), As (B), Zn (C), Cr (D), Pb (E) and Cu (F). Dashed lines represent apparent additional correlations.

In the lower Au-enriched horizon, Au content generally increases with that of Fe and As, but is also significantly correlated with Mn content (Figure 9.55). The mineralogical analysis shows a lack of well crystalline iron oxide minerals (Appendix 4), which possibly indicates occurrences of Fe within the amorphous and /or clay materials. The relationship between Au and Mn in Fe-rich zones needs further investigation, including detailed microanalysis of components.

In CBAC204 the Fe–enriched zone consists of pink saprolite. The identified iron-oxide/oxyhydroxide minerals in this zone are goethite (8.6 wt%) and hematite (1.2 wt%; Appendix 7). Iron is associated with As and Au and the highest Au value coincides with highest As and Fe contents (Figure 9.56). A positive correlation between Au enrichment and Fe_2O_3 abundance possibly indicates adsorption of Au and As onto Fe oxides/oxyhydroxides during chemical weathering of Au-rich materials.

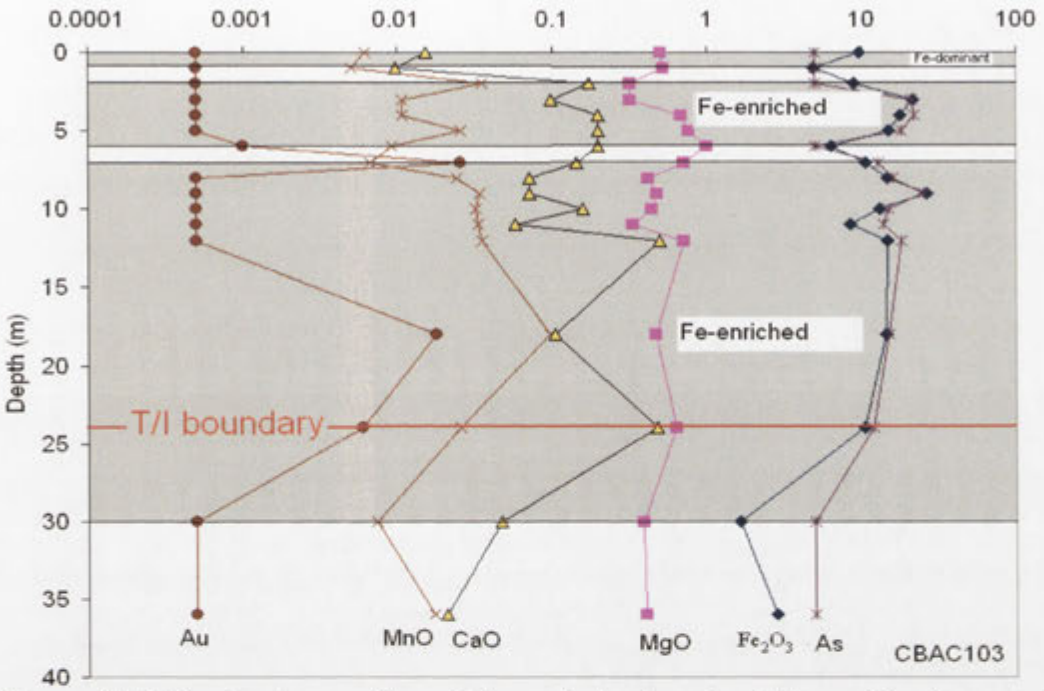

Figure 9.55 Distribution profiles of Au and As (ppm) and the major elements Fe_2O_3 (total), MnO, CaO and MgO (wt%) in the Fe-enriched horizons of drill hole CBAC103.

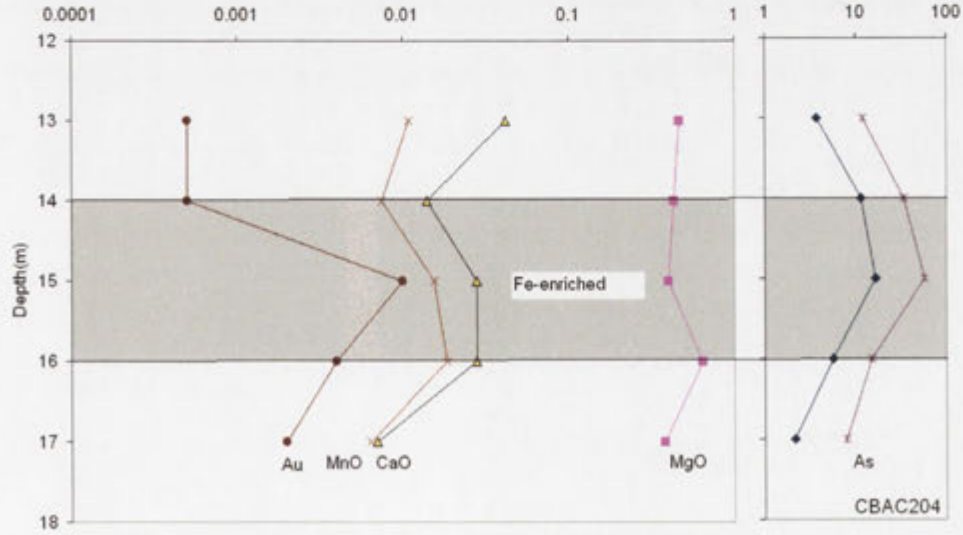

Figure 9.56 Distribution profiles of Au and As (ppm) and the major elements Fe_2O_3 total, MnO, CaO and MgO (wt%) in the Fe-enriched horizons of drill hole CBAC204.

9.4.3.2 ZINC, COPPER AND LEAD ASSOCIATED WITH Fe OXIDES/ OXYHYDROXIDES

Because of the economic significance of gossans, there have been many studies, which have shown a strong correlation between Cu and Fe content of weathered rocks (see Taylor and Eggleton, 2001). Eh, pH and CO_2 (g) pressure are important factors in controlling the Cu-Fe relationship (e.g. Thornber, 1985; Mosser and Zeegers, 1988). In a similar context a comparative study of iron oxides (Rose and Bianchi-Mosquera, 1993) showed that under neutral conditions (pH=7) goethite adsorbed all the available metal, whereas hematite preferentially adsorbed all the Pb, Zn, Co and Ni with only 70 % of Cu and Ag.

In the Girilambone region there is significant correlation between elevated Fe values and high concentration of Cu, Zn and Pb. Distribution patterns in the regolith profiles strongly suggests that these metals were preferably adsorbed or accommodated by Fe-oxides/ oxyhydroxides. In drill holes CBAC27 and CBAC246 there is a comparable relationship between Fe and Zn content within and above the Fe-enriched horizons (Figures 9.57-58). In CBAC27, XRD analysis shows 11.2 wt% of goethite in the upper horizon (9-19 m depth) and 17.9 wt% goethite with 0.3 wt% hematite in the lower horizon (Appendix 4). Similarly, two Fe-enriched horizons with elevated Zn and Cu concentrations occur in drill hole CBAC 246 with 0.7 wt% and 6.7wt% of goethite (the only detected iron oxide mineral) in the upper and the lower horizons respectively (Figure 9.58, Appendix 4)). Petrographic and field observation show the Fe-enriched zone consists of finely laminated siltstone with ferruginous rock chips in CBAC27 and granitic saprolite with schistose-like texture and ferruginous induration in CBAC 246 (Chan *et al.*, 2001; 2004).

The significant correlation between Fe and Zn content and distribution of ferruginous weathered bedrock suggest that the Fe-Zn association reflects an original bedrock association in CBAC27 and /or the mobilised Zn during the weathering of the bedrock accompanied afterward with Fe in goethite.

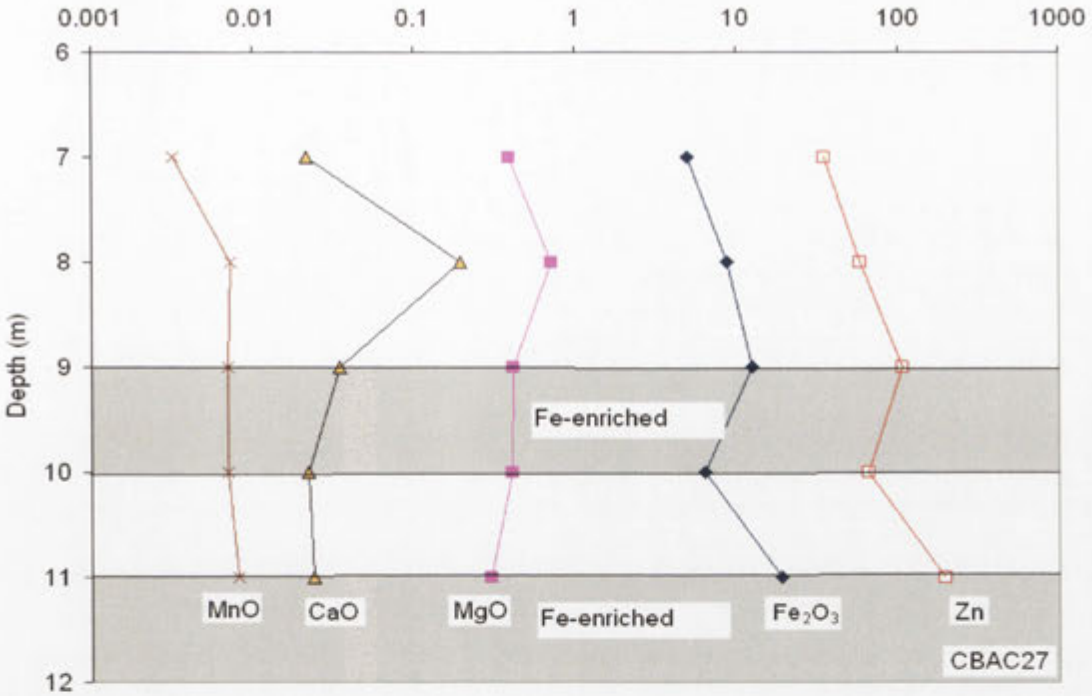

Figure 9.57 Distribution profiles of Zn (ppm) and the major elements Fe_2O_3 (total), MnO, CaO and MgO (wt %) in the Fe- enriched horizons of drill hole CBAC27.

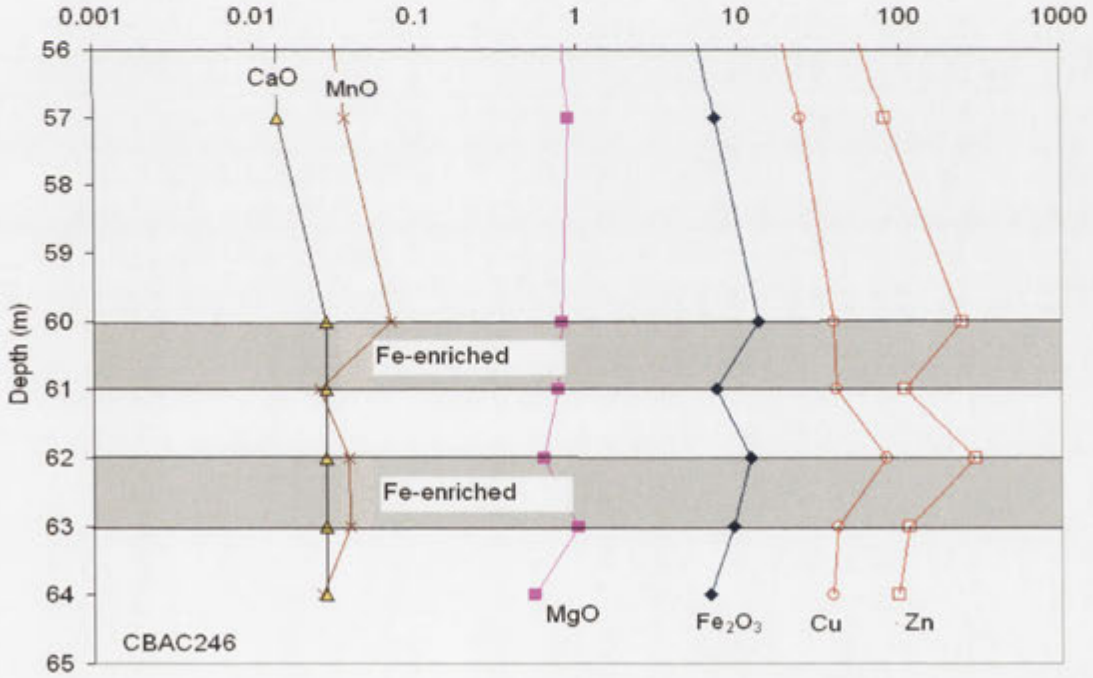

Figure 9.58 Distribution profiles of Zn and Cu (ppm) and the major elements Fe_2O_3 (total), MnO, CaO and MgO (wt%) in the Fe- enriched horizons of drill hole CBAC246.

In CBAC243 the elevated Zn and Cu values are also significantly correlated with Fe in the Fe-enriched zone, coinciding with the highest Fe content (Figure 9.59). The predominant iron mineral in this zone is goethite, which ranges between 9.1 wt% in the base of the zone (25 m) to 42.4wt % at 23-21 m depth (Appendix 4). This Fe-enriched zone is developed on mafic and altered magnetic sedimentary rocks with Fe staining and ferruginous indurations. This is again another original bedrock (mafic rock) association between Fe, Zn and Cu preserved within goethite.

Elevated Cu values (357-403 ppm) occur in the Fe-enriched zone of drill hole CBAC200 (4-6m), where the distribution pattern of Fe is significantly correlated with that of Cu (Figure 9.60). The mineralogy of the Fe-enriched horizon is characterised by 4.3 wt% of hematite and 2.7 wt% of goethite (Appendix 4). This correlation extends down the first ten meters of this drill hole regardless of regolith type. The carbonate-rich regolith zones that are interbedded with the Fe-enriched zone also show a comparable Fe-Cu association, which possibly indicates that the distribution of these elements is not affected by the development of the calcrete or pH conditions (alkaline or non-alkaline) during the weathering process. In other words, the Fe-Cu association possibly represents a bedrock association and the enrichment of these elements is significantly related to increased abundance of ferruginous clasts.

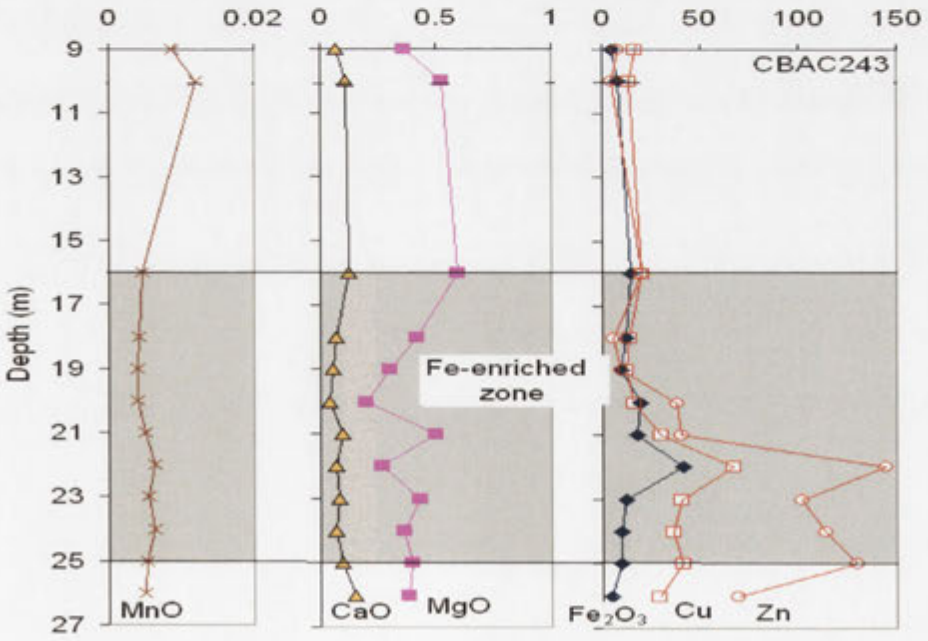

Figure 9.59 Distribution profiles of Zn and Cu (ppm) and the major elements Fe_2O_3 (total), MnO, CaO and MgO (wt%) in the Fe-enriched horizons of drill hole CBAC243.

The correlation between Fe, Zn and Cu contents has also been reported in other regolith studies in the western New South Wales and Western Australia. This correlation has been related to hosting of Zn and Cu by iron oxide/oxyhydroxide minerals (i.e., hematite, goethite, Lintern and Scott, 1990; Brand and Butt, 2001). Alipour et al. (1995) noticed a significant relationship between Fe and Cu in ferrolithic lag that was derived from an original Fe-rich lithology near Cobar.

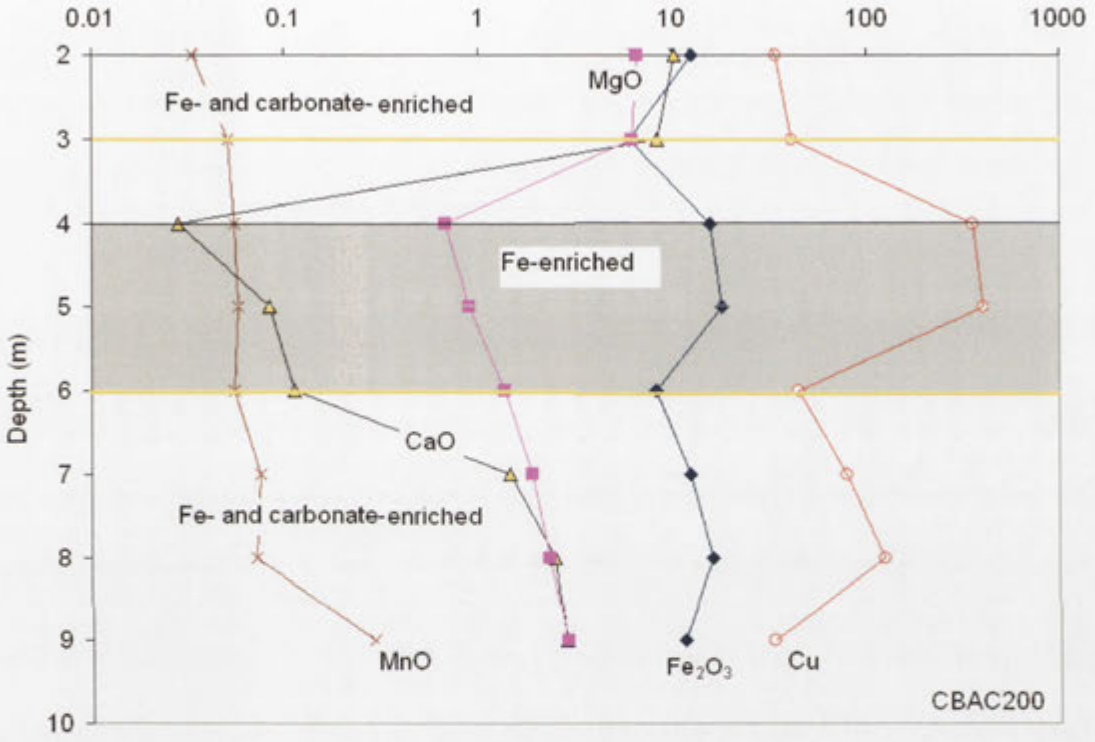

Figure 9.60 Distribution profiles of Cu (ppm) and the major elements Fe_2O_3 (total), MnO, CaO and MgO (wt%) in the Fe- enriched horizons of drill hole CBAC200.

In CBAC205 the Fe-enriched regolith consists of pink saprolite claystone ane meta-shale and phyllite (Chan *et al.*, 2004). The distribution patterns of elements show that the Pb contents follow those of Fe. The highest Pb value was observed in the lower Fe-enriched horizon (15-18 m). This enrichment is associated with increasing Fe and Mn content (Figure 9.61). XRD analysis shows that the only detected iron oxide mineral in this horizon is goethite (1.9 wt%, Appendix 4). Elevated Pb is also observed within the Fe-enriched horizons of drill hole CBAC218 and CBAC224. In CBAC 218 the elevated Pb is associated with elevated Zn, Cu, Fe and Mn (Figure 9.73) in the transported regolith, which is rich in sand and gravel. XRD analysis shows 3.6 wt % of hematite

and 0.6 wt% of goethite (Appendix 4). Similarly in CBAC224 the Fe-enriched horizon (15-16 m) was observed in a succession of transported sand, silt and gravel where Pb and Zn concentrations show comparable patterns to Fe and Mn (Figure 9.63). This horizon includes the highest Pb value (103 ppm) with 3.6 wt% of hematite and 3.3wt % of goethite (Appendix 4). There are mafic rocks recorded in these drill holes (Chan *et al.*, 2002) and the high concentrations and association of Fe, Zn and Cu may have been inherited from these mafic parent rocks. However, occurrences of pink to red coloured claystone indicate the presence of iron oxide minerals (possibly hematite) in association with clay material. These iron oxides also have the potential to accommodate some of the mobilised Pb, Zn and Cu during weathering. The relative enrichment in hematite in these drill holes possibly explains the increased Pb concentration due to its preferential adsorption by hematite. Other observations from the Cobar region have shown that hematite generally has higher Pb but lower Cu and Zn content than goethite (i.e., Scott, 1992).

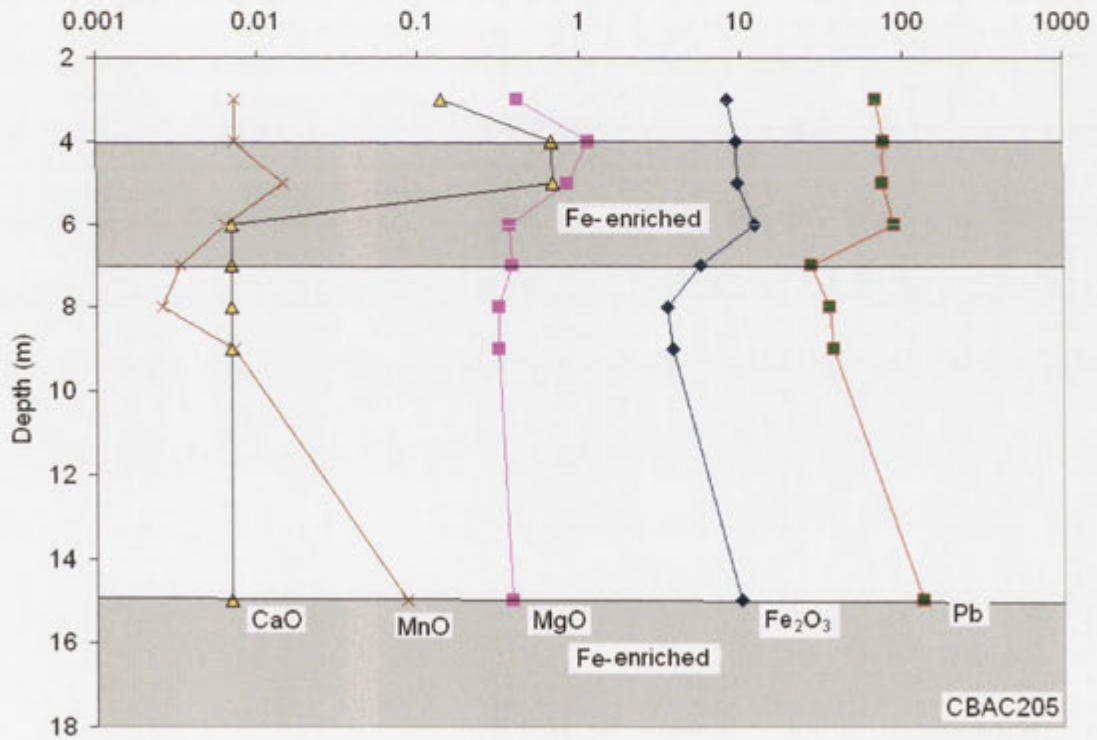

Figure 9.61 Distribution profiles of Pb (ppm) and the major elements Fe_2O_3 (total), MnO, CaO and MgO (wt %) in the Fe-enriched horizons of drill hole CBAC205.

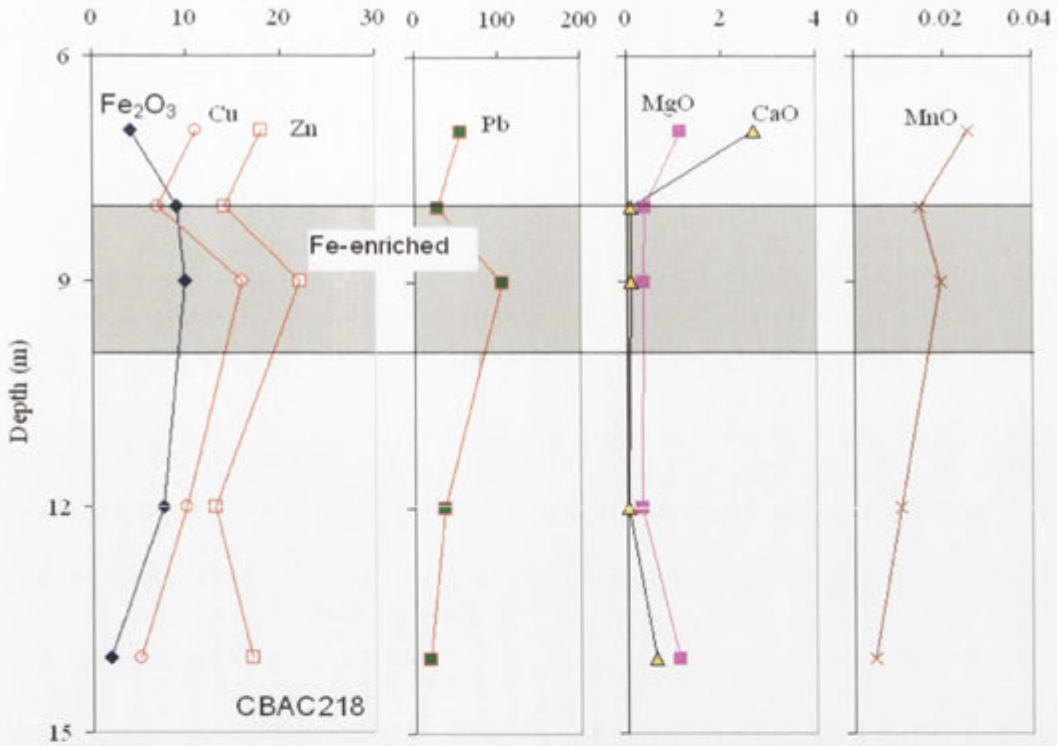

Figure 9.62 Distribution profiles of Pb, Cu and Zn (ppm) and the major elements Fe_2O_3 (total), MnO, CaO and MgO (wt%) in the Fe-enriched horizons of drill hole CBAC218.

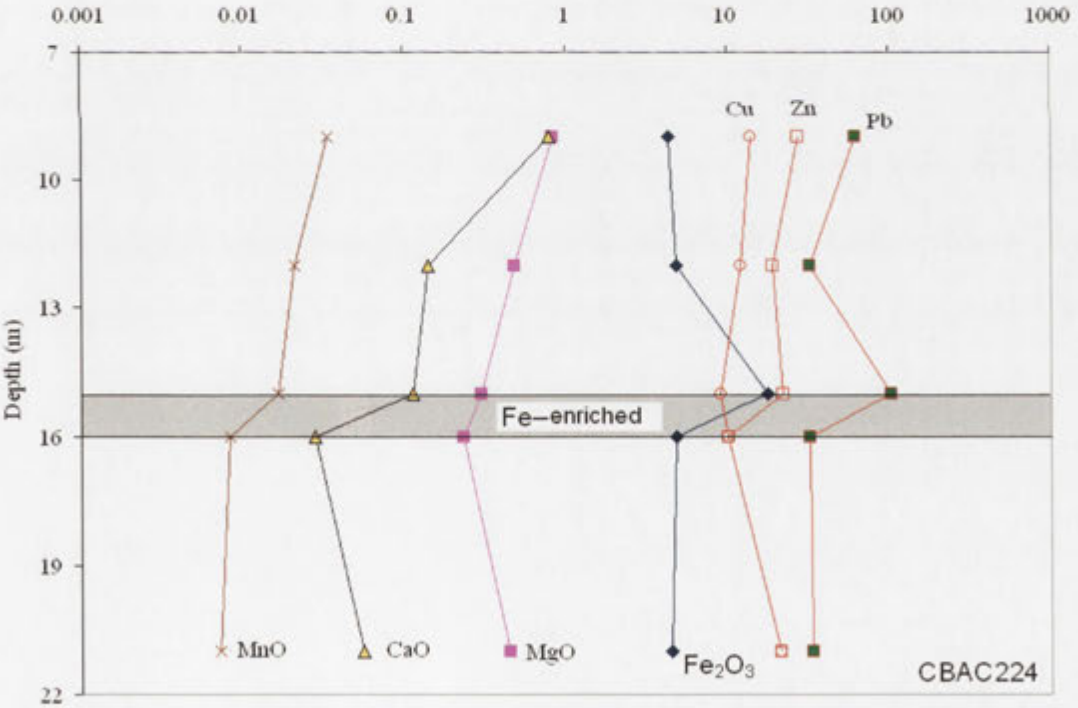

Figure 9.63 Distribution profiles of Pb, Cu and Zn (ppm) and the major elements Fe_2O_3 (total), MnO, CaO and MgO (wt%) in the Fe-enriched horizons of drill hole CBAC224.

9.4.4 SUMMARY AND CONCLUSIONS

Iron-enriched zones are unevenly distributed in the regolith profiles of the Girilambone region. Iron- enrichment predominantly occurs in the central part of the study area (Sussex area) where Fe is concentrated in the transported regolith. This significantly decreases towards the south (Hermidale area). In the northern Byrock area, Fe-enrichment is observed in the in-situ regolith in the west generally in the transported regolith in the east.

Some enrichment of Au and As is associated with the increased abundance of ferruginous magnetic gravels in the Fe-enriched zone, which possibly indicates a mechanical dispersion of remnant primary Au in ferruginous regolith.

Higher contents of Fe, Zn and Cu occur in areas where there are weathered mafic rocks. There is generally not a strong correlation between hematite or goethite content and concentration of Au, As, Zn, Cu and Pb in the Fe-enriched zones. This suggests that for these background sites the known propensity for iron oxides/oxyhydroxides to take up these elements is not strongly expressed, probably because of the low abundances of the trace elements.

10. CHAPTER TEN: CONCLUSIONS AND RECOMMENDATIONS

This study has used a combination of geochemical analysis of the regolith materials and groundwater in the Girilambone region and made the following key findings:

- Threshold and anomaly values for target and pathfinder elements vary in different regolith materials and facies. The spatial distribution of anomalous values in the top metre, transported and *in situ* regolith have been identified.
- Multivariate cluster analysis and principal component analysis can be used to identify major element associations in the regolith. Four major element associations have been identified in the Girilambone regolith using these methods.
- Groundwater can be used to vector toward potential mineralisation and ^{36}Cl isotope data can be used to identify the possible age of groundwater.
- Key geochemical signatures can be used to discriminate the main bedrock units (i.e., Girilambone Group and Cobar Supergroup) through the overlying saprolith. The A-CN-K diagram can be used to determine the likely original source composition, weathering and metasomatism trends of the saprolith materials;
- Secondary enrichments of calcrete, manganese and iron oxides significantly control the target and pathfinder elements dispersions in the regolith.
- The highest Au contents in the regolith carbonate zone are not necessarily associated with the position of maximum calcrete development and Au enrichment has occurred at the top of the calcrete zone;
- The stratified occurrence of Mn in the *in situ* regolith is due to precipitation of Mn along previous water table levels. There is a significant correlation between Mn oxides/oxyhydroxides and As, Co, Ni, Cu and Zn in these Mn-enriched zones;
- There are significant concentrations of Au in some Fe-enriched horizons, although there is no direct correlation between Au and Fe content; and
- There are significant correlations between Fe and elevated Zn and Cu in areas where there are mafic rocks.

10.1 ANOMALY, BACKGROUND AND ELEMENT ASSOCIATIONS

The threshold values of target and pathfinder elements are calculated in the clay-silt-gravel facies, regolith carbonate facies, Fe-dominant facies and Mn-dominant facies of the top meter, transported and *in situ* regolith material using Boxplot and MAD methods. The boxplot method is more efficient in separating anomalies from the background "noise" in the regolith. Potential mineralisation in the northeast of the central part of the region (Sussex area) was identified based on anomalous enrichments of Au, Cu, Zn and to some extent Pb along the regolith profile from drill hole CBAC119 to CBAC125. High threshold values for As, Cr and V are observed in the Fe-enriched facies where weathered mafic rocks are present. These elements are accommodated by the secondary Fe oxide/oxyhydroxide minerals (hematite and goethite). Establishing appropriate threshold values will greatly assist future mineral exploration in the Girilambone region.

Four major element associations are identified by cluster analysis. These are element suites associated with Ca and Mg (carbonate group), with MnO (Mn-oxide/ oxyhydroxide), with Fe_2O_3 (iron oxide/oxyhydroxide) and with mafic rock (Ni and Cr). Principal component analysis indicates similar groups, representing calcretization (Ca+Mg), adsorption (Fe-Mn oxides) and bedrock influences. Recognising these important regolith-related element associations will assist in selection of the most suitable sampling media and geochemical interpretation during mineral exploration.

10.2 GROUNDWATER CHEMISTRY AND HYDROGEOLOGY

Groundwater aquifers are present within the *in situ* regolith where there are weathered phyllitic siltstone-sandstone units. Water levels mirror topography, indicating an unconfined aquifer system, and groundwater is flowing in general to the northeast in the Hermidale area and similarly in part of the Byrock area. The groundwater in the region is mainly chloride type, rich in Na, Cl and SO_4 .The other calcium-bicarbonate and bicarbonate-chloride types are less common. The main processes that have affected the groundwater composition are evaporation, water–rock interaction and mixing. Each of these processes left a compositional touch, which can be recognised by significant

changes in Na/Br and Cl/Br ratios. A significant increase in the $^{36}Cl/Cl$ ratio along the groundwater flow path indicates mixing of groundwaters of different ages. Groundwater ages calculated from $^{36}Cl/Cl$ indicate that the groundwater in the Byrock area is older (418000-516000 years) than that in the Hermidale area (241000-492000 years). The waters are undersaturated with respect to oxidised copper and zinc minerals. Calculated saturation indices of $ZnSiO_3$, malachite and tenorite for the Hermidale groundwaters appear to show a vector towards known mineralisation (i.e. the Budgery deposit northwest of drill hole 150 and the Glengarry gossan south of drill hole CBAC173). The correlation between the groundwater and regolith composition suggests at least another two sites (drill holes 217 and 219) of potential mineralisation.

10.3 SEDIMENTARY WEATHERING PROCESSES AND SOURCE COMPOSITION

The degree of weathering of saprolith in the Girilambone region can be determined using the Chemical Index of Alteration (CIA) and plots of major components (A-CN-K diagram). Four zones of weathering I to IV are recognised based on CIA values. Zone IV is the least weathered and zone I the most weathered. The A-CN-K diagram gives good results for the finer grained lithologies but is not useful for sandstones particularly where they are poorly sorted. Deviations from the weathering trends infer chemical changes resulting from diagenesis or metasomatism.

Immobile element ratios Zr/Sc versus Th/Sc can be used to identify sedimentary recycling in source rocks for the regolith. A significant increase in Zr/Sc with insignificant or no increase in Th/Sc, suggests significant recycling of sediment making up the protolith. Comparing these ratios with those for known rock composition indicate a wide range of igneous rock compositions for the sediment source.

Al_2O_3/SiO_2 and TiO_2/Zr ratios can be used in association with the $15Al_2O_3$-$300TiO_2$-Zr diagram to discriminate between sandstone, shale and mafic to felsic igneous compositions. Sandstone-dominant saprolith plots trend toward immature sandstone indicating a significant amount of silt and clay within these samples. This diagram also discriminates the saprolith derived from mafic igneous rocks (eg. in drill holes CBAC163, 166, 198, 200, 201, 234) from that derived from an intermediate (granodioritic) igneous source (eg. in drill holes CBAC167, 233, 237 and 247).

Ti/Th and Ce/La ratios can be used to discriminate between saprolith materials that are derived from the Cobar Supergroup and the Girilambone Group. Cobar Supergroup rocks show a limited range of Ti/Th ratios (0.039 - 0.03) and of Ce/La ratios (2.2- 1.9), whereas those related to the Girilambone Group are characterised by relatively lower ranges of Ti/Th (0.005- 0.03) and Ce/La (1.8- 2.3).

10.4 ELEMENT DISPERSION IN CALCRETE- MANGANESE-IRON –DOMINANT REGOLITH

Calcrete, Fe-Mn oxides or oxyhydroxides are important host regolith materials for Au and base metals (Cu, Zn, Pb) in transported and *in situ* regolith in the Girilambone region. Calcrete is widespread within a zone of variable thickness in the upper 10 m of the regolith. The calcrete typically consists of dispersed calcite-dolomite, generally with calcite predominating in the upper part of the zone and dolomite predominant towards the base. The highest Au contents in a profile are not necessary associated with the position of maximum calcrete development. Typically, the highest Au concentration is at the top of the calcrete zone, but not in all cases. There is generally a negative correlation between elevated Au and Fe_2O_3 content in this part of the regolith. Some *in situ* profiles show an association of elevated Au with higher Fe_2O_3 content, but this is probably remnant primary Au in ferruginous saprolite.

The association of Au with calcrete in the Girilambone region appears to reflect a chemical environment within both transported and *in situ* regolith that is conducive to precipitation of both carbonate and mobilised gold rather than a direct control on gold fixation by calcrete. There is no positive correlation between Cu, Zn, Pb, Cr, Ni and Ti concentrations and CaO and MgO contents in the calcrete zone. However, these elements show positive correlation with Fe_2O_3 content suggesting these elements are contained within iron oxide/oxyhydroxide impurities in the carbonate zone.

The Mn-enriched zone is variably distributed in the regolith of the Girilambone region, but is generally best developed in the *in situ* regolith. The highest MnO content is in the southwest of the Hermidale area and generally decreases toward the east. Lithiophorite, cryptomelane, pyrolusite and hollandite are the dominant Mn minerals. They are

generally present as microcrystalline masses or well-developed platy crystals in cavities and spaces in Mn-rich zones.

Manganese oxide content is positively correlated with multi-element enrichments of Fe, Mg, As, Co, Ni, Cu and Zn, typically in mafic rock dominant areas. This indicates a mafic suite of elements that has been released during weathering. Gold enrichment is not associated with this multi-element enrichment and it is not correlated with MnO abundance, which probably indicates an independent host mechanism. A stratified concentration of Mn oxides above the present water level along the groundwater flow path indicates previous water levels where the manganese oxides were precipitated due to redox changes.

Iron-enriched zones are unevenly distributed in the regolith profile of the Girilambone region with predominant enrichment in the central part of the study area (Sussex area) where Fe is concentrated in the transported regolith. This significantly decreases towards the south (Hermidale area). In the northern part (Byrock area) Fe- enrichment is observed in the *in situ* regolith in the west and in the transported regolith in the east. Enrichments of Au and As are associated with ferruginous magnetic gravels in the Fe-enriched zone, which possibly indicates a mechanical dispersion of Au in ferruginous regolith.

Elevated Fe, Zn and Cu contents are associated with weathered mafic rocks in the region. These enrichments reflect higher background level of these elements in the original mafic bedrock and possibly scavenging of Pb by more abundant Fe oxides. Generally across the region there is no clear correlation between hematite or goethite content (identified by high Fe-contents) and concentration of Au, As, Zn, Cu and Pb. This suggests that the well-known preferential adsorption of these elements by these minerals has not been sufficient to produce an observable correlation on a regional scale.

10.5 RECOMMENDATIONS FOR FURTHER WORK

- Sampling and analysis of separate regolith lithotypes is important in identifying appropriate pathfinders for mineral exploration. Composite sampling over 1 metre

intervals is a successful and convenient method to detect variations, particularly within the first ten-meters of the regolith profile. Surface (top metre) composite samples are not recommended for exploration and should only be utilised when the regolith mixing facies are well recognised.

- Groundwater samples collected by sample bailer have been found useful for detecting regional variation in groundwater geochemistry. This type of sampling is recommended for regional exploration, particularly when the recharge times are too long for preliminary pumping to be practical. They can provide a better understanding of water-rock and water- regolith interactions and the resulting presence of some dissolved metal complexes.

- Roadside drilling is too restricted to provide a full understanding of the spatial distribution of the regolith, groundwater and geochemical anomalies. In any drilling project in the future, the drill holes should be selected to provide greater coverage of the region.
- Sampling the upper part of the calcrete zone within shallow transported and *in situ* regolith during air-core drilling is recommended, as part of the strategy for gold exploration in this region. Identifying this zone from drill cuttings in the field is probably best done by testing samples with hydrochloric acid and careful visual observation. This can be verified from the Ca and Mg content of samples, following chemical analysis.
- Threshold values of elements need to be established for different types of regolith material and also tested, particularly in an area of known mineral occurrences by implementation of an orientation survey around and away from the mineral occurrence.
- Geochemical anomalies in different regolith facies showed enrichments of Au, Cu, Zn and to some extent Pb in a profile extending from drill hole CBAC119 to CBAC125 in the northwest Sussex area. Further detailed investigation is strongly recommended for this area.
- Anomalous Zn and Cu in the groundwater from drill holes CBAC217 and CBAC219 (Byrock area) suggest further investigation is warranted around these areas probably southeast of CBAC217.
- The scarcity of hydrogeologic information suggests a need for further work on the groundwater in the Girilambone region.

- For a better understanding of weathering process, CIA, A-CN-K diagram and other element ratios techniques need to be applied across the regolith profile (as a study case, particularly in areas of known bedrock geology) to establish the weathering history from fresh bedrock to deeply weathered regolith.

- Further investigation of some underlying bedrock compositions (particularly for the Girilambone Group) is required to fully evaluate the application of Ti/Th and Ce/La geochemical signatures.

REFERENCES

Abonyi, J., Tamas, F.D. and Tritthart, J., 2004. Exploratory Data Analysis of trace elements in Clinker. Advances in Cement Research, 16: 9-16.

Ackerman, B.R., 2005. Regolith geochemical exploration in the Girilambone district of New South Wales. Ph D Thesis, University of Wollongong, 631 pp.

Ackerman, B.R. and Chivas, A.R., 2004. The subsurface geochemical expression of concealed mineralistion, Tritton copper deposit, Girilambone district. In: McQueen, K.G. and Scott, K.M. (Editors), Exploration field workshop Cobar region, 2004. CRC LEME, Cobar, pp. 1-4.

Aitchison, J., 1986. Statistical analysis of compositional data. Methuen Inc, New York, 416 pp.

Aitchison, J., Barcelo-Vidal, C., Martin-Fernandez, J.A. and Pawelowsky-Glahn, V., 2000. Ratio analysis and compositional distance. Mathematical Geology, 32: 271-275.

Alchin, B., 1980. Soil conservation and reclamation of areas of eolian soil in western NSW. In: Wasson, R. (Editor), Quaternary dust mantles of China, New Zealand and Australia. Australian National University, Canberra, pp. 243-249.

Alipour, S., Cohen, D.R. and Dunlop, A.C., 1995. Geochemical characteristic of lag in the Cobar area, NSW. IGES abstracts, 17: 119-121.

Alipour, S., Cohen, D.R. and Dunlop, A.C., 1997. Characteristics of magnetic and non-magnetic lag in the Cobar area, NSW. Journal of Geochemical Exploration, 58: 15-28

Alipour, S., Dunlop, A.C. and Cohen, D.R., 1996. Morphology of lag in the Cobar region, New South Wales. AGSO Journal of Australian Geology & Geophysics, 16: 253-262.

Aller, R.C., 1980. Diagenetic processes near the sediment-water interface of Long Island Sound II. Fe and Mn. Advances in Geophysics, 22: 351-415.

Anderson, B.J., Jenne, E.A. and Chao, T.T., 1973. The sorption of silver by poorly crystallized manganese oxides. Geochimica et Cosmochimica Acta, 37: 611-622.

Andrews, E.C., 1915. The Canbelego , Budgery and Budgerygar mines, Part II of the Cobar Copper and Gold- Field. Mineral Resources, 18. NSW Department of Mines, Sydney, 121 pp.

Andrews, J.N. and Fontes, J.C., 1991. Importance of *in situ* production of Chlorine-36, Argon-36 and Carbon-14 in hydrology and hydrogeochemistry, isotope techniques in water resources development, International Atomic Energy Agency, Vienna, 245-269 pp.

Australian Bureau of Meteorology. www.bom.gov.au, accessed in 2006.

Baes, C.F. and Mesmer, R.E., 1976. The hydrolysis of cations. Wiley, New York, 487 pp.

Barnett, V. and Toby, L., 1994. Outliers in statistical data. Wiley, New York, 463 pp.

Barrett, T.J. and MacLean, W.H., 1991. Chemical, mass and oxygen isotope changes during extreme hydrothermal alteration of an Archean rhyolite, Noranda, Quebec. Economic Geology, 86: 406-414.

Baudo, R., Barbero, P., Beltrami, M. and Rossi, D., 2000. Chemical composition of the sediment from lake 20 (Antarctica). Journal of Limnology, 59: 55-60.

Bentley, H.W., Phillips, F.M. and Davis, S.N., 1986. Chlorine-36 in the terrestrial environment. In: Fritz, P. and Fontes, J.C. (Editors), Handbook of environmental isotope geochemistry. Elsevier, New York, pp. 422-475.

Bentley, H.W., Phillips, F.M., Davis, S.N., Habermehl, M.A., Airey, P.L., Calf, G.E., Elmore, D., Grove, H.E. and Torgeson, T., 1986. Chlorine-36 dating of very old groundwater. The Great Artesian Basin, Australia. Water Resources Research, 22: 1991-2001.

Berthelsen, R., 1998. The geology of the Tritton copper deposit. Australian Institute of Geoscientists Bulletin, 23: 15-23.

Bethke, C.M., 2005. The Geochemist's Workbench Release 6.0. RockWare, Golden, USA.

Bird, J.R., Davie, R.F., Chivas, A.R., Fifield, L.K. and Ophel, T.R., 1991. ^{36}Cl production and distribution in Australia. Palaeography, Palaeoclimatology, Palaeoecology, 84: 299-307.

Blevin, P.L. and Jones, M., 2004. Granites of the Bourke-Byrock-Brewarrina region, NSW. In: McQueen, K.G. and Scott, K.M. (Editors), Exploration field workshop Cobar region 2004. CRC LEME, pp. 10-14.

Borrego, P. and Gutierrez, M., 2000. Mapping soil geochemical anomalies in the Mesa Quadrangle, Arizona, using NURE data. Environmental Geoscience, 7: 80-89.

Brand, N.W. and Butt, C.R.M., 2001. Weathering element distribution and geochemical dispersion at Mt Keith, Western Australia: Implication for nickel sulphide exploration. Geochemistry: Exploration, Environment, Analysis, 1: 391-407.

Brunker, R.L., 1970. Explanatory notes on the Cobar 1:250 000 geological sheet. Geological Survey of New South Wales, Sydney, 33 pp.

Bucker, C., Shimeld, J., Hunze, S. and Bruckmann, W., 2000. Data report: Logging while drilling data analysis of Leg 171A, a multivariate statistical approach. In: Moore, J.C. and Klaus, A. (Editors), Proceedings of the Ocean Drilling Program, pp. 1-29.

Burns, R.G. and Burns, V.M., 1975. Manganese oxides. In: Burns, R.G. (Editor), Marine Minerals. Mineralogical Society of America, Washington D. C., pp. 1-46.

Burns, R.G. and Burns, V.M., 1979. Manganese oxides. In: Burns, R.G. (Editor), Marine Minerals. Reviews in Mineralogy. Mineralogical Society of American, Washington, D.C., pp. 1-46.

Butt, C.R.M., 1987. A basis for geochemical exploration models for tropical terrains. Chemical Geology, 60: 5-16.

Butt, C.R.M., 1991. Dispersion of gold and associated elements in the lateritic regolith, Mystery Zone, Mt Percy, Kalgoorlie, Western Australia, 1. CSIRO Division of exploration geoscience restricted report 156R, 60 pp.

Butt, C.R.M., 1998. Geochemical background, Mt Percy, Kalgoorlie, Western Australia, CRC LEME Open File Report 54, 103 pp.

Butt, C.R.M., Lintern, M.J. and Anand, R.R., 2000. Evolution of regoliths and landscapes in deeply weathered terrain- implications for geochemical exploration. Ore Geology Reviews, 16: 167-183.

Butt, C.R.M., Robertson, I.D.M., Scott, K.M. and Cornelius, M., 2005. Regolith expression of Australian ore systems. CRC LEME, Perth, 424 pp.

Butt, C.R.M., Williams, P.A., Gray, D.J., Robertson, I.D.M., Schorin, K.H., Churchward, H.M., McAndrew, J., Barnes, S.J. and Tenhaeff, M.F.J., 1992. Geochemical exploration for platinum group elements in weathered terrain. Final report. 332, CSIRO Division of Exploration Gescience.

Butt, C.R.M. and Zeegers, H., 1989. Classification of geochemical exploration models for tropically weathered terrains. Journal of Geochemical Exploration, 32: 65-74.

Byrnes, J.G., 1993. Bourke 1:250 000 metallogenic map SH/55-10: Metallogenic study and mineral deposits data sheets. Geological survey of New South Wales, Sydney, 127 pp.

Bystrom, A. and Bystrom, A.M., 1950. The crystal structure of hollandite, the related manganese oxide minerals and MnO_2. Acta Crystallogr, 3: 146-154.

Cairns, C.J., McQueen, K.G. and Leah, P.A., 2001. Mineralogical controls on element dispersion in regolith over two mineralised shear zones near the Peak, Cobar, New South Wales. Journal of Geochemical Exploration, 72: 1-21.

Cameron, E.M., Hamilton, S.M., Leybourne, M.I., Hall, G.E.M. and McClenaghan, M.B., 2004. Finding deeply buried deposits using geochemistry. Geochemistry: Exploration, Environment, Analysis, 4: 7-32.

Campbell, I.B. and Claridge, G.G.C., 1992. Soil of cold climate regions. In: Martini, I.P. and Chesworth, W. (Editors), Weathering, soil and paleosols. Elsevier, pp. 183-201.

Caritat, P.de. and Kirste, D., 2004. Groundwater geochemistry as a tool for mineral exploration under cover- the Curnemona Province, PACRIM 2004 Congress: Hi Tech and World Competitive Mineral Success Stories Around the Pacific Rim. AusIMM, Adelaide, Series 5/2004:219.

Caritat, P.de., Kirste, D., Carr, G. and McCulloh, M., 2003. Vectoring towards mineralisation under cover using groundwater geochemistry: an example from the Curnamona province. In: Roach, I.C. (Editor), Advances in Regolith. CRCLEME, pp. 49-52.

Caritat, P.de., Kirste, D. Carr, G and McCulloh, M., 2005. Groundwater in the Broken Hill region, Australia: recognising interaction with bedrock and mineralisation using S, Sr and Pb isotopes. Applied Geochemistry, 20: 767-787.

Carr, G., Andrew, A., Denton, G., Giblin, A., Korsch, M. and Whitford, D., 1999. The "Glass Earth" - Geochemical frontiers in exploration through cover. http://www.smedg.org.au/Sym99glass. Accessed in 2005

Carr, P.F., Fergusson, C.L., Pemberton, J.W., Colquhoun, G.P., Murray, S.L. and Watkins, J., 2003. Late Ordovician island-arc volcanic rocks, Northern Capertee Zone, Lachlan Fold Belt, New South Wales. Australian Journal of Earth Sciences, 50: 319-330.

Cartwright, I., Weaver, T.R., Fulton, S., Nichol, C., Reid, M. and Cheng, X., 2004. Hydrogeochemical and isotopic constraints on the origins of dryland salinity, Murray basin, Victoria, Australia. Applied Geochemistry, 19: 1233-1254.

Chan, R.A., Greene, R.S.B., De Souzakovacs, N., Maly, B.E.R., McQueen, K.G. and Scott, K.M., 2001. Regolith, geomorphology, geochemistry and mineralisation of the Sussex-Coolabah area in the Cobar-Girilambone region, north-western Lachlan Fold Belt, NSW. 166, CRC LEME, 56 pp.

Chan, R.A., Greene, R. S. B., Hicks, M., Le Gleuher, M., McQueen, K. G., Scott, K. M. and Tate, S. E., 2004. Regolith architecture and geochemistry of the Byrock area, Girilambone region, North-Western NSW. 159, CRC LEME, 71 pp.

Chan, R.A., Greene, R.S.B., Hicks, M., Maly, B.E.R., McQueen, K.G. and Scott, K.M., 2002. Regolith architecture and geochemistry of the Hermidale area of the Girilambone region, north-western Lachlan Fold Belt, NSW. 179, CRC LEME, 48 pp.

Chappell, B.W., 1998. Basement of the Lachlan Fold Belt: the evidence from S-type granites. GEMOC Abstract.

Chen, X.Y., Lintern, M.J. and Roach, I.C., 2002. Calcrete characteristics, distribution and use in mineral exploration. CRC LEME, 160 pp.

Chen, X.Y., McKenzie, N.J. and Roach, I.C., 2002. Distribution in Australia: calcrete landscapes. In: Chen, X.Y., Lintern, M.J. and Roach, I.C. (Editors), Calcrete: characteristics, distribution and use in mineral exploration. CRC LEME, pp. 110-138.

Childs, C.W., 1975. Composition of iron-manganese minerals concretions from some New Zealand soils. Geoderma, 13: 141-152.

Clesceri, L.S., Greenberg, A.E. and Trussell, R.R. (Editors), 1989. Standard methods for the examination of water and wastewater, 17th edition, Washington D.C.

Coakes, S. and Steed, L., 2001. SPSS: analysis without anguish: version 10.0 for Windows. John Wiley & Sons Australia, Ltd, Brisbane, 266 pp.

Cohen, D.R., 2001. Exploration geochemical data processing course notes, Guide to software and data sets. University of New South Wales.

Cohen, D.R., Rutherford, N.F., Dunlop, A.C. and Alipour, S., 1996. Geochemical exploration in the Cobar region. In: Cook, W.G., Ford, A.J.H., McDermott, J.J., Standish, P.N., Stegman, C.L. and Stegman, T.M. (Editors), The Cobar mineral field-A 1996 perspective. The Australasian Institute of Mining and Metallurgy, pp. 125-155.

Cohen, D.R., Shen, X.C., Dunlop, A.C. and Rutherford, N.F., 1998. A comparison of selective extraction soil geochemistry and biogeochemistry in the Cobar area, New South Wales. Journal of Geochemical Exploration, 61: 173-189.

Condie, K.C., 1991. Another look at rare earth elements in shale. Geochimica et Cosmochimica Acta, 55: 2527-2531.

Cornu, S., Deschatrettes, V., Salvador-Blanes, S., Clozel, B., Haerdy, M., Branchut, S. and Forestier, L.L., 2005. Trace element accumulation in Mn-Fe-oxide nodules of a planosolic horizon. Geoderma, 125: 11-24.

Cresswell, R.G., Wischusen, J.D.H., Fifield, L.K. and Jacobson, G., 1999. Assessment of recharge to groundwater systems in the arid southwestern part of Northern Territory, Australia, using chlorine-36. Hydrogeology Journal, 7: 393-404.

Cullers, R., Barrett, T., Carlson, R. and Robinson, B., 1987. Rare-Earth element and mineralogic changes in Holocene soil and stream sediments: A case study in the Wet Mountains, Colorado, USA. Chemical Geology, 63: 275-297.

Cunningham, G.M., 1981. Plants of western New South Wales, Soil Conservation Service of New South Wales, Sydney, 32 pp.

Dale, M.B., 1995. Exploratory data analysis. Advanced Systems Institute, National Resource Information Centre, ACT, 344 pp.

Dart, R.C., Barovich, K.M. and Chittleborough, D., 2005. Pedogenic carbonates strontium isotopes and their relationship with Australian dust processes. In: Roach, I.C. (Editor), Regolith 2005: Ten years of CRC LEME, pp. 64-66.

David, M., 1977. Geostatistical ore reserve estimation. Elsevier, Amsterdam, 364 pp.

Davie, R.F., Kellet, J.R., Fifield, L.K., Evans, W.R., Calf, G.E., Bird, J.R., Topham, S. and Ophel, T.R., 1989. Chlorine-36 measurements in the Murray Basin: preliminary results from the Victorian and South Australia Mallee region. BMR Journal of Geology and Geophysics, 11: 261-272.

Davis, J.C., 2002. Statistics and data analysis in geology. Wily, New York, 638 pp.

Day, F.H., 1963. The chemical elements in nature. Harrap, London, 372 pp.

De Ross, G.J., 1978. Report on exploration on EL 1087,Beanbah- Cobar region. GS1978/362, Geological Survey of New South Wales, pp.

Deer, W.A., Howie, R.A. and Zussman, J., 1992. An introduction to the rock forming minerals. Pearson-Prentice Hall, 696 pp.

Deutsch, W.J., 1997. Groundwater geochemistry, fundamentals and applications to contamination. Lewis Publishers, Boca Raton, 220 pp.

Dogramaci, S.S., Herczeg, A.L., Schiff, S.L. and Bone, Y., 2001. Controls on ^{34}S and ^{18}O of dissolved sulfate in aquifers of the Murray Basin, Australia and their use as indicators of flow processes. Applied Geochemistry, 16: 475-488.

Dong, D., Derry, L.A. and Lion, L.W., 2003. Pb scavenging from a freshwater lake by Mn Oxides in heterogeneous surface coating materials. Water Research, 37: 1662-1666

Dong, D. and Hua, Y.L.X., 2001. Investigation of Fe, Mn oxides and organic material in surface coating and Pb, Cd adsorption to surface coating developed in different natural waters. Microchemical Journal, 70: 25-33.

Drever, J.I., 1997. The geochemistry of natural waters: surface and groundwater environments. Prentice Hall, Upper Saddle River, 436 pp.

Duk-Rodkin, A., Chan, R.A. and McQueen, K.G., 2003. Drainage evolution and implications for neotectonics and mineral exploration in the Cobar uplands, NSW. In: Roach, I.C. (Editor), Advances in Regolith. CRCLEME, pp. 104-109.

Dunlop, A.C., Atherden, P.R. and Govett, G.J.S., 1983. Lead distribution in drainage channels about the Elura zinc- lead- silver deposit, Cobar, New South Wales, Australia. Journal of Geochemical Exploration, 18: 195-204.

Durand, N., Gunnell, Y., Curmi, P. and Ahmad, S.M., 2006. Pathways of calcrete development on weathered silicate rocks in Tamil Nadu, India: Mineralogy, Chemistry and paleoenvironmental implications. Sedimentary Geology, 192: 1-18.

Eastmet Minerals, N.L., 1970. E.L. 1977 (Application No.437) report for the fourth quarter of Tenure (incorporating the second and third quarter). GS1970/463, Mineral search and development, 5 pp.

Eaton, A.D., Clesceri, L.S. and Greenberg, A.E., 1995. Standard methods for the examination of water and wastewater. Am. Public Health Association, Washington, DC, 2-25- 2-28 pp.

Edwards, D.S., Kennard, J.M., Preston, J.C., Summons, R.E., Boreham, C.J. and Zumberge, J.E., 2000. Bonaparte Basin, Geochemical characteristics of hydrocarbon families and petroleum systems. AGSO Research Newsletter: pp. 14- 19.

Eggleton, R.A., 2001. The regolith glossary surficial geology, soils and landscape. CRC LEME, Canberra, 144 pp.

Elliotts, J. and Martin, A.R., 1991. Alaskan-type intrusive complexes of the Fifield belt, central New South Wales. In: Elliott, S.J. and Martin, A.R. (Editors), Geology and Mineralization of the Fifield Platinum Province, New South Wales. Geological Society of Australia, pp. 4-11.

Ellis, J.C. and Gilbert, C.F., 1980. How to handle " less-than" data when forming summaries. ER764, Water Research Centre, Medmenham, England,

Elmore, D., Fulton, B.R., Clover, M.R., Marsden, J.R., Gove, H.E., Naylor, H., Purser, K.H., Kilius, L.K., Beukens, R.P. and Litherland, A.E., 1979. Analysis of ^{36}Cl in environmental water samples using an electrostatic accelerator. Nature, 277: 22-25.

Fedo, C.M., Nesbitt, H.W. and Young, G.M., 1995. Unraveling the effects of potassium metasomatism in sedimentary rocks and paleosols, with implications for paleoweathering conditions and provenance. Geology, 23: 921-924.

Fedo, C.M., Young, G. M, Nesbitt, H. W. and Hancher, J.M., 1997. Potassic and sodic metasomatism in the Southern Province of Canadian Shield: Evidence from Paleoproterozoic Serpent Formation, Huronian Supergroup, Canada. Precambrian Research, 84: 17-36.

Feitknecht, W., 1965. Oxidation of Fe_3O_4 and Fe. Colloq Int. CNRS, 122: 121-126.

Felton, A., 1981. Geology of the Canbelego 1:100 000 geological sheet 8134. Geological Survey of New South Wales, Sydney, 171 pp.

Fergusson, C.L., 2003. Ordovician-Silurian accretion tectonics of the Lachlan Fold Belt, southeastern Australia. Australian Journal of Earth Sciences, 50: 475-490.

Fergusson, C.L. and Coney, P.J., 1992. Convergence and interplate deformation in the Lachlan Fold Belt of southeastern Australia. Tectonophysics, 214: 417-439.

Fifield, L.K., Ophel, T.R., Bird, J.R., Calf, G.E., Allison, G.B. and Chivas, A.R., 1987. The ^{36}Cl measurement program at the Australian National University. Nuclear Instruments and Methods in Physics Research, 29: 114-119.

Fleming, G. and Hicks, M., 2002. Second programme of shallow reconnaissance aircore drilling, Hermidale area, Cobar NSW., NSW Department of Mineral resources GS2002/018.

Fleming, G., Hicks, M. and Barron, L., 2001. First programme of shallow reconnaissance aircore drilling, Sussex area, Cobar NSW, Geological Survey of New South Wales, GS2001/200 & GS2001/319.

Fleming, G., Hicks, M., Buckley, P., Needham, J., Barron, L. and Spencer, R., 2002. Cobar project, Preliminary magnetic basement interpretation. Department of Mineral Resources New South Wales.

Fletcher , W.K., 1981. Analytical methods in geochemical prospecting, Amsterdam, 255 pp.

Fogarty, J.M., 1996. Exploration for leachable copper deposits in the Girilambone district. In: Cook, W.G., Ford, A.J.H., McDermott, J.J., Standish, P.N., Stegman, C.L. and Stegman, T.M. (Editors), The Cobar Mineral Field - a 1996 perspective. Australasian Institute of Mining and Metallurgy, pp. 179-193.

Fogarty, J.M., 1998. Girilambone district copper deposits. In: Berkman, D.A. and Mackenzie, D.H. (Editors), Geology of Australia and Papua New Guinean Mineral deposits. Australasian Institute of Mining and Metallurgy Monograph 22, pp. 593-600.

Fogarty, J.M., 2001. Tritton Copper deposit Project Update. Minfo, 69: 34-36.

Forelich, P.N., Klinkhammer, G.P., Bender, M.L., Luedtke, N.A., Heath, G.R., Cullen, D., Dauphin, P., Hammond, D., Hartman, B. and Maynard, V., 1979. Early oxidation of organic matter in pelagic sediments of the eastern equatorial Atlantic: Suboxic diagenesis. Geochimica et Cosmochimica Acta, 43:1075-1090.

Foster, D.A., Gray, D.R. and Bucher, M., 1999. Chronology of deformation within the turbidite-dominated Lachlan Fold Belt: implications for the tectonic evolution of eastern Australia and Gondwana. Tectonics, 18: 452-485.

Fralick, P., 2003. Geochemistry of clastic sedimentary rocks: ratio techniques. In: Lentz, D.R. (Editor), Geochemistry of sediments and sedimentary rocks: evolutionary considerations to mineral deposit-forming environments. Geological Association of Canada, pp. 85-103.

Freeze, A.R. and Cherry, J.A., 1979. Groundwater. Prentice Hall, Englewood Cliffs, 604 pp.

Friedl, G., Wehrli, B. and Manceau, A., 1997. Solid phases in the cycling of manganese in eutrophic lakes: New insights from EXAFS spectroscopy. Geochimica et Cosmochimica Acta, 61: 275-290.

Garcia, D., Fonteilles, M.and Moutte, J., 1994. Sedimentary fractionations between Al, Ti and Zr and the genesis of strongly peraluminous granites. Journal of Geology, 102: 411-322.

Gedeon, A.Z. and Butt, C.R.M., 1990. Morphology and geochemistry of particulate gold in the lateritic regolith, Mystery Zone, Mt.Percy, Kalgoorlie, Western Australia. Report No:124R,, Australian Mineral Industries Research association Limited, 41pp.

Giblin, A.M., 1996a. Applications of groundwater geochemistry to mineral exploration in the Narromine-Nyngan region of NSW. GS1996/201, NSW Department of Mineral Resources.

Giblin, A.M., 1996b. Applications of groundwater geochemistry to the detection of prospective basement beneath Mesozoic cover, Mesozoic Geology of the Eastern Australian Plate Extended Abstracts No 43. Geological Society of Australia, pp. 186-194.

Giblin, A.M., 2001. Groundwaters, geochemical pathfinders to concealed ore deposits. CSIRO, 70 pp.

Giblin, A.M. and Dickson, B.L., 1992. Source, distribution and economic significance of trace element in groundwaters from Lake Tyrrell, Victoria, Australia. Chemical Geology, 96: 133-149.

Giblin, A. M. and Rutherford, N.F., 2003. Groundwaters as pathfinders to concealed ore deposits. Australian Institute of Geoscientists AIG News Quarterly Newsletter, 71: 1-5.

Giles, A.D. and Marshall, B., 2004. Genetic significance of fluid inclusions in the CSA Cu-Pb- Zn deposit, Cobar, Australia. Ore Geology Reviews, 24: 241-266.

Gilligan, L.B., 1982. The origin and evolution of the Mount Boppy gold deposit, Canbelego and related mineralisation. MAS Thesis, New South Wales Institute of Technology, Sydney, 198 pp.

Gilligan, L.B. and Byrnes, J.G., 1995. Cobar 1:250 000 Metallogenic Map SH/55-14: Metallogenic study and mineral deposit data sheet. Geological Survey of New South Wales, Sydney, 240 pp.

Giovanoli, R., Buhler, H. and Sokolowaka, K., 1973. Synthetic lithiophorite: electron micrography and X-ray diffraction. Journal of Microscopy, 18: 271-84.

Glanville, D.H., Roach, I.C. and McQueen, K.G., 2003. Regolith-landform mapping, leucitite basalt and the landscape evolution of the Byrock region, NW NSW. In: Roach, I.C. (Editor), Advances in regolith. CRC LEME, pp. 144-148.

Gleit, A., 1985. Estimation for small normal data sets with detection limits. Environmental Science and Technology, 19: 1201-1206.

Glen, R.A., 1985. Basement control on the deformation of cover basins: an example from the Cobar district in the Lachlan Fold Belt, Australia. Journal of Structural Geology, 7: 301-315.

Glen, R.A., 1987. Copper and gold-rich deposits in deformed turbidites at Cobar, Australia: their structural control and hydrothermal origin. Economic Geology, 82: 124-140.

Glen, R.A., 1988. Basin inversion, thrusts and ore deposits at Cobar, New South Wales: A preliminary report, Geological Survey New South Wales, 21-26 pp.

Glen, R.A., 1990. Inversion of transtensional basins in the western part of the Lachlan Fold Belt New South Wales, with emphasis on the Cobar basin. Journal of Structural Geology, 12: 601-620.

Glen, R.A., 1992. Thrust, extensional and strike-slip tectonics in an evolving Paleozoic orogen- a structural synthesis of the Lachlan orogen of southeastern Australia. Tectonophysics, 214: 314-380.

Glen, R.A., 1994. Geology of the Cobar 1:100,000 sheet 8035, Geological Survey of New South Wales, Sydney.

Glen, R.A., 1995. Thrusts and thrust-associated mineralization in the Lachlan Orogen. Economic Geology, 90: 1402-1429.

Glen, R.A., Clare, A. and Spencer, R., 1996. Extrapolating the Cobar basin model to the regional scale: Devonian basin-formation and inversion in west New South Wales. In: Cook W. G., Ford A.J.H., McDermott, J.J., Standish, P.N., Stegman, C.L. and Stegman, T.M. (Editors), The Cobar Mineral Field- A 1996 perspective. The Australasian Institute for Mining and Metallurgy, pp 43-83.

Glen, R.A., Dallmeyer, R.D. and Black, L.P., 1992. Isotopic dating of basin inversion- the Paleozoic Cobar basin, Lachlan Orogen, Australia. Tectonophysics, 214: 249-268.

Glen, R.A. and Fleming, G., 2000. A new exploration province in New South Wales: The Girilambone Group. In: McQueen, K.G. and Stegman, C.L. (Editors), Central West Symposium, Cobar 2000: Extended Abstract. CRC LEME, Perth, pp. 36-37.

Golden, D.C., Dixon, J.B. and Kanehiro, Y., 1993. The manganese oxide mineral, lithiophorite, in an Oxisol from Hawaii. Australian Journal of Soil Research, 31: 51-66.

Gomez-Gras, D. and Zarza, A.M.A., 2003. Reworked calcrete: their significance in the reconstruction of alluvial sequences (Permian and Triassic, Minorca, Balearic Islands, Spain. Sedimentary Geology, 158: 299-319.

Goncalves, C.A. and Ewert, L., 1998. Evaluation of the geochemical logging data in hole 959d: Cte D'ivoire-ghana transform margin. In: Mascle, J., Lohmann, G.P. and Moullade, M. (Editors), Proceeding of the Ocean Drilling Program, Scientific Results, pp. 171-179.

Goudie, A.S., 1973. Duricrusts in tropical and subtropical landscapes. Clarendon Press, Oxford, 174 pp.

Goudie, A., 1983. Calcrete. In: Goudie, A. and Pye, P. (Editors), Chemical sediments and geomorphology. Academic Press, New York, pp. 93-131.

Govett, G.J.S., Dunlop, A.C. and Atherden, P.R., 1984. Electrogeochemical techniques in deeply weathered terrain in Australia. Journal of Geochemical Exploration, 21: 311-331.

Gray, D.J., 1991. Hydrogeochemistry in the Mount Gibson gold district. 120R, CSIRO Australia, Division of exploration geoscience, 80 pp.

Gray, D.R., 1997. Tectonics of the southeastern Australia Lachlan Fold Belt: Structural and thermal aspects. In: Burg, J.P. and Ford, M. (Editors), Orogeny Through Time. Geological Society of London Special Publication, pp. 149-177.

Gray, D.R. and Foster, D.A., 1997. Orogenic concepts-application and definition: Lachlan Fold Belt, Eastern Australia. American Journal of Science, 297: 859-891.

Gray, D.R. and Foster, D.A., 1998. Character and kinematics of faults within turbidite-dominated Lachlan Orogen: implications for tectonic evolution of eastern Australia. Journal of Structural Geology, 20: 1691-1720.

Gray, D.R., Foster, D.A. and Bierlein, F.P., 2002. Geodynamics and metallogeny of the Lachlan Fold Belt. Australian Journal of Earth Sciences, 49: 1041-1056.

Gray, J.M. and Murphy, B.W., 1999. Parent material and soils: A guide to the influence of parent material on soil distribution in Eastern Australia. Technical report No.45, NSW Department of Land and water Conservation, Sydney.

Gray, J.M. and Murphy, B.W., 2002. Parent material and soil distribution. Natural Resource Management, 5: 1-12.

Grunfeld, K., 2005. Dealing with outliers and censored values in multi-element geochemical data- a visualization approach using XmdvTool. Applied Geochemistry, 20: 341-352.

Grunsky, E.C. and Smee, B.W., 1999. The differentiation of soil types and mineralization from multi-element geochemistry using multivariate methods and digital topography. Journal of Geochemical Exploration, 67: 287-299.

Guerzoni, S., Portaro, R., Trincardi, F., Molinaroli, E., Langone, L., Correggiari, A., Vigliotti, L., Pistolato, M., De Falco, G. and Boccini, V., 1996. Statistical analysis of grain-size, geochemical and mineralogical data in core CM92-43, Central Adriatic basin. Mem. Ist. Ital. Idrobiol., 55: 231-245.

Hall, G.E.M., 1998. Analytical perspective on trace element species of interest in exploration. Journal of Geochemical Exploration, 61: 1-19.

Hall, Relph and Associates, 1969. Quarterly report on exploration license No.177, 3 pp.

Hartigan, J.A., 1975. Clustering algorithms. Wiley, New York, 332 pp.

Hawkes, H.E. and Webb, J.S., 1962. Geochemistry in mineral exploration. Harper and Row, New York, 415 pp.

Heins, W.A., 1993. Source rock texture versus climate and topography as controls on the composition of modern, plutoniclastic sand. In: Johnsson, M.J. and Basu, A. (Editors), Processes controlling the composition of clastic sediments. Geological Society of America, Special Paper no.284, pp. 135-146.

Helgeson, H., Garrels, R.M. and Mackenzie, F.T., 1969. Evaluation of irreversible reactions in geochemical processes involving minerals and aqueous solutions: I Applications. Geochimica et Cosmochimica Acta, 33: 455-481.

Helsel, D.R., 1990. Less than obvious: statistical treatment of data below the detection limit. Environmental Science and Technology, 24: 1767-1774.

Helsel, D.R. and Hirsch, R.M., 1992. Statistical methods in water resources. Elsevier, Amsterdam, 294 pp.

Hem, J.D., 1964. Deposition and solution of manganese oxides. U.S. Geol. Survey Water Supply Paper 1667B.

Hem, J.D., 1985. Study and interpretation of the chemical characteristics of natural water, U.S. Geological Survey Water-Supply Paper 2254.

Hema, A. and Navin, S., 2004. Pedogenic calcretes from Coimbatore area, Tamil Nadu: micromorphology, geochemistry and paleoclimate significance, UNESCO and IAEA, 38 pp.

Herczeg, A.L., Torgersen, T., Chivas, A.R. and Habermehl, M.A., 1991. Geochemistry of groundwaters from the Great Artesian Basin, Australia. Journal of Hydrology, 126: 225-245.

Hesp, W.R. and Rigby, D., 1975. Aspects of tin metallogensis in the Tasman geosyncline, eastern Australia, as reflected by cluster and factor analyses. Journal of Geochemical Exploration, 4: 331-347.

Hill, S.M., McQueen, K.G. and Foster, K.A., 1999. Regolith carbonate accumulations in western and central NSW: characteristics and potential as an exploration sampling medium. In: Taylor, G.M. and Pain, C.F. (Editors), New approaches to an old continent. Proceedings of Regolith 98 Conference. CRCLEME, Kalgoorlie, WA, pp. 191-208.

Hill, S.M., Taylor, G.M. and McQueen, K.G., 1998. Discussion genesis of some calcretes in the southern Yilgarn Craton, Western Australia: implications for mineral exploration. Australian Journal of Earth Sciences, 45: 177-178.

Hornung, R.W. and Reed, L.D., 1990. Estimation of average concentration in the presence of non-detectable values. Applied Occupational and Environmental Hygiene, 5: 46-51.

Hudak, P.F., 1999. Chloride and nitrate distributions in the Hickory aquifer, central Texas, USA. Environment International, 25: 393-401.

Hwang, C.K., Cha, J.M., Kim, K.W. and Lee, H.K., 2001. Application of multivariate statistical analysis and a geographic information system to trace element contamination in the Chungnam Coal Mine area, Korea. Applied Geochemistry, 16: 1455-1464.

James, C.H., 1970. A rapid method for calculating the statistical precision of geochemical prospecting analysis. Institution of Mining and Metallurgy, 79: B88-B90.

Jeong, C.H., 2001. Mineral-water interaction and hydrogeochemistry in the Samkwang mine area, Korea. Journal of Geochemistry, 35: 1-12.

Jerram, D.A. and Cheadle, M.J., 2000. On the cluster analysis of grains and crystals in rocks. American Mineralogist, 85: 47-67.

Johnson, R.A. and Wichern, D.W., 1982. Applied multivariate statistical analysis. Prentice-Hall, 594 pp.

Johnsson, M.J., 1993. The system controlling the composition of clastic sediments. In: Johnsson, M.J. and Basu, A. (Editors), Processes controlling the composition of clastic sediments. Geological Society of America Special Paper no. 284, 342 pp.

Joplin, G.A., 1963. Chemical analysis of Australian rocks. Part I: Igneous and Metamorphic. BMR Geology and Geophysics, Bulletin No.65.

Joplin, G.A., 1965. Chemical analysis of Australian rocks. Part II: Sedimentary rocks. BMR Geology and Geophysics, Bulletin No.78.

Kabata-Pendias, A. and Pendias, H., 1984. Trace elements in soils and plants. CRC Press, Boca Raton, 315 pp.

Kauranne, L.K., Salminen, R. and Eriksson, K., 1992. Regolith exploration geochemistry in Arctic and Temperate terrains. Elsevier, 444 pp.

Kelly, W., Ratliff, T.A.J. and Nenadic, C., 1992. Basic statistics for laboratories. Van Nostrand Reinhold, New York. 175pp.

Keywood, M.D., 1995. Origins and sources of atmospheric precipitation from Australia: Chlorine-36 and major ion chemistry. PhD Thesis, Australian National University, 207 pp.

Keywood, M.D., Chivas, A.R., Fifield, L.K., Cresswell, R.G. and Ayers, G.P., 1997. The accession of chloride to the western half of the Australian Continent. Australian Journal of Soil Research, 35: 1177-1189.

Khadkikar, A.S., Merh, S.S., Malik, J.N. and Chamyal, L.S., 1998. Calcretes in Semi-arid alluvial system: formative pathways and sinks. Sedimentary Geology, 116: 251-260.

Khider, K., 2004. Geochemical dispersion of elements in Byrock- Hermidale groundwaters, Cobar region NSW. In: Roach, I.C. (Editor), Regolith 2004. CRC LEME, pp. 175-180.

Khider, K. and McPhail, D.C., 2005. Hydrogeology and hydrogeochemistry in the Herimidale area, NSW. In: Roach, I.C. (Editor), Ten years of CRC LEME. CRC LEME, pp. 165-169.

Khider, K. and McQueen, K.G., 2005. Geochemical discrimination of weathered bedrock in the Hermidale-Byrock region of northwestern NSW. In: Roach, I.C. (Editor), Ten years of CRC LEME. CRC LEME, pp. 170-175.

Khider, K. and McQueen, K.G., 2006. Gold dispersion in calcrete-bearing regolith of the Girilambone region, western NSW. In: Fitzpatrick, R.W. and Shand, P. (Editors), Regolith 2006: consolidation and dispersion of ideas. CRC LEME, pp. 190-195.

Kilpatrick, D. and Fleming, D.P., 1980. Lower Ordovician sediments in the Wagga Trough: discovery of early Bendigonian graptolites near Eskdale, northeast Victoria. Journal Geological Society of Australia, 27: 69-73.

Kotlyard, B.B., Singer, D.A., Jachens, R.C. and Theodore, T.G., 1998. Regional analysis the distribution of gold deposits in northeast Nevada using NURE arsenic data and geophysical data, Open-file. 338, 234-242 pp.

Krige, D.G., 1960. On the departure of ore value distributions from the lognormal model in South African gold mines. J. S. Afr. Inst. Min. Metall. (November): 231-244.

Kronberg, B.I., Fyfe, W.S., Leonardos, J.O.H. and Santos, A.M., 1979. The chemistry of some Brazilian soils: element mobility during intense weathering. Chemical Geology, 24: 211-229.

Krumbein, W.C. and Graybill, F.A., 1965. An introduction to statistical models in geology. International series in the earth sciences. McGraw-Hill Book Comp., New York.

Lalor, G.C. and Zhang, C.S., 2002. Multivariate outlier detection and remediation in geochemical databases. Science of the Total Environment., 281: 99-109.

Last, J.M. (Editor), 1988. A dictionary of epidemiology. Oxford Medical Publications, Oxford University, New York.

Leah, P.A., 1996. relict lateritic weathering profiles in the Cobar district, NSW. In: Cook W. G., Ford, A.J.H., McDermott, J.J., Standish, P.N., Stegman, C.L. and Stegman, T.M. (Editors), The Cobar Mineral Field- A 1996 Perspective. Australasian Institute of Mining and Metallurgy, Melbourne, pp. 157-177.

Lee, J.Y., Cheon, J.Y., Lee, K.K., Lee, S.Y. and Lee, M.H., 2001. Statistical evaluation of geochemical parameters distribution in a ground water system contaminated with petroleum hydrocarbons. Journal of Environmental Quality, 35: 1548-1563.

Lehmann, B.E., Love, A., Purtschert, R., Collon, P., Loosli, H.H., Kutschera, W., Beyerle, Aeschbach-Hertig, W., Kipfer, R., Frape, S.K., Herczeg, A., Moran, J., Tolstikhin, I.N. and Groning, M., 2003. A comparison of groundwater dating with ^{81}Kr, ^{36}Cl and ^{4}He in four wells of the Great Artesian Basin, Australia. Earth and Planetary Science Letters, 211: 237-2550.

Lentz, D.R., 2003. Geochemistry of sediments and sedimentary rocks: historical to research perspectives. In: Lentz, D.R. (Editor), Geochemistry of sediments and sedimentary rocks: Evolutionary considerations to mineral deposit-forming environments. Geological Association of Canada, pp. 1-6.

Levinson, A.A., 1974. Introduction to exploration geochemistry. Applied Publishing Ltd., Wilmette, Illinois, 924 pp.

Leybourne, M.I., Goodfellow, W.D. and Boyle, D.R., 2002. Sulfide oxidation and groundwater transport of base metals at the Halfmile Lake and Restigouche Zn-Pb massive sulfide deposits, Bathurst Mining Camp, New Brunswick. Geochemistry: Exploration, Environment, Analysis, 2: 37-44.

Limpert, E., Stahel, W.A. and Abbt, M., 2001. Log-normal distributions across the sciences: keys and clues. Bioscience, 51: 341-352.

Lintern, M.J., 1997. Calcrete sampling for gold exploration. MESA Journal, 5: 5-8.

Lintern, M.J. and Butt, C.R.M., 1993. Pedogenic carbonate; an important sampling medium for gold exploration in semi- arid areas. Explor. Res. News, 7: 7-11.

Lintern, M.J. and Butt, C.R.M., 1998. Gold exploration using pedogenic carbonate (calcrete). Geol. Soc. Aust. Spec. Publ., 20: 200 -208.

Lintern, M.J. and Scott, K.M., 1990. The distribution of gold and other elements in soils and vegetation at Panglo, Western Australia., CSIRO, Report No.129R.

Loganathan, P. and Burau, R.G., 1973. Sorption of metal ions by a hydrous manganese oxide. Geochimica et Cosmochimica Acta, 37: 1277-1293.

Love, A.J., Herczeg, A.L., Samson, L., Cresswell, R.G. and Fifield, L.K., 2000. Sources of chloride and implications for Cl-36 dating of old groundwater, southwestern Great Artesian Basin, Australia. Water Resources Research, 36: 1561-1574.

Lovely, D.R. and Phillips, E.J.P., 1988. Manganese inhibition of microbial iron reduction in anaerobic sediments. Geomicrobiology Journal, 6: 145-155.

Lubin, J.H., Colt, J.S., D., C., Davis, S., Cerhan, J.R., Severson, R.K., Bernstein, L. and Hartge, P., 2004. Epidemiologic evaluation of measurement data in the presence of detection limits. Environmental Health Perspectives, 112: 1691-1696.

MacLean, W.H., 1990. Mass change calculations in altered rock series. Mineralium Deposita, 25: 44-49.

Maerz, N.H. and Zhou, W., 1999. Multivariate analysis of bore hole discontinuity data, Rock mechanics for Industry, Proceedings of the 37th US Rock Mechanics Symposium, Vail, Colorado, pp. 431-438.

Manceau, A., Llorca, S. and Galas, G., 1987. Crystal chemistry of cobalt and nickel in lithiophorite and asbolane from New Caledonia. Geochimica et Cosmochimica Acta, 51: 105-114.

Manceau, A., Tamura, N., Marcus, M.A., MacDowell, A.A., Celestre, R.S., Sublett, R.E., Sposito, G. and Pandore, H.A., 2002. Deciphering Ni sequestration in soil ferromanganese nodules by combined X-ray fluorescence, absorption and diffraction at micrometer scale of resolution. American Mineralogist, 87: 1494-1499.

Mantei, E.J., Gutierrez, M. and Zhou, Y., 1996. Use of normalized metal concentrations in the Mn oxides/ hydrous oxides extraction phase of stream sediments to enhance the difference between a landfill emission plume and background. Applied Geochemistry, 11: 803-810.

Martinez, P., Bertrand, P., Shimmield, G.B., Cochrane K., Jorissen, F.J., Foster, J. and Dignan, M., 1999. Upwelling intensity and ocean productivity changes off Cape Blanc (northwest Africa) during the last 70,000 years: Geochemical and micropaleontological evidence. Marine Geology, 158: 57-74.

McKeague, J.A., Damman, A.W. and Heringa, P.K., 1968. Iron-manganese and other pans in some soils of Newfoundland. Canadian Journal of Soil Science, 48: 243-253.

McKenzie, R.M., 1970. The reaction of cobalt with manganese dioxide minerals. Australian Journal of Soil Research, 8: 97-106.

McKenzie, R.M., 1975. An electron microprobe study of the relationships between heavy metals and manganese and iron in soils and ocean floor nodules. Australian Journal of Soil Research, 13: 177-188.

McLaren, R.G. and Crawford, D.V., 1973. Studies on soil copper II. The specific adsorption of copper by soil. Journal of Soil Sciences, 24: 172-181.

McLennan, S.M., Bock, B., Hemming, S.R., Hurowitz, J.A., Lev, S.M. and McDaniel, D.K., 2003. The roles of provenance and sedimentary processes in the geochemistry of sedimentary rocks. In: Lentz, D.R. (Editor), Geochemistry of sediments and sedimentary rocks: evolutionary considerations to mineral deposit-forming environments. Geological Association of Canada, pp. 7-37.

McLennan, S.M., Hemming, S., McDaniel, D.K. and Hanson, G.N., 1993. Geochemical approaches to sedimentation, provenance, and tectonics. In: Johnsson, M.J. and Basu, A. (Editors), Processes controlling the composition of clastic sediments. Geological Society of America, Special Paper, no.284, pp. 21-40p.

McLennan, S.M. and Murray, R.W., 1999. Geochemistry of sediments. In: Marshall, C.P. and Fairbridge, R.W. (Editors), Encyclopedia of Geochemistry. Kluwer Academic Publishers, pp. 282-292.

McLennan, S.M., Taylor, S.R., McCulloch, M.T. and Maynard, J.B., 1990. Geochemical and Nd-Sr isotopic composition of deep-sea turbidites: Crustal evolution and plate tectonic associations. Geochimica et Cosmochimica Acta, 54: 2015-2050.

McPhail, D.C., Summerhayes, E., Welch, S. and Brugger, J., 2003. The geochemistry and mobility of zinc in the regolith. In: Roach, I.C. (Editor), Advances in regolith. CRC LEME, pp. 287-291.

McQueen, K.G., 2004a. Element fractionation and mineral hosts in the regolith, Abstracts-LEME AMEC Mineral Exploration Seminar, pp. 19-22.

McQueen, K.G., 2004b. Field trip guide and locality descriptions. CRC LEME, 32 pp.

McQueen, K.G., 2004c. Girilambone synthesis. Abstracts-LEME AMEC Mineral Exploration Seminar, 4-7 pp.

McQueen, K.G., 2006. Calcrete geochemistry in the Cobar-Girilambone region, New South Wales, CRC LEME open file report 200, 31 pp.

McQueen, K.G., Hill, S.M. and Foster, K.A., 1999. The nature and distribution of regolith carbonate accumulations in southeastern Australia and their potential as a sampling medium in geochemical exploration. Journal of Geochemical Exploration, 67: 67-82

McQueen, K.G. and Munro, D.C., 2003. Weathering- controlled fractionations of ore pathfinder elements at Cobar, NSW. In: Roach, I.C. (Editor), Advances in Regolith. CRCLEME, pp. 296-300.

McQueen, K.G., Munro, D.C., Gray, D.J. and Le Gleuher, M., 2004. Weathering-controlled fractionation of ore and pathfinder elements Part II: the lag story unfolds. In: Roach, I.C. (Editor), Regolith 2004. CRC LEME, pp. 231-246.

Menzies, I., 1969. Hydrogeology. In: Brunker, R.L. (Editor), 1; 250,000 Geological Series ,Explanatory notes Nymagee, pp. 31.

Miesch, A.T., 1967. Theory of error in geochemical data. U.S. Geol. Surv. Prof. Paper 574A, 17 pp.

Mongelli, G., Cullers, R.L., Dinelli, E. and Ruttura, A., 1998. Elemental mobility during the weathering of exposed lower crust: the kinzigitic paragneisse from the Serre, Calabria, southern Italy. Terra Nova, 10: 190-195.

Morgan, J.J. and Stumm, W., 1964. Colloid chemical properties of manganese dioxide. Journal of Colloid Science, 19: 347-59.

Morris, P.A., Pirajno, F. and Shevchenko, S., 2003. Proterozoic mineralization identified by integrated regional regolith geochemistry, geophysics and bedrock mapping in Western Australia. Geochemistry: Exploration, Environment, Analysis, 3: 13-28.

Mosser, C. and Zeegers, H., 1988. The mineralogy and geochemistry of two copper-rich weathering profiles in Burkina Faso, West Africa. Journal of Geochemical Exploration, 30: 145-166.

Munro, D.C., 2003. Regolith geology and geochemical dispersion of the Yarrawonga-Peak area, Cobar, New South Wales, Honours Thesis, University of Canberra, 49 pp.

Murray, R.W., 1979. Iron oxides. In: Burns, R.G. (Editor), Marine minerals. Mineralogical Society of America, Washington, D.C., pp. 47-98.

Nahon, D., 1991. Introduction to the petrology of soils and chemical weathering. Wiley, New York, 313 pp.

Nahon, D., Boulange, B. and Colin, F., 1992. Metallogeny of weathering: an introduction. In: Martini, I.P. and Chesworth, W. (Editors), Weathering, soils and paleosols. Developments in earth surface processes 2. Elsevier, Amsterdam, pp. 445-471.

Nahon, D., Herbillon, A. and Beauvais, A., 1989. The epigenetic replacement of kaolinite by lithiophorite in a manganese-lateritic profile, Brazil. Geoderma, 44: 247-259.

Nahon, D. and Parc, S., 1990. Lateritic concentration of manganese oxyhydroxides and oxides. International Journal of Earth Sciences, 79: 319-326.

Nash, J.T., Day, W.C. and Wilson, A.B., 2001. Geochemical data for historic mining areas, central western slope, Colorado. Open- File Report 01-003, USGS, 13 pp.

Nash, D. and McLaren, S.J., 2003. Kalahari valley calcretes: their nature, origin, and environmental significance. Quaternary International, 111: 3-22.

Native, R., Adar, E., Dahan, E. and Nissim, I., 1997. Water salinization on arid regions-observations from Negev desert. Journal of Hydrology, 196: 271-296.

Neaman, A., Mouele, F., Trolard, F. and Bourrie, G., 2004. Improved methods for selective dissolution of Mn oxides: applications for studying trace element associations. Applied Geochemistry, 19: 973-979.

Neef, G., 2004. Stratigraphy, sedimentology, structure and tectonics of lower Ordovician and Devonian strata of south Mootwingee, Darling basin, western New South Wales. Australian Journal of Earth Sciences, 51: 15-29

Neef, G. and Bottrill, R.S., 2001. Stratigraphy, structure and tectonics of Lower Ordovician and Devonian strata of the central part of the Wonominta Block, western New South Wales. Australian Journal of Earth Sciences, 48: 317-330.

Negra, C., Ross, D.S. and Lanzirotti, A., 2005. Oxidizing behavior of soil manganese: Interactions among abundance, oxidation state, and pH. Soil Sci. Soc. Am. J., 69: 87-95.

Nesbitt, H.W., 2003. Petrogenesis of siliciclastic sediments and sedimentary rocks. In: Lentz, D.R. (Editor), Geochemistry of sediments and sedimentary rocks: evolutionary considerations to mineral deposit-forming environments. Geological Association of Canada, pp. 39-51.

Nesbitt, H.W., Fedo, C.M. and Young, G.M., 1997. Quartz and feldspar stability, steady and non-steady state weathering and petrogenesis of siliciclastic sands and muds. Journal of Geology, 105: 173-191.

Nesbitt, H.W. and Young, G.M., 1982. Early Proterozoic climates and plate motions inferred from major element chemistry of lutites. Nature, 299: 715-717.

Nesbitt, H.W. and Young, G.M., 1984. Prediction of some weathering trends of plutonic and volcanic rocks based on thermodynamic and kinetic considerations. Geochimica et Cosmochimica Acta, 48: 1523-34.

Nesbitt, H.W. and Young, G.M., 1989. Formation and diagenesis of weathering profiles. Journal of Geology, 97: 129-147.

Nesbitt, H.W. and Young, G.M., 1996. Petrogenesis of sediments in the absence of chemical weathering: effects of abrasion and sorting on bulk composition and mineralogy. Sedimentology, 43: 341-358.

Nesbitt, H.W. and Young, G.M., 1997. Sedimentation in the Venezuelan Basin, circulation in the Caribbean Sea, and onset of North Hemisphere glaciation. Journal of Geology, 105: 531-544.

Nesbitt, H.W., Young, G.M., McLennan, S.M. and Keays, R.R., 1996. Effects of chemical weathering and sorting on the petrogenesis of siliciclastic sediments, with implications for provenance studies. Journal of Geology, 104: 525-542.

Nicholson, K., 1992. Contrasting mineralogical-geochemical signatures of manganese oxides: guides to metallogenesis. Economic Geology, 87:1253-1264.

NIST/SEMATECH, 2005. e Handbook of statistical methods, http://www.itl.nist.gov.

Nord Pacific Ltd, 1998. Tritton copper deposit. Minfo, 61: 33-36.

Norrish, K. and Chappell, B.W., 1967. X-ray fluorescence spectrography. In: Zussman, J. (Editor), Physical methods in determinative mineralogy. Academic Press, New York, pp. 201-272.

Northcote, K.H., 1975. Atlas of Australian soils. CSIRO, Melbourne.

Obial, R.C. and James, C.H., 1973. Use of cluster analysis in geochemical prospecting, with particular references to southern Derbyshire, England. In: Jones, M.J. (Editor), Geochemical exploration 1972. The Institution of Mining and Metallurgy, pp. 237-257.

Ohta, A., Imai, N.,Terashima, S. and Tachibana,Y., 2005. Application of multi-element statistical analysis for regional geochemical mapping in Central Japan. Applied Geochemistry, 20:1017-1037.

Ohta, A., Imai, N., Terashima, S., Tachibana, Y., Ikehara, K. and Nakajima, T., 2004. Geochemical mapping in Hokuriku, Japan: Influence of surface geology, mineral occurrences and mass movement from terrestrial to marine environments. Applied Geochemistry, 19: 1453-1469.

Ollier, C. and Pain, C., 1996. Regolith, soils and landforms. Wiley, Chichester, 316 pp.

Oren, O., Yechieli, Y., Bohlke, J.K. and Doby, A., 2004. Contamination of groundwater under cultivated fields in an arid environment central Arave Valley, Israel. Journal of Hydrology, 290: 312-328.

Ostwald, J., 1984. Two varieties of lithiophorite in some Australian deposits. Mineralogical Magazine, 48: 383-388.

Palomares, M. and Arribas, J., 1993. Modern stream sands from compound crystalline sources: composition and sand generation index. In: Johnsson, M.J. and Basu, A. (Editors), Processes controlling the composition of clastic sediments. Geological Society of America, Special Paper No.284, pp. 313-322.

Pan Australian Mining Ltd, 1986. Exploration reports, ELs 2339 and 2405, Crowal Creek-Yarran Creek-Harts Tank area. GS1986/262, Geological Survey of New South Wales.

Parc, S., Nahon, D., Tardy, Y. and Vieillard, P., 1989. Estimated solubility products and fields of stability for cryptomelane, nsutite, birnessite and lithiophorite based on natural lateritic weathering sequences. American Mineralogist, 74: 466-475.

Parkhurst, D.L. and Appelo, C.A.J., 1999. User's guide to PHREEQC (version 2) a computer program for speciation, batch reaction, one dimensional transport, and inverse geochemical calculations. Water-Resources Investigations Report 99-4259. United State Geological Survey, 312 pp.

Peruzzo, L. and Busa, T., 2000. Geochemical correlation and distinction between similar Meta-sedimentary unite from the Eastern Alps. Journal of Conference Abstracts "Goldschmidt 2000", 5: 786.

Phillips, F.M., Bentley, H.W., Davis, S.N., Elmore, D. and B., S.G., 1986. Chlorine-36 dating of very old groundwater 2, Milk River aquifer, Alberta Canada. Water Resources Research, 22: 2003-2016.

Phillips, F.M., Bentley, H.W. and Elmore, D., 1986. Chlorine-36 dating of old ground water in sedimentary basins., The third Canadian/American conference on hydrology. National water well association, Dublin, Ohio, USA,, Banff, Alberta, Canada,, pp. 143-150.

Phillips, F.M., Zreda, M.G., Smith, S.S., Elmore, D., Kubik, P.W., Dorn, R.I. and Roddy, D.J., 1991. Age and geomorphic history of Meteor Crater, Arizona, from cosmogenic ^{36}Cl and ^{14}C in rock varnish. Geochimica et Cosmochimica Acta, 55: 2695-2698.

Phipps, G.C., Boyle, D.R. and Clark, I.D., 2004. Groundwater geochemistry and exploration methods: Myra Falls volcanogenic massive-sulphide deposits, Vancouver Island, British Columbia, Canada. Geochemistry: Exploration, Environment, Analysis, 4: 329-340.

Piang, T.K., 1996. A study of Element dispersion, secondary mineral distribution and weathering history at the McKinnons gold deposit, Cobar, N.S.W., Australia. Honours Thesis, University of Canberra, Canberra, 126 pp.

Pilro, M.C. and Giblin, A.M., 2004. Application of groundwater-mineral equilibrium calculations to geochemical exploration for sediment-hosted uranium: observation from the Embayment, South Australia. Geochemistry: Exploration, Environment, Analysis, 4: 113-127.

Plant, J., Jeffery, K. Gill, E. and Fage, C., 1975. The systematic determination of accuracy and precision in geochemical exploration data. Journal of Geochemical Exploration, 4: 467-486.

Plouffe, A. and Bond, J.D., 2003. Till geochemistry of the Finlayson lake (105G), Glenlyon (105L) and east Carmacks (1151) map areas, Yukon Territory. Geological Survey of Canada, Open file 4479: 17pp.

Pogson, D.J., 1982. Stratigraphy, structure and tectonics: Nymagee-Melrose, central western New South Wales. M.A.Sc. Thesis, New South Wales Institute of Technology, Sydney.

Pogson, D.J., 1991. Geology of the Bobadah 1; 100 000 Geological sheet, Geological Survay of New South Wales, Sydney.

Popov, K., 2002. Geochemical associations in Radka Ore Distric. Annual of the University of Mining and geology "St.Ivan Rilski", 45 part 1, Geology: 57-63.

Post, J.E., 1999. Manganese oxide minerals: crystals structures and economic and environmental significance. Proceedings of the National Academy of Science, 96: 3447-3454.

Powell, C.M., 1984. Uluru and Adelaide regimes Ordovician to earliest Silurian marginal sea and island arc. Phanerozoic earth history of Australia. Oxford University Press., 290-303 pp.

Pwa, A., McQueen, K.G., Scott, K.M. and Van Moort, J.C., 1999. Regolith geochemical exploration using acid insoluble residues as a sample medium for gold and base metal deposits in the Cobar region, N.S.W., Australia. Journal of Geochemical Exploration, 67: 15-31.

Pwa, A., Siegele, R. Cohen, D.R. Stelcer, E. and van Moort, J.C., 2002. Proton included X-ray emission and proton induced gamma ray emission analysis in geochemical exploration for gold and base metal deposits. Nuclear Instruments and Methods in Physics Research, B190: 501-504.

Quantin, C., Becquer, T. and Berthelin, J., 2002. Mn-oxides: a major source of easily mobilisable Co and Ni under reducing conditions in New Caledonia ferralsols. C.R. Geoscience, 334: 273-278.

Rabemanana, V., Violette, S., Marsily, G.D., Robain, H., Deffontaines, B., Andrieux, P., Bensimon, M. and Parriaux, A., 2005. Origin of the high variability of water mineral content in the bedrock aquifer of Southern Madagascar. Journal of Hydrology, 310: 143-156.

Rainbird, R.H., Nesbitt, H.W. and Donaldson, J.A., 1990. Formation and diagenesis of a sub-Huronian saprolith: comparison with a modern weathering profile. Journal of Geology, 98: 801-822.

Ramsey, M.H., Thompson, M. and Hale, M., 1992. Objective evaluation of precision requirements for geochemical analysis using robust analysis of variance. Journal of Geochemical Exploration, 44: 23-36.

Rayner, E.O., 1961. The Peak area, Cobar mineral field, New South Wales. Technical Report 6, Department of Mines, New South Wales, 49-62 pp.

Rayner, E.O., 1969. The copper ores of the Cobar region, New South Wales, Geological Survey New South Wales, 131 pp.

Reese, R.A., 2005. Boxplots, or box-and-whisker plots, offer simple visual summaries of samples of data. Significance, September: 134-135.

Register of Australian Mining, 2003/2004. Resource Information Unit, 739 pp.

Reimann, C. and Filzmoser, P., 2000. Normal and lognormal data distribution in geochemistry: death of a myth. Consequences for the statistical treatment of geochemical and environmental data. Environmental Geology, 39: 1001-1014.

Reimann, C., Filzmoser, P. and Garrett, R.G., 2005. Background and threshold: critical comparison of methods of determination. Science of the Total Environment., 346: 1-16.

Reinders, J., Hanesch, M. and Dearing, J.A., 2003. Statistical analysis of a multiparameter database of Welsh topsoils and rock magnetic characterisation of pollution cluster. Geophysical Research Abstract, 5.

Rendu, J.M., 1988. Applications in geology. In: Crow, E.L. and Shimizu, K. (Editors), Lognormal distributions theory and applications. Marcel Dekker, INC., New York, pp. 357 -365.

Robertson, I.D.M. and Taylor, G.F., 1987. Depletion haloes in fresh rocks surrounding the Cobar ore bodies, N.S.W., Australia: Implications for exploration and ore genesis. Journal of Geochemical Exploration, 27: 77-101.

Rollinson, H., 1993. Using geochemical data: evaluation, presentation, interpretation. Pearson Prentice Hall, London, 352 pp.

Rose, A.W. and Bianchi-Mosquera, G.C., 1993. Adsorption of Cu, Pb, Zn, Co, Ni and Ag on goethite and hematite: a control on metal mobilization from red beds into stratiform copper deposits. Economic Geology, 88: 1226-1236.

Roser, B.P., Coombs, D.S., Korsch, R.J. and Campbell, J.D., 2002. Whole-rock geochemical variations and evolution of the arc-derived Murihiku Terrane, New Zealand. Geological Magazine, 139: 665-685.

Roy, A., 1981. Application of cluster analysis in the interpretation of geochemical data from the Sargilpalli lead-zinc mine area, Sundergarh district, Orissa (India). Journal of Geochemical Exploration, 14: 245-264.

Roy, M., Clark, P.U., Raisbeck, G.M. and Yiou, F., 2004. Geochemical constraints on the regolith hypothesis for the middle Pleistocene transition. Earth and Planetary Science Letters, 227: 281-296.

Rutherford, N.F., 2000. Geochemistry in the weathered profile, Cobar, NSW, Central West Symposium Cobar 2000: Geology, Landscapes and Mineral Exploration. Extended Abstracts. CRCLEME.

Salman, S.R. and Rukah, Y.H., 1999. Multivariate and principal component statistical analysis of contamination in urban and agricultural soils from north Jordan. Environmental Geology, 38: 265-270.

Sato, M., 1960. Oxidation of sulfide ore bodies, 1. Geochemical environment in terms of Eh and pH. Economic Geology, 55: 928-961.

Sawyer, E.W., 1986. The influence of source rock type, chemical weathering and sorting on the geochemistry of clastic sediments from the Quetico Metasedimentry Belt, Superior Province. Chemical Geology, 55: 77-95.

Scheibner, E., 1983. Suspect terranes in the Tasman Fold Belt System (Eastern Australia), Circum- Pacific Terrane Conference, Stanford University, pp. 170-174.

Scheibner, E., 1999. The geological evolution of New South Wales-a brief review. Geological Survey of New South Wales, Sydney, 32 pp.

Scheibner, E. and Basden, H. (Editors), 1996. Geology of New South Wales- Synthesis, Volume 1 Structural Framework. Memoir Geology, 13. Geological survey of New South Wales, 295 pp.

Schenau, S.J., Prins, M.A., De Lange, G.J. and Monnin, C., 2001. Barium accumulation in the Arabian Sea: Controls on barite preservation in marine sediments. Geochimica et Cosmochimica Acta, 65: 1545-1556.

Schwertmann, U. and Taylor, R.M., 1972. The influence of silicate on the transformation of lepidocrocite to goethite. Clay and Clay Minerals, 20: 159-164.

Scott, K.M., 1992. The geochemistry of minerals at the polymetallic Wagga Tank deposit. CSIRO, Report No.344R, pp.

Scott, K.M., 2002. Behaviour of geochemical pathfinder elements during weathering and pedogenesis in SE Australia. Transactions of the 17th World Congress of Soil Science, Thailand,, pp. 11.

Scott, K.M., Rabone, G. and Chaffee, M.A., 1991. Weathering and its effect upon geochemical dispersion at the polymetallic Wagga Tank deposit, N.S.W., Australia. Journal of Geochemical Exploration, 40: 413-426.

Scott, K.M. and Taylor, G.F., 1989. Weathering of pyritic and pyrrhotitic ore on 1 drill level and above, Elura Zn-Pb-Ag orebody, N. S. W., CSIRO, Report no. 55R, pp.

Shen, X.C., Dunlop, A.C. and Cohen, D.R., 1998. Geochemical dispersion in residual and transported regolith along drainage systems near the CSA mine, Cobar, New South Wales. In: Taylor, G. and Pain, C. (Editors), Regolith 98 Australian regolith and mineral exploration: new approaches to an old continent. CRCLEME, Kalgoorlie, WA, pp. 263-270.

Shields, P., 1996. Geology of the Girilambone Copper deposit. In: Cook W. G., Ford A.J.H., McDermott, J.J., Standish, P.N., Stegman, C.L. and Stegman, T.M. (Editors), The Cobar Mineral Field - a 1996 perspective. Australasian Institute of Mining and Metallurgy, Melbourne, pp. 293-304.

Shimmield, G.B. and Mowbray, S.R., 1991. The inorganic geochemical record of the northwest Arabian Sea: A history of productivity variation over the last 400 ka from Sites 722 and 724. Proceedings of Ocean Drilling Program Science Results, 117: 409-429.

Sokal, R.R. and Sneath, P.H.A., 1963. Principles of numerical taxonomy. Freeman, San Francisco, 359 pp.

Staufer, R.E., 1990. Granite weathering and the sensitivity of alpine lakes to acid deposition. Limnol. Oceanogr., 35: 1112-1134.

Stegman, C.L. and Pocock, J.A., 1996. The Cobar gold field- a geological perspective. In: Cook W. G., Ford, A.J.H., McDermott, J.J., Standish, P.N., Stegman, C.L. and Stegman, T.M. (Editors), The Cobar Mineral Field -A 1996 Perspective. Australasian Institute of Mining and Metallurgy, Melbourne, pp. 229-264.

Stegman, C.L. and Stegman, T., 1996. The history of mining in the Cobar field. In: Cook W. G., Ford, A.J.H., McDermott, J.J., Standish, P.N., Stegman, C.L. and Stegman, T.M. (Editors), The Cobar Mineral Field - a 1996 perspective. Australasian Institute of Mining and Metallurgy, Melbourne, pp. 3-39.

Stumm, W. and Morgan, J.J., 1981. Aquatic Chemistry. Wiley, New York, 780 pp.

Sun, Y. and Seccombe, P.K., 2000. Fluid evolution and stable isotope constraints on component sources at the Elura deposit, Cobar. In: McQueen, K.G. and Stegman, C.L. (Editors), Central West Symposium Cobar, Extended abstracts. CSIRO, Perth, WA, pp. 117-121.

Suppel, D.W. and Gilligan, L.B., 1993. Nymagee 1:250 000 Metallogenic map SI/55 -2: Metallogenic study and mineral deposits data sheet. Geological Survey of New South Wales, Sydney.

SWDIV and EFAWEST, 1998. Procedural guidance for statistically analyzing environmental background data. Naval facilities engineering command, 56 pp.

Tan, W.F., Liu, F., Li, Y.H., Hu, H.Q. and Huang, Q.Y., 2006. Elemental composition and geochemical characteristics of iron-manganese nodules in main soils of China. Pedosphere, 16: 72-81.

Tate, S.E., 2003. Characterisation of aeolian materials in the Girilambone region, north-western Lachlan Fold Belt, NSW. Honours Thesis, Australian National University, 208 pp.

Taylor, G. and Eggleton, R.A., 2001. Regolith geology and geomorphology. John Wiley & Sons, Chichester, 375 pp.

Taylor, G. and Butt, C.R.M., 1998. The Australian regolith and mineral exploration. AGSO Journal of Australian Geology & Geophysics, 17: 55-67.

Taylor, G. and Ruxton, B.P., 1987. A duricrust catena in south-east Australia. Zeitschrift fur Geomorphologie, 31: 385-410.

Taylor, G. and Shirtliff, G., 2003. Weathering: cyclical or continuous? An Australian perspective. Australian Journal of Earth Sciences, 50: 1-9.

Taylor, G.F., Wilmshurst, J.R., Togashi, Y. and Andrew, A.S., 1984. Geochemical and mineralogical haloes about the Elura Zn- Pb-Ag orebody, western New South Wales. Journal of Geochemical Exploration, 22: 265-290.

Taylor, J.H., Smith, E.J., Davison, W. and Sugiyama, M., 2005. Resolving and modeling the effects of Fe and Mn redox cycling on trace metal behavior in a seasonally anoxic lake. Geochimica et Cosmochimica Acta, 69: 1947-1960.

Taylor, R.M., 1968. The association of manganese and cobalt in soils-further observations. Journal of Soil Sciences, 19: 77-80.

Taylor, R.M., McKenzie, R.M., Fordham, A.W. and Gilman, G.P., 1983. Oxide minerals, In: Soil: an Australian viewpoint. Division of Soils, CSIRO, Melbourne.

Taylor, S.R. and McLennan, S.M., 1985. The Continental Crust: its composition and evolution. Oxford :Blackwell Scientific, 312 pp.

Thamdrup, B., 2000. Bacterial manganese and iron reduction in aquatic sediments. Advances in Microbial Ecology, 16: 41-48.

Thomas, J.M., Welch, A.H. and Preissler, A.M., 1989. Geochemical evolution of groundwater in Smith Creek Valley- a hydrologically closed basin in Central Nevada, USA. Applied Geochemistry, 4: 493-510.

Thompson, M., 1983. Control procedures in geochemical analysis. In: Howarth, R.J. (Editor), Statistics and data analysis in geochemical prospecting. Elsevier, Amsterdam, pp. 39-58.

Thompson, M., 1992. data quality in applied geochemistry: the requirements, and how to achieve them. Journal of Geochemical Exploration, 44: 3-22.

Thompson, M. and Howarth, R.J., 1978. A new approach to the estimation of analytical precision. Journal of Geochemical Exploration, 9: 23-3-.

Thornber, M.R., 1985. Supergene alteration of sulphides.vii. Distribution of elements during the gossan-forming process. Chemical Geology, 53: 270-301.

Tonuie, E., Caritat, P. and Leyh, W., 2003. Geochemical signature of mineralization in weathered sediments and bedrock, Thunderdome prospect, Broken Hill region, western New South Wales, Australia: implications for mineral exploration under cover. Geochemistry: Exploration, Environment, Analysis, 3: 263-280.

Torgeson, T., Habermehl, M.A., Phillips, F.M., Elmore, D., Kubik, P., Geoffrey-Jones, B., Hemmick, T. and Gove, H.E., 1991. Chlorine 36 dating of very old groundwater? Further studies in the Great Artesian Basin, Australia. Water Resources Research, 27: 3201-3213.

Torrey, C. and White, P.D., 2004. The Pipeline Ridge discovery. In: McQueen, K.G. and Scott, K.M. (Editors), Exploration field workshop Cobar region 2004. CRCLEME, pp. 101-104.

Tritton Resources Limited, 2003. Overview of the Tritton assets.

Tukey, J.M., 1977. Exploratory data analysis. Behavioral science: Quantitative methods. Addison-Wesley, Reading, 688 pp.

Vandenberg, A.H.M. and Stewart, I.R., 1992. Ordovician terranes of the southeastern

Lachlan Fold Belt : stratigraphy, structure and paleogeographic reconstruction. Tectonophysics, 214: 159-176.

Vaniman, D.T., Chipera, S.J., Bish, D.L., Duff, M.C. and Hunter, D.B., 2002. Crystal chemistry of clay-Mn oxides associations in soils, fractures, and matrix of the Bandelier Tuff Pajarito Mesa, New Mexico. Geochimica et Cosmochimica Acta, 66: 1349-1374.

Ward, J.H., 1963. Hierarchical grouping to optimize an objective function. Journal of the American Statistical Association, 58: 236-244.

Whitbread, M.A.I., 2004. Lithogeochemical alteration around the Century and Elura Zn-Pb-Ag deposits: detecting alteration expressions in deep and near surface environments. Ph.D. Thesis, University of Canberra, 330 pp.

Whitbread, M.A. and Moore, C.L., 2004. Two lithogeochemical approaches to the identification of alteration patterns at the Elura Zn-Pb-Ag deposit, Cobar, New South Wales, Australia: use of Pearce Element Ratio analysis and Isocon analysis. Geochemistry: Exploration, Environment, Analysis, 4: 129-141.

White, D.E., Hem, J.D. and Waring, G.A., 1963. Chemical composition of subsurface waters, U.S. Geological Survey Professional Paper 440-F, 67 pp.

White, G.N. and Dixon, J.B., 1996. Iron and manganese distribution in nodules from a young Texas vertisol. Soil Sci. Soc. Am. J., 60: 1254-1262.

Whitford, D.J., Andrew, A.S., Carr, G.R. and Giblin, A.M., 1998. Application of isotope studies of Australian groundwater to mineral exploration: The Abra Prospect, western Australia. In: Arehart, G.B. and Hulston, J.R. (Editors), Proceeding of the 9th International Symposium on Water- Rock Interaction, pp. 583-586.

Whiticar, M.J. and Harris, S.A., 2000. Compound Specific Isotope Correlation (CSIC):Biogeochemical Fingerprints of Organic Compounds. GeoCanada: 1-4.

Wischusen, J.D.H., Fifield, L.K. and Cresswell, R.G., 2004. Hydrogeology of Palm Valley, central Australia; a Pleistocene flora refuge? Journal of Hydrology, 293: 20-46.

Wolfgang, C.A. and White, I., 2000. Pilliga Sandstone hydrogeochemistry, Great Artesian Basin, Australia, Proceedings of the IAH Congress on Groundwater, vol 30, pp 683-687.

Wright, V.P. and Tucker, M.E., 1991. Calcretes: an introduction. In: Wright, V.P. and Tucker, M.E. (Editors), Calcrete. International Association of Sedimentologists Reprint Series 2, pp. 1-22.

Wyborn, D. and Chappell, B.W., 1986. The petrogenetic significance of chemically related plutonic and volcanic rock units. Geological Magazine, 123: 619-628.

Yarincik, K.M., Murray, R.W. and Peterson, L.C., 2000. Climatically sensitive eolian and hemipelagic deposition in the Cariaco Basin,Venezuela, over the past 578,000 years: Results from Al/Ti and K/Al. Paleoceanography, 15: 210-228.

Young, C.J., Merchant, B.J. and Aster, C., 2001. Comparison of cluster analysis methods for identifying regional events. 23rd Seismic Research review: Worldwide Monitoring of Nuclear Explosions: 229-238.

Yu, K.C., Tsai, L.J., Chen, S.H. and Ho, S.T., 2001. Correlation analysis on binding behavior of heavy metals with sediment matrices. Water Research, 35: 2417-2428.

Zabel, M., Schneider, R.R., Wagner, T., Adegbie, A.T., Vries, U. and Kolonic, S., 2001. Late Quaternary climate changes in Central Africa as inferred from terrigenous input to the Niger Fan. Quaternary Research, 56: 207-217.

Zaidelman, F.R. and Nikiforova, A.S., 1998. Manganese-iron concentration in soils and their change under the effect of gleyification on parent materials of different genesis. Euasian Soil Sci., 31: 817-825.

Zhang, C. and Lalor, G., 2003. Multivariate relationships and spatial distribution of geochemical features of soils in Jamaica. Chemical Speciation and Bioavailability, 14: 57 -65.

Zhang, L., Sun, M., Wang, S. and Yu, X., 1998. The composition of shale from the Ordos basin, China: effects of sources weathering and diagenesis. Sedimentary Geology, 116: 129-141.

Zhou, W. and Maerz, N.H., 2001. Multivariate clustering analysis of discontinuity data; Implementation and applications, Rock mechanics in the national interest; Proceeding of the 38th U.S. rock mechanics symposium, Washington, D.C., pp. 861-868.

APPENDICES

The attached CD includes a digital copy for all the appendices. These appendices are:

Appendix 1: Includes the data of ICP multi acid digestion analysis for the regolith of the Byrock, Sussex and Hermidale areas in the Girilambone region.

Appendix 2: Includes the data of ICP and XRF analysis for bottom of the hole samples in the Girilambone region.

Appendix 3: Includes the data of geochemical analysis of groundwater in the Byrock and Hermidale areas.

Appendix 4: Includes the data of XRD analysis data for selective samples from the calcrete bearing, Mn- and Fe- enriched zones in the regolith of the Girilambone region.

Appendix 5: Includes standard, blanks, replicates and duplicates data.

Appendix 6: Includes the data of saturation indices for minerals as calculated from the groundwaters.

Appendix 7: Includes all the regolith facies and the anomaly table of pathfinders

Appendix 8: Includes the probability P-P diagram for the important elements (i.e., As, Au, Cu, Co, Cr, Ni, Pb, Zn) in all the studied facies (i.e., clay-enriched, carbonate-enriched, iron-enriched and manganese-enriched) of the top metre, transported and *in situ* regolith in the study area.